FDOT Work Program Number:
0510757

FINAL REPORT

EVALUATION OF PLASTIC PIPING FOR CULVERTS AND STORM SEWERS

Contractor:

Florida Atlantic University
Department of Ocean Engineering
777 Glades Road Boca Raton, FL
33431

Principal Investigator:

Dr. D. V. Reddy Professor and Director Center
for Marine Structures and Geotechnique (561)
297-3443

April 1999

FOREWORD

The objectives of this study are to evaluate, through experimental and analytical investigation, the feasibility of high density polyethylene pipes (HDPE) for cost-effective applications in the transportation infrastructure, that would enhance the utilization of public funds for highway construction and maintenance operations.

The literature is replete with references on laboratory and field testing, and computer analysis of plastic piping, with particular emphasis on HDPE for subsurface drainage of transportation facilities. The handbooks of the manufacturers outline the product lists, structural, hydraulic, and durability properties, and specifications. The National Cooperative Highways Research Program developed guide specifications for HDPE piping, based on evaluation of criteria for the selection of plastic materials, design procedures, and installation guidelines. The work included laboratory and full scale tests in cooperation with several States, and monitoring of an ongoing field installation. Based on the findings, over 40 States use HDPE pipe, as part of a 40% annual growth for the use of thermoplastics (primarily HDPE and PVC), in transportation drainage facilities.

Notwithstanding, concerns have been expressed about inadequacies of HDPE flexible piping, primarily based on recent experiences in three field sites in California. These concerns include 1) long-term strength and stiffness (dimensional reliability) characteristics, 2) variation in soil properties, 3) longitudinal bending, 4) buckling, 5) tearing of corrugations and circumferential cracking of the inner liner, 6) opening of joints leading to infiltration and exfiltration of water, 7) creep to creep-rupture transition, and 8) life prediction. Since a sizable number of DOT reports have indicated favorable performance of this type of pipe, with many national organizations like AASHTO and the Bureau of Reclamation approving its use, these concerns must be resolved.

ACKNOWLEDGEMENTS

The Principal Investigator would like to thank the Florida Department of Transportation (State Project # 99700-3312, Work Program # 0511757) for its generous financial support. Gratitude is expressed to Mr. R. Powers, Assistant State Corrosion Engineer, Materials Division FDOT, Gainesville, FL, Contract Monitor, and Mr. S. McLemore, State Drainage Engineer, Drainage Division FDOT, Tallahassee, for their continuing interaction with invaluable input, encouragement, and guidance.

Thanks are due to the following persons for their enthusiastic support.

FDOT, Materials Division, Gainesville, FL	i) Mr. R. Kessler, State Corrosion Engineer, Contract Monitor
FDOT, Drainage Division, Ft. Lauderdale, FL	ii) Mr. R. Renna, District Drainage Engineer
Advanced Drainage Systems Inc., Columbia, OH	iii) Mr. J. Goddard, Chief Engineer iv) Mr. J. Erickson, Field Salesman v) Mr. Yunis, Former Area Engineer
Hancor Inc., Findlay, OH	vi) Mr. B. Little, Former National Engineering Manager vii) Ms. V. Daley, Research Engineer viii) Mr. A. Quijada, International Sales Manager.
University of Western Ontario, London, ONT., Canada	ix) Dr. I. Moore (Program WANFE)
University of Florida, Gainesville, FL	x) McTrans Center (Program CANDE)

Appreciation is due to Dr. W. Ahn, former Graduate Assistant, who was the principal contributor, with his Ph.D. dissertation based on the project. Other Graduate Assistants who participated were Ms. N. Azem, Mr. M. Barnes, Mr. K. Bethune, Mr. T. Gavin, Mr. C. Gazagnaire, Mr. G. Gervois, Mr. C. Gonzalez, Mr. T. Phillips, Mr. T. Pierro, Mr. E. Shanahan, and Mr. G. Sitomer.

The administrative support of Dr. S. E. Dunn, Professor and Chairman, Department of Ocean Engineering and Dr. J. T. Jurewicz, Dean of Engineering, Florida Atlantic University, is gratefully acknowledged.

ABSTRACT

An overview of the current issues of HDPE pipe-soil systems is followed by a comprehensive review addressing current specifications, design methods, and relevant research projects. The following experimental tasks were carried out: i) environmental stress cracking resistance (modified AASHTO M294), ii) creep (10,000 hour parallel plate loading at super ambient temperatures), iii) performance of buried pipes, subjected to live loading in a soil chamber, iv) longitudinal bending test to evaluate the ultimate flexural strength of a simply-supported pipe (single piece and jointed with a soil-tight coupler) without the soil medium, subjected to distributed loading, and v) field monitoring. The findings include a) satisfactory short-term environmental stress cracking resistance, b) temperature dependency of the flexural modulus, c) the evidence of transition between slow crack growth and rapid crack propagation due to imperfect installation, d) high load carrying capacity for the properly installed pipe in uniform backfill, showing an over-deflection failure mode with top flattening, e) failure by yielding without debonding (between the inner and outer liner) or cracking, and flexibility of the coupler with the joint separation at a mid-span deflection of 7 in., and f) most cracking on inner liner near the concrete header/end wall due to poor initial installation and ignoring of proper gap filling (right next to the concrete wall).

The analytical investigations were as follows: i) Bidirectional shift-constructed master curve, based on accelerated creep test values for long-term modulus prediction that showed good agreement with the Arrhenius equation-based analysis, ii) Development of a seven-degree Voigt Kelvin viscoelastic model based on the bi-directional shift-constructed master curve for analytical prediction of the long-term modulus, iii) Comparison of two-dimensional and three-dimensional harmonic Finite Element Method analyses with the measured response of pipe-soil interaction that demonstrated that the pattern of deformation and stress distribution can be analytically predicted, iv) Determination of axial stress distribution along the pipe in non-uniform backfill condition, evaluated by approximate analysis, based on finite differencing the deflection profile and introducing deflection compatibility at the soil interfaces by regression analysis. This overcomes the limitation of the harmonic FEM analysis for pipe-soil interaction involving non-uniform soil conditions longitudinally and/or varying soil thickness circumferentially, and v) Joint integrity analysis. The findings include a) importance of axial stress contribution at failure, b) top flattening failure mode due to over-deflection preceding buckling or yielding, c) critical adverse effect of the non-uniform backfill condition that can lead to joint opening, localized buckling, liner tearing/debonding, or cracking, and d) adequacy of the approximate finite element analysis for simulating non-uniform soil conditions.

TABLE OF CONTENTS

LIST OF TABLES

CHAPTER

Table

Page No.

LIST OF FIGURES

CHAPTER

Figure

Page No.

6. ANALYTICAL INVESTIGATION

CHAPTER 1

INTRODUCTION

A pipe can be classified as either flexible or rigid, depending on how it behaves when installed. Flexible pipe, manufactured from either plastics or metals, takes advantages of its ability to bend without structural damage. Plastics exhibit viscoelastic properties in contrast to the elastic behavior of metals. It is this difference that is the source of much confusion in understanding the thermoplastic pipe and its installed performance as compared to other types of flexible pipe [CPPA, 1996]. The behavior of viscoelastic materials differs from elastic ones. For example, when a thermoplastic material is subjected to constant force, the stress/strain curve gives the impression that the material loses strength with time.

High density polyethylene pipe (HDPE) has good potential for economic use for marine oil and gas pipelines, underdrains, storm sewers, culverts, and other subsurface drainage structures. In view of its inherent chemical and corrosion resistance, light weight, toughness, flexibility, easy splicing, and consequent easy handling, and installation, over forty states use HDPE pipe as part of a 40% annual growth for the use of thermoplastic, HDPE pipe in transportation construction projects [Goddard, 1995], Fig. 1.1. The long

term performance of HDPE is of particular interest, in view of highly organic and salt water (coastal) conditions.

Fig. 1.1 Lightweight HDPE

Recently, based on field experiences in California, concerns have been expressed [Johnson, 1993], [Strand, 1993], and [Hall and Foreman, 1993] about certain inadequacies of high density polyethylene piping. These include long-term strength and stiffness (dimensional reliability) characteristics, delamination of the interior liner,

inconsistency of physical properties, buckling, opening of joints leading to infiltration and exfiltration of water, tearing of corrugations and circumferential cracking of inner liner, flammability, the requirement for excessive trench widths. But, thirty state DOT (Department of Transportation) reports have indicated favorable performance of this type of pipe. Additionally, many national organizations like AASHTO (American Association of State Highway and Transportation Officials) and TRB (Transportation Research Board) approved its use.

The necessary considerations to ensure long-term performance of HDPE pipe are as follows: 1) resin quality (strength and cracking), 2) profile stability (buckling resistance), 3) adequate installation stiffness and backfill control, and 4) installed pipe deflection levels. Items 1 and 2 are especially important in these long-term applications due to the timedependent nature of the materials involved. Local buckling can occur when sufficient compressive strain due to any combination of deflection and ring compression occurs for each specific profile. Cracking occurs due to localized tension stresses (strains) and stress concentration factors in the profile. For long-term applications, both pipe deflection levels and the specific grade of the material used must be controlled.

Inclusion of HDPE in competition with other pipe materials is essential to assure cost-effective applications, which would provide the maximum utilization of public funds [Reddy, 1995 - 98, 1997 - 99]. This study involved laboratory testing, together with computer based pipe-soil interaction analysis for long-term 'strength and durability, Ahn and Reddy [1998]. The findings enable the setting up of product performance limits and the development of practical guidelines for the selection, design, specification, and installation of HDPE piping for subsurface drainage of transportation facilities.

CHAPTER 2

BACKGROUND

2.1 CHARACTERISTICS OF THERMOPLASTIC PIPING MATERIAL

Flexible thermoplastic piping materials include polyvinyl chloride (PVC), chlorinated polyvinyl chloride (CPVC), high density polyethylene (HDPE), polybutene (PB), polypropylene (PP), and polyvinylidene fluoride (PVDF). Thermoplastics are generally time and temperature-dependent, and exhibit viscoelastic response. Consequently, their behavior is not sufficiently understood well enough for a comparable base of design and evaluation information to exist. Since thermoplastics are softened by heating, they can be shaped into articles by operations, such as by molding or extrusion. They are organic materials, that is, they are based on carbon and hydrogen atoms, joined together. They have crystalline (ordered) or amorphous (random) molecular structures. The presence of crystallinity is dependent on the thermal history and hence the processing conditions. Plastics used for pipe exhibit a wide range of properties, derived from the chemical composition of the basic synthetic polymer, the kind and amount of additives, the nature of reinforcement, and manufacturing process [Hashash, 1991].

The molecular weight and its distribution determine many of the mechanical and chemical properties of the pipe. The longer the main molecular chain, the greater the molecular weight. The arrangement of molecular chains influence the property characteristics. Therefore, the number and chemical characteristics of chains determine, in the large part, density, stiffness, tensile strength, flexibility, hardness, brittleness, elongation, creep characteristics, melt viscosity of the polymer.

2.1.1 POLYETHYLENE

The polymer, polyethylene (PE), with repeat unit structure [-CH2 CH2-]$_n$ is produced by the polymerization of ethylene. It is the largest tonnage plastic material produced and is obtained in a variety of forms with various degree crystallinity. The earliest type of commercial polyethylene was produced by free radical polymerization of ethylene at very high temperatures and pressures. It is, therefore, sometimes referred to as high pressure polyethylene which does not crystallize as readily as linear polyethylene and is of density, 33.0-33.41b/in3 (0.915-0.925 g/cm^3)-Low Density Polyethylene (LDPE). Ethylene may also be polymerized at normal pressures using very active catalysts to give Medium Density Polyethylene (MDPE). These polymers are more linear and crystallize to a greater extent and are, therefore, intermediate density (medium density polyethylene, MDPE), in the range , 33.4-33.9 lb/in^3 (0.925-0.94 g/cm^3). High Density Polyethylene (HDPE) is even more crystalline (about 90%) and is of high density (about 34.71b/in^3, 0.96 g/cm^3). Typical molecular weights of commercial polyethylenes are in range 20,00040,000 (number average) with a polydispersity of about 20-50 for LDPE and 10,00050,000 with a polydispersity of about 5-15 for HDPE.

The crystalline melting behavior is dependent on density. Typically, LDPE melts over a wide range of 176-230 OF, (80-110 OC) and HDPE over a range of about 248-275 °F, (120-135 OC). Several transitions (α, (β, and γ) exist apart from T_m (melting temperature). The a transition is associated with motions in the crystalline phase and occurs at about +122 OF (+50 OC) although the value is crystallinity dependent. The β transition is at about -4 OF (-20 OC) and is associated with motions involving branch points. The y transition is at. about -184 OF (-120 OC) and involves motions of sequences of a few -CH2- groups. Considerable controversy exists as to whether the β or γ transition should be called, glass transition at temperature, T_g.

The mechanical behavior of PE depends on density. LDPE is a soft and flexible material, with a typical elastic modulus of 29 ksi (0.2 GPa), a tensile strength of 1.45 ksi (10 MPa), and elongation at break of 800 %. HDPE is a harder, stiffer material, typically with a modulus of 145 ksi (1.0 GPa) , tensile strength of 4.35 ksi (30 MPa), and

2.2 LOADS ON BURIED PIPES

The loads to which buried pipes are subjected to in service and their supporting strength under various installation conditions can be determined by means of the Marston Theory of Loads on Underground Conduits [Spangler and Handy, 1982]. The basis of the theory is that the load due to the weight of the soil column above a buried pipe is modified by arching action, in which part of its weight is transferred to the adjacent side prisms, making the load on the pipe less than the weight of the overlying column of soil.

from the side prisms is transferred to the soil over the pipe. The direction of load transfer by an arching action is in the direction of relative movement or tendency for movement, between the overlaying prism of soil and the adjacent side prisms, as shown in Figs. 2.1 and 2.2. The transfer force associated with arching action at the plane of relative movement is the resultant of the vertical and horizontal force components.

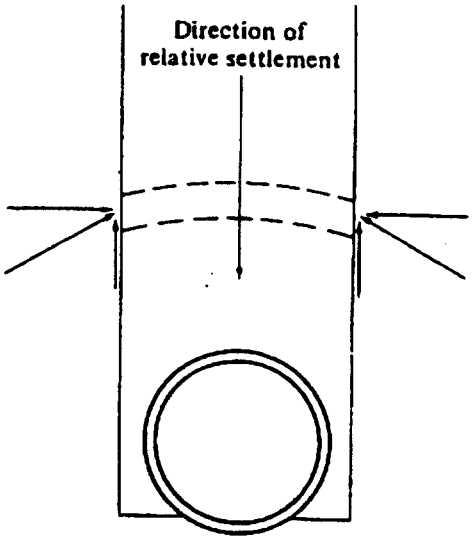

Fig. 2.1 Arching action

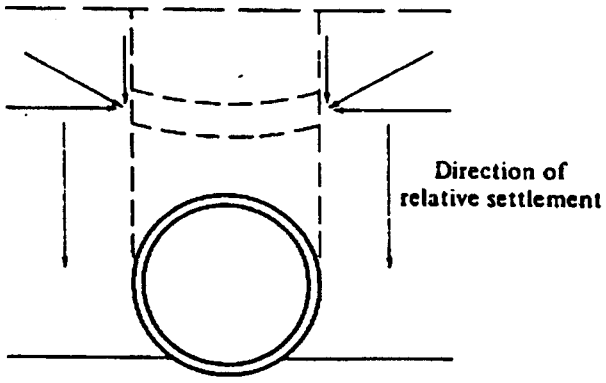

Fig. 2.2 Inverted arching action

2.3 VISCOELASTICITY

Plastics are viscoelastic materials, with deformation and strength properties varying with temperature and duration of loading, and also affected by certain environmental conditions. As the name implies, viscoelastic materials respond to stress as superposition of elastic and viscous elements. The springs in the highly simplified model of Fig. 2.3 represent the elastic elements of a polymer (e.g., chain rigidity, chemical bonds, and crystallinity), each spring having a different constant that represents a time-independent modulus of elasticity. The dashpots represent the viscous fluid elements (e.g., molecules slipping past each other), each one having a different viscosity or time-dependent response.

When a constant load is applied and sustained on this model, it results in an initial deformation which continues to increase indefinitely, Fig. 2.4. This phenomenon of continuing deformation, which also occurs in concrete, soft metals, wood, and structural metals at very high temperatures, is called creep. If the load is removed after a certain time (say, at point ti in Fig. 2.4), there is a rapid initial strain recovery followed by a continuing recovery that occurs at a steadily decreasing rate; in this model recovery is never complete. However, if the creep strain does not cause irreversible structural changes and sufficient time is allowed, the strain recovery will be almost complete. The rate and extent of deformation and recovery are sensitive to temperature, and can also be influenced by environmental effects, such as by absorption of solvents or other materials with which the plastics may have come in contact with while under stress. An analogous response of viscoelastic materials is stress-relaxation. The initial load required to achieve a certain deformation will tend to gradually relax when that deformation is kept constant, Fig. 2.5. Initially, stress-relaxation occurs rapidly and then steadily decreases with increasing time.

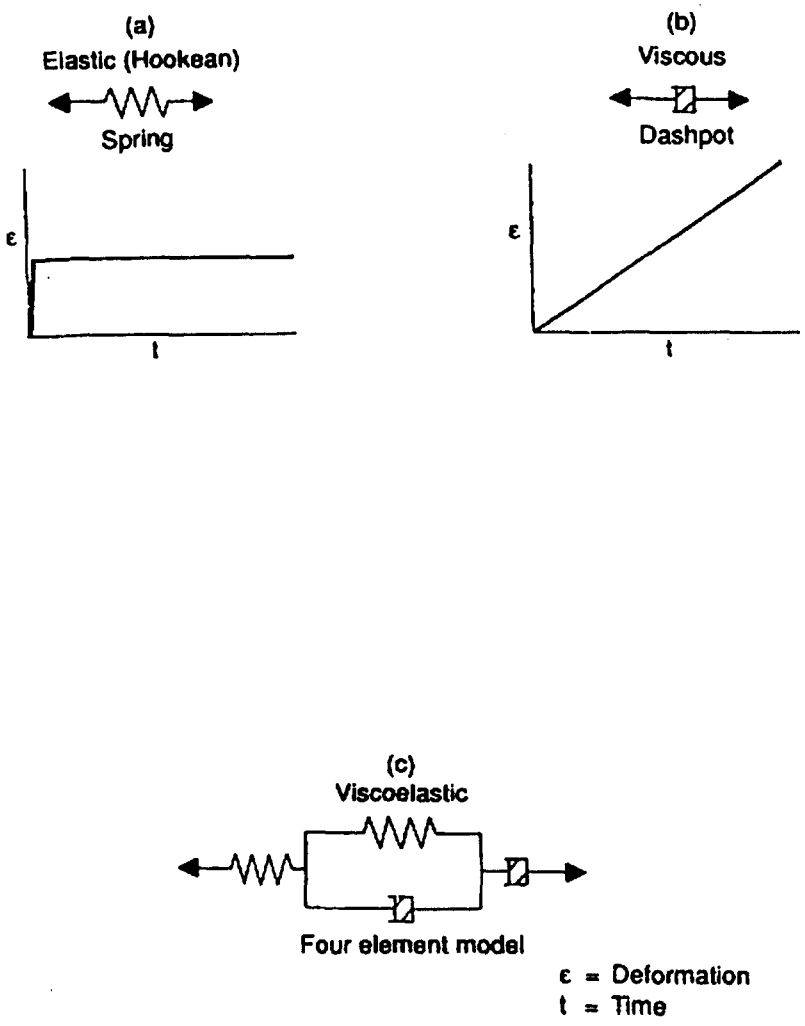

Fig. 2.3 Model of viscoelastic behavior

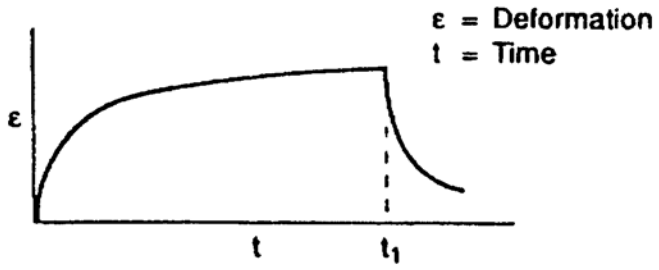

Fig. 2.4 Viscoelastic response, creep (constant load)

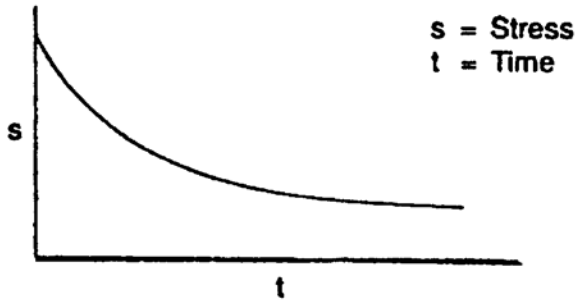

Fig. 2.5 Viscoelastic response, stress relaxation (constant deformation)

CHAPTER 3

LITERATURE REVIEW

3.1 THERMOPLASTIC PIPE FOR NONPRESSURE APPLICATIONS

More than half of all the thermoplastic pipe made is used for nonpressure applications. Most drainage systems, including those for building foundations, leaching fields, agriculture, and road construction now consist of thermoplastics piping, mostly PE and PVC. Both PE and PVC are increasingly used for larger-diameter sewers and culverts. Plastics, being nonconductors, are immune to the corrosion process induced by electrolytes, such as acids and salts. In addition, plastic pipe materials are not vulnerable to biological attack. This results in negligible costs for maintenance and external protection, such as painting, coating, or cathodic protection. Their lower specific gravity contributes to ease of handling, storage, and installation, as well as lower transportation costs. They also offer very good abrasion resistance, even when conveying slurries. High deformation capacity provides positive pipe-soil interaction, which is capable of supporting earth fills and surface live loads of considerable magnitude without fracture. Therefore a sizable number of DOT (Department of Transportation) reports have indicated favorable performance of this type of pipe, and many national organizations including AASHTO (American Association of State Highway and Transportation Officials) approve its use.

Based on some recent experience in three field sites in California, concerns have been expressed about the inadequacies of HDPE flexible piping, and, by implication, about all thermoplastics for this application area; e.g. Johnson [1993], Strand [1993], and Hall and Foreman [1993]. These concerns which must be resolved include long-term strength and stiffness (dimensional reliability) characteristics; delamination of the interior liner, inconsistency of physical properties, buckling, opening of joints leading to infiltration, and exfiltration of water, tearing of corrugations and circumferential cracking of the inner liner, flammability, and the requirement for excessive trench widths. The development of data and methodologies for the safe and reliable use of thermoplastics as pipe materials is essential to assure cost-effective applications, which, in turn, would enhance the utilization of public funds for highway construction and maintenance operations.

To ensure long-term performance, the individual pipe wall profile must be evaluated in regard to its specific geometry, and the stresses and strains quantified to properly determine the long term capacity of the specific materials allowed. Local buckling will occur when sufficient compressive strain due to any combination of deflection and ring compression occurs for each specific profile. Cracking occurs due to localized tension stresses (strains) due to stress concentrations and residual stresses in the profile. For longterm applications, both pipe deflection levels and the specific grade of the plastic used must be controlled. Specific items for control include the following:

1) Resin quality (strength and cracking)
2) Profile stability (buckling resistance)
3) Adequate installation stiffness and backfill control.
4) Pipe deflection levels.

Items 1 and 2 are especially important in long term applications.

The long-term performance limits depend very much on the design method. The proof of any design theory should be how accurately it predicts the location, and the mode of failure of the product under service loading conditions. Unfortunately, current nonpressure pipe design procedures do not pass this test, regardless of major pipe types [Goddard, 1994]. Performance limits that have been suggested for the design of buried gravity flow thermoplastic pipes include: 1) deflection, 2) wall buckling, 3) wall strain, 4) wall crushing, 5) longitudinal bending, 6) stress concentration, and 7) yielding.

A recent study on PE pipe specifications carried out at California State University by Gabriel et al. [1996], indicated that the HDB (Hydrostatic Design Basis) testing has only marginal value in its ability to predict the long term service performance of gravity flow non-pressure pipes, and that its cost/benefit aspects are not persuasive. However, a quantitative evaluation was not made to set up performance limits and develop practical guidelines for selection, design, specification, and installation.

Moser [1993, 1994] observed that "the normal and real modulus is the instantaneous stress divided into the instantaneous short term strain parameter for design and most materials must be designed on a life basis". This was based on Hydrostatic Design Basis (HDB) strength testing of the PVC pipe that had been in service for 15 years, in which the modulus after unloading was the same as that when the pipe was manufactured. The properties of HDPE pipe (viscoelastic material), however, are dependent on time, temperature, stress and rate of loading; thus instantaneous testing cannot be expected to simulate material behavior, when subjected to stress or deformation

for extended periods of time. For life prediction, consideration should be given to the estimation of long term property values of the modulus and strength under exposure conditions (pipe-soil interaction) that simulate the end-use applications. The use of a pseudoviscoelastic modulus for the elastic modulus implies the tacit use of a principle of viscoelasticity known as the "correspondence principle". This principle states that the stresses in a viscoelastic body subjected only to constant applied forces, will be exactly the same as they are in an elastic body subjected to the same set of tractions. Compared to constant internally pressurized pipe in the gas industry, non-pressure pipe is subjected to mixed force and displacement boundary conditions, which make creep and relaxation characterization testing essential for an analysis of the potential for service failure.

3.2 HDPE MANUFACTURING, CLASSIFICATION, AND PROPERTIES

Polyethylene is possibly the best known member of the polyolefin family, derived from polymerization of olefin gases. PE is a partly crystalline and partly amorphous material. The properties of PE are determined by its molecular structure. PE consists of a backbone of long molecular chain from which short chain branches occasionally project. The length, type, and frequency of distribution of these branches, as well as other parameters such as molecular weight and distribution, determine the degree of crystallinity and network of molecules that anchor the crystal-like regions to one another. These structural characteristics affect the short and long-term mechanical properties. The extent of crystallinity of PE is reflected by density. The higher density materials have more crystalline regions, which results in greater stiffness and tensile strength.

To protect the polymer during processing, storage, and service, small quantities of heat stabilizers, anti-oxidants, and ultra-violet (UV) screens or stabilizers are added. The primary specification for identifying and classifying PE piping materials is ASTM D3350, entitled "Standard Specification for Polyethylene Pipe and Fitting Materials", Table 3.1. This specification identifies polyethylene pipe and fitting materials according to a cell class format based on physical property criteria. The PE pipe compounds are classified according to density, melt index, flexural modulus, tensile strength at yield, environmental stress crack resistance, hydrostatic design basis at 73.4 ºF (23 ºC), color, and UV stabilizers. The order of these various properties is constant as shown in Table 3.1.

3.3 PIPE-SOIL INTERACTION

Pipe-soil interaction addresses the mutual contributions of pipe and soil in a structural system, as soil supports much of the vertical pressure in arching action, over the pipe. The basic concept of the theory is that the load due to weight of the soil column above the buried pipe is modified by arching action, in which a part of its weight is transferred to the adjacent side prisms, with the result that in some cases the load on the pipe may be less than the weight of the overlaying column of soil, Figs 2.1 and 2.2. Conversely, the load on the pipe may be increased by an inverted arch action, in which the load from the side prisms is transferred to the soil over the pipe. The transferred force, associated with arching action at the plane of the relative movement, is the resultant of the vertical and horizontal components of force Spangler [1982].

Table 3.1 Primary Properties: Cell Classification Limits for PE Materials in Accordance with ASTM D3350

Destination order no.	Property	Test method	Cell limits 0	1	2	3	4	5	6
1	Density, g/cm^3	D 1505	...	0.910-0.925	0.926-0.940	0.941-0.955	>0.955	...	
2	Melt index	D 1238	...	> 1.0	1.0 to 0.4	<0.4 to 0.15	<0.15	*	†
3	Flexural modulus, psi	D 790	...	<20,000	20,000 to <40.000	40,000 to 80,000	80,00010	110,000 to < 160,010	> 160,00
4	Tensile strength at yield, psi	D 638	...	<2,200	2,200-<2,600	2,600-<3,000	3,000-<3,500	3,500-<4,000	>4,000
5	Environmental stress crack resistance	D 1693	...				...		
	a. Test condition			A	B	C			
	b. Test duration, h			48	24	192			
	c. Failure, max, %			50	50	20			
6	Hydrostatic design basis, psi(23'C)	D 2837	NPR#	800	1,000	1,250	1,600	...	

'Materials with melt index less than cell 4 but which have flow rate <4.0 8/10 min when tested in accordance with D 1238, Condition F.

†Materials with melt index less than cell 4 but which have flow rate <0.30 8/10 min when tested in accordance with D 1238 but at 310'C with total load of 12,480 8.

$Nonpressure rated.

The "bedding" condition has a very important effect on both circumferential and longitudinal bending moments. For instance, active lateral earth pressure can reduce the circumferential moment by 25 % [Spangler, 1982]. The longitudinal bending moments can also be affected similarly. Rajani et al. [1996] have indicated that flexural action due to inadequate bedding support or swelling of underlying clay imposes longitudinal tensile stresses, Fig. 3.1. Tensile stresses in the pipe can also be induced if clays with a high montmorillonite mineral content undergo substantial volume change, when subjected to seasonal wet and dry conditions. Clark [1971] and Morris [1967] report that volumetric shrinkage for clays in Texas can be in the range of 14-40 percent.

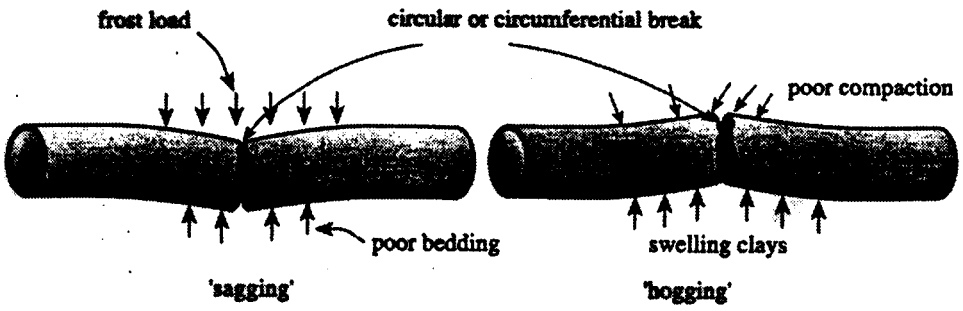

Fig. 3.1 Bending or flexural failure [Rajani et al. 1996]

A simple relationship to express soil-pipe interaction in the transverse plane is that given by the Iowa Method (Modified Spangler Equation, ASTM D2412, 1995) CPPA [1996], which is applicable up to a deflection of 5 % of the diameter i.e.

$$\Delta y = \frac{K(D_L W_C + W_L)}{0.149PS + 0.061E'} \qquad (3.1)$$

where

Δy=deflection

K=bedding constant,dimensionless (ASTM D 3839, X1.3.2)

D_L=deflection lag factor, (ASTM D3839, X1.3.1)

γ=unit weight

H=burial depth

OD=outside diameter of pipe

$W_C=\gamma HOD$=soil column load on pipe

W_L=live load

$PS=EI/0.149Fr^3$=pipe stiffness

E=flexural modulus of the pipe

I=moment of inertia of the pipe wall

E'=backfill modulus

This clearly indicates that the deflection of a soil-embedded pipe depends on the relative stiffness of the pipe and soil. There is a likelihood of long-term decomposition in organic soil, which can reduce the arching action. Also, the physico-chemical stability of certain limestone gravel can be detrimentally affected by dissolution due to groundwater changes. The change in the degree of compaction near the pipe, and the consequent change in K, can occur during installation, and/or service due to soil saturation or pumping. This can also cause separation of the pipe wall from the soil. Therefore, it is important to address the possible decrease of the arching effect in the life prediction of HDPE pipe. The same type of soil changes can induce significant longitudinal stresses due to differential settlement induced beam action with non-uniform subgrade modulus.

3.4 FAILURE MECHANISMS OF BURIED HDPE PIPE

The major failure modes for thermoplastic pipes include buckling, and ductile/brittle failures. Some of these are characterized by slow crack growth or rapid crack propagation. For pressurized pipes, ductile and brittle failures are of the utmost importance, as buckling is seldom a major concern. In contrast, buckling is the most common failure mechanism in non-pressure applications, with the remaining two failure modes being possible only in highly unusual conditions. Note that in this discussion "brittle" is one that is produced in a long time period under relatively low stress, is accompanied by little or no ductility, and is initiated at an intrinsic weakness, (i.e. impurities, notches) in the material. Slow crack growth (SCG), which is a similar process, is used to describe failures that initiate from stress concentration geometry introduced in installation or service.

3.4.1 STRESS CRACKING

Stress cracking is a macro-brittle cracking phenomenon that occurs at a constant stress, significantly less than the yield or break stress of the material. It is initiated at an internal or external "defect" in the material, such as an inclusion or scratch. In HDPE components, although the stress crack is not associated with any apparent adjacent material deformation, the fracture face itself provides evidence of ductility on a microscopic scale. In most cases, failure occurs as a result of some unknown material performance characteristic, or some unexpected local service condition that initiates a crack at a "flaw" in the material. It is necessary to identify such unexpected failure-initiating defects, and to understand at what rate induced cracks will propagate, and how much they reduce the service life [Reddy, 1996].

The predominant mode of premature failure of thermoplastic pipe is a quasi-brittle fracture initiated at stress concentrating surface notch geometry and/or unexpected point stress [Peggs and Kanninen, 1995]. Such failures occur due to the fundamental stress cracking susceptibility. The stress cracking is often called "Slow Crack Growth (SCG)", which occurs at stress levels lower than the tensile yield strength, and at any time during the life of a pipe.

The material does not become brittle, it simply shows the appearance of brittleness. Stress cracking is a synergistic function of applied stress, temperature, and many material parameters (e.g., molecular weight and its distribution, comonomer type and content, and crystallinity). Stress cracking is most commonly thought to occur when the tie molecules , which link crystalline and amorphous regions, slowly slip out from the region of crystallinity involving entangled loose ends of tie molecules [Lustiger, 1983]. Fracture thus occurs between crystalline regions involving amorphous polymer only, without apparent deformation, and with relatively smooth fracture face morphology in HDPE. In contrast, when HDPE is subjected to rapid increase in stress, as in a typical uniaxial tensile test, the tie molecules do not have time to slip out of their entanglement, but instead, pull segments of the crystalline region with them, producing the necking and elongation associated with yielding.

In the design of HDPE for storm-water sewer applications, a number of performance limits need to be considered. In addition to well established limit states, such as buckling and excessive deflection, the maximum circumferential bending stresses in the pipe have to be considered to avoid tensile yield or rupture of the pipe. Recently, it has also been suggested that buried plastic pipe may be susceptible to slow crack growth, following environmental stress cracking or some other crack initiation mechanism. Slow

crack growth will only occur in a tensile stress field [Kuhlman, et al., 1995]. Furthermore, index tests developed for the gas pressure pipeline industry reveal that the speed at which slow crack growth occurs is affected by the magnitude of that maximum tensile stress. Materials exhibiting low ductility can fail prematurely in a crack-like fashion (brittle fracture) by slow crack growth.

The potential for stress cracking of plastic pipe is not a function of material properties alone, as geometry plays an important role [Gabriel et al., 1996]. The NCTL (Notch Constant Tensile Load) test, ASTM D5397, does not address the relationship between stiffness and stress crack initiation with the focus on geometry. It is necessary to identify unexpected failure-initiated defects and to understand their rate of propagation, and the associated possible effects on excessive deflection and buckling. Stress cracking failure in pipe, which is well presented in the Gas Research Institute's Field Failure Catalog for Polyethylene Gas Piping, occurs predominantly at notch geometries associated with joints. It also occurs at locations where rocks impinge against the pipe surface, and at locations that have been improperly squeezed off, while making repairs [Peggs and Kanninen 1995]. The stress cracking problem in HDPE pipe was identified in the late 1970's. It was subject of much research in the early 1980's, resulting in significant improvements in stress cracking resistance of pipe grade resins.

3.4.2 Creep and Creep Rupture

HDPE is viscoelastic material for which the history of deformation has an effect on the response. For example, if a load is continuously applied, it creates an instantaneous initial deformation, that then increases over time. The stress and strain are related by a modulus that depends on the duration of load and magnitude of the applied stress at a given

temperature, Fig. 3.2. Viscoelastic behavior becomes nonlinear at high stress or strain or elevated temperatures exihibiting logarithmic decay of modulus over time, Figs. 3.2 and 3.3.

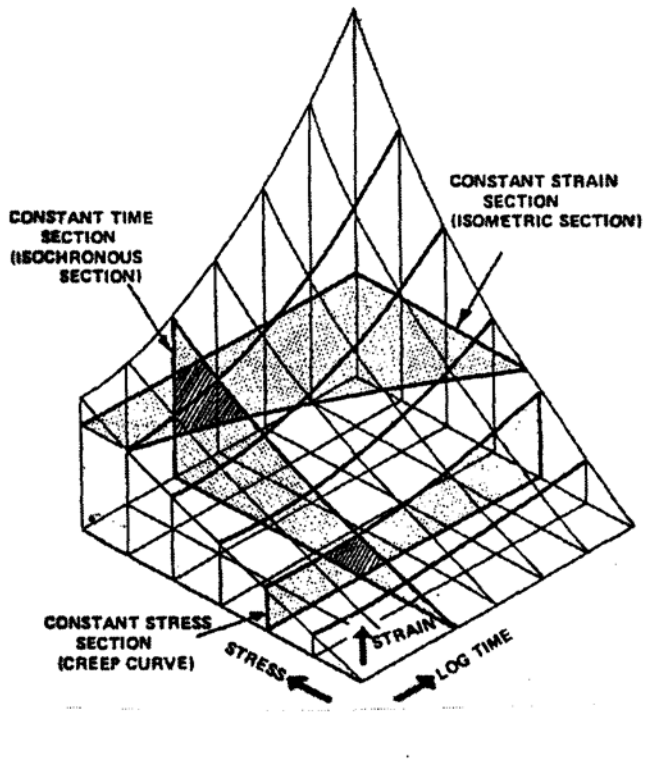

Fig. 3.2 Constant stress-strain time coordinates [ASTM D 2990]

Creep, expressed in terms of the increasing compliance contributing to increasing deformation, (i.e. loss of stiffness), and creep-rupture, expressed in terms of decreasing life with increasing stress and temperature, are important parameters for life prediction. The transition from ductile to brittle behavior enables the realistic estimation of life from the creep-rupture plot.

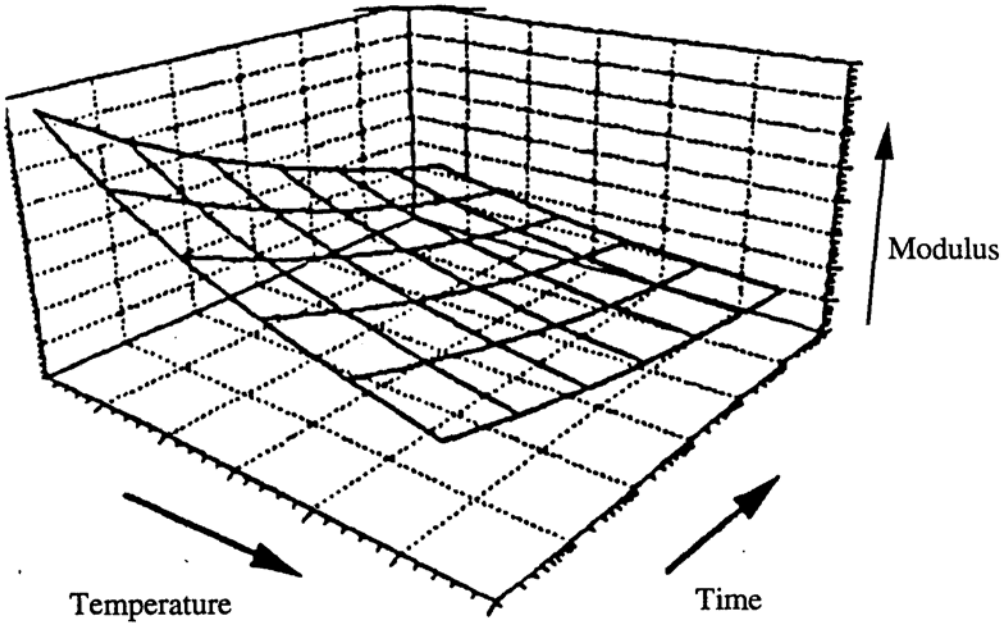

Fig. 3.3 Schematic of the viscoelastic behavior of polymers

Woods et al. [1996] conducted tensile creep-rupture testing on HDPE pipe material, based on ASTM D 638, and observed the occurrence of the ductile-brittle transition at a very early stage with a high stress level; no "knee", Fig. 3.4, was seen in the tensile stress vs. time plot.

The predominant mode of premature failure of thermoplastic pipe, as indicated earlier is quasi-brittle fracture, initiated at stress concentrating surface notch geometries, imperfections (initial pinpoint depressions, etc.) and/or unexpected point stresses. Prediction of life, based on only long term material properties, ignoring the geometry, would overestimate the predicted life. Geometry, associated with the pipe curvature and the connectivity of the corrugations with lining, can effect the creep and creep-rupture

behavior. It can also reduce the buckling strength at the wall. The creep and creep-rupture schematics for life prediction are shown in Figs. 3.2 , 3.3, and 3.4. It is necessary to identify unexpected failure-initiating defects, and to understand at what rate induced cracks will propagate, and how much they affect the reduction of service life.

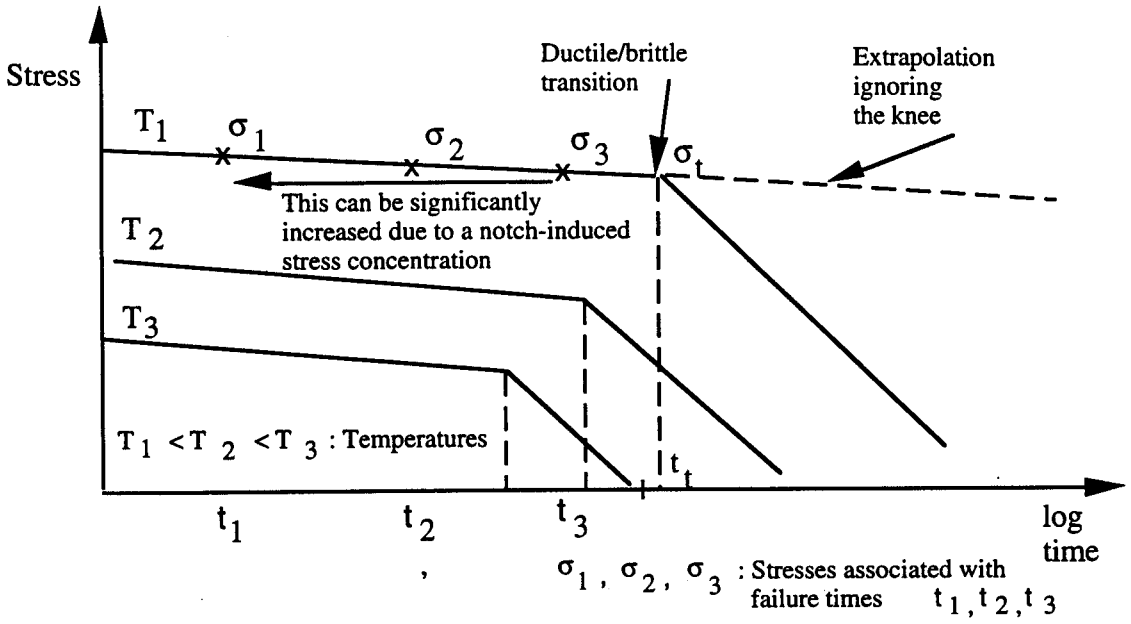

Fig. 3.4 Creep- rupture behavior for semi-crystalline polymers

3.4.3 BUCKLING

Circumferential and longitudinal moments can induce local buckling in the corrugated wall of the HDPE pipe. The more flexible the pipe, the lower the resistance to buckling. Caution should be exercised when considering large diameter pipes or pipes in shallow burial. Moser [1990] developed a buckling equation that has been shown to be

conservative for thermoplastic pipe, with the modification of the Euler buckling formula, as follows:

$$P_{cr} = 2\sqrt{\frac{E'}{1-\nu}\left(\frac{EI}{R^3}\right)} \quad \text{----------(3.2)}$$

where

P_{cr} =critical buckling pressure, (Mpa, psi)

E'=soil modulus, (MPa, psi)

ν=Poisson's ratio, (dimensionless)

E=modulus of elasticity, (MPa, psi)

I=moment of inertia, ($mm^4/mm.$, $in.^4/in.$)

R=pipe radius, (mm, in.)

AASHTO and ASCE use a somewhat different approach; the current AASHTO, [1992] version is as follows:

$$f_{cr} = 0.77(R / A\phi)\sqrt{\frac{BE'EI}{0.149R^3}} \quad \text{----------(3.3)}$$

where

B=water buoyancy factor (dimensionless)=$1 - 0.33h_w/h$

h_w =height of water above top of pipe, (m, ft.)

h=height of ground surface above top of pipe, (m, ft.)

E=long term modulus of elasticity (50 year), (MPa, psi)

I=moment of inertia, (mm^4/mm, $in.^4/in.$)

E'= soil modulus, (MPa, psi)

f_{cr}=critical buckling stress, (MPa, psi)

R=effective radius, (mm, in.)=c+ID/2

c=distance from the inside surface to the neutral axis, (mm, in.)

A_{ϕ}=pipe wall area (0.083 min ^{2}/mm, in. ^{2}/ft.)

*For side fills conforming to the minimum soil cover required, a value of f_{cr}=11.7 MPa may be used. AASHTO LRFD Bridge Design Specification, Article 12.6.6.3

HDPE is a viscoelastic material which shows creep behavior. Therefore, the buckling strength of HDPE pipes decreases for long-term service. The AASHTO standard specification for highway bridges (Section 18.2.2. buckling) requires the use of the 50year modulus of elasticity for conservative buckling analysis, instead of the initial modulus of elasticity.

Based on the hoop compression test carried out by Selig et al. [1993], Moore and Laidlaw [1997] evaluated local buckling in the side wall of the corrugation, the valley, and the crown. Local sidewall buckling was characterized by the development of waviness in the element or sidewall. The phenomenon typically commenced at one location, spread, and became more pronounced at higher hoop strains, thus involving most of the pipe circumference. Valley buckling typically featured a lateral torsional response. This was generally at a location, where the sidewall buckling was also present, with possible significant interaction between the two elements of the profile. In his field inspection of pipe, buried under Route I-279 north of Pittsburgh, PA, Selig [1990-1993], observed buckling of the unsupported parts of the liner (between corrugation crests). These buckles were located in the bottom half of the pipe [Selig, 1995]. This is a natural consequence of the ring compression of the wall. In addition, circumferential cracking of inside crests was also observed in the corrugated sections with the area covered by the coupling. It was indicated that this was probably a longitudinal stress problem.

For a pipe tested under hoop compression, a numerical prediction of critical hoop strain was made using a stiffened plate model and with buckling expressed in terms of critical hoop strain [Selig et al., 1993]. Local soil support was found to have an important effect on the edge restraint which influences the buckling strength, Moore and Laidlaw [1997]. It was assumed that the pipe was subjected to uniform radial stress acting around the pipe circumference, due to arching. However, when the arching action is affected by degradation in soil properties, the vertical pressure in the soil above the pipe is greater than the lateral pressure, and an ovaling deformation results. Interactive longitudinal and circumferential bending can cause local wall buckling due to changes in bedding uniformity over a long term, possible poor installation, or ground saturation. Therefore, it is necessary to investigate the buckling strength under combined circumferential and longitudinal bending. The time-dependent buckling strength needs to be correlated with creep and creep-rupture; the effect of possible damage should be considered for the long-term performance of HDPE pipe.

3.5 PERFORMANCE LIMITS

Prior to developing a design procedure, performance limits must be established. The performance limits of buried HDPE pipe are related to stress, strain, deflection, or buckling. The values of these limits depends on the design method used. The following is a list of performance limits that are suggested by the literature for the design of buried, HDPE pipe and culverts [Goddard, 1994]:

i) Deflection: This limit is quite important due to relatively low bending stiffness compared to concrete or metal pipes. Also, the stiffness decreases with time during the service period. Excessive deformation can limit the flow or joint leakage. The limits are set to avoid pipe flattening, reversal of curvature, limit bending stresses, or bending strains. However, deflection of pipes which are flexible in bending is controlled mainly by the method of installation and in-situ soil envelope properties, Fig. 3.5.

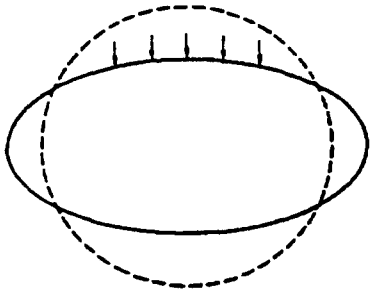

Fig. 3.5 a) Ring deflection in a flexible pipe, [Moser, 1994]

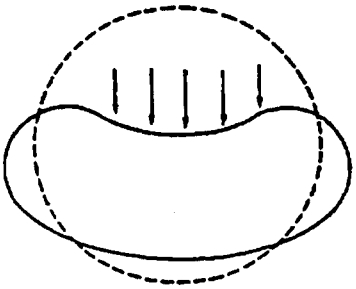

Fig. 3.5 b) Reversal of curvature due to over-deflection [Moser, 1994]

ii) Wall buckling: Insufficient bending stiffness or stiffness of soil envelope can cause wall buckling, Fig. 3.6. Buckling should be considered because it represents pipe cave in. Large diameter pipe design may be governed by buckling, particularly when subjected to high soil pressure in low stiffness soil.

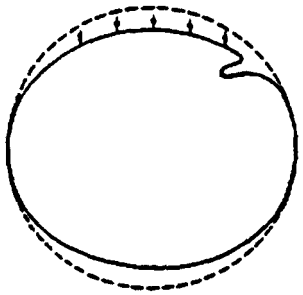

Fig. 3.6 Localized wall buckling [Moser, 1994]

iii) Wall crushing: Wall stress in compression can lead to wall crushing if excessive. If the ring compressive stress exceeds the compressive strength of the wall of the pipe, wall crushing can generally occur at the 3 and 9 o'clock positions on a pipe, Fig 3.7.

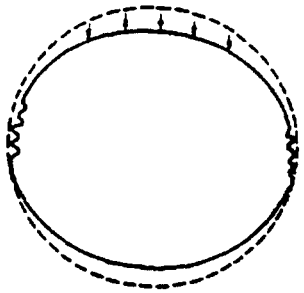

Fig. 3.7 Wall crushing at the 3 and 9 o'clock positions [Moser, 1994]

The situation is generally only of concern for small 0 thinner walled pipes under deep burial. The thrust in the wall is as follows:

$$T = \frac{PD}{2} \quad \text{----------(3.4)}$$

in which

T=thrust (Mmm, lb/in)

P=distributed design load (psi, kPa)

D=diameter of the pipe, (in., mm)

iv) Longitudinal bending: Circumferential cracking indicates failure due to longitudinal tensile stress. Bending action due to inadequate bedding support imposes additional tensile stresses. The inevitable variation of the spring coefficient for bedding, along the pipe length, can cause longitudinal stresses and opening/cracking of the joint or lateral buckling. So the flow inside of the pipe may be limited or leak.

3.6 LIFE PREDICTION

There is an identified need to investigate the long-term behavior in relatively short laboratory time scale, by evaluating the effect of soil degradation mechanisms at field related temperatures and stresses, compounded by synergistic effects, with accelerated testing, high stress, elevated temperatures, and/or aggressive liquids.

It is noteworthy that the type of material qualification testing, used for natural gas distribution piping has very effectively screened out one failure mode; ductile failure. This has been done by testing of pressurized pipe at temperatures and pressures, that are well above the expected operating conditions. Because of the strong time and temperature dependence of polyethylene and other thermoplastic materials, it is both possible and necessary to accelerate the failure mechanism. The key is the use of time-temperature shifting functions that can reliably connect high temperature/high pressure performance to actual service conditions.

The long-term properties can be predicted based on viscoelastic behavior: i) the time-temperature (WLF) superposition [Aklonis and Macknight,1983], which describes the equivalence of time and temperature, ii) the Arrhenius equation [Koerner, 1994], which describes the temperature dependency of the degradation reaction on time and temperature iii) the rate process method, describing which curve fits time-to-failure test data at elevated temperatures to enable predictions of times-to-failure at lower temperatures [Popelar, 1993].

3.6.1 WLF METHOD

Based on the time-temperature (WLF) superposition principle, for each of the three load levels, creep curves are plotted for different temperatures, and superposed by horizontal shifts along a logarithmic time scale to give a single curve covering a large range of times, termed a master curve. The shift factor, $a_{T'}$, is a function of the temperature and described as follows:

$$\log a_{T'} = [-C_1 \times (T-T_r)] / [C_2 + (T-T_r)] \quad \text{----------(3.5)}$$

where

$a_{T'}$ = shift factor

C_1 and C_2 = universal constants, which vary from polymer to polymer

T_r = reference temperature.

Vertical temperature shifting is necessary to accommodate the change of the degree of crystallinity with the temperature for the HDPE pipe specimens, which are made of semicrystalline polymeric material [Tobolsky,1960]. The vertical shift factor, b_T, can be defined as follows [Miyano, 1996]:

$$b_T(T) = \frac{E(t,T)}{E(t,T_r)} \quad \text{----------(6.8)}$$

The extended time-scale master curve enables the determination of the long term mechanical properties and service life, Fig. 3.8 [Aklonis and MacKnight, 1983]. Fig. 3.9 shows the three master curves (modulus-time curves at three different stress levels) obtained by time shifting. The extrapolation equation for any other loading condition will be determined, similar to the procedure used for the Hydrostatic Design Basis (HDB) test described in the ASTM Standard D2837.

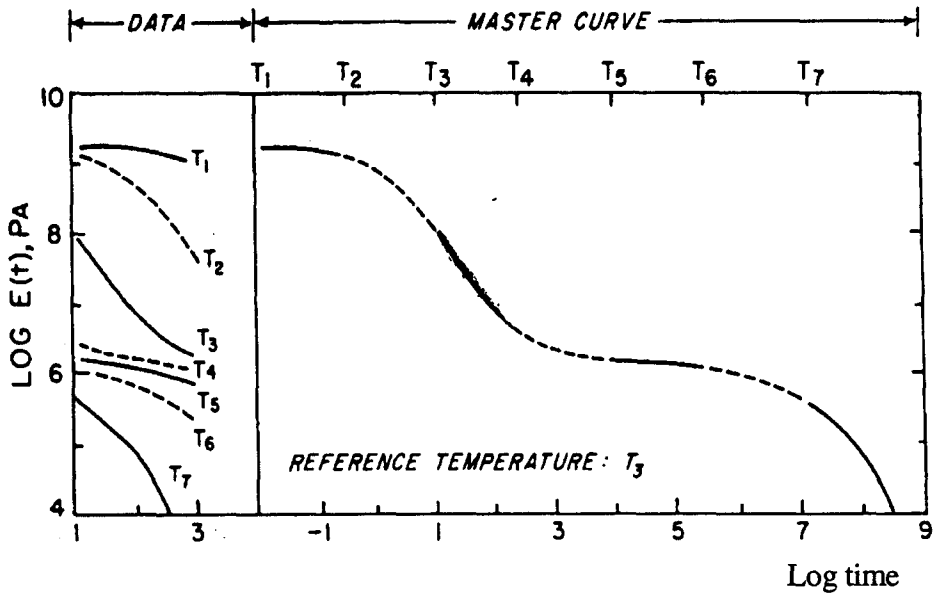

Fig. 3.8 Master curve from experimentally measured modulus-time curves at various temperatures [Aklonis and MacKnight, 1983]

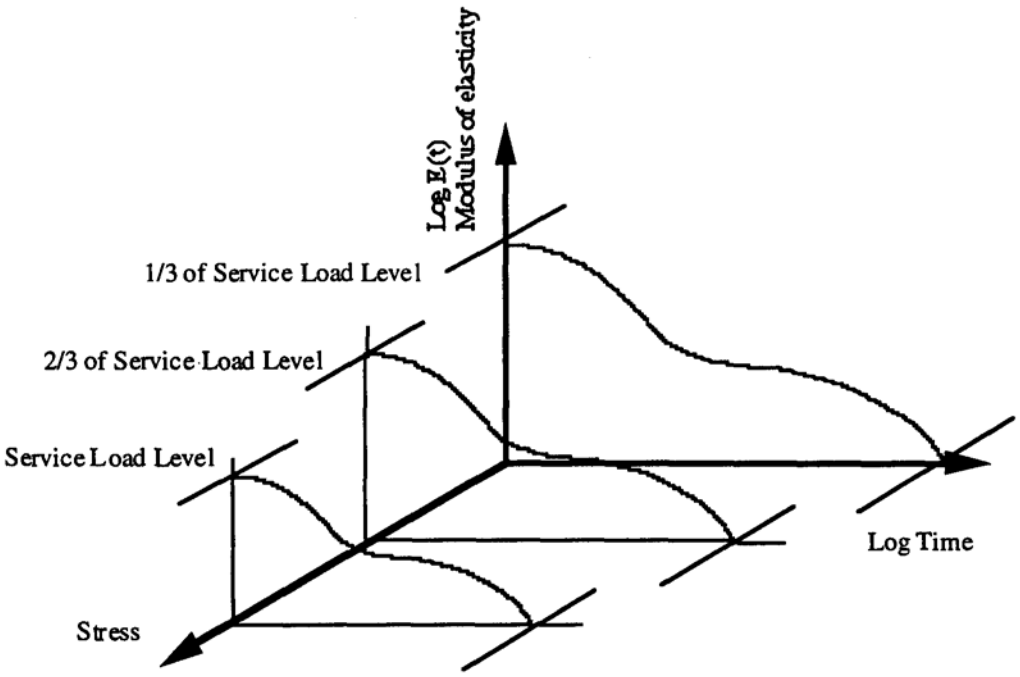

Fig. 3.9 Master curves at different load levels

3.6.2 ARRHENIUS EQUATION

A considerable amount of data shows that the rate of most chemical reactions have a strong dependence on the temperature and the concentration of reagents involved. In fact, such dependence can be used advantageously to develop relationships which can be used for extrapolation purposes. A common form of this important extrapolation tool is as follows:

$$\ln (t/t_o)=(E_{act}/R)(1/T - 1/T_o) \quad \text{----------(3.6)}$$

where

t=time to given strength loss, usually 50%, at the test conditions

T=temperature of the test environment, in ^oK

t_o=time to the same given strength loss as for t, but in the in-situ environment

T_o=temperature of the in-situ environment, in ^oK

R=universal gas constant, which is 8.314 J/mole

E_{act}=effective activation energy, J/mole

In the Arrhenius plot, degradation is plotted as the logarithm of the reciprocal of time versus the reciprocal of temperature using Equation 3.6. A schematic plot is presented in Fig. 3.10. It is noted that the temperature has an exponential effect on the time required for a specified level of degradation based on this model, and the data used in Equation 3.6 is obtained at a constant level of degradation (indicated by the modulus decay) in the material. The extrapolation for failure time is similar to that used in the WLF Method. The WLF method and Arrhenius equation-based analysis are accurate for amorphous polymers, but catastrophic failure that occurs at ductile-brittle transition make the prediction difficult for semi-crystalline polymers. This problem should be addressed, and the life predictions given by the two methods compared, and their equivalence studied using the procedure developed by Miyano [1996].

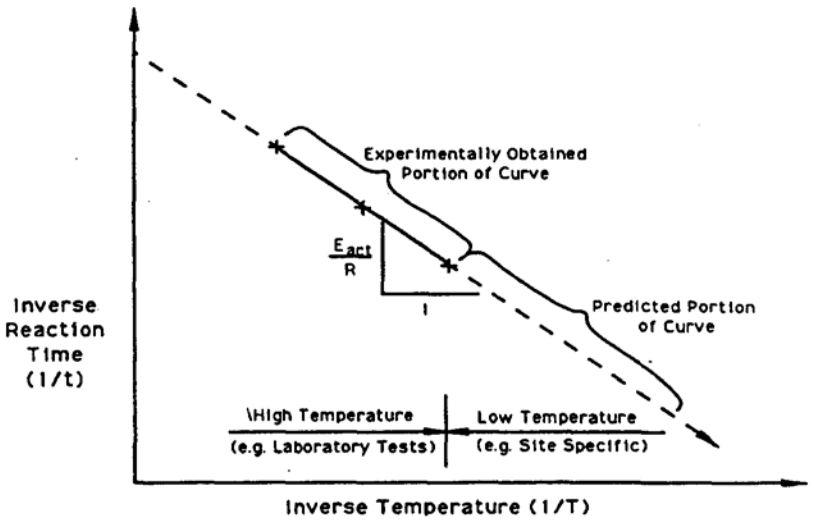

Fig. 3. 10 Generalized Arrhenius plot, for a specified stress level, used for life prediction from super-ambient temperature experimental data [Koerner, 1992]

3.6.3 RATE PROCESS METHOD (RPM)

The conventional time-temperature shifting procedure for pressurized pipe is the rate process method (RPM) which, in essence, curve fits time-to-failure test data at two elevated temperatures to enable predictions of times-to-failure at lower temperatures. The time to failure for thermoplastic pipe depends upon the operating temperature and the induced stress. The RPM has been used by the gas industry to extrapolate design parameters at the operating temperature from elevated temperature, sustained hydrostatic pressure tests of pipes [Poplelar, 1993] and [Koerner, 1994]. RPM, that has evolved from analyzing numerous test data, assumes that the time to failure is governed by an Arrhenius

relation, wherein the activation energy varies linearly with the logarithm of stress [Poplelar, 1993] and [Koerner, 1994].

The RPM equation for the time to failure, t_f, at the absolute temperature, T, and hoop stress, 6, is expressed as follows:

$$\log t_f = A + (B/T) + (C/T)\log\sigma \quad \text{(3.7)}$$

An implication of Equation 3.7 is that the data plots as a straight line in the $\log t_f$-logo plane. The coefficients A, B, and C are determined through a least square fit of Equation 3.5 to the data. The fitting of Equation 3.7 requires that the time-to-failure data be available for a minimum of two temperatures.

CHAPTER 4

EXPERIMENTAL PROCEDURE

4.1 MATERIALS AND SPECIMEN CONFIGURATION

Two types of corrugated HDPE pipe specimens of nominal inside diameters 12 and 24 in. (305 and 610 mm) were considered. Both types had the same cell classification, i.e. 335420C with density = 33.97-34.48 lb/in^3 (0.941-0.955 g/cm^3), melt index = 0.4-0.15, flexural modulus = 110,000-160,000 psi (758-1,103 MPa), tensile strength at yield = 80,000-110,000 psi (552-758 MPa), and Color and UV stabilizer = black with 2% minimum carbon black, referred to Table 3.1. There were small geometrical property differences between the two types, Table 4.1 and Fig. 4.1.

Table 4.1 Specimen Geometries and Section Properties

Types of specimens, nominal diameter	Type I 12 in. (305 mm)	Type I 24 in. (610 mm)	Type II 12 in. (305 mm)	Type II 24 in. (610 mm)
Wall thickness	0.275 (7)	0.55 (14)	0.275 (7)	0.55 (14)
Inside diameter, "ID", in. (mm)	12 (305)	24.08 (612)	12 (305)	24 (610)
Outside diameter, "OD", in. (mm)	14.2 (361)	27.80 (719)	14.2 (361)	28.40 (721)
Section area, "A", in^2/in, (mm^2/mm)	0.188 (4.78)	0.338 (8.59)	0.198 (5.03)	0.308 (7.82)
Moment of inertia, "I", $in.^4/in.$, (mm^4/mm)	0.041 (26.45)	0.231 (149)	0.0319 (20.58)	0.1838 (118.6)
Pipe stiffness, "PS", psi (kN/m^2)	50 (340)	34 (240)	50 (340)	34 (240)
Distance from inside surface to neutral axis, "C", in. (mm)	0.53 (13.5)	1.07 (27.2)	0.436 (11.1)	0.8574 (21.8)

4.2 ENVIRONMENTAL STRESS CRACKING RESISTANCE TESTING (ESCR)

The ESCR tank was designed and fabricated, taking into account the possible hazard from IGEPAL CO-630, a trade name for nonylphenoxy poly (ethyleneoxy) ethanol solution. The specimens, 90^0 arc length, were bent in a loading jig to shorten the inside chord length 20%, AASHTO M294-93, Standard Section 9.4,. Figs 4.2, 4.3 and 4.4 show the specimens and the loading jig. They were then exposed at an elevated temperature of 122^0F (50^0C) to IGEPAL, for 24 hours, Figs 4.5 and 4.6 After 24 hours of exposure, all the specimens were removed and inspected by petrographic examination (using a 5-20x microscope). The changes of chord length, after unloading, were measured for IGEPAL-exposed and air-exposed (room temperature) specimens to determine the relative degree of deformation.

Specimen Details. (Table 4.2)

Type: I and II

Cell Classification: 335420C

Corrugation Design: Annular

Size: 1/4 of 12 in.(304.8 mm) inside diameter 4 in. (152.4 mm) length.

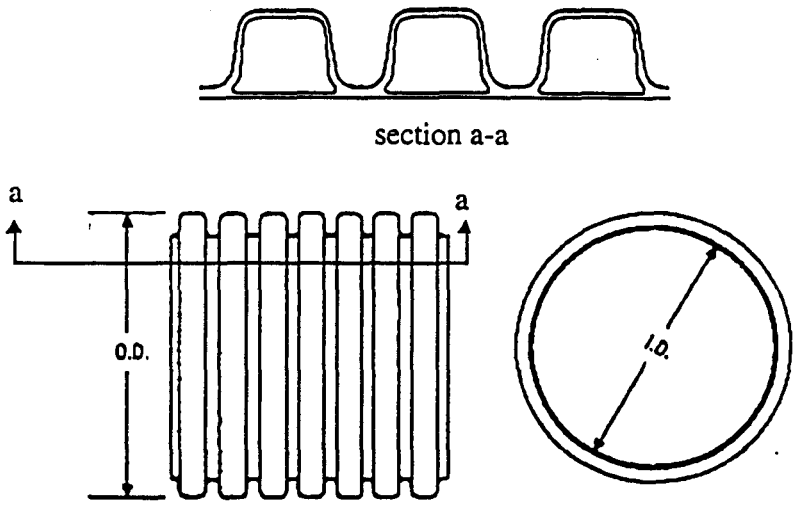

Fig. 4.1 Specimen geometry

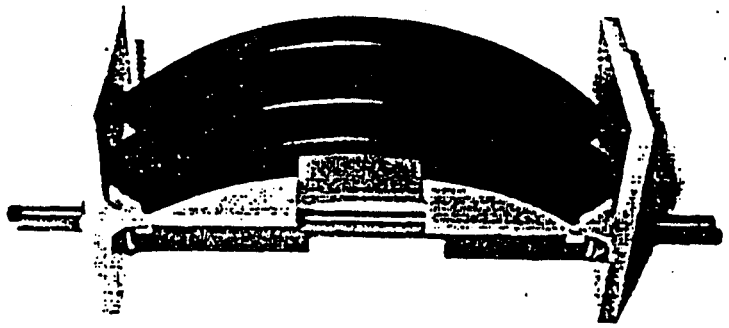

Fig. 4.2 Specimen 90° arc length for ESCR testing

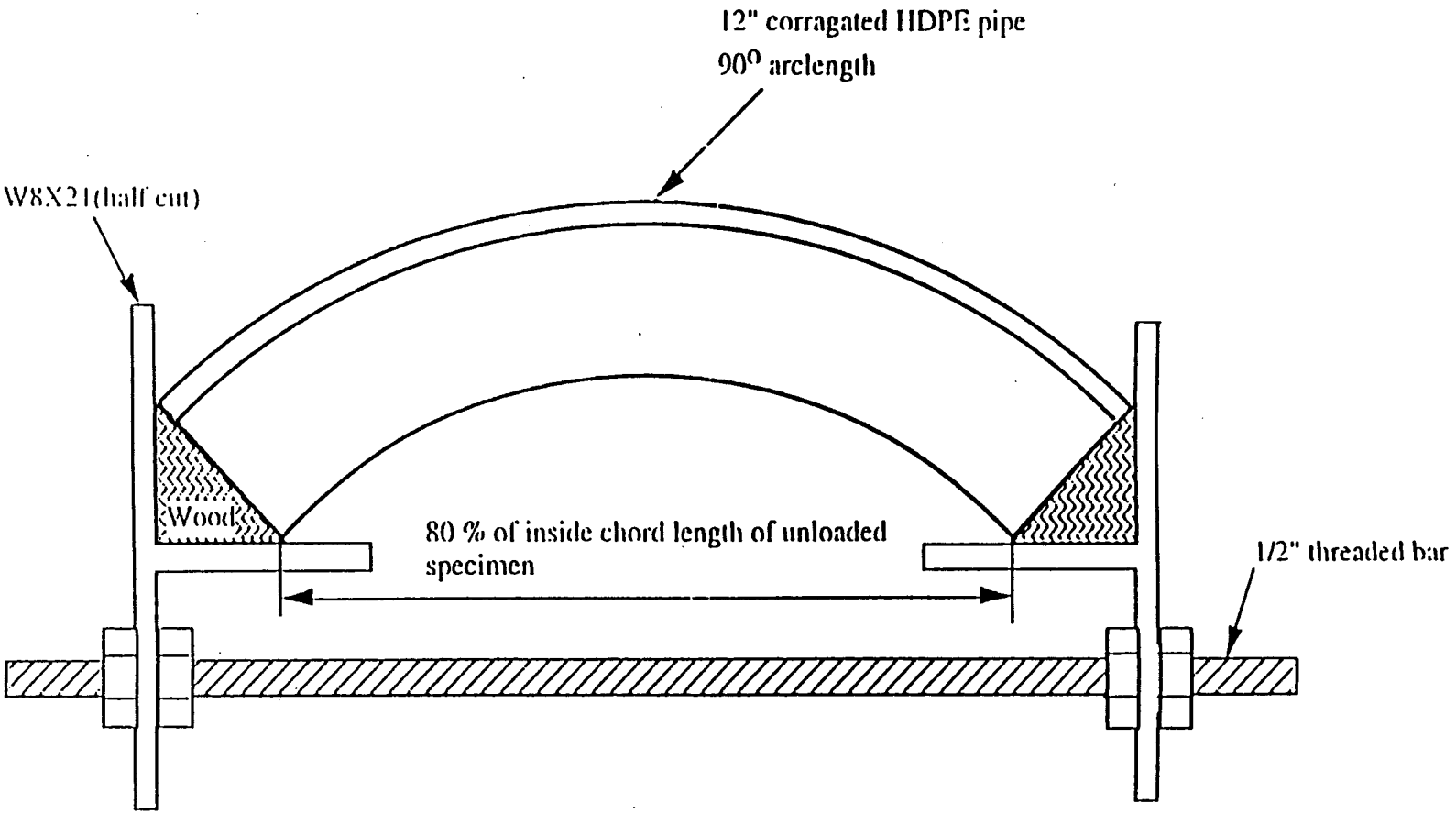

Fig. 4.3 Schematic of ESCR test setup

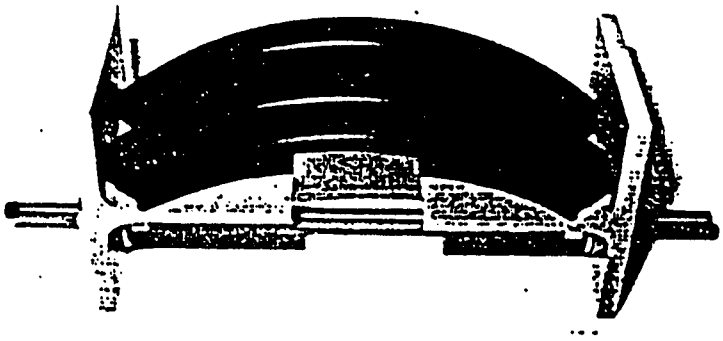

Fig. 4.4 ESCR specimen in a loading jig

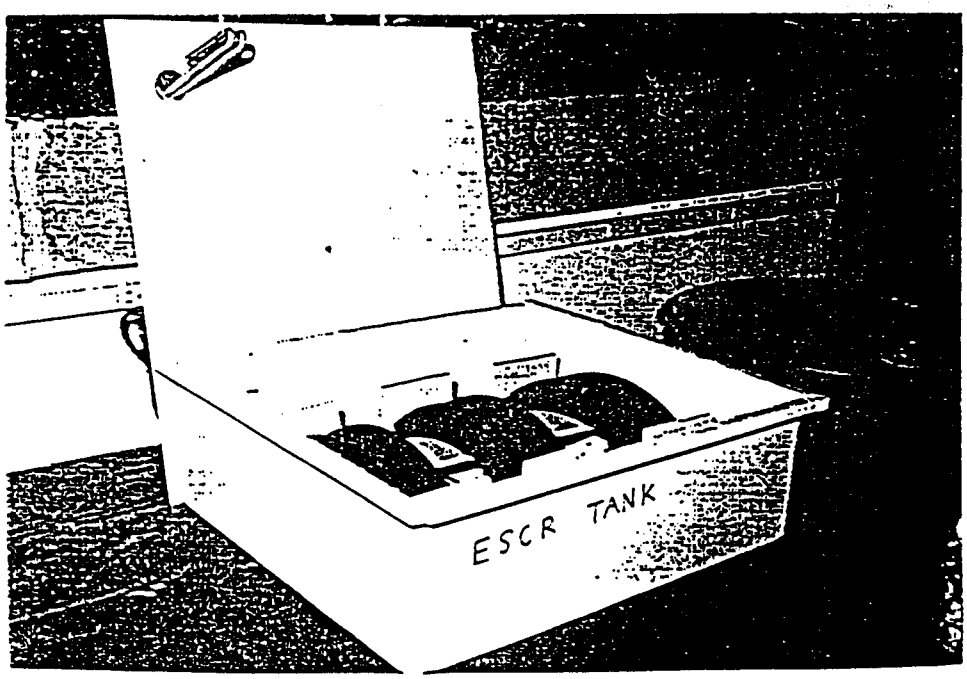

Fig. 4.5 Arrangement of the specimens in the IGEPAL tank

Table 4.2 Number of ESCR Specimens

Exposure Conditions	Number of Type I specimens	Number of Type II specimens
Shorten the inside chord length 20% in 100% IGEPAL, 122 ^{o}F (50 ^{o}C)	3	3
Air, Room Temperature 70 ^{o}F (21 ^{o}C)	3	3

Total number of specimens = 12

4.3 RING BENDING TEST BY PARALLEL PLATE LOADING

The ring bending tests, using the modified ASTM D 2412-92 Standard Test Method for Determination of External Loading Characteristics of Plastic Pipe by Parallel-Plate Loading, were carried out to determine the viscoelastic mechanical properties of HDPE pipe prior to creep test. The properties, evaluated from the test results, enable the determination of the applied load level for the creep test.

A properly calibrated compression testing machine of the constant-rate-of-head movement type, was used for the specimens exposed to ambient temperature, Fig. 4.7.

The rate of head approach was 0.5±0.02 in. (12.5±0.5 mm)/min. The specimens, exposed to super ambient temperature levels 95, 122, 126, and 140 OF (35, 50, 52, and 60 °C), were tested in the creep test tanks by increasing the deadweight with the rate of the loading, 0.5±0.02 in. (12.5±0.5 mm) /min., Fig. 4.8. The vertical deflection was measured with dial gages accurate to the nearest 0.001 in. (0.0254 mm). Specimen details are shown in Table 4.3.

4.4 CREEP

Short lengths of pipes, 12 in. (305 mm) diameter and 6 in. (152 mm) long, subjected to five different temperatures, 68, 95, 122, 126, and 140 OF (20, 35, 50, 52, and 60 ºC), were loaded between two rigid parallel flat plates with constant loading to evaluate the time-temperature-dependent behavior of HDPE pipe, Fig. 4.9. Vertical changes of diameter were periodically measured by dial gages, accurate to the nearest 0.001 in. (0.0254 mm). The magnitude of the constant loading was based on Eqn. (4.1).

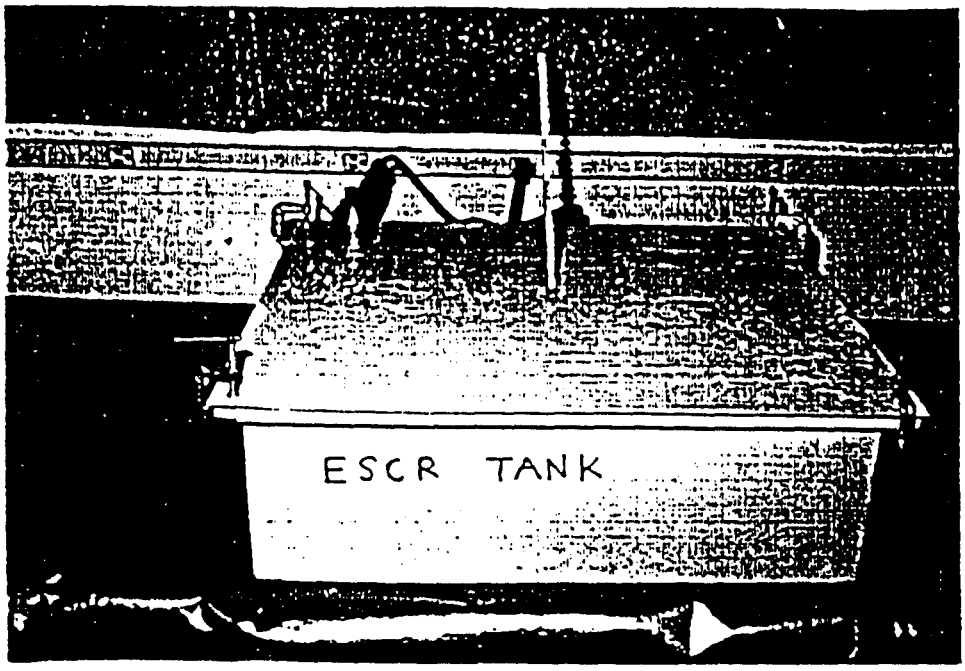

Fig. 4 6 ESCR testing setup

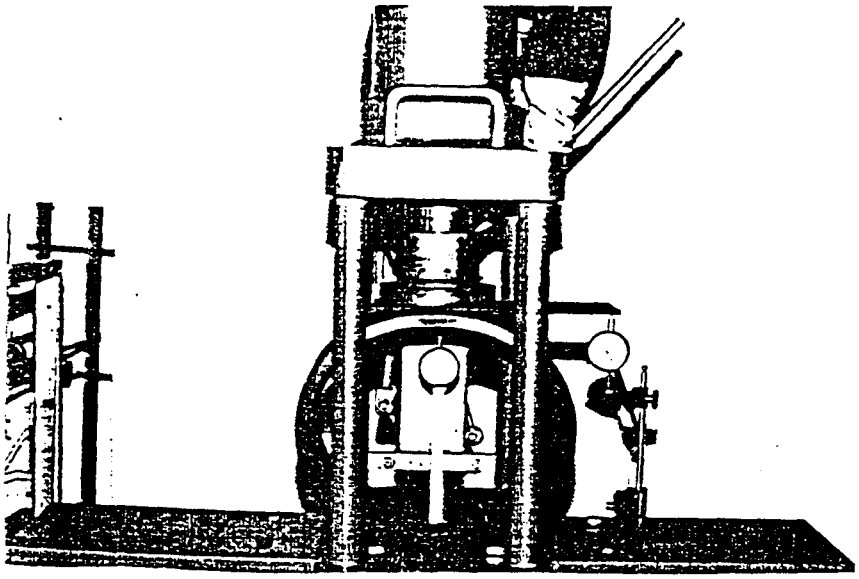

Fig. 4.7 Parallel plate loading at ambient temperature

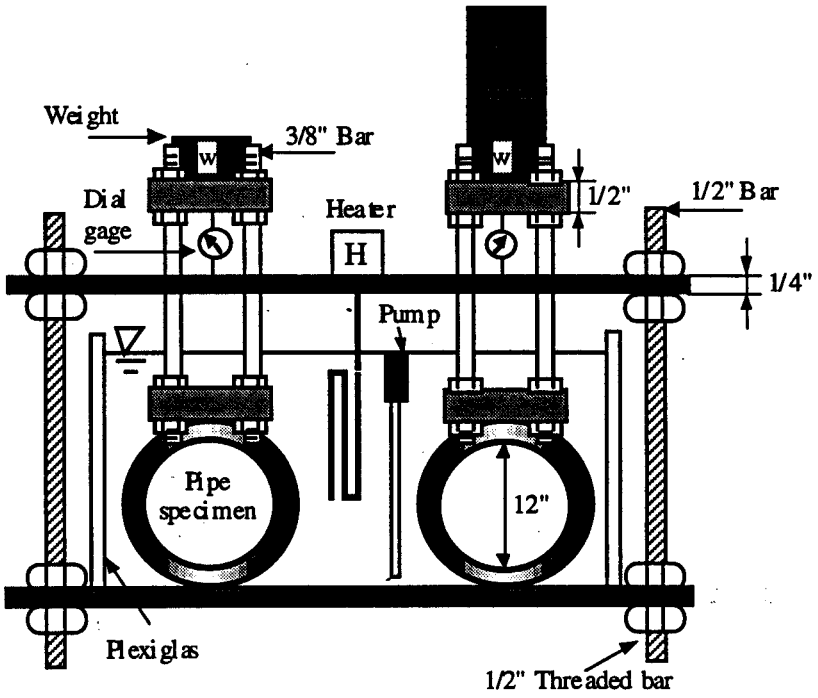

Fig. 4.8 Parallel plate loading at super ambient temperature

Table 4.3 Details of Specimens for the Ring Bending Test

Manufacturor	Type I and II
Cell classification	335420C
Dimension	12 in.(305 mm) inside diameter x 6 in.(152) long
Temperature	20, 35 , 50, and 60 degree of Celcius
Legend: 1st Character: I for Type I and II for Type II 2nd Character: 20, 35, 50, and 60 for each temperature levels	
Combinations: I20, I35, I50, I60 II20, II35, II50, II60	
Number of combinations : 8 Number of specimens per combinations: 3	
Total number of specimens: 24	

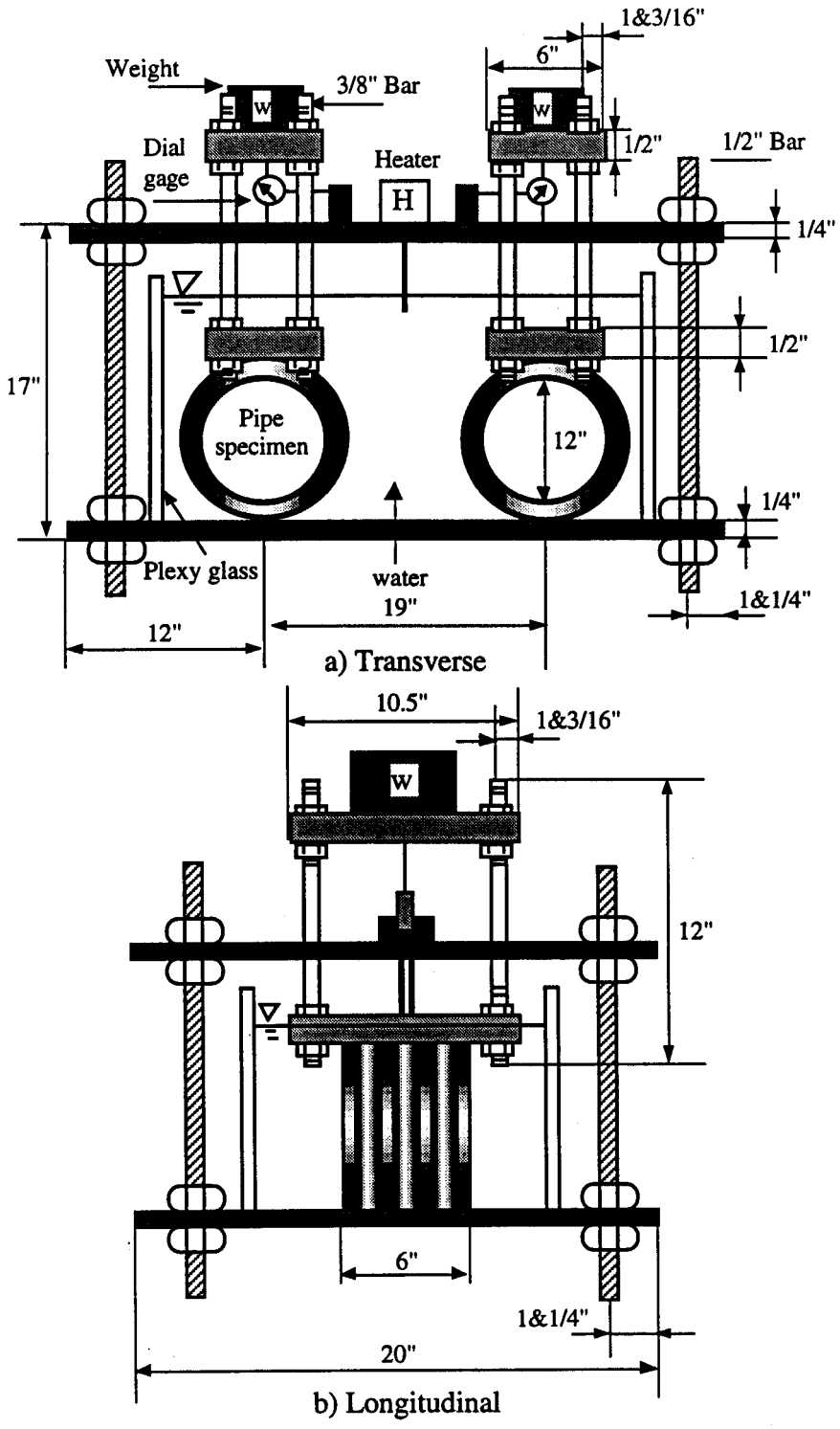

Fig. 4.9 Schematic of creep test setup

With the applied load (simulated service load) levels of 321b/in. (0.57 kg/mm) for type I specimens, and 26.5 lb/in. (0.47 kg/mm) for type II specimens, that cause the initial 2.5% of the change of inside diameter for the given pipe stiffness, [Eqn. (4.1)]. The load levels differ due to small geometrical differences between the two specimens. Figs. 4.10 and 4.11 show the arrangement of the test setups.

$$EI=0.149\ Pr^3/\Delta y \quad \text{----------(4.1)}$$

where

E=flexural modulus, psi (MPa)

I=moment of inertia, $in^4/in.$ (mm^4/mm)

F=applied load, lb, (N)

P=actual load applied=F/SF

SF=safety factor, 2

r=mean radius, in (mm)

Δy=vertical deflection, in. (mm)

Specimen Details. (Table 4.4)

Types: I and II

Cell Classification: 335420C

Corrugation Design: Annular

Size: 12 in.(304.8 mm) inside diameter 6 in. (152.4 mm) length

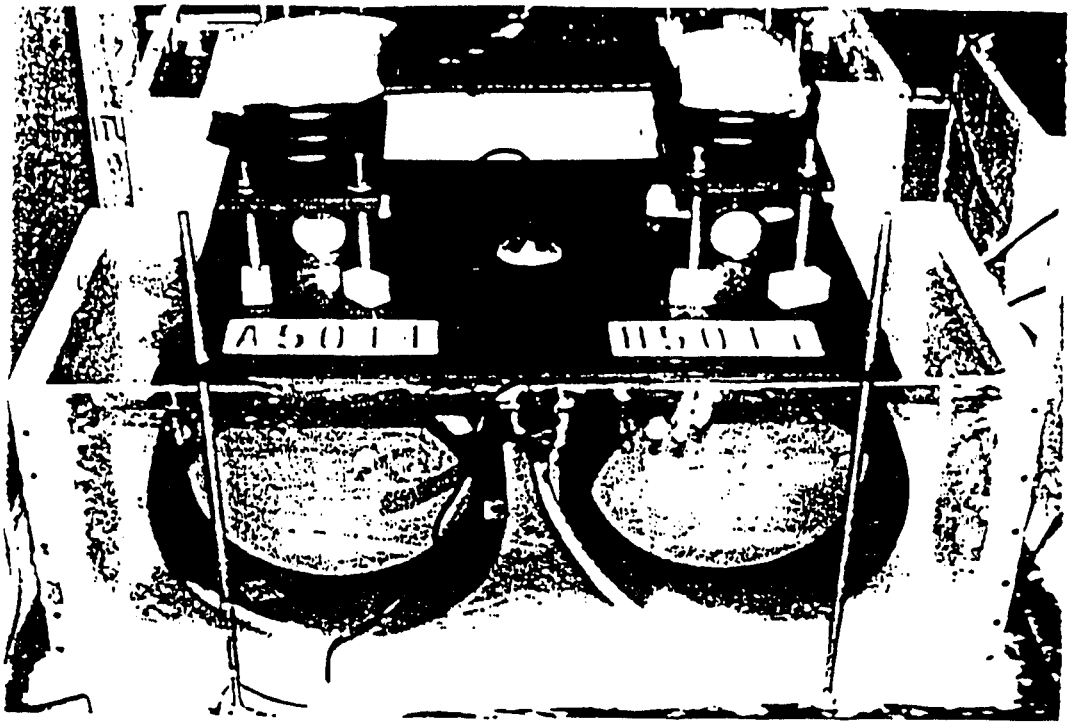

Fig. 4 10 Creep test at constant temperature, 60 °C

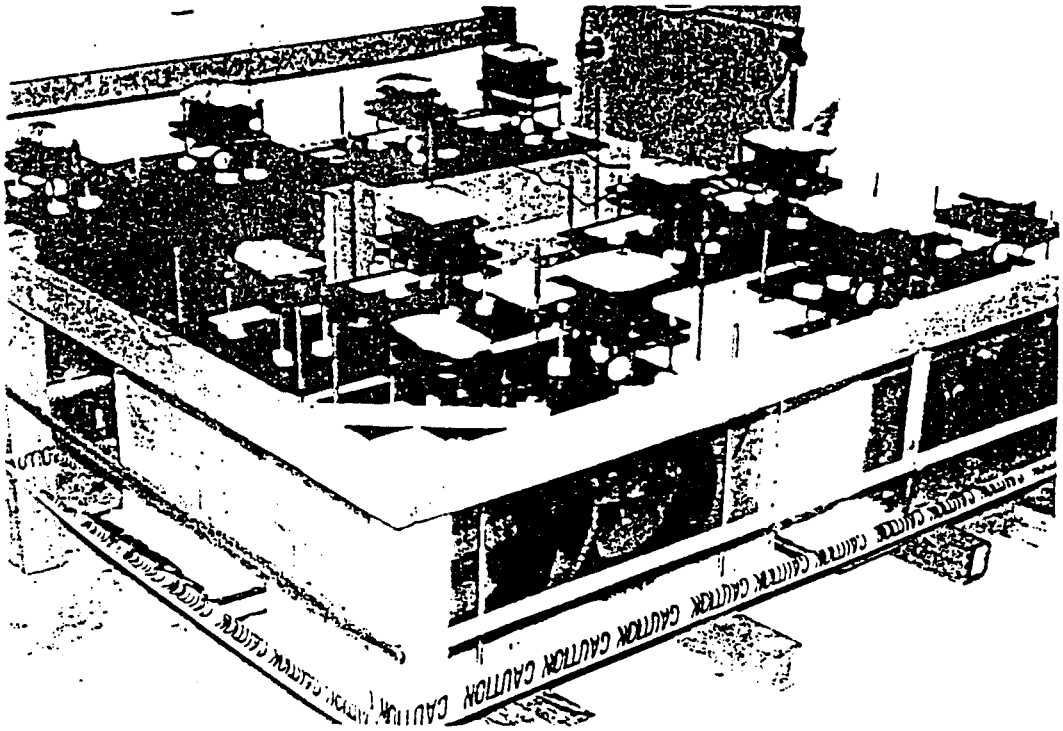

Fig. 4.11 Arrangements of creep test setups

Table 4.4 Creep Specimens

Exposure Conditions	Number of Type I specimens	Number of Type II specimens
68 ºf (20 ^{0} C), 10,000 hours	3	3
95 ºf (35 ^{0}C), 10,000 hours	3	3
122 °f (50 ^{0} C), 10,000 hours	3	3
126 ºf (52 ^{0} C), 100 hours	2	2
140 °F (60 ^{0} C), 1,000 hours	2	2

Total number of specimens = 22

4.5 PERFORMANCE OF BURIED PIPE, SUBJECTED TO LIVE LOAD

Buried pipes are subjected to earth pressure and traffic load, that induce hoop compression, ring bending, and longitudinal stresses. No standard laboratory test exists for the performance of buried pipe in hoop compression and longitudinal bending, and the few laboratory investigations for soil-pipe interacting systems address only a restricted number of parameters. Therefore, a laboratory test setup was developed, for a more comprehensive investigation of the failure modes of the HDPE pipe, with realistically simulated soil cover. Since most states use HDPE culverts across roads (Amarasiri et al. [1999]), the loading was simulated by uniform distribution over the pipe.

4.5.1 FABRICATION OF SOIL CHAMBER, LOADING PLATE AND TEST FRAME

The test setup, including the frame, loading plate, and soil chamber was designed and fabricated in Florida Atlantic University's Structural Laboratory. The dimensions of

the frame and chamber were determined based on the standard size of the backfill (ASTM D2321 and FDOT Roadway and Traffic Design Standards Section 205). The maximum capacities were 400 kips (1,780 kN) for the test frame and loading plate, and 116 psi (800 kPa) for the soil chamber. The cover was equal to one pipe diameter, which is considerably more than the minimum 1 ft. required by CPPA [96]. This is also in conformance with the cover used by the sizable number of State DOTS, Amarasiri et al. [1999]. The soil was South Florida clean sand, SW, with more than 85% Standard Protor Compaction. A three-dimensional structural analysis program, 3D MULTI FRAME, was used for the design of the test setup. The design criteria were as follows: the maximum deflection due to point load should not exceed the member length, divided by 1,000 for the frame and loading plate. ii) the maximum deflection due to hydrostatic pressure should not exceed half the tank wall thickness. Arc welding and fastener jointing were used for the fabrication with plates, angles, I beams, and channels. Details of the test setup design and fabrication are shown in Figs 4.12 to 4.18.

4.5.2. INSTALLATION OF LOADING AND MEASURING DEVICES

Two hydraulic jacks (maximum capacity=100 tons) were installed on the loading plate to load the top of the backfill, Figs. 4. 12 and 13. Eight dial gages were mounted on guide rail to measure vertical and horizontal changes of inside diameter at mid-section, L (span)/4, and 3L/4. Figs. 4.19 and 4.20 show pilot testing of the dial gage installation on the guide rail and locations of measurement.

A number of uniaxial, foil type, and encapsulated strain gages were affixed circumferentially and longitudinally to the internal wall of the pipe at both single and twin-wall locations at mid-section of the pipe. Circumferential and longitudinal strains, on both

single and twin-wall locations were measured by channel switches and digital indicators. Figs 4.19, 4.20, 4.21, and 4.22 show the locations of the strain gages and the setup for deflection/strain measurement devices in the pipe.

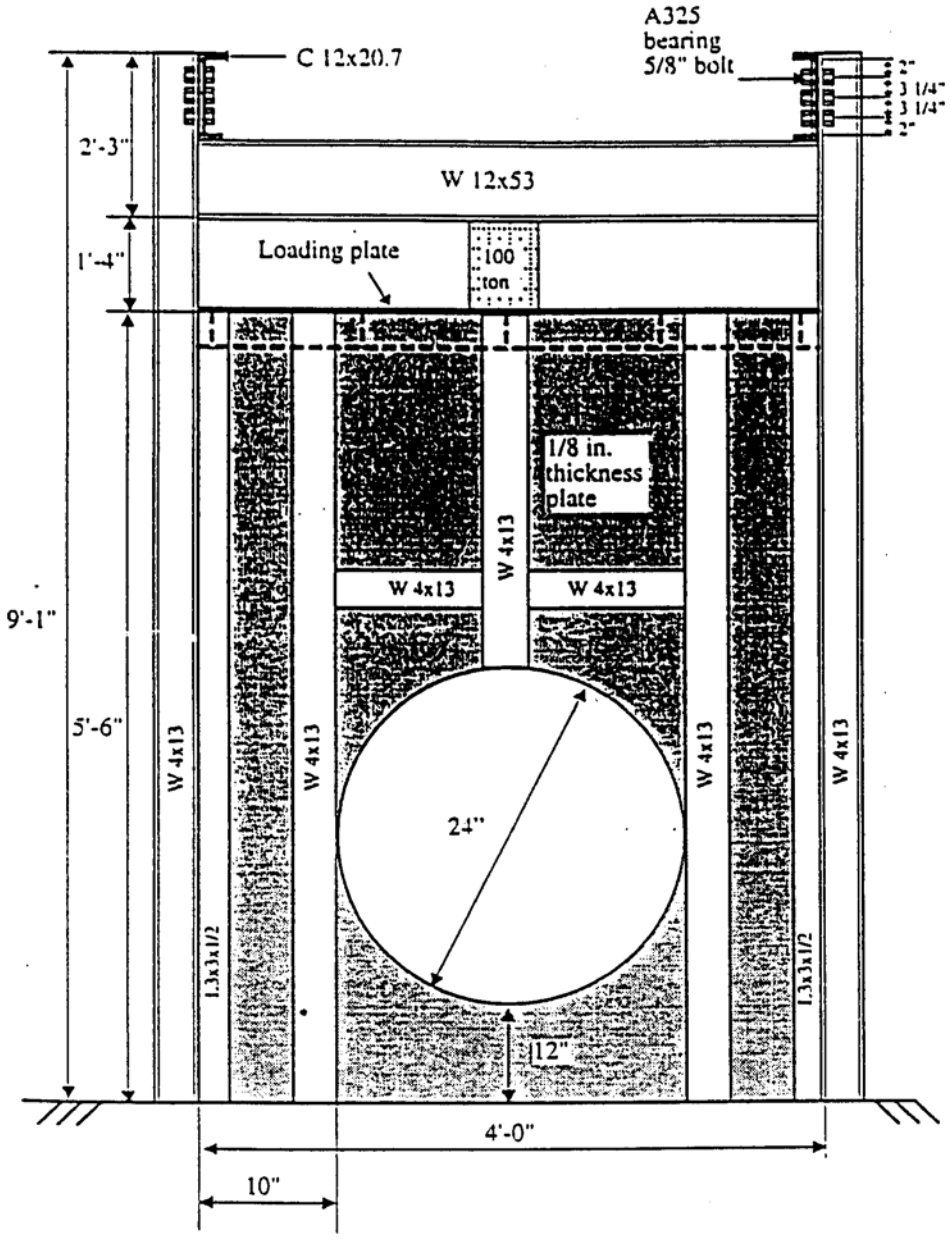

Fig. 4.12 Schematic of the soil chamber and test frame (transverse view of front)

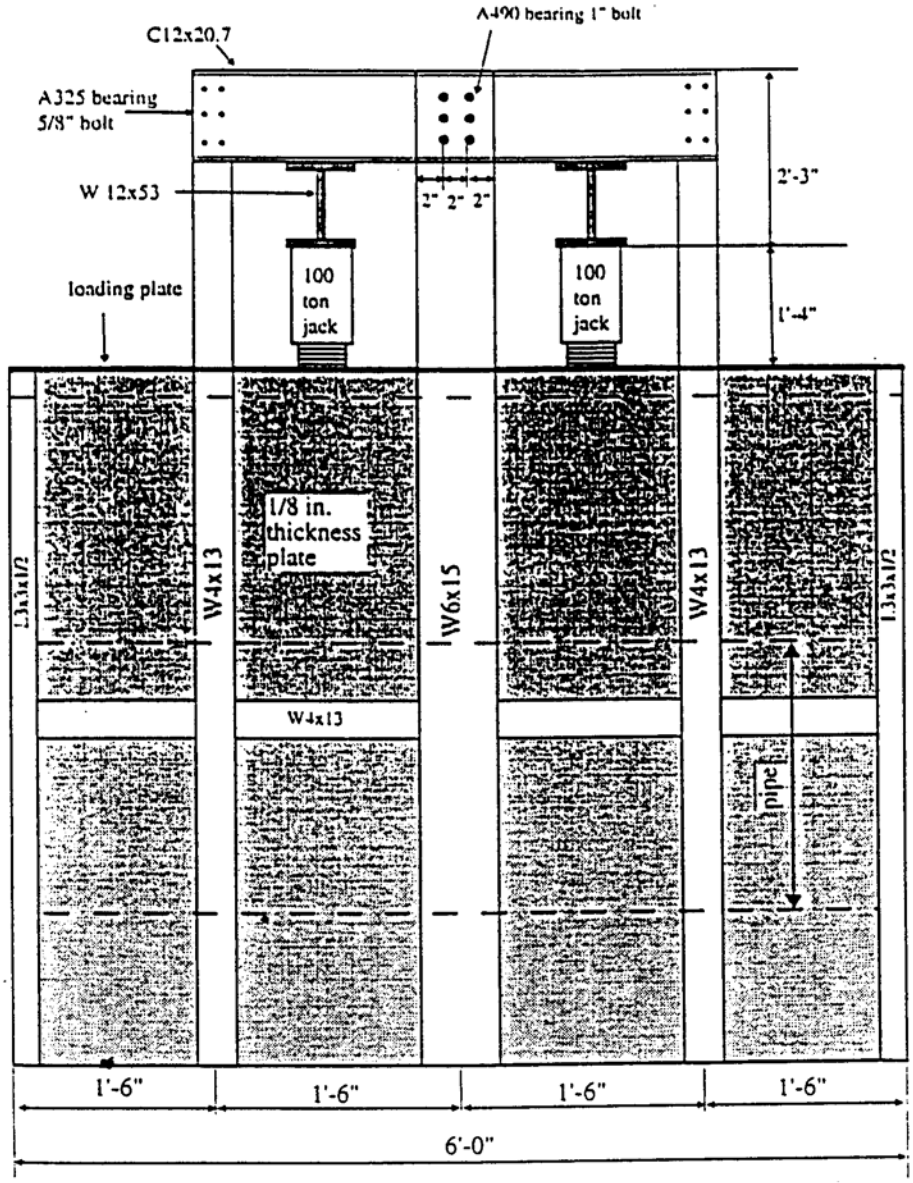

Fig. 4.13 Schematic of the soil chamber and test frame (longitudinal view)

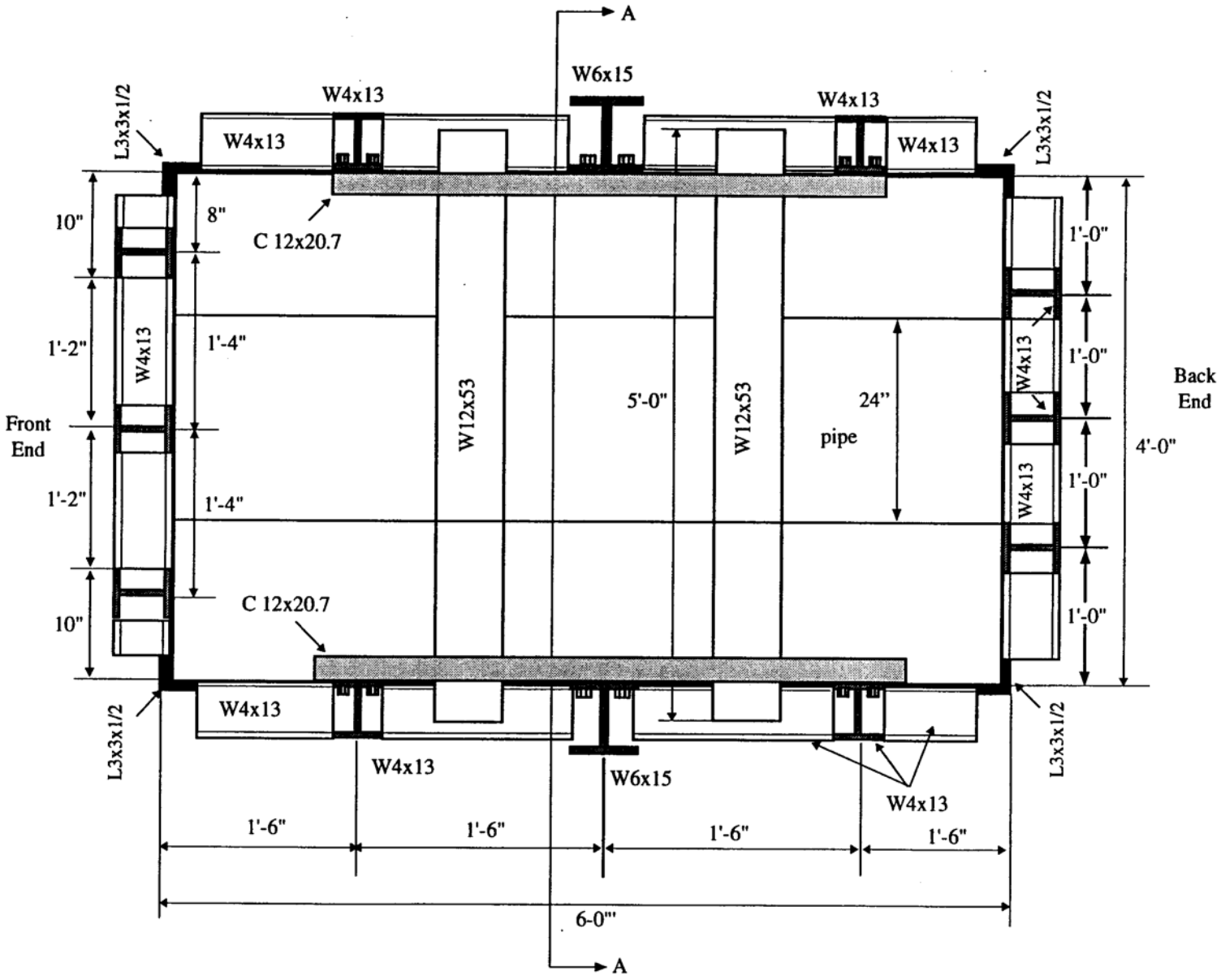

Fig. 4.14 Schematic of the soil chamber and test frame (plan)

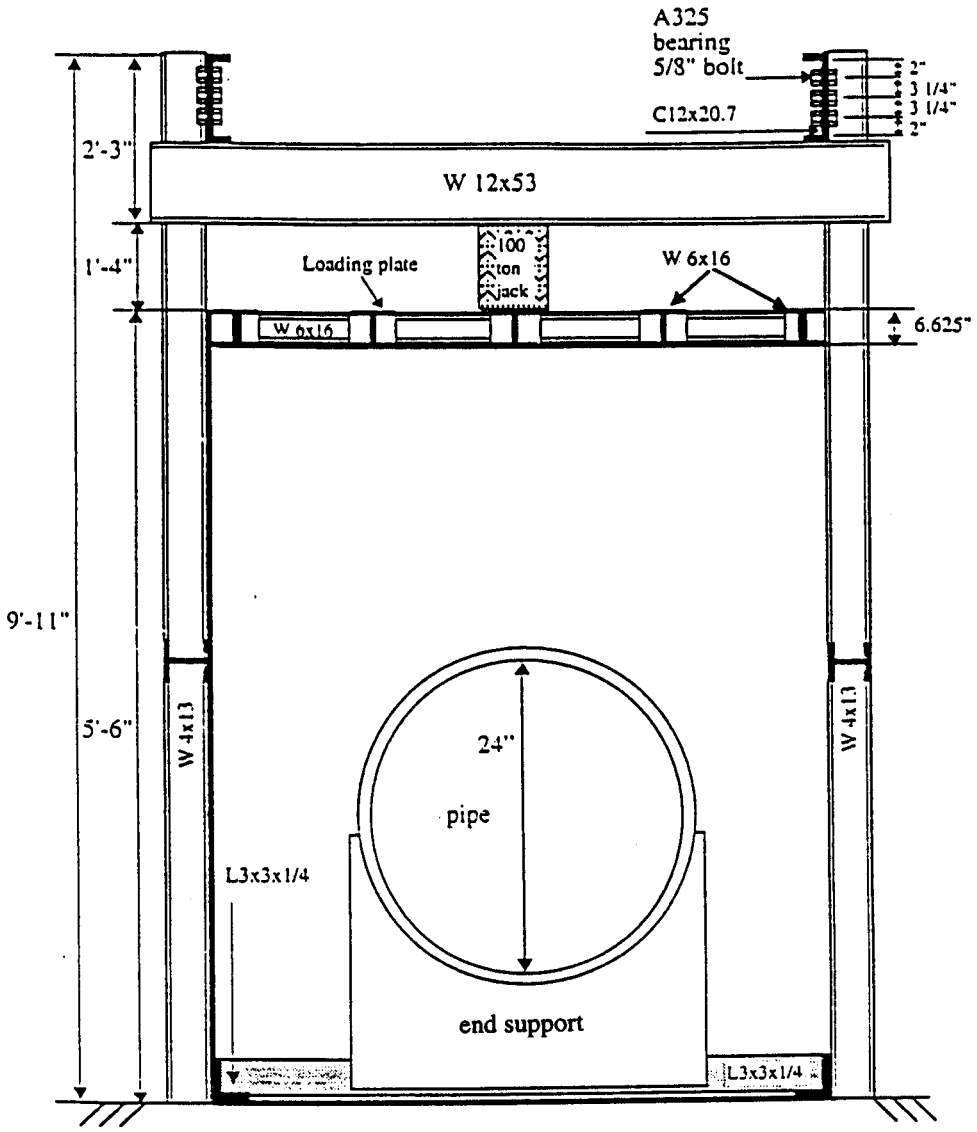

Fig. 4.15 Schematic of the soil chamber and test frame (cross section A-A)

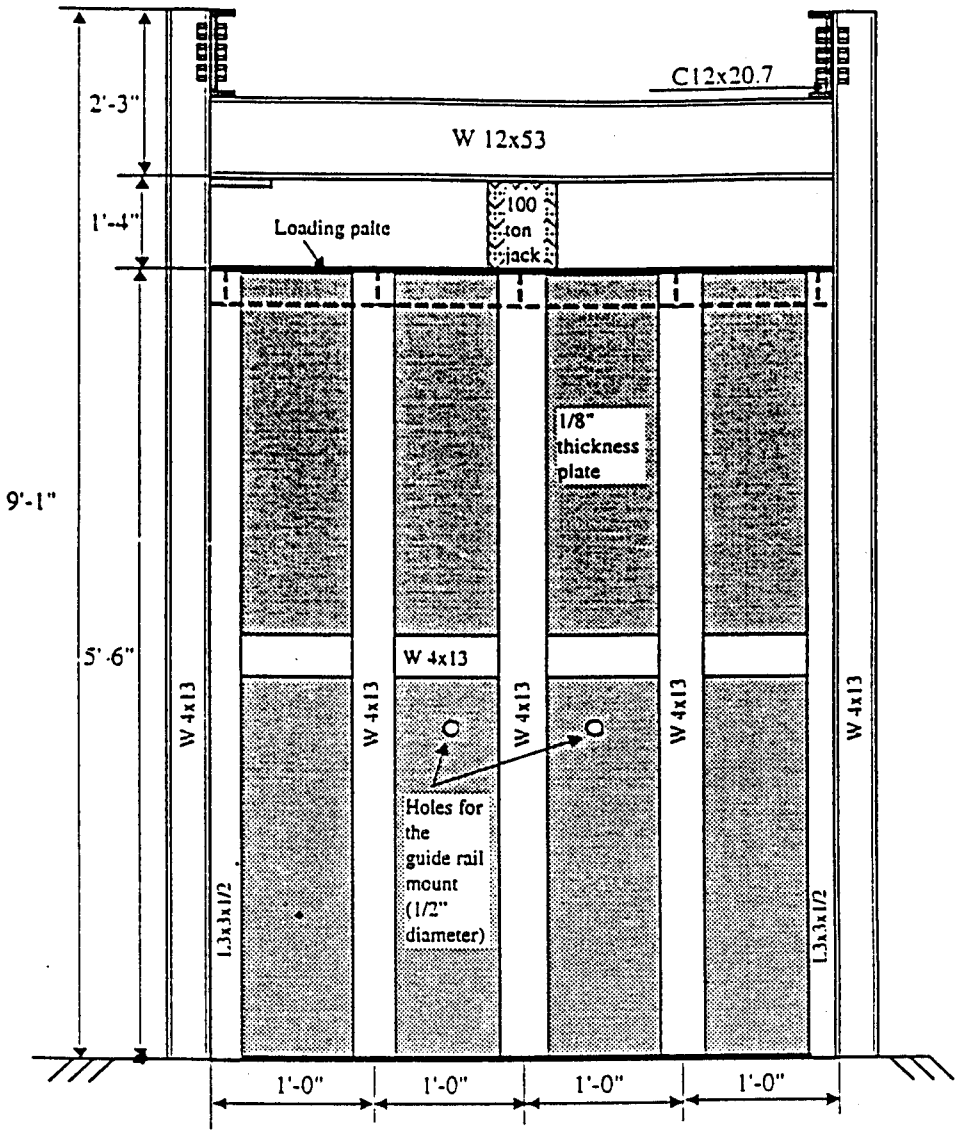

Fig. 4.16 Schematic of the soil chamber and test frame (transverse view of back)

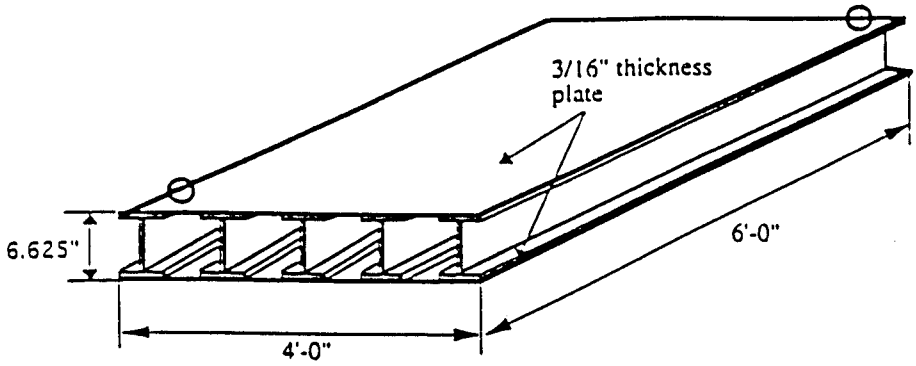

a) Schematic of the loading plate

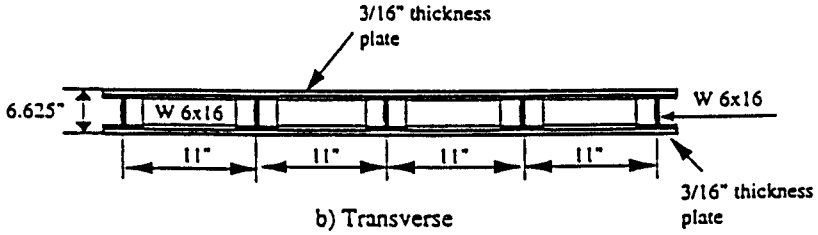

b) Transverse

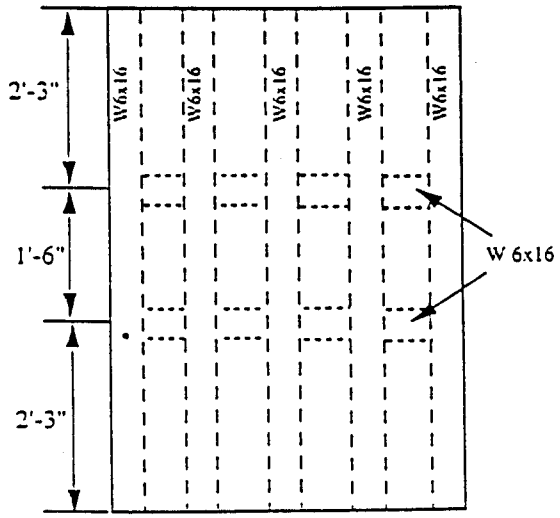

c) Plan

Fig. 4.17 Details of the loading plate

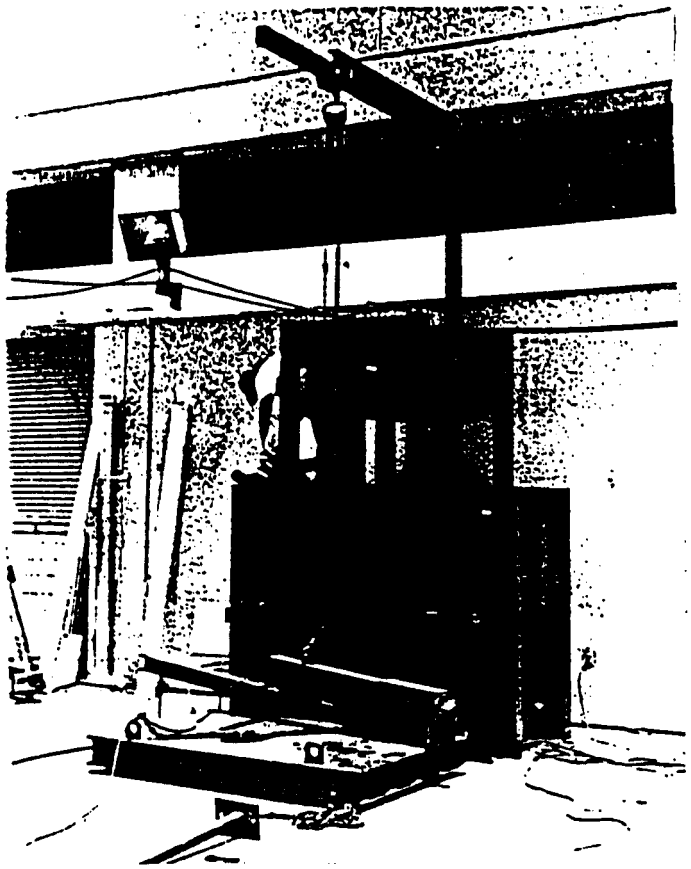

Fig. 4.18 Fabrication of the test frame and soil chamber

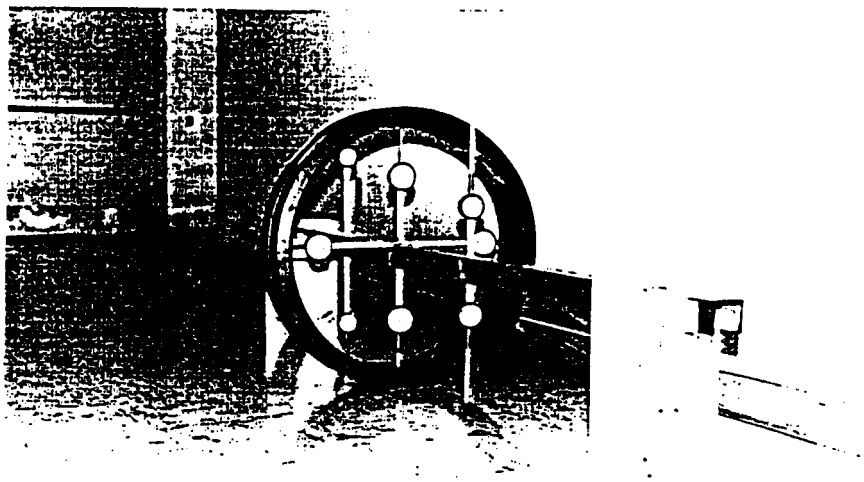

Fig. 4.19 Installation of dial gages on guide rail

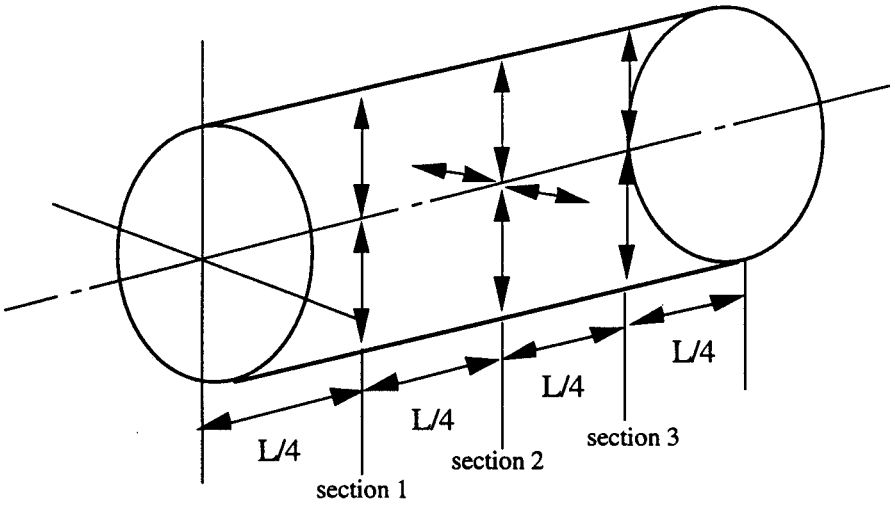

Fig. 4.20 Locations for measurement of diametral changes

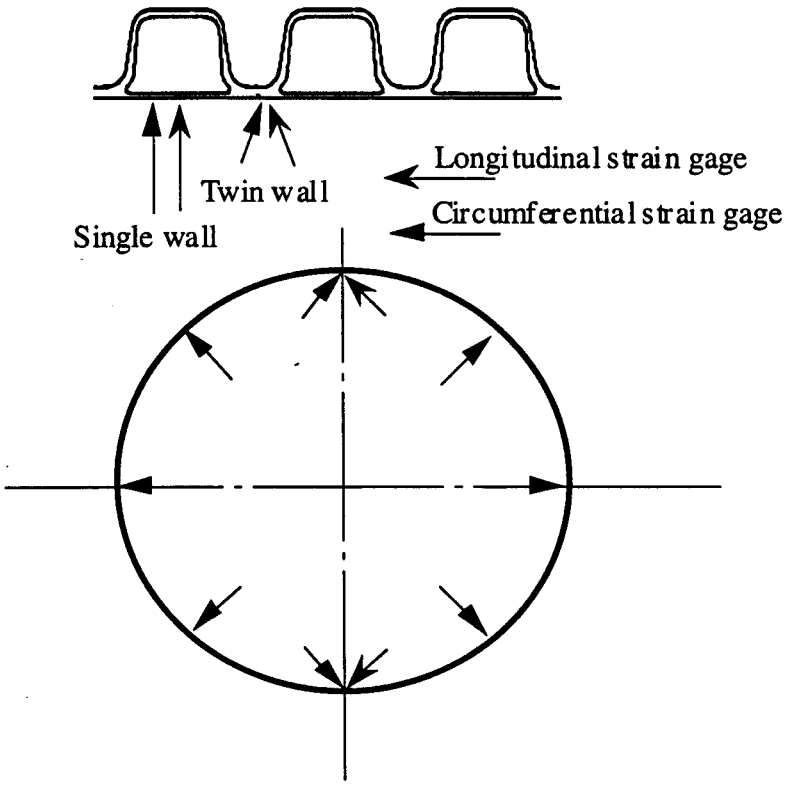

Fig. 4.21 Locations for strain gages

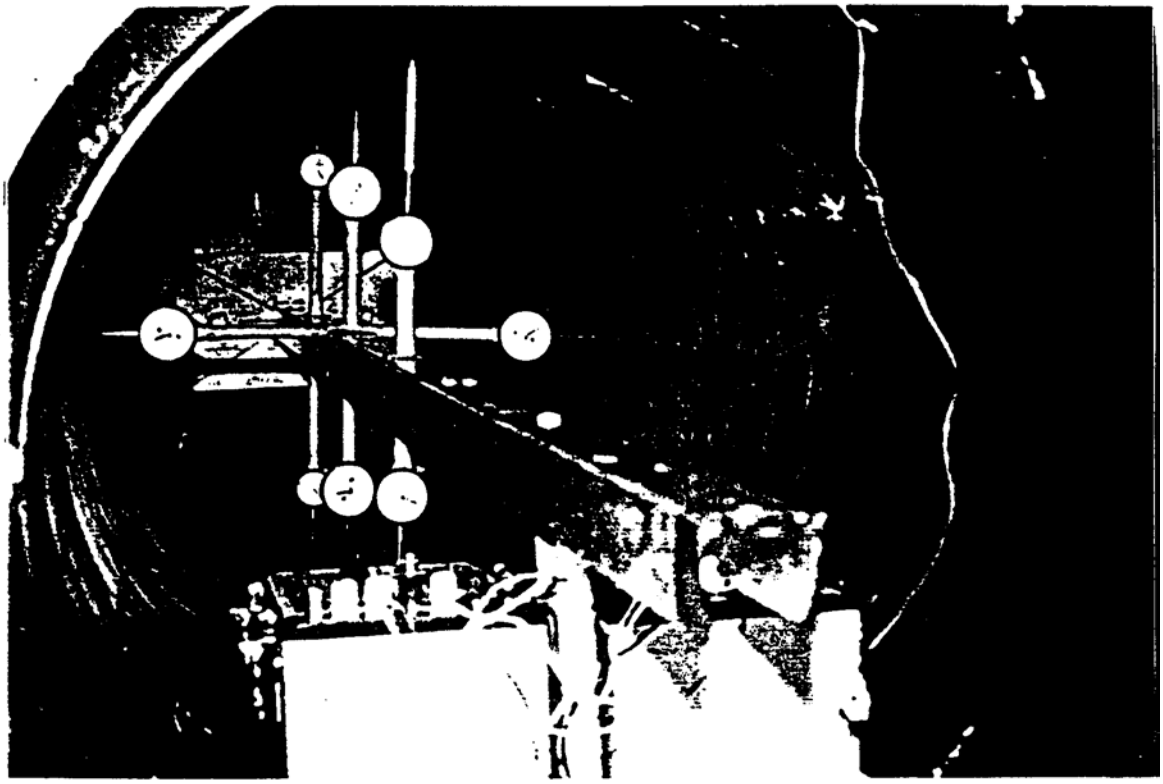

Fig. 4 22 Arrangement of strain and dial gages

4.5.3 TEST PROCEDURE

The testing was carried out in the following stages: i) Compaction of the bedding with vibrating compactor, placing of the pipe, and haunch/backfill compaction with an optimum moisture content. ii) Loading to simulate the overburden due to soil and truck weights. The incremental loading was held constant for periods ranging from 1 day to 1 week to allow creep to develop in the soil-pipe system. The ultimate loads were set at those corresponding to maximum diametral change of 7.5 % of the inside diameter. The bedding, surrounding and backfill material, used was South Florida clean sand, Class III SP, and more than 85% Standard Protor Compaction, with a Poisson's ratio of, ν=0.3, angle of friction, ϕ=30^0, and soil cohesion, c=0. The cover to the pipe and thickness of bedding were 30 in. and 12 in. (FDOT Roadway and Traffic Design Standards Section

Specimen Details

Types: I and II

Cell Classification: 335420C Corrugation Design: Annular

Size: 24 in.(610 mm) inside diameter, 6 ft. (1.83 m) length

Number of Specimens: 6 = 3 Type I + 3 Type II

Fig. 4.23 Performance testing of the buried

4.6 FLEXURAL TESTING IN AIR

The longitudinal bending stiffness and maximum moment capacity of the HDPE pipe of cell classification, 335420C, were evaluated by flexural testing in air. Two sizes, 12 in. and 24 in. inside diameter, made by the two manufacturers, and designated Type I and Type II, were selected for the testing. The specimen details are shown in Table 4.5.

Table 4.5 Specimens for Flexural Testing

Type: I and II Cell Classification: 335420C Corrugation Design:

Annular Joint: Soil-tight joint with foam O ring

Details	Type I specimen	Type II specimen	Type II specimen with soil-tight joints
Inside Diameter	12 & 24 in.	12 in.	12 in.
San Len th	10 & 15 ft	10 ft	loft
Number of specimens	3 & 3	3	3
Temperature at testing oC	38°C	38°C	38°C

The specimens were simply supported and subjected to uniform loading by applying sand bags on the top of the specimens. The test setups are shown in Figs. 4.24, 4.25, and 4.26. Uniaxial, foil type strain gages were affixed longitudinally at mid-span on the internal wall of the 24 in. inside diameter pipe (top and bottom), and the outer wall of the 12 in. pipe (top and bottom). The strain gages, used for the 24 in. diameter pipe, were long enough (2.5 in.) to cover both the twin and single wall locations, but the 0.24 in. long 65

gages for the 12 in. pipe were mounted only at the twin wall locations at the valley. The strain values were measured by digital indicators, and the deflections at the midspan by dial gages.

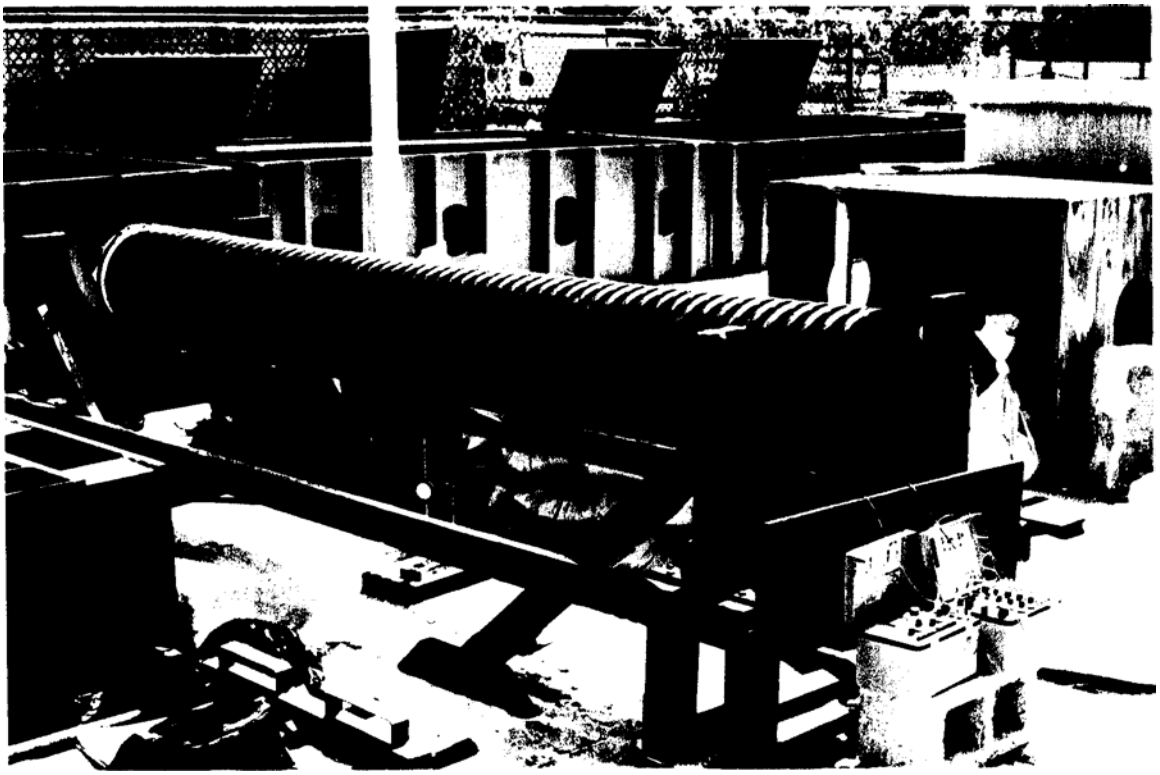

Fig. 4.24 Flexural test setup for the 12 in. inside diameter

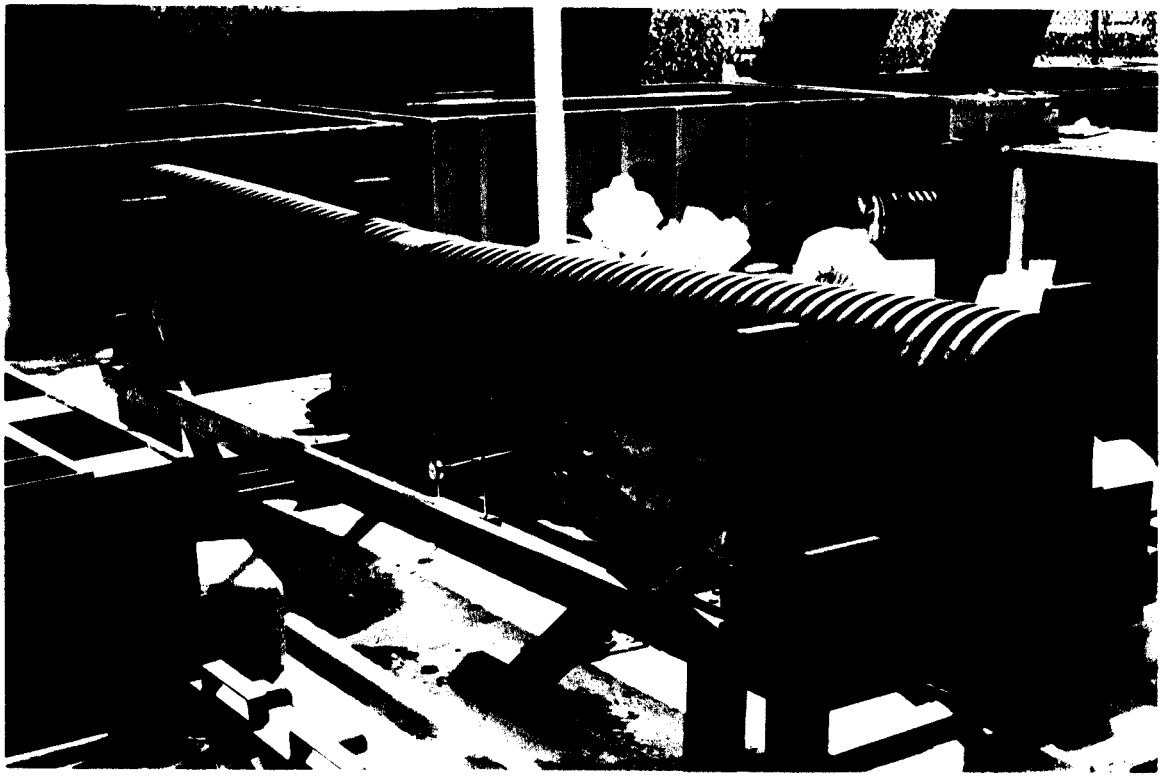

Fig. 4.25 Flexural test setup for the 12 in. inside diameter soil-tight jointed pipe

Fig. 4.26 Sand bag load testing of the 24 in. inside diameter pipe

CHAPTER 5

RESULTS OF THE EXPERIMENTAL INVESTIGATION

This chapter is divided into three parts: i) small scale laboratory testing, ii) large scale laboratory testing, and iii) field inspection.

5.1 RESULTS OF ENVIRONMENTAL STRESS CRACKING RESISTANCE (ESCR) TESTING

The modified ESCR test (AASHTO M294-93, Standard Section 9.4) was carried out to ensure cracking resistance of the new cell class for the melt index, 3, with the average molecular weight of the PE resin chains as low as 0.15-0.4. The bent specimens, exposed at super ambient temperature of 122 OF (50 ºC) to 100 % IGEPAL, a trade name for nonylphenoxy poly (ethyleneoxy) ethanol solution, for 24 hours were removed and inspected visually and with a microscope (5-20x).

None of the specimens showed any visible cracking or damage. The initial pinpoint surface depressions on the inside surface of the pipe, Figs. 5.1, did not lead to any

cracking or further damage. The changes of the inside chord length, after unloading, were measured for the test (exposed at super ambient temperature, 100 % IGEPAL) and control (atmospheric exposure, room temperature) specimens to determine the difference in the degree of deformation, Fig. 5.2. The measurements were carried out within 10 minutes after unloading. Table 5.1 shows the percentage shortening of the inside chord length. From Table 1, the relative degree of deformation can be estimated as follows:

$$D_f = \frac{C_E - C_A}{100 - C_A} \times 100 \quad \text{----------(5.1)}$$

where

D_f=relative degree of deformation, %

C_A=change of chord length when exposed to air, %

C_E=change of chord length after ESCR test, %

Table 5.2 shows the relative degree of deformation for the two different specimens based on equation 5.1. Type I specimens performed better than the Type II ones. From the viewpoint of the AASHTO requirement, the specimens, both Types I and II, showed quite good environmental stress cracking resistance without any visible damage. Therefore, the new melt index (molecular weight range, 0.15-0.4), which is lower than the one the range 0.4 to 1.00 for the conventional HDPE pipe, meets the required environmental stress cracking resistance of the AASHTO M294 specification [AASHTO M294, 1993].

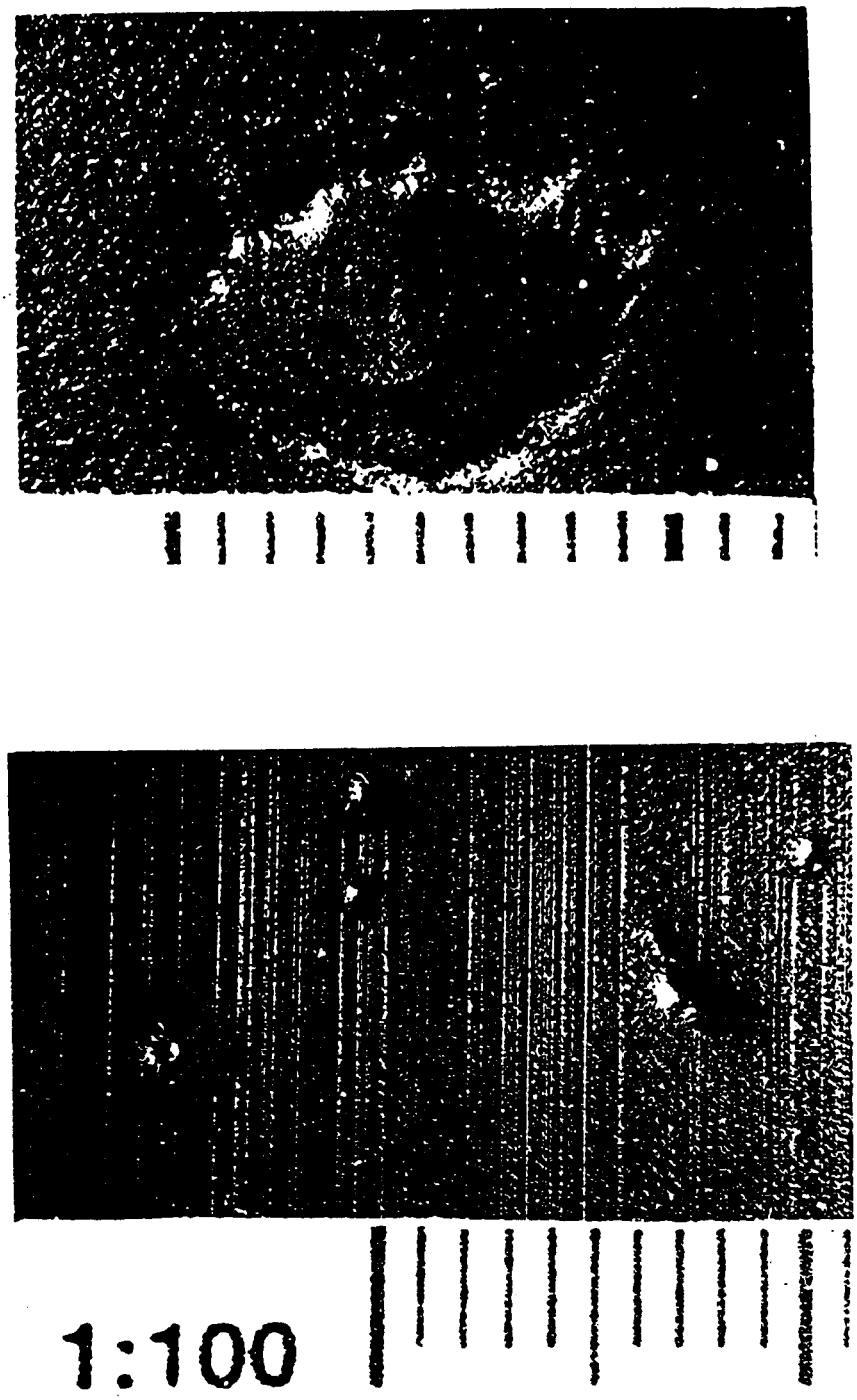

Fig. 5.1 Pin-point depressions on the inside pipe surface (after the exposure)

Table 5.1 Inside Chord Length Change

Manufacturer	Change of chord length (average), control specimens	Change of chord length (average), test specimens
Type I	6.73 %	10.48 %
Type II	6.48 %	14.01

Table 5 2 Relative Degree of Deformation

Manufacturer	Relative degree of degradation, %
Type I	4.02
Type II	8.05

5.2 RESULTS OF RING BENDING TEST BY PARALLEL PLATE LOADING

The ring bending tests were carried out by parallel plate loading, and the flexural modulus of HDPE pipes exposed at different temperature levels, 68, 95, 122, 126, and 140 OF (20, 35, 50, 52, and 60 °C) were evaluated. Table 5.3 and Fig. 5.3 show the temperature-dependent flexural modulus for Type I and II specimens. Both types have higher values of flexural modulus than the cell classification limit of flexural modulus at ambient temperature (class number 5, 110,000 psi = 758 MPa) [ASTM D3350, 1995]. The flexural modulus decreases almost linearly with increasing temperature for both types

of specimens. Type II specimens have the higher modulus than those of Type I at ambient temperature. Both types have similar values and decaying trends, with almost the same slope at temperature levels higher than 95 OF (35 °C). These test results were used for determining the long-term properties of HDPE pipe by creep testing.

Table 5 3 Flexural Modulus at Different Temperatures, Based on the Ring Bending Test

Type I, E (si)	Type II, E (si)	Temperatures (°C)
115,090	134,686	20
94,364	97,053	35
59,692	61,017	50
55,473	56,899	52
37,534	38,414	60

1 psi =6.895 kPa

Fig. 5.2 Chord length changes before and after the testing

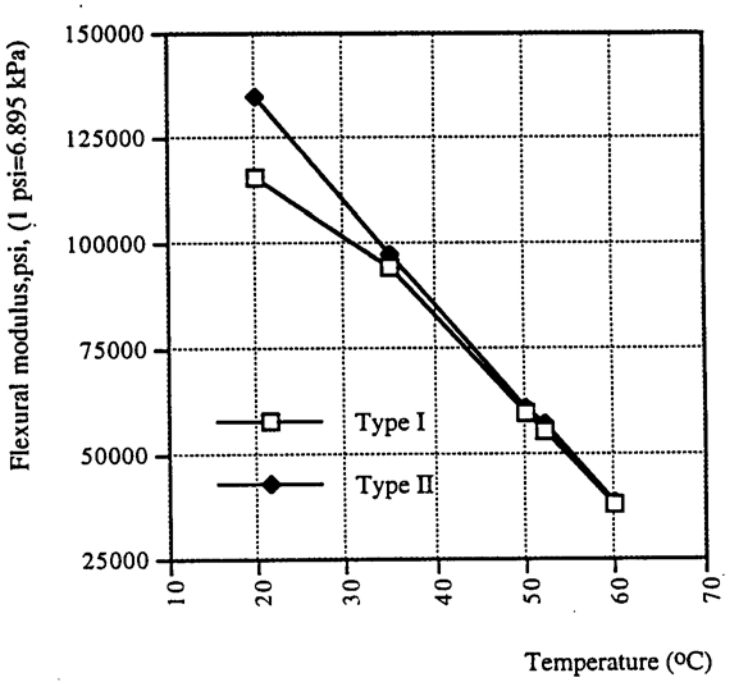

Fig. 5.3 Flexural modulus at different temperatures

5.3 CREEP TEST RESULTS

Constant parallel plate loading creep testing was carried out to predict the long-term properties of HDPE pipe with the maximum duration of the test, 10,000 hours. Periodic measurements of the vertical changes of diameter are shown in Figs. 5.4, 5.5, 5.6, and 5.7. For higher temperatures, i.e. 52°C and 60°C, the duration was restricted to 1,000 hours as the deflection limit is reached sooner. It was observed that i) the ring specimens (same type), exposed at the same temperature, showed similar behavior of time transient deformation, ii) the behavior for Type I and II was also quite similar, iii) approximately after 3,500 hours, both specimens Types I and II at 20 °C became quite stable with little changes.

Average values of the time dependent flexural modulus at each temperature level were calculated from the test results, based on equation (4.1) and plotted in Figs. 5.8 and 5.9. There were only marginal differences in the modulus decay slopes (log time scale) at all the temperature levels for both Type I and H specimens. No cracking or damage were found from all the specimens, subjected to 1,000-10,000 hours of creep testing at superambient temperature levels. The results of the maximum 10,000-hour tests at various temperatures were shifted to construct the long-term master curves. The applicability of the current available procedures in extrapolating these results to longer time intervals is compared and studied in Chapter 6.

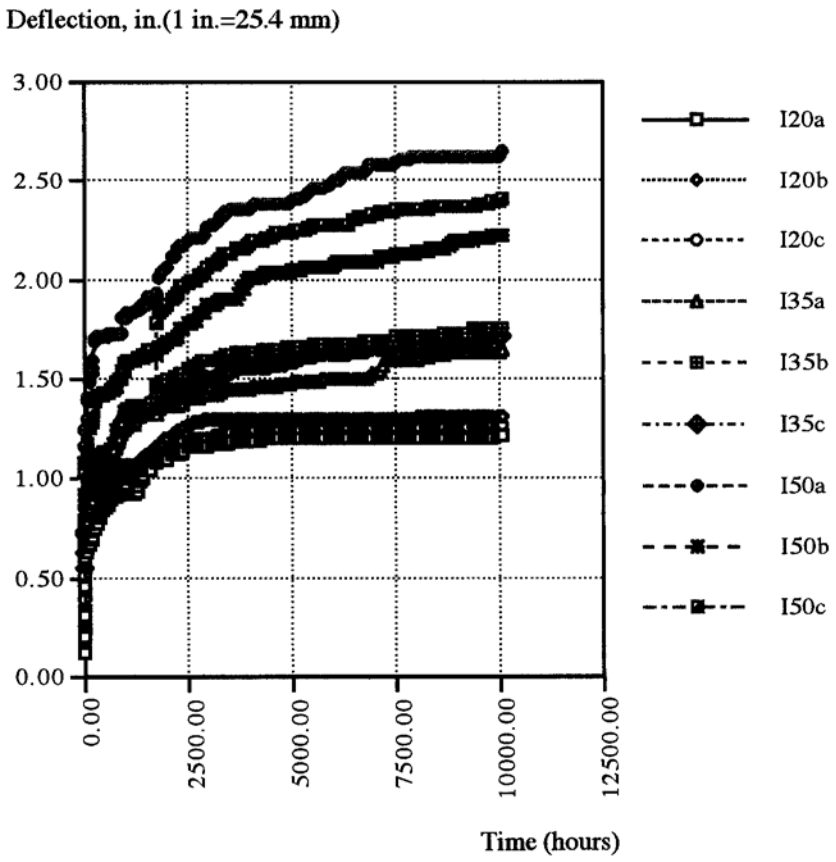

Fig. 5.4 Creep deflection vs. time curves for Type I specimens at 20, 35, and 50 °C

Legend

Ist Character: specimen type, I for Type I and II for Type II

2nd Character: temperature (°C), 20, 35, 50, 52, and 60 °C 3rd

Character: specimen number, a, b, and c

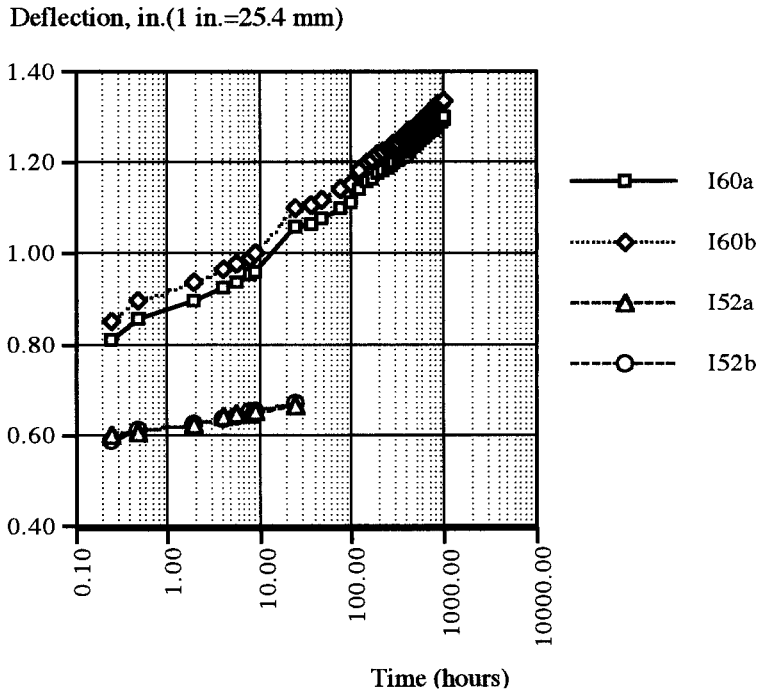

Fig. 5.5 Creep deflection vs. time curves for Type I specimens at 52 and 60 °C

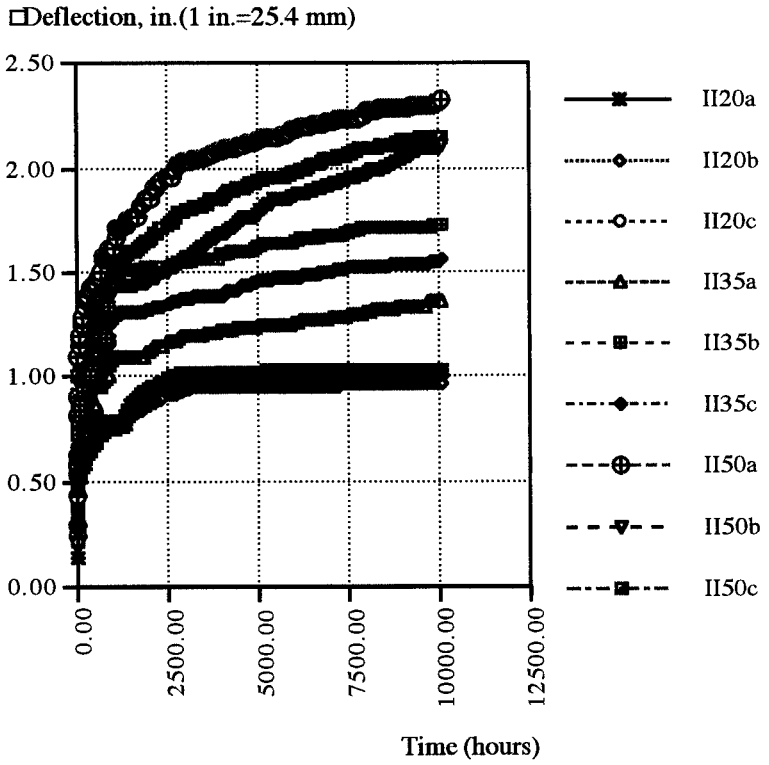

Fig. 5.6 Creep deflection vs. time curves for Type II specimens at 20, 35, and 50 °C

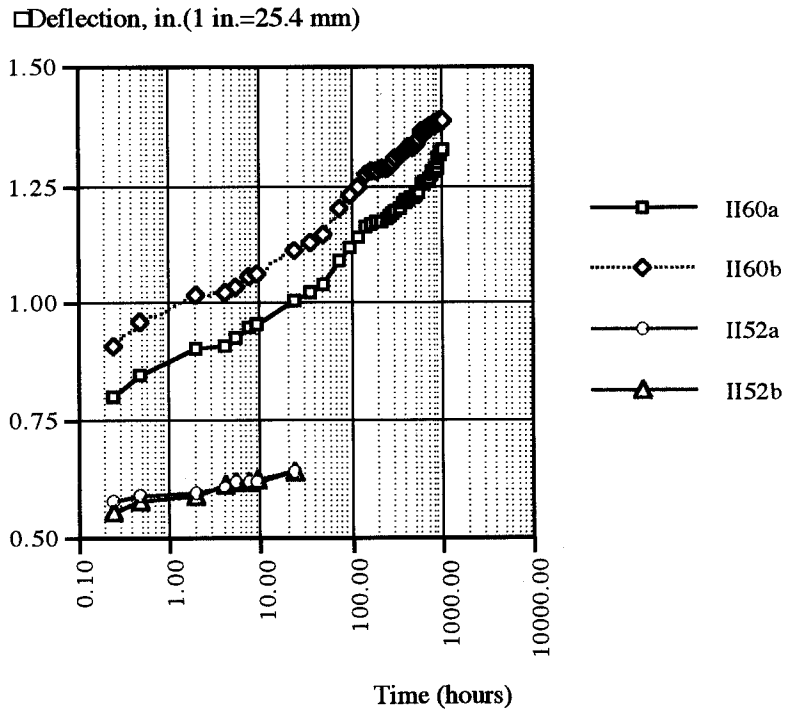

Fig. 5.7 Creep deflection vs. time curves for Type II specimens at 52 and 60 °C

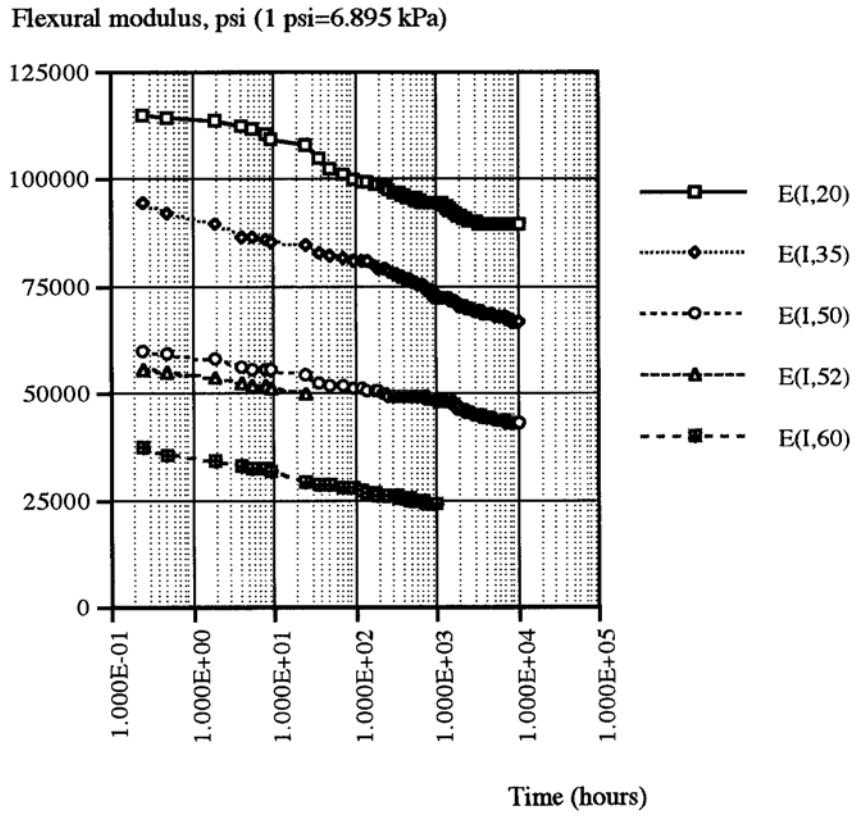

Fig. 5.8 Flexural modulus vs. time curves for Type I specimens

Legend for E(*,)**

E: Flexural modulus

*: Specimen types, I and II

**: Temperatures, 20, 35, 50, 52, 60 °C

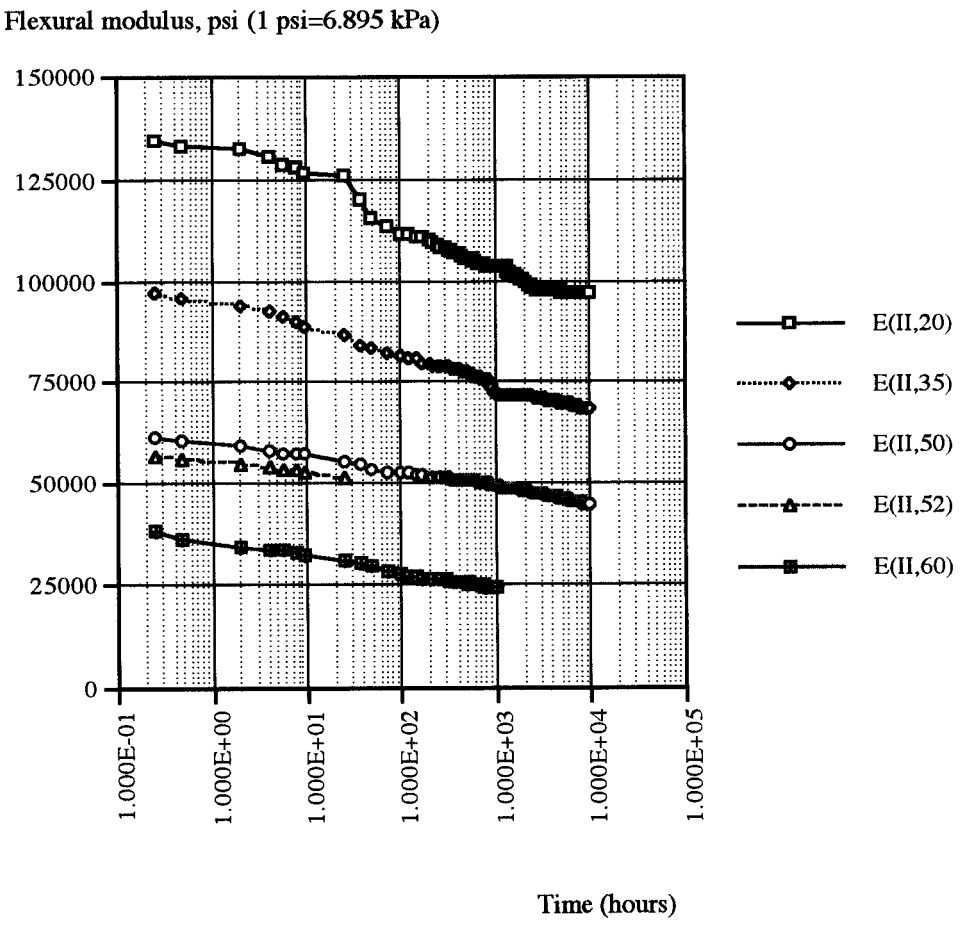

Fig. 5.9 Flexural modulus vs. time curves for Type II specimens

5.4 SIEVE ANALYSIS

Two different Florida local soil samples were prepared for the sieve analysis (modified ASTM D2487-92), to investigate the validity of backfill material for the installation of HDPE pipe. South Florida clean sand was collected from a nearby coastal location for the laboratory testing of the buried pipe . Central Florida local sand, which was used as a backfill material for the HDPE culvert buried under the median of US I-75 (Wildwood Florida), was excavated from the backfill and haunch zones during field inspection. The percentages of the total weight of soil that passed through different sieves are plotted in Figs. 5.10, 5.11, and 5.12.

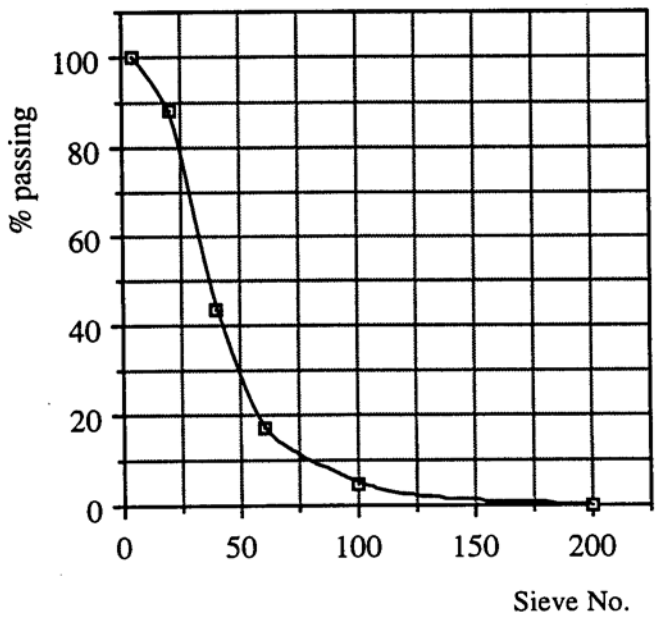

Fig. 5.10 Sieve analysis of the South Florida soil sample

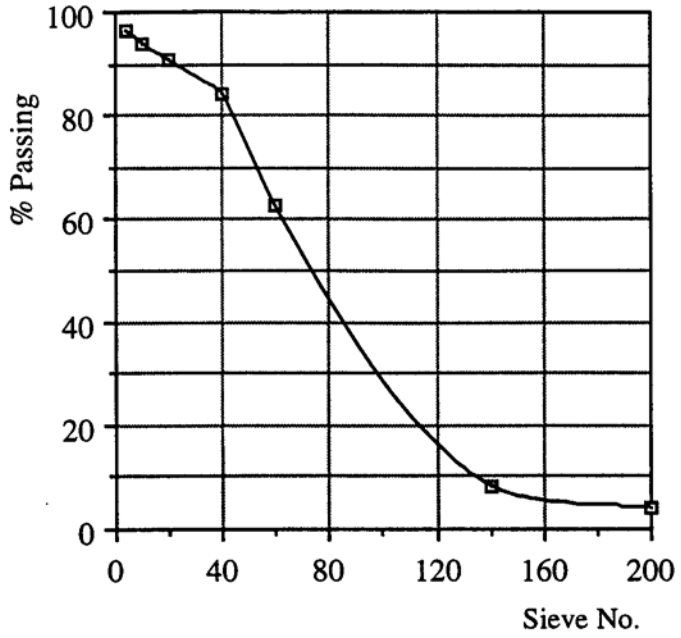

Fig. 5.11 Sieve analysis of the Central Florida soil sample from the backfill zone

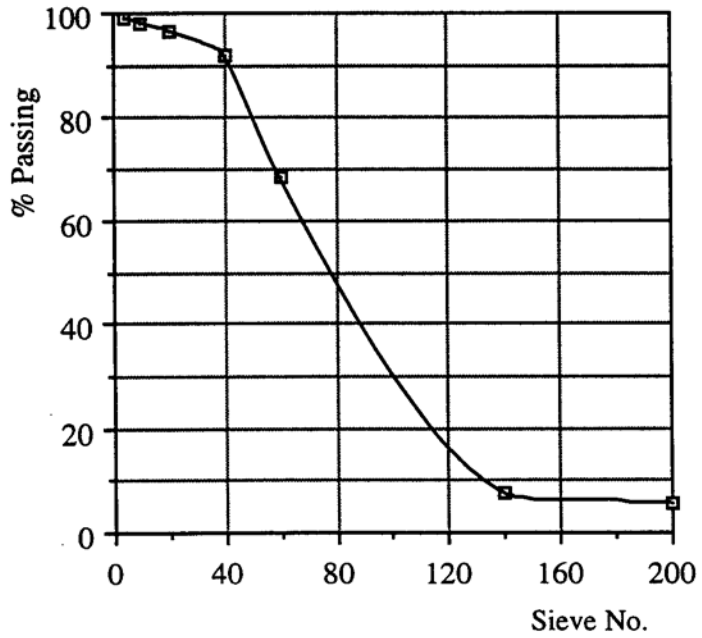

Fig. 5.12 Sieve analysis of the Central Florida soil sample from the haunch zone

The South Florida soil, which was used for the performance of buried pipe test, was classified as **SP** (poorly-grained sands and gravely sands, little or no fines) in **Class II** (coarse-grained one, clean) [ASTM D2321 and D2487]. The analysis indicated the percentage passing sieve No 200 (0.075 mm=0.003 in.) was less than 5% the coefficient of uniformity, C_u=3.75 < 6, and the coefficient of curvature C_c=0.82 < 1, as calculated by equations 5.2 and 5.3. Therefore, the backfill modulus, E', can be increased to 2,000 psi (13.8 MPa) with relative compaction, 85 to 95%, based on ASTM D3839.

$$C_u = D_{60}/D_{10} \quad \text{----------(5.2)}$$

$$C_c = \frac{(D_{30})^2}{(D_{10} \times D_{60})} \quad \text{----------(5.3)}$$

where

D_{10}, D_{30}, and D_{60} are the particle size diameters corresponding to 10, 30 ,and 60%, respectively, passing on the cumulative particle size distribution curve, Fig. 5.10.

The Central Florida soil samples which were collected from the backfill and haunch zones of HDPE sewer pipe, buried in the median of the route I-75 were classified separately by two different batch of sieve analysis. Similarly, the soil in the backfill zone was classified as Class II, SP soil, with the percentage passing sieve No 200 (0.075 mm=0.003 in.) < 5% , the coefficient of uniformity, C_u=2.18 < 6, and the coefficient of curvature C_c=0.97 < 1, Figs 5.11 and 5.12. However, the soil sample from the haunch zone was classified as Class II, SP-SM (sands and gravels, which are in the borderline

between clean and with fines), with the percentage passing sieve No 200 (0.075 mm=0.003 in.) < 12% , the coefficient of uniformity, C_u=1.83 < 6, and the coefficient of curvature C_c=0.85 < 1. Therefore, both Central Florida soil samples were identified as stable backfill materials with proper relative compaction.

5.5 FIELD INSPECTION OF THE BURIED HDPE SEWER PIPES

A field inspection of HDPE pipe, buried in the median of the route I-75 was carried out near Wildwood exit and Florida Turnpike intersection, Wildwood Florida. Visual inspections for the number of sections were carried out by a remote control robot vehicle, equipped with rotational video camera, Fig. 5.13, and followed by soil and pipe sample (cracked) collection, to analyze the properties of the backfill materials and the pipe failure patterns.

Fig. 5.13 Remote control device for visual inspection of buried HDPE

Specimen Details

Type: II

Cell Classification: 324420C

Corrugation Design: Annular

Size: Inside diameter 18 in. (457 mm)

Most cracking on the inner liner occurred near the concrete header/end wall due to poor initial installation, and ignoring of the proper gap filling (right next to the concrete structure). Diagonal cracking resulted due to excessive combined bending and circumferential stresses, Fig 5.14. The level of unexpected stresses was high enough to start slow crack growth from initial defects or pin hole depressions followed by rapid crack propagation. Such failure occurred due to fundamental stress cracking susceptibility. The failure process can be outlined as follows:

Stage 1: SCG initiated at a small installation-induced surface defect

Stage 2: Transition from SCG to Rapid Crack Propagation (RCP)

Stage 3: Catastrophic RCP results

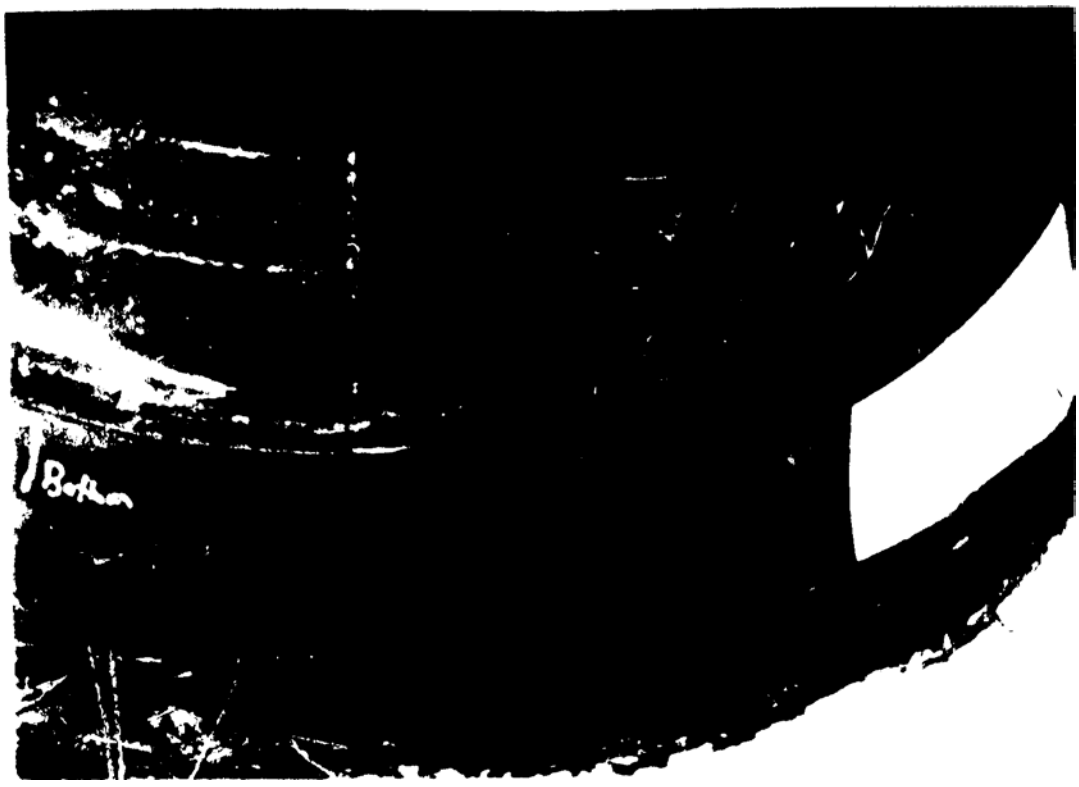

Fig. 5.14 Diagonal cracking near concrete

The typical long term-failure process of a HDPE geomembrane is shown in Fig. 5.15 [Kanninen et al., 1993]. SEM (Scanning Electron Microscope) fractographic examinations of the crack surface features of the field HDPE pipe specimens, indicated the failure mode as the SCG (Slow Crack Growth) in the initial stage, followed by RCP (Rapid Crack Propagation). Figs 5.16, 5.17, 5.18, and 5.19 SEM fractographies, clearly show stages 1,2, and 3, referred to above. Fig. 5.16 emphasizes the part of the crack face that was subjected to SCG. The surface features are representative of the SCG mechanism showing some initial fibrils, which were stretched in the direction of parallel to the applied stress, similar to the example for SEM fractography for SCG on HDPE gas pipe, shown in Fig 5.20. The fibrils continued to stretch until those nearest the crack tip weakened and broke (rupture), Figs. 5.17 and 5.18.

This case showed the importance of HDPE sewer pipe installation procedures. Mostly proper backfill materials (based on 5.4 test results of sieve analysis) were used but a piece of bituminous paving was found in the soil sample, excavated at the haunch zone. This indicates uncertainty about backfill compaction. Gap filling (near the bottom portion of pipe/concrete wall connection) with proper material is an important installation procedure, and should not be overlooked to avoid the occurrence of any excessive stresses.

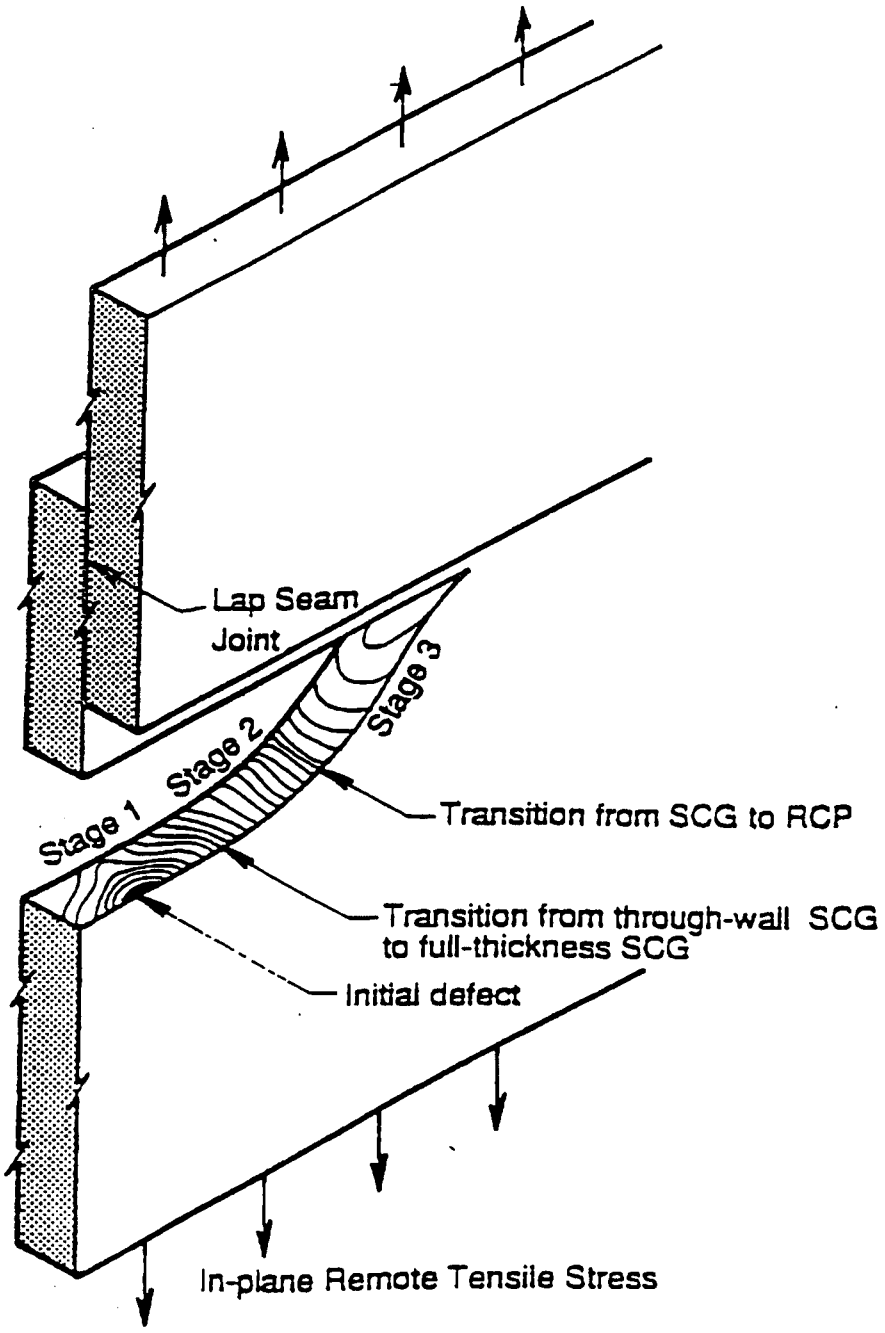

Fig. 5.15 Schematic view of long-term failure process in a seamed geomembrane [Kanninen et al, 1993]

Fig. 5.16 Crack surface near the initially defective zone (X600)

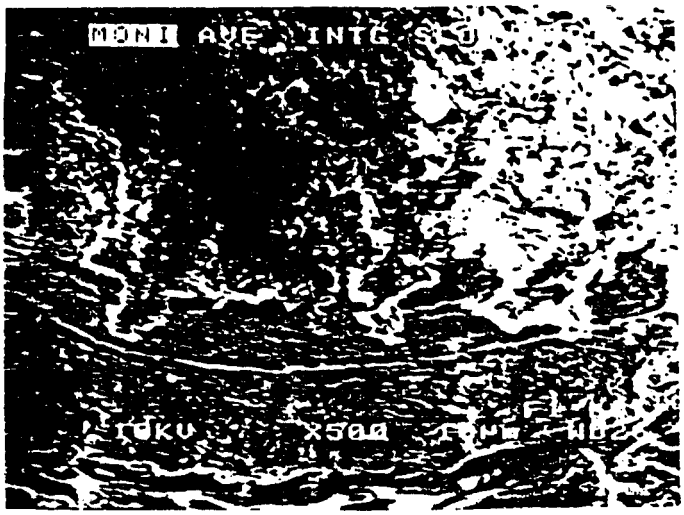

Fig. 5.17 Transition from SCG to RCP (X500)

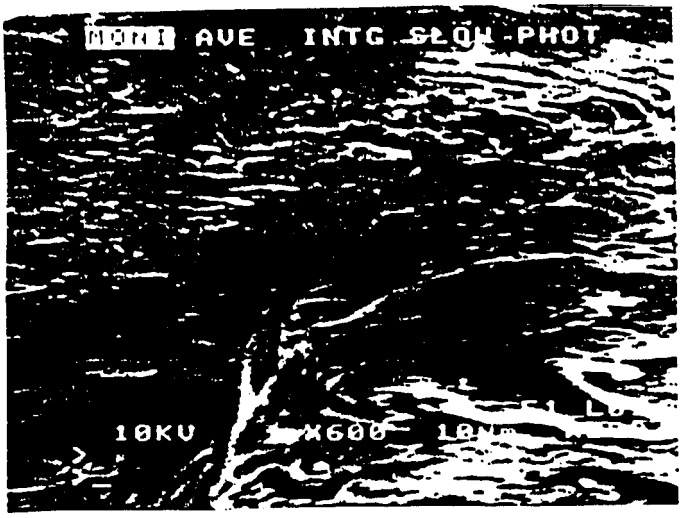

Fig. 5.18 Rapid crack propagation (X600)

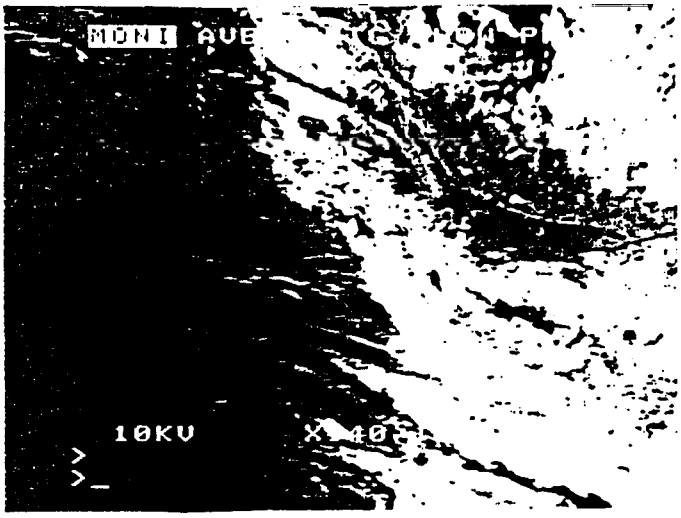

Fig. 5.19 Direction change in crack propagation (X140)

5.6 SOIL COMPACTION

Laboratory (Standard Proctor Test, ASTM D698) and in-situ compaction tests were carried out to confirm the required degree of compaction of the soil in the chamber for the task of performance of buried pipe.

1) The soil was mixed with varying amounts of water and then compacted in three equal layers by a hammer (5.5 lb, 2.5 kg) that delivers 25 blows to each layer in the mold (1/30 ft^3, $9.43x10^5$ mm^3). The moisture content of the soil for each test was determined by drying it in the oven. With known moisture content, the dry unit weight γ_d can be calculated as follows:

$$\gamma_d = \frac{\left(W/V_m\right)}{(1+0.01w)} \quad \text{----------(5.4)}$$

where

γ_d=dry unit weight

W=weight of compacted soil in the mold

V_m=volume of the mold

w=the percentage of moisture content

2) In-situ compactions of the soil in bedding, haunch, and backfill zones in the chamber were carried out by the vibrating compactor after the mold was buried. The molds were carefully taken out after proper compaction process, and the moisture contents and

dry unit weights of the samples found in a manner similar to that for the standard compaction test, Figs 5.21 and 5.22.

Laboratory Standard Proctor Test tests were carried out prior to the in-situ compaction tests, and the relationship between the dry unit weight and moisture content the soil was evaluated, Fig. 5.23. It was found that the maximum dry unit weight was 105 lb/ft^3 (16.51 kN/m^3), with the optimum moisture content 10.5 %. Based on the laboratory and in-situ test results, the degree of compaction can be determined as follows:

$$R(\%) = \left[\frac{\gamma_{d(in-situ)}}{\gamma_{d(\max-lab)}} \right] \times 100 \quad \text{----------(5.5)}$$

where R=relative compaction

γ_d(in-situ)=dry unit weight of in-situ sample

γ_d(max-lab)=maximum dry unit weight, obtained in the laboratory

The required degree of compaction of the soil, in the soil chamber was confirmed for each specimen installation. Table 5.4 shows the relative compaction, for the bedding and backfill regions. It was proved that proper in-situ compaction was carried out with small variations (91-96 %), and the relative compactions were higher than the minimum, required (85 % Standard Proctor, ASTM D2321) for the soil.

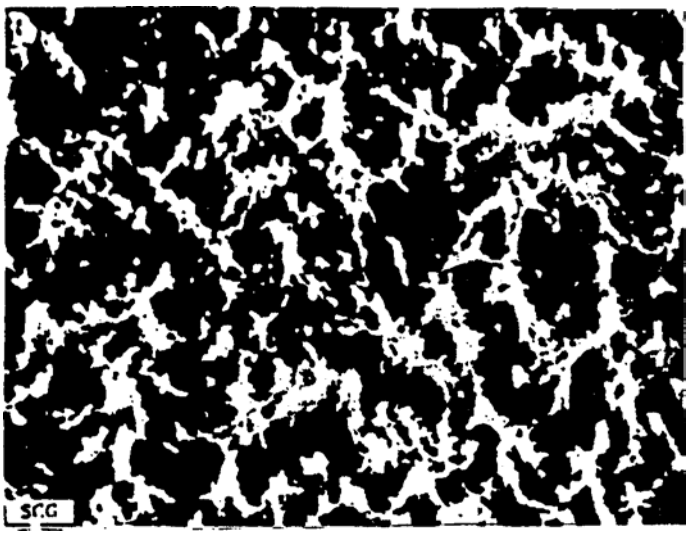

SCG test fracture 500X

Fig. 5.20 Typical SCG test fracture [Plastic Pipe Line, 1994]

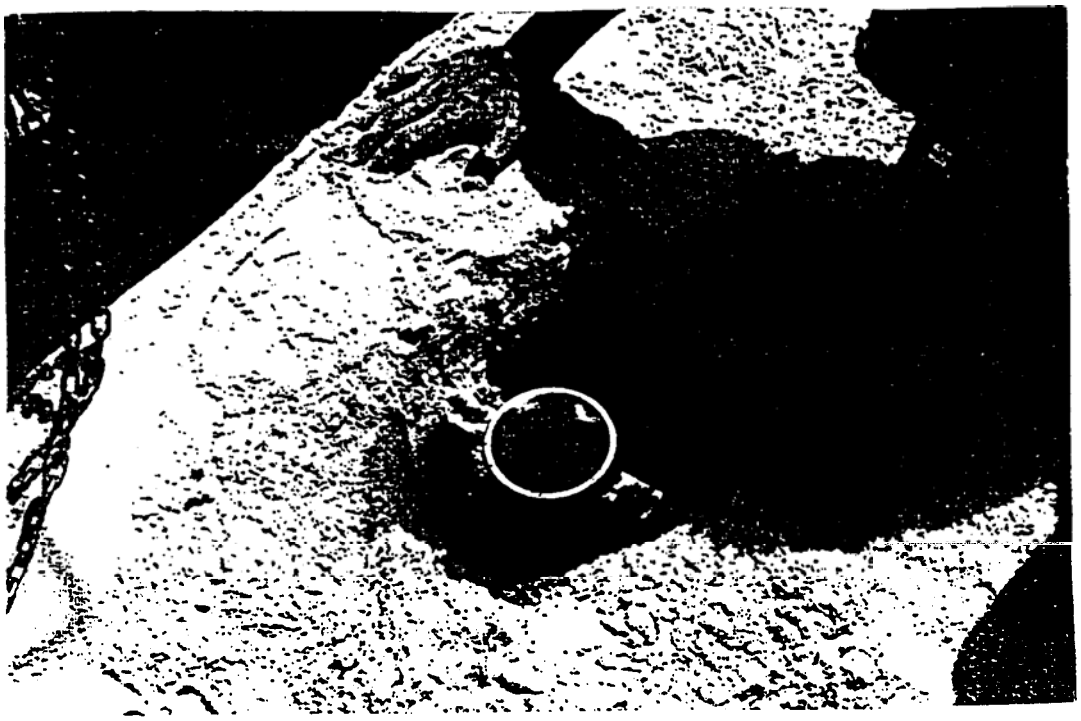

Fig. 5.21 In-situ test for relative compaction 93

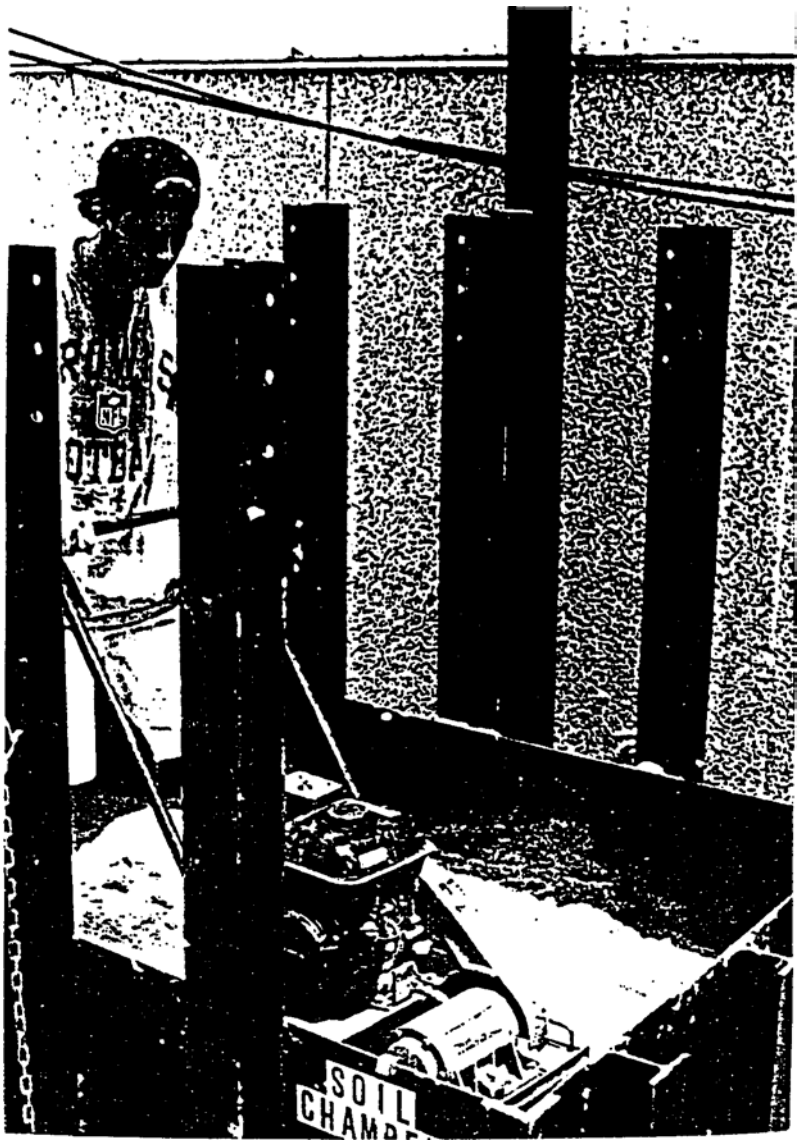

Fig. 5.22 Backfill compaction in the soil chamber

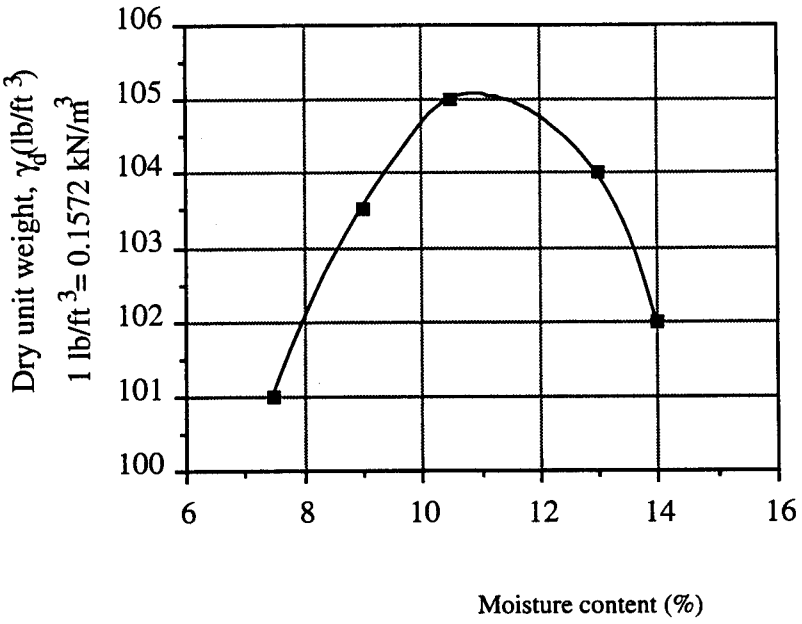

Fig. 5.23 Plot of dry unit weight vs. moisture content for the laboratory test results

Table 5.4 Relative compactions at the bedding and backfill zones in the soil chamber

Soil Samples (Beddings)	Relative Compaction, R (%)	Soil sample (Backfills)	Relative Compaction, R (%)
1	96	1	95
2	96	2	93
3	94	3	91
4	92	4	92
5	95	5	95
6	94	6	94

5.7 TEST RESULTS OF THE PERFORMANCE OF BURIED HDPE PIPE, SUBJECTED TO LIVE LOAD

The testing for the performance of buried pipe in the soil chamber was carried out after Standard Proctor-based compaction of the bedding, placing of the pipe, and Standard Protor-based backfill and cover compaction with an optimum moisture content. Loading to simulate the overburden of the soil and truck weights was applied by two hydraulic jacks and a loading plate, and diametral and longitudinal measurements of deflection and strain were taken using dial and strain gages.

The results are shown in Figs 5.24 -5.29. Three separate test results, for each type of specimen, indicated that changes of deflections and strains vs. live load increment are quite similar for all three specimens. The average values of the deflection at each section are shown in Figs. 5.24 and 5.25 for Type I and II specimens. The average values of longitudinal and circumferential strains are shown in Figs.5.26 to 5.31. The response to incremental loading, which was held constant for periods ranging from 1 day to 1 week to allow creep to develop in the soil-pipe system, is shown in Fig 5.32. The maximum midsection deflections for AASHTO H-20 live load level (40 kips) were very small [approximately 0.19 in. (4.8 mm) for Type I and 0.11 in. (2.8 mm) for Type II specimens]. Both types of specimens failed at the live load level, approximately 260 kips (1.16 MN), with excessive deflection (7.5% of inside diameter) at the top of specimens at mid-section [ASTM F894, 1995]. The failure mode was characterized by the top flattening due to overdeflection, without cracking and buckling, for both Type I and II specimens. The details of the longitudinal and cross-sectional deformations at different live load levels are shown in Figs. 5.33, 5.34, 5.35, and 5.36.

Vertical changes of the inside diameter with live load at section 2 were greater than those at sections 1 and 3 for both Type I and II specimens, Fig. 5.24 and 5.25. Therefore, the deformation of the mid-section is quite important and should be evaluated prior to that of other sections. Load vs. longitudinal strain curves, Fig. 5.26 and 5.27, show that there is no gage sensitivity (single/double liner and top and bottom) at the mid-section of the pipe specimen. Both Type I and II specimens showed sudden increase of circumferential and longitudinal strains, right before the pipes failed at about six times the AASHTO H-20 Highway live load level, 40 kips (178 kN) [CPPA, 1996].

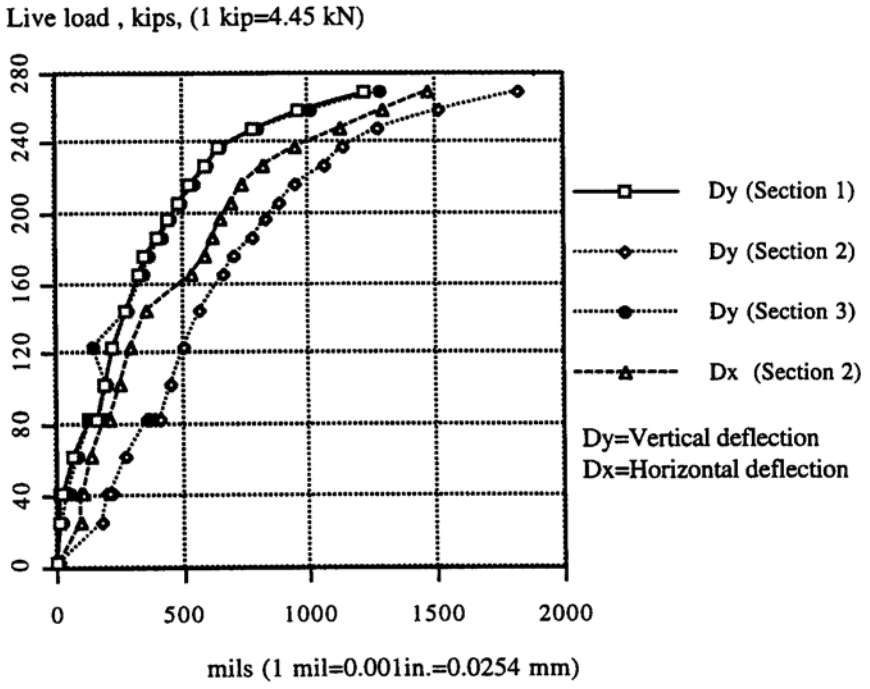

Fig. 5.24 Load vs. deflection curve at each section for Type I specimen

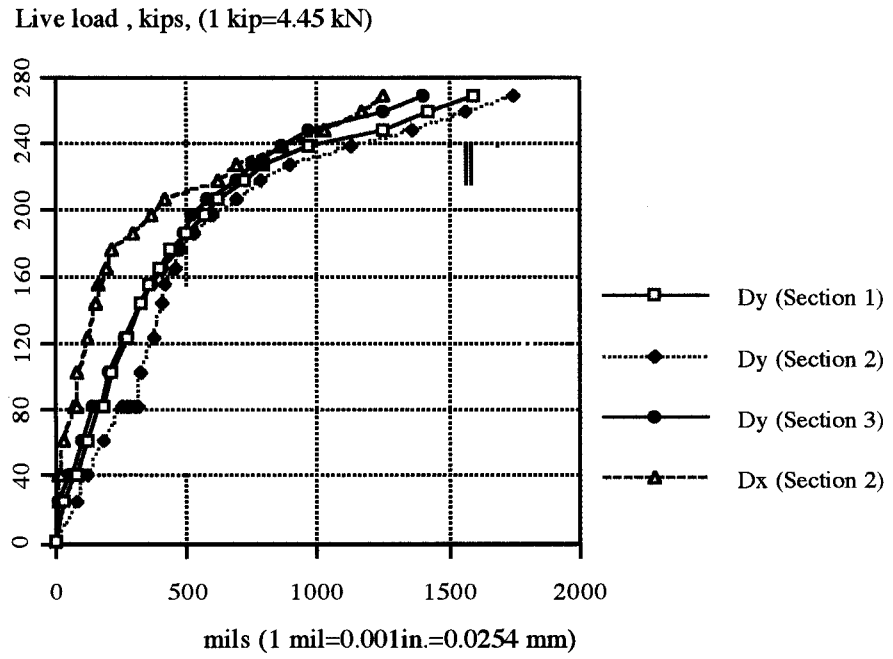

Fig. 5.25 Load vs. deflection curve at each section for Type II specimen

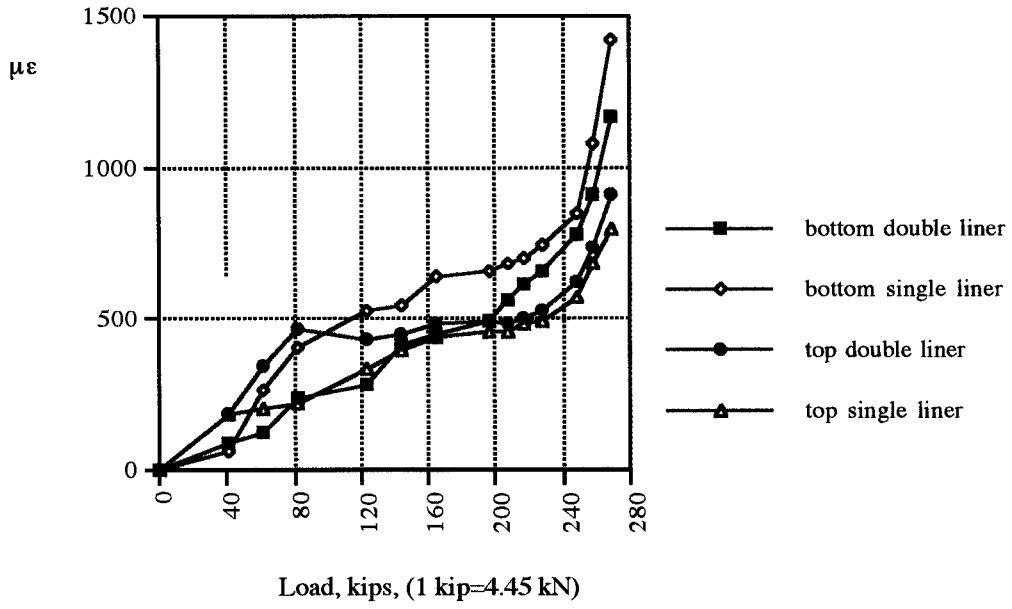

Fig. 5.26 Load vs. strain (longitudinal) curves for Type I specimen

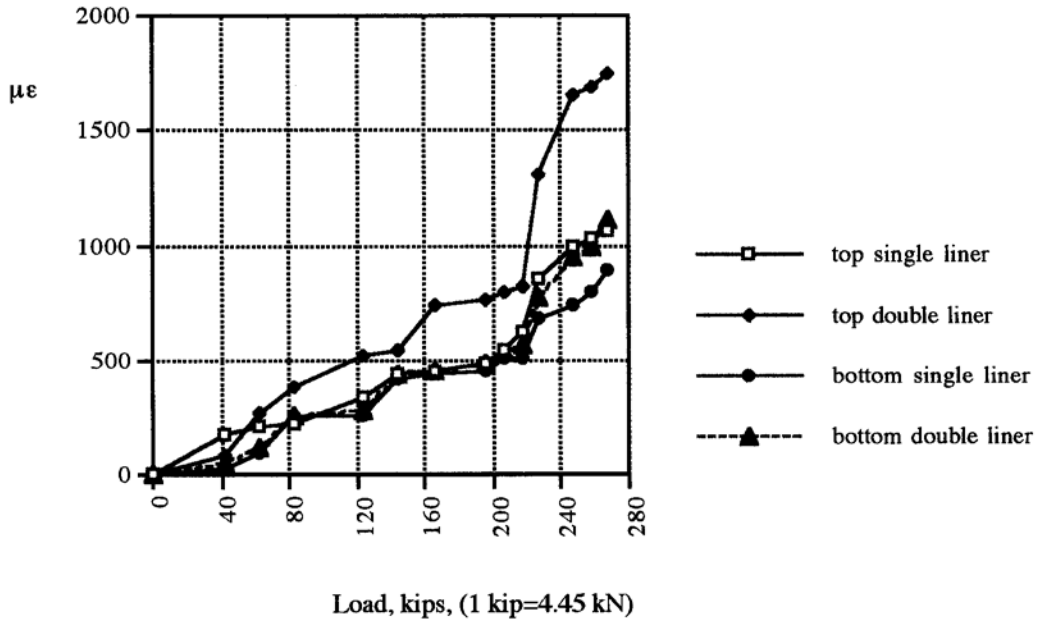

Fig. 5.27 Load vs. strain (longitudinal) curve for Type II specimen

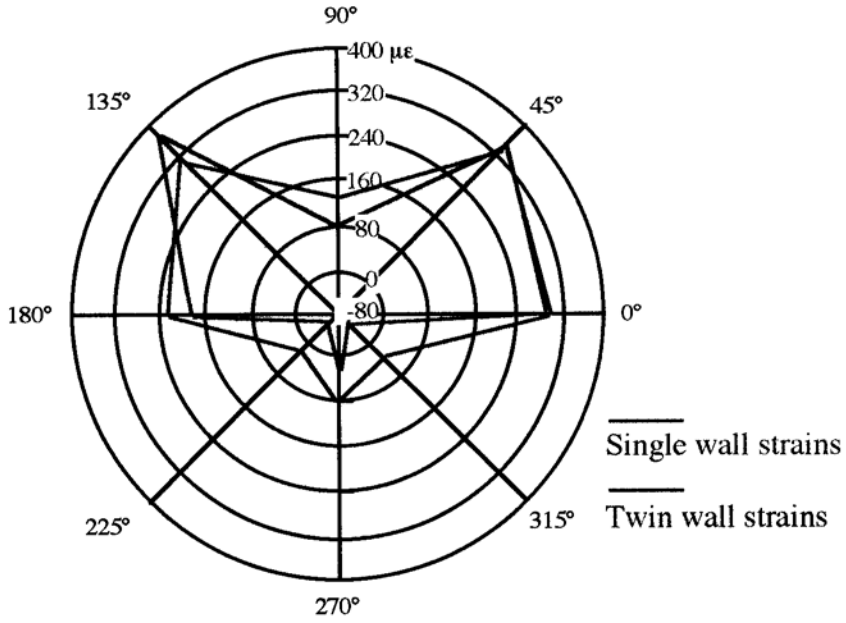

Fig. 5.28 Circumferential strains caused by live load, 40 kips (178 kN) for Type I specimen

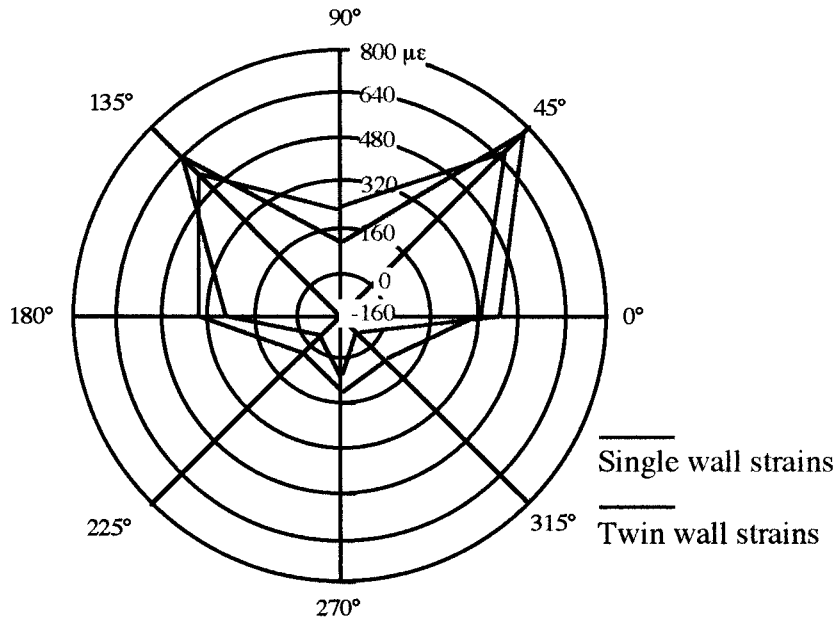

Fig. 5.29 Circumferential strains caused by live load, 80 kips (356 kN) for Type I specimen

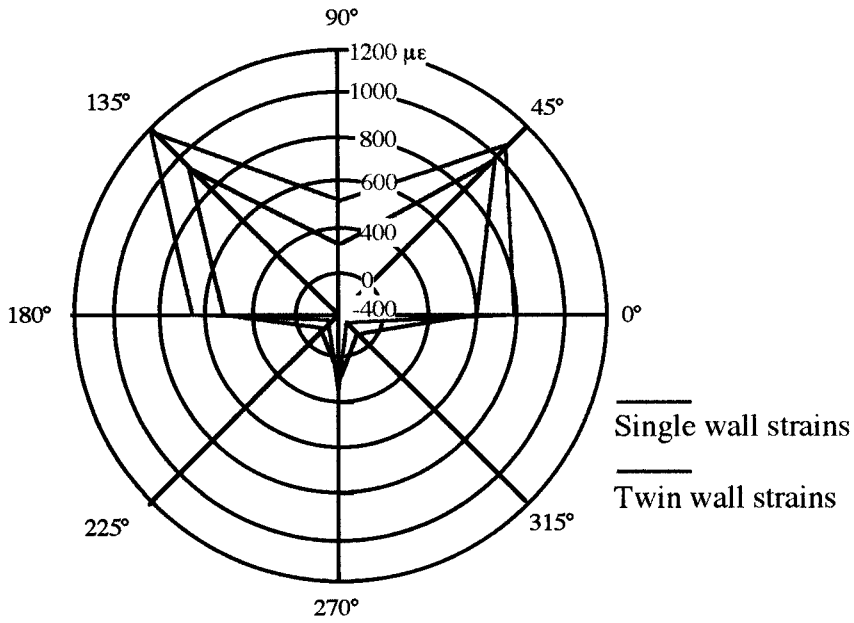

Fig. 5.30 Circumferential strains caused by live load, 160 kips (712 kN) for Type I specimen

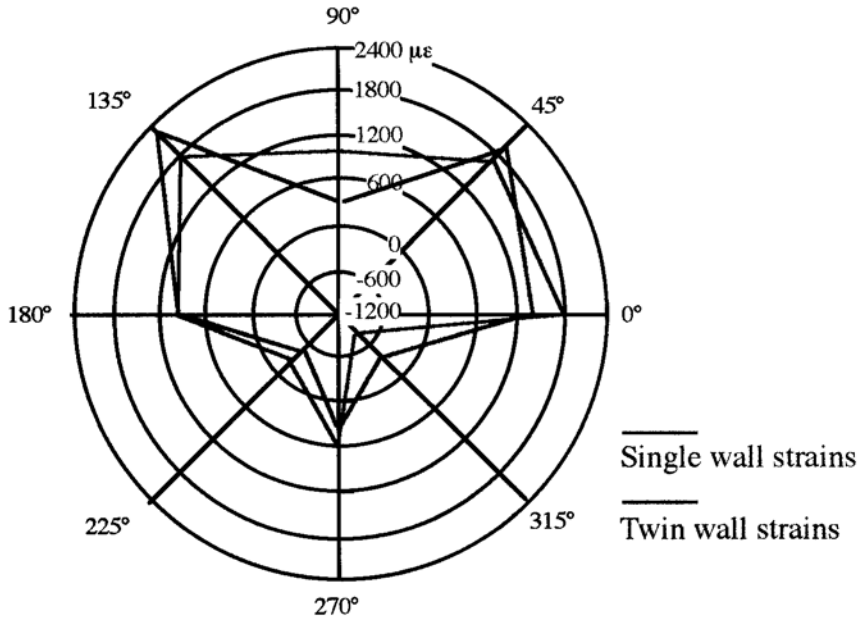

Fig. 5.31 Circumferential strains caused by live load, 260 kips (1,157 kN) for Type I specimen

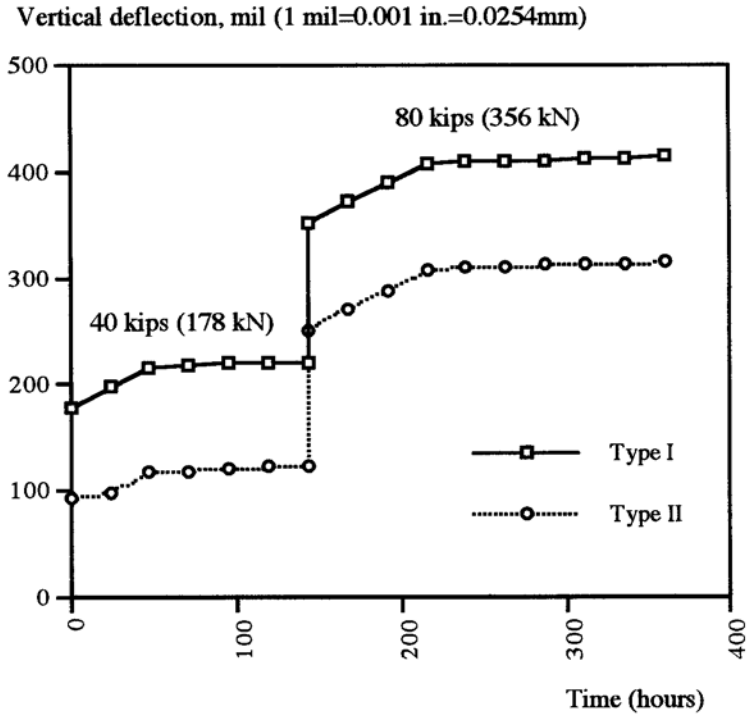

Fig. 5.32 Vertical deflection at midsection vs. time

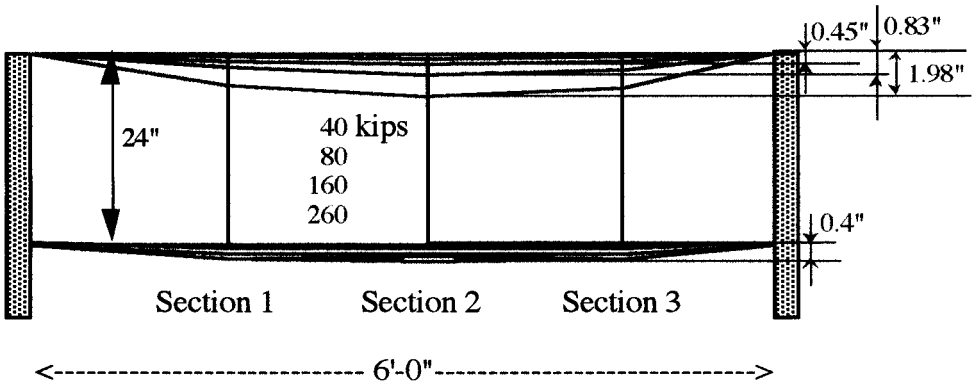

Fig. 5.33 Longitudinal deformation at different live load levels for Type I specimen

Fig. 5.34 Longitudinal deformation at different live load levels for Type II specimen

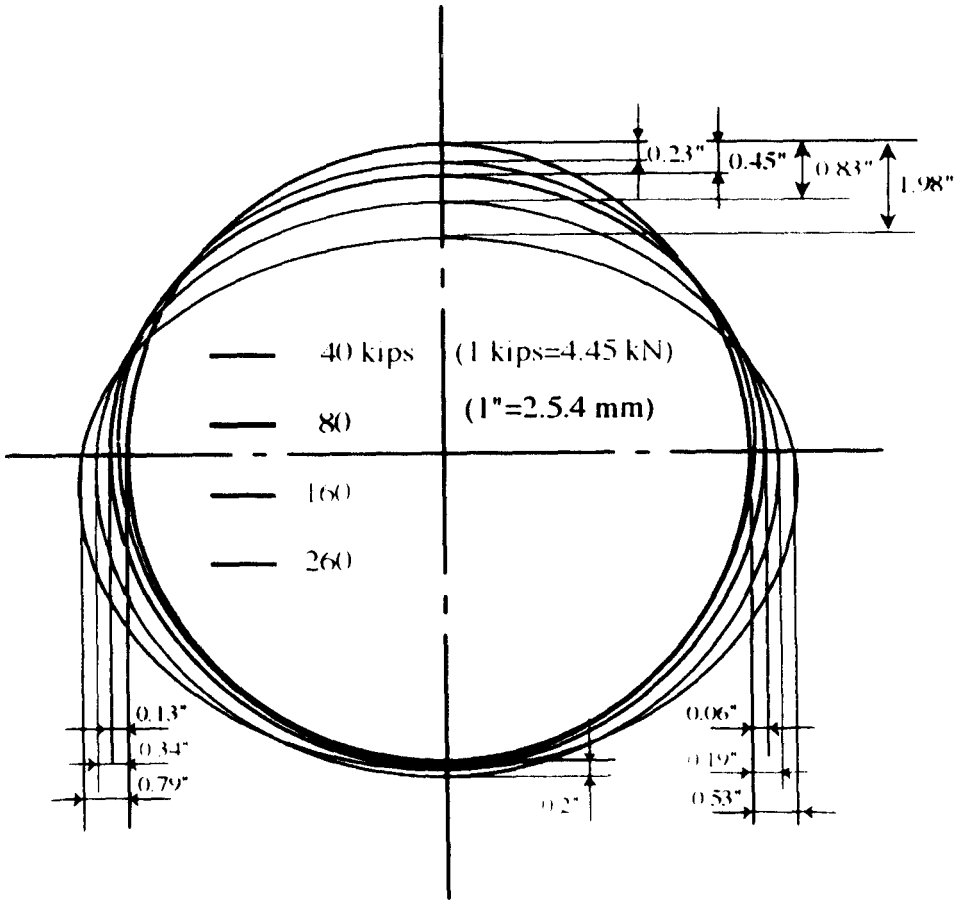

Fig. 5.35 Midsection deformation at different live load levels for Type I specimen

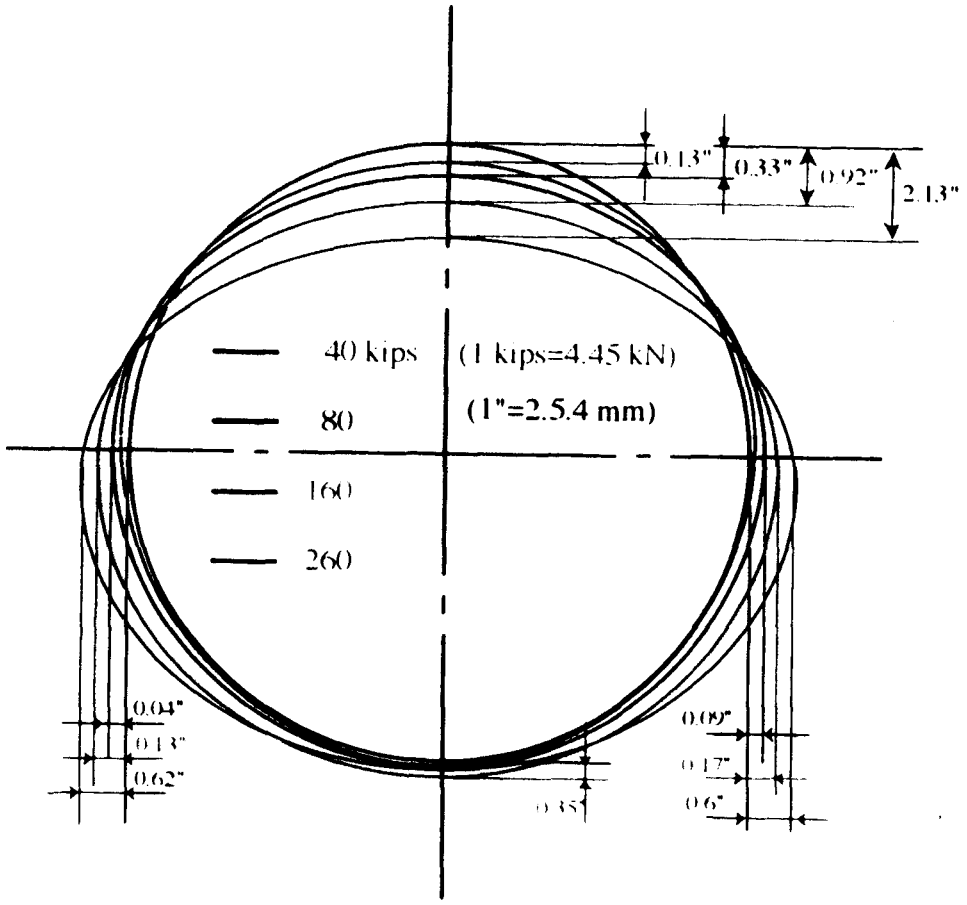

Fig. 5.36 Midsection deformation at different live load levels for Type II specimen

For HDPE piping, the longitudinal stress should not exceed 3,000 psi (20.7 MPa) and the bending strain should not exceed 0.05, [CPPA, 1996]. However, the test results indicated that the maximum axial strain at failure is approximately 0.0015 which is much less than CPPA limit referred above. It seems that the limit, which is based on yielding due to longitudinal bending, is not reasonable for the general failure criteria of the buried HDPE pipe, subjected to live load. The maximum circumferential strain occurred at the shoulder region (45° or 135^0) of the specimen, whereas the minimum circumferential strain occurred at the haunch (225° or 315°) for each live load level, from Figs 5.28 to 5.31. Tensile circumferential strains occurred at all the regions except at the haunch (225° or 315°) for all the live load levels. This is quite similar to test results of the research, carried out on "Buried Plastic Pipe-Performance Versus Prediction" by Rogers et al, (1995). The strain values measured at the single and double wall locations are close to each other. Similar to the test results for longitudinal strains, there was also no significant difference between the single and double wall locations for the circumferential strain measurement.

Figs 5.33 and 5.34 show the longitudinal deformations which combine vertical deflections, measured at sections 1, 2, and 3 at each live load level. These figures clearly show that the maximum deformation occurred at section 2 for each load level for both Type I and II specimens. The interesting finding is that the deflection, measured at the bottom of each section, increased with the load to 160 kips (712 kN), and then started to decrease with increasing load values higher than 160 kips (712 kN), Figs 5.33 to 5.36. Figs. 5.35 and 5.36 also indicate the effect of arching action which caused less change in the horizontal diameter, compared to that in the vertical diameter. The load, applied above the buried pipe specimens, was modified by the beneficial effect of arching action, in which a part of the load is transferred to adjacent side soil prisms. The bottom half of the section showed less deformation than the top half, indicating good soil support at the embedment

and the haunch zone. Therefore, it is inferred that the rate of deformation increases at live load levels higher than 160 kips (712 kN). The bottom half of the section resulted in less deformation than the top half, indicating good soil support at embedment and the haunch zone.

The response to live load levels, 40 and 80 kips (178 and 356 kN), which were held constant for period for 1 week to allow creep to develop in the soil-pipe system, is shown in Fig 5.32. It took about 48 hours for the increase of deflection to be stabilized at the load level 40 kips (178 kN), and 72 hours for 80 kips for both Type I and II specimens. The creep responses of both the types of specimens were quite similar, so the curve fitting for each response was carried out and compared, Fig. 5.37. The specimens, subjected to 80 kips (356 kN), have higher rates of deflection increment than those of the other specimens, subjected to 40 _kips. It is clearly indicated that the isochronous effect also exists for the HDPE pipe-soil system, Fig. 3.2, [ASTM D2990, 1995]. Therefore, it is quite important to evaluate the effect of the applied load level for long-term performance of HDPE pipe in service. The long-term changes of inside diameter, were approximately predicted for the 50 and 100 years of service at the constant load levels by conservative extrapolation in Fig. 5.37, and the values are shown in Tables 5.5 and 5.6. The changes of inside diameter, predicted for 100 years of service at 80 kips (356 kN), are 2.24% and 2.04% for Type I and II specimens. Therefore, the buried HDPE pipe specimen, subjected to the live load level, twice the AASHTO H-20 Highway Loading level, may perform well for 100 years, provided uniform backfill and notch-free conditions are guaranteed, based on i) selection of proper cover thickness, ii) uniform relative compaction and degree of saturation , iii) stable backfill material, and iv) imperfection free geometry.

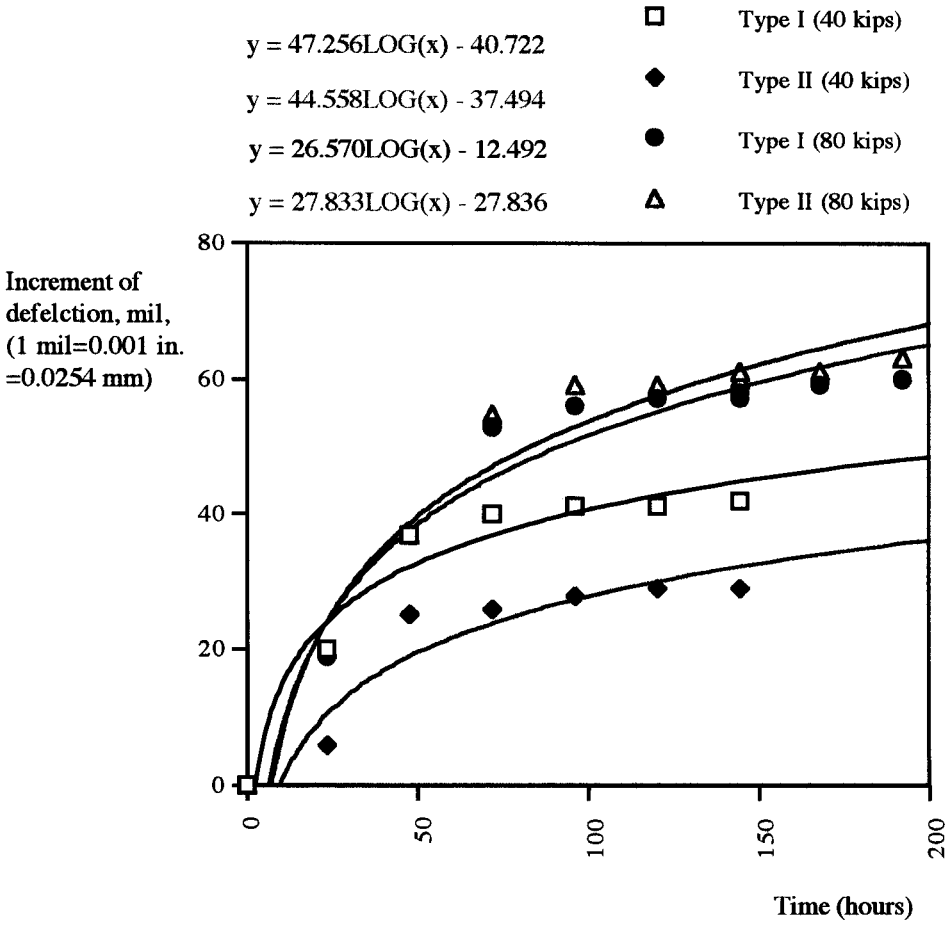

Fig. 5.37 Creep at live load levels 40 and 80 kips (178 and 356 kN)

Table 5.5 Long-term Deformation of Buried HDPE Pipe, Subjected to AASHTO H-20 Highway Loading level, Based on Direct Extrapolation Technique

	Type I specimen	Type H specimen
Change of 'diameter at 50 ears of service (%)	1.31	0.93
Change of diameter at 100 ears of service (%)	1.35	0.96

Table 5.6 Long-term Deformation of Buried HDPE Pipe, Subjected to Twice the AASHTO H-20 Highway Loading level, based on direct Expolation Technique

	Type]E[IpESimen
Change of diameter at 50 F 2.36 year of service (%)	1.98
Change of diameter at 100 2.42 year of service (%)	2.04

5.8 RESULTS OF FLEXURAL TESTING IN AIR

Flexural testing was carried out for 10 ft. long (12 in. inside diameter) and 15 ft. (24 in. inside diameter) pipe specimens, with classification 335420C. The details of the test setup and instrumentation were presented in Chapter 4. This type of testing was performed to determine i) the longitudinal stiffness of the pipes, ii) the failure modes under flexural loading, and iii) structural integrity of the joint connections. Failure was defined as the state at which the specimen continues to deflect without any increment of loading. The deflections and strains were almost identical for replicate specimens. The

5.8.1 MIDSPAN MOMENT - DEFLECTION / AXIAL STRAIN RELATIONSHIPS

Deflections and axial strains were measured at the midspan of each specimen. Figs. 5.38, and 5.39 show the deflection of the pipes during the test.

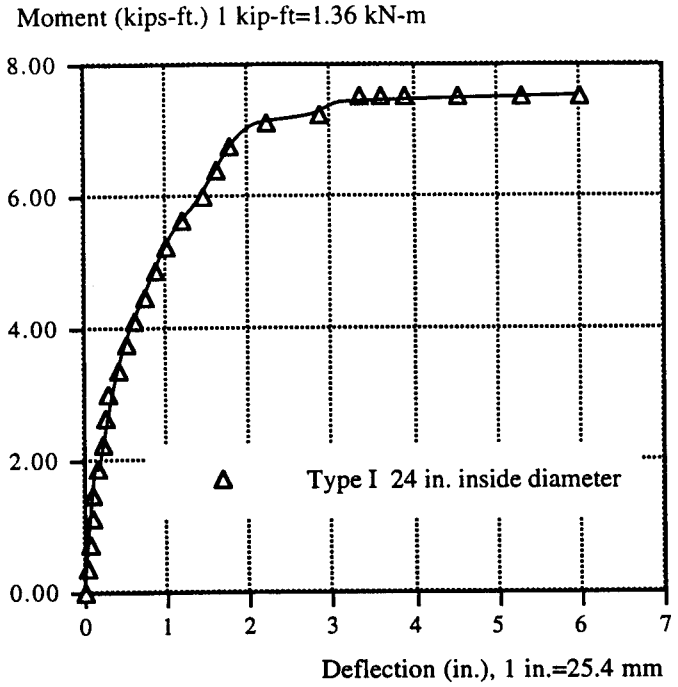

Fig. 5.38 Moment vs. midspan deflection for 24 in. inside diameter pipe

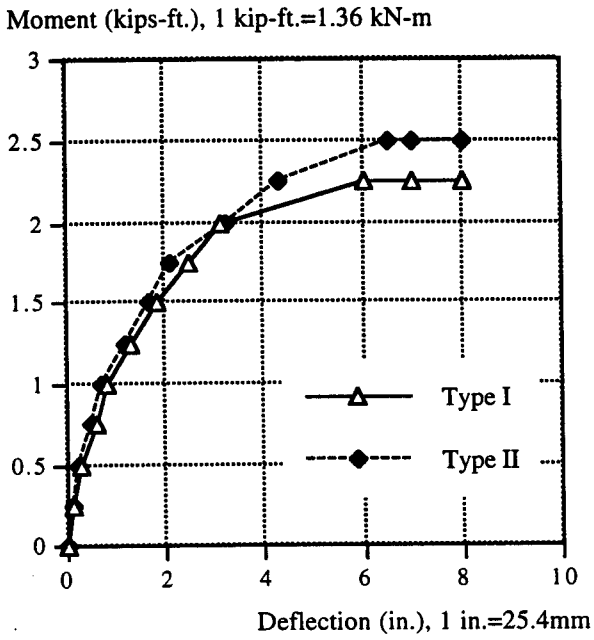

Fig. 5.39 Moment vs. midspan deflection for 12 in. inside diameter pipe

The initially linear moment/deflection curves became nonlinear at higher moment values indicating yielding. All the specimens failed due to excessive deflection at the midspan without cracking, buckling, or debonding between inner and outer liners. This mode was similar to the modes obtained by Klaiber et al. [19961 in four-point flexural testing of HDPE pipe.

The schematics of the measured deflected shapes and strains (tensile and compression), are shown in Fig. 5.40. Figs. 5.41, 5.42, and 5.43 show the axial strain changes with increasing applied moment at midspan.

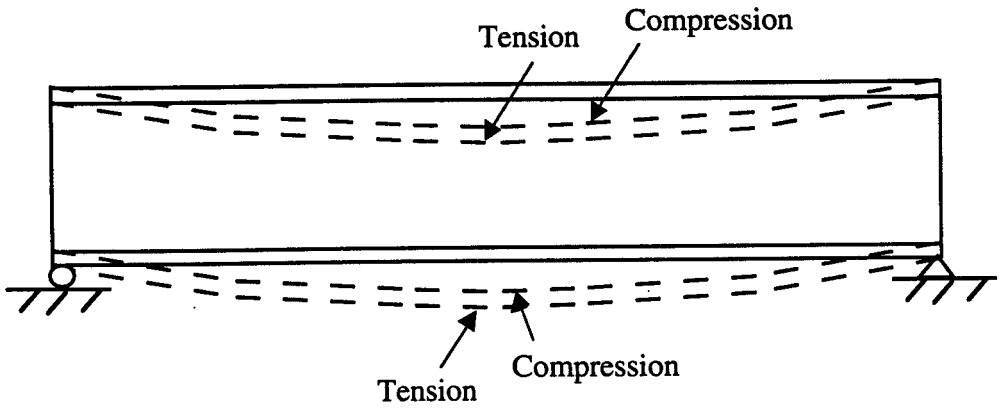

Fig. 5.40 Axial liner strains and deflected shape for specimen

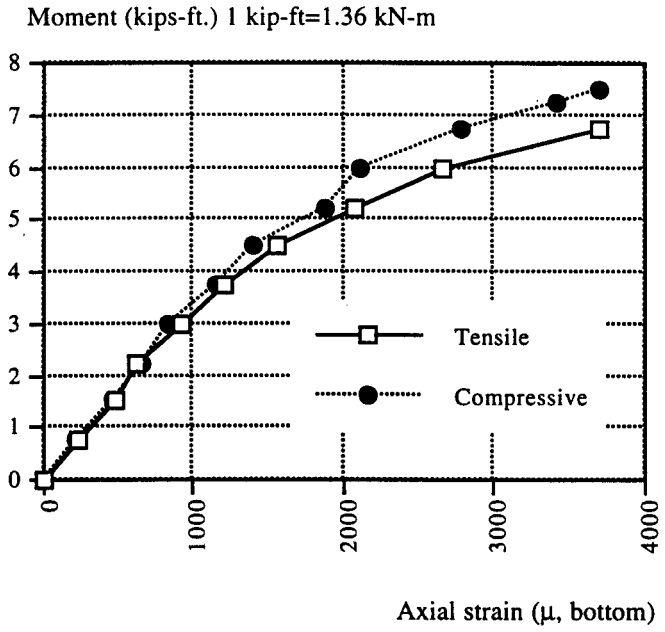

Fig. 5.41 Moment vs. axial strain (tensile) for 24 in. inside diameter pipe

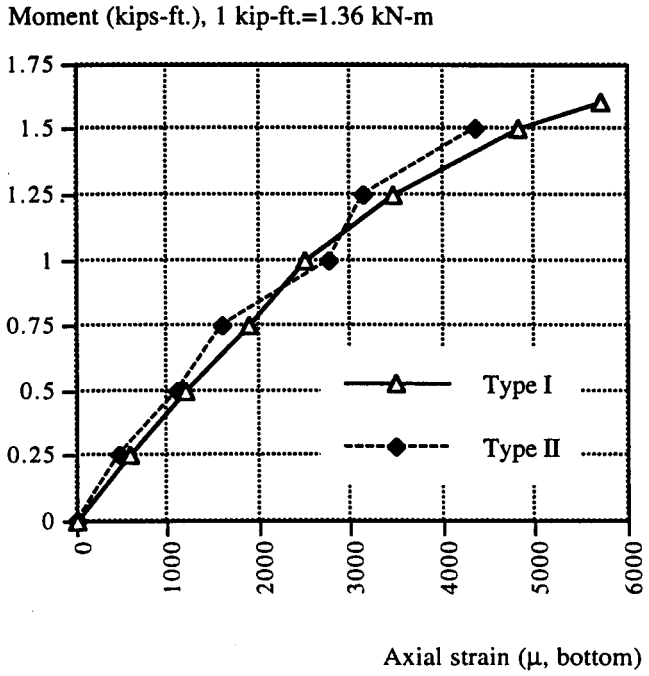

Fig. 5.42 Moment vs. axial strain (tensile) for 12 in. inside diameter pipe

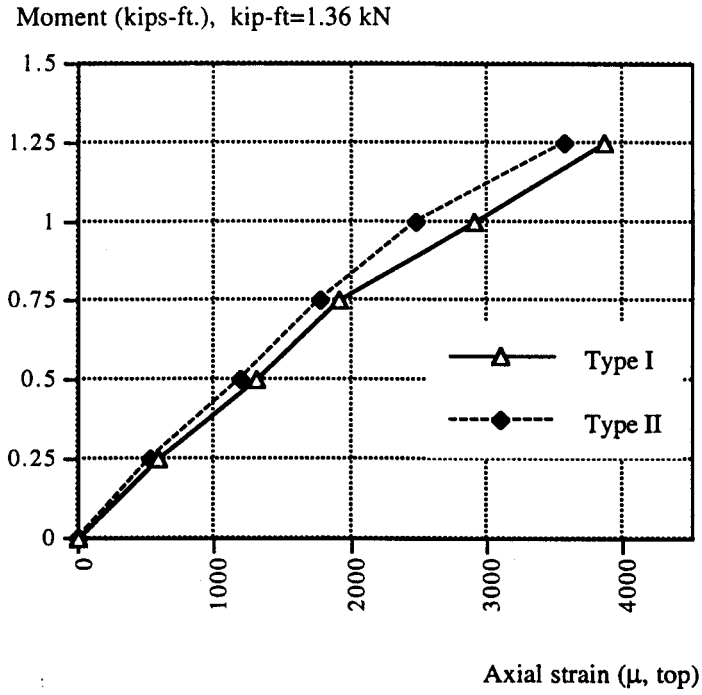

Fig. 5.43 Moment vs. axial strain (compressive) for 12 in. inside diameter pipe

Both Type I and Type II specimens showed generally similar trends, for both changes of deflection and strains, with increasing moment at the midspan. However, Type I pipe showed a little more deformation than Type II. This difference in flexural behavior can be attributed to the slight difference in pipe wall geometry. It was also found that the axial strain at the top was slightly larger than that at the bottom of the pipe specimens. When the specimen started yielding, the range of maximum axial strain at the midspan was about 2,500-6,000 μ (0.25-0.6%). Fig. 5.44 shows the excessively bent top part of the pipe at failure.

Fig. 5.44 Flexural failure of pipe

5.8.2 FLEXURAL TESTING OF THE PIPE WITH SOIL-TIGHT JOINT CONNECTION

Another set of flexural tests were carried out for pipes connected with soil-tight joints at the midspan to evaluate the structural integrity of the joints. The specimen deflected 3.5 in. due to the self weight due to rotation at the joint connection. Fig. 5.45 shows the applied moment versus midspan deflection curve.

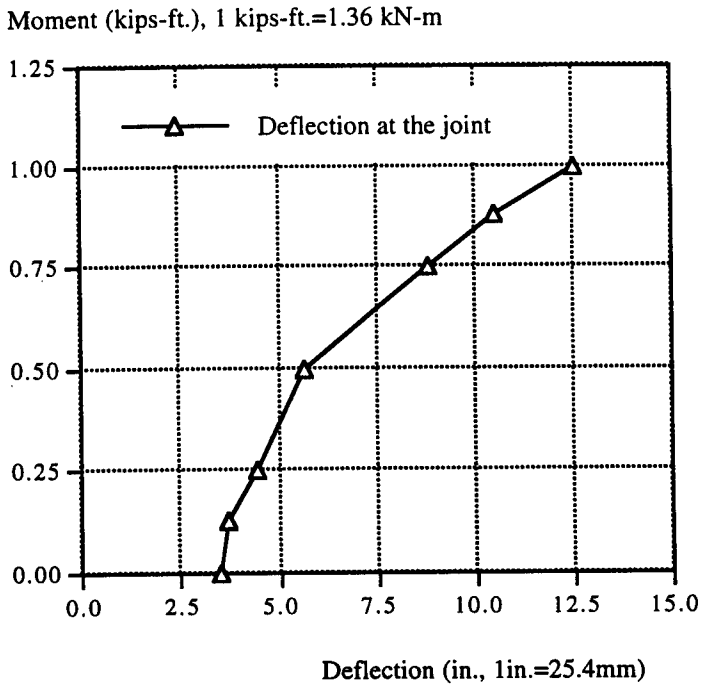

Fig. 5.45 Moment vs. midspan deflection for the pipe connected with the soil-tight joint

Inspite of the large deflection, the joints did not open up until the maximum moment applied was about 1 kip-ft. The joint had the capacity to deflect up to 9 in. Therefore, it can be inferred that the excellent rotation capability of the soil-tight joint can permit differential settlements due to possible non-uniform backfill conditions.

CHAPTER 6

ANALYTICAL INVESTIGATION

Analytical investigations are needed to evaluate the short-term and long-term performance and the predictive capacity of pipe-soil interaction. The results in Chapter 5 were used for the analytical study. This chapter is divided into three parts: i) prediction of long term properties, ii) finite element analysis, and iii) comparison of experimental and analytical investigations

6.1 PREDICTION OF LONG-TERM PROPERTIES

It is important to evaluate the viscoelastic behavior of buried HDPE pipe in service. Therefore, the long-term properties of HDPE pipe material need to be predicted prior for analysis of pipe soil interaction. Test results of creep in Chapter 5 with three different well known prediction methods were used.

6.1.1 EVALUATION OF THE LONG-TERM MODULUS USING EQUATION (AE)

Using the Arrhenius Equation (AE) approach described in Chapter 3, Section 3.6.2, the long term modulus of the HDPE can possibly be evaluated. Based on the creep test results, the Arrhenius plot for the 50% reduction of the initial flexural modulus for Type I and II specimens are shown in Figs. 6.1 [Koerner et al., 1992]. The Arrhenius plot, in which degradation data is plotted as the natural logarithm of the reciprocal of time versus the reciprocal of temperature based on equation 3.6, is used to extrapolate data. The effective activation energy, E_{act}, which is proportional to the slope of Arrhenius plot was evaluated from Fig. 6.1, as follows:

$$\frac{E_{act}}{R} = \frac{\ln(1/t_1) - \ln(1/t_2)}{(1/T_1) - (1/T_2)} \quad \text{----------(6.1)}$$

where

t=time, hour

T=temperature, °K

R=universal gas constant, which is 8.314 J/mol-K (1.987 cal/mol-K)

E_{act}=effective activation energy, J/mol (cal/mol)

The effective activation energies calculated were 153 and 141 kcal/mol (641 and 590 kJ/mol) for Type I and II specimens. Based on the equation 3.6, the time for the specified modulus decay, 50%, was evaluated for temperature levels, 20, 25, and 30 °C. These temperature levels were based on direct measurement of temperature variation around the buried pipe. Fig. 6.2 shows the inverse of the Arrhenius plot, which describes the time-temperature relationship for the HDPE pipe specimens.

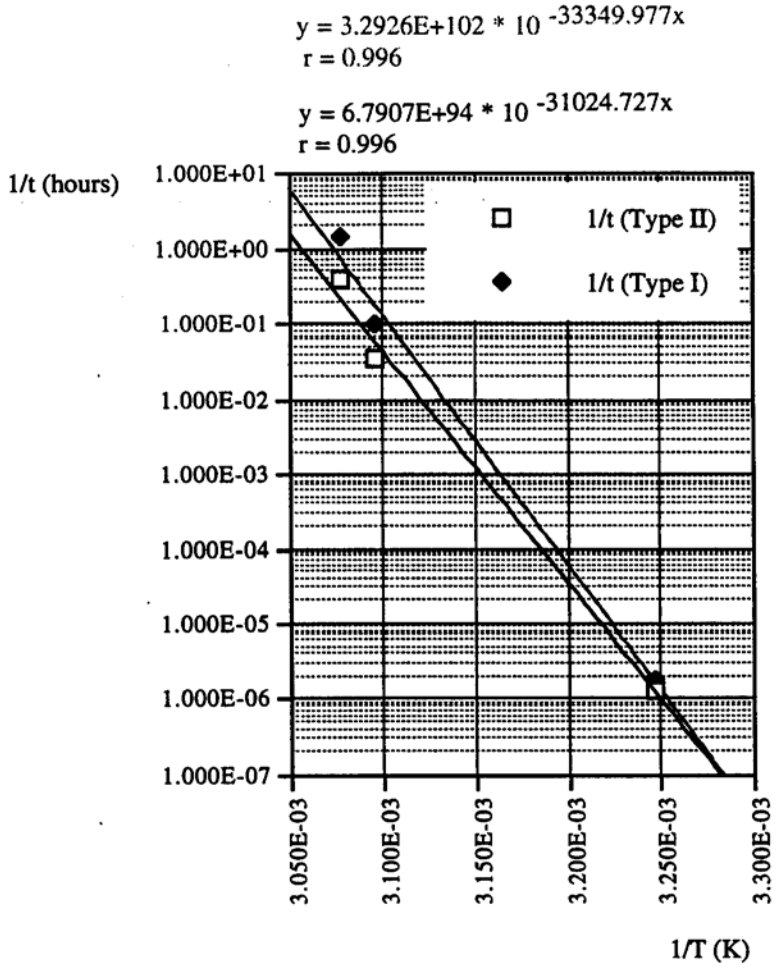

Fig. 6.1 Arrhenius plot corresponding to 50% flexural modulus reduction of HDPE

Time-temperature relations for Type I and II specimens are quite similar to each other with a marginal difference. It is implied, from Fig. 6.2, that the modulus decay rate of Type II specimen is higher than that for Type I.

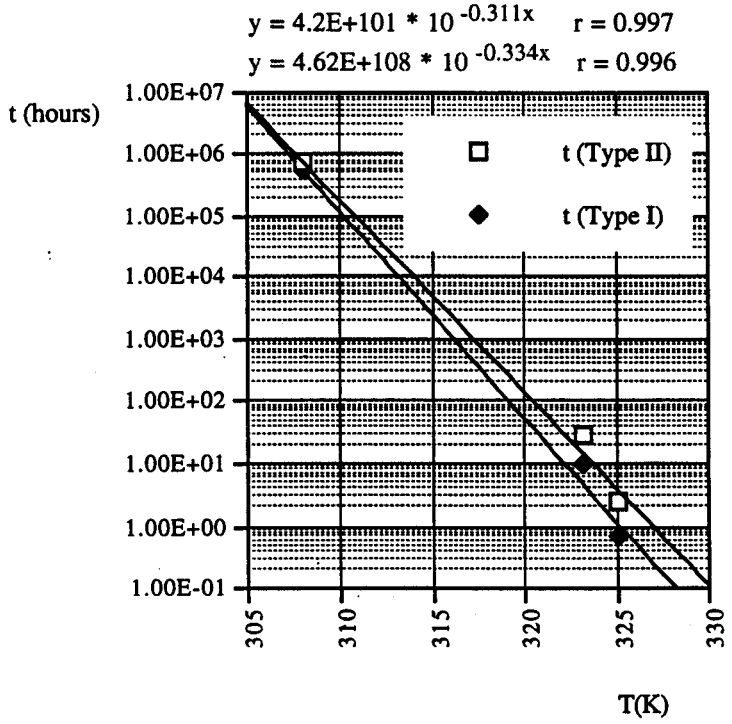

Fig. 6.2 Inverse Arrhenius plot for the time-temperature relation

6.1.2 EVALUATION OF THE LONG-TERM MODULUS* USING THE WLF EQUATION FOR TIME TEMPERATURE SUPERPOSITION

The results of the maximum 10,000 hour creep tests at different temperature levels were used to establish the longer time scale master curve. An empirical equation, referenced in equation 3.5 (WLF equation) for the horizontal shift factor, a_T, was used to construct the master curve. The established shift factors were then used to predict the long-term modulus at longer time intervals.

Several criteria, summarized by Ferry [1995] were checked to satisfy the applicability of the time-temperature shift factors on the creep test results as follows: i) exact matching of the shapes of adjacent curves of the viscoelastic function vs. log time at different temperature levels, ii) superposition of all the viscoelastic functions by the calculated values of the shift factors, a_T and b_T, and iii) taking into account of the temperature dependence of a_T and b_T.

The individual creep curves in Figs 5.9 and 5.10 show similarity of slope with temperature increase. The curves show quite good matches of the shapes at higher temperatures. Typical values of the universal constants, C_1g and C_2g (17.4 and 51.6), of the WLF equation were used for the glass transition temperature, T_g= -80 OC (-112 OF) for the HDPE pipe specimens [Aklonis and Macknight, 1983]. The WLF equation can be written using any convenient temperature as a reference temperature, T_r. The form of the

---

* In view of the need for using long-term modulus for flexure-induced circumferential and longitudinal buckling and the requirement of the time intergral in the characterization of viscoelastic materials, modulus decay is an important parameter.

equation remains the same, but the values of the constants C_1 and C_2 change. Therefore, using the universal constants $C_1 g$ and $C_2 g$ (17.4 and 51.6), and the semiempirical Doolittle equation [Aklonis and Macknight, 1983], C_1 and C_2 for the reference temperature 20 ^oC (68 ^oF) were evaluated for the calculation of the shift factor [Aklonis and Macknight, 1983]. The starting point is the Doolittle equation: [Aklonis and Macknight, 1983]:

$$\ln \eta = \ln A + B\left(\frac{V - V_f}{V_f}\right) \quad \text{----------(6.2)}$$

where

η=tensile viscosity

A and B=constants for the tensile viscosity

V=total volume

V_f=free volume available

The fractional free volume increases linearly with the temperature [Aklonis and Macknight, 1983] i.e.

$$f = f_g + \alpha_f (T - T_g) \quad \text{----------(6,3)}$$

where

f--fractional free volume at T, $T>T_g$

f_g=fractional free volume at T_g

α_f--coefficient of thermal expansion of the fractional free volume above T_g

In terms of equation 6.3, the Doolittle equation becomes:

$$\log a_T = -\frac{B}{2.303 f_g}\left[\frac{T-T_g}{\left(f_g/\alpha_f\right)+T-T_g}\right] = -C_1\left[\frac{T-T_g}{C_2+T-T_g}\right] \quad \text{----------(6.4)}$$

Using equations 6.3 and 6.4, C_1 and C_2 can be simplified as follows:

$$C_1 = \frac{C_1^g C_2^g}{C_2^g + (T_r - T_g)} = 5.92 \quad \text{----------(6.5)}$$

$$C_2 = C_2^g + (T_r - T_g) = 151.6 \quad \text{----------(6.6)}$$

Therefore, the horizontal shift factor can be caculated for the HDPE pipe specimen as follows:

$$\log a_T = -5.92\left(\frac{T-T_r}{151.6+T-T_r}\right) \quad \text{----------(6.7)}$$

Fig.6.3 shows the change of the horizontal shift factor at different temperature levels.

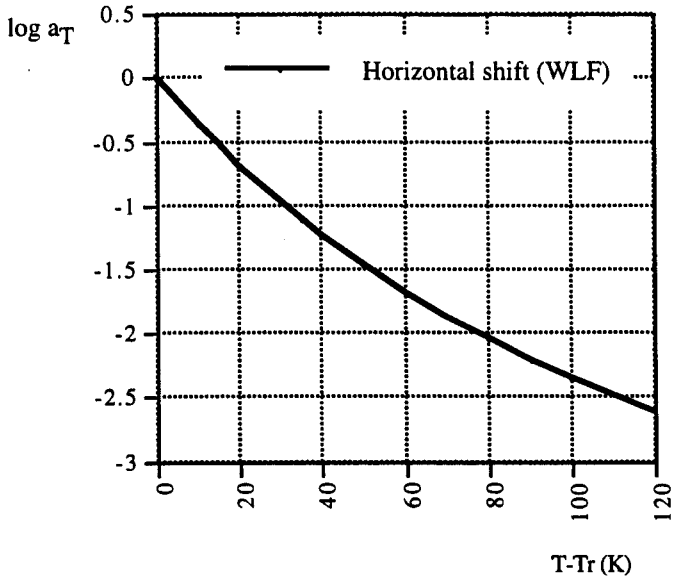

Fig.6.3 Horizontal shift factors based on the WLF equation

Vertical temperature shifting is necessary to accommodate the change of the degree of crystallinity with the temperature for the HDPE pipe specimens, which are made of semicrystalline polymeric material [Tobolsky,1960]. The vertical shift factor, b_T, can be defined as follows [Miyano, 1996]:

$$b_T(T) = \frac{E(t,T)}{E(t,T_r)} \quad \text{----------(6.8)}$$

The vertical shift factors at different temperatures and the master curve are shown in Figs. 6.4 , 6.5, and 6.6. From Figs. 6.5 and 6.6, the long term (25, 50, and 100 years)

moduli were estimated, Table 6.1. Master curves for the prediction of long-term modulus were constructed by appropriate horizontal shifts for each temperature level with vertical correction shifts.

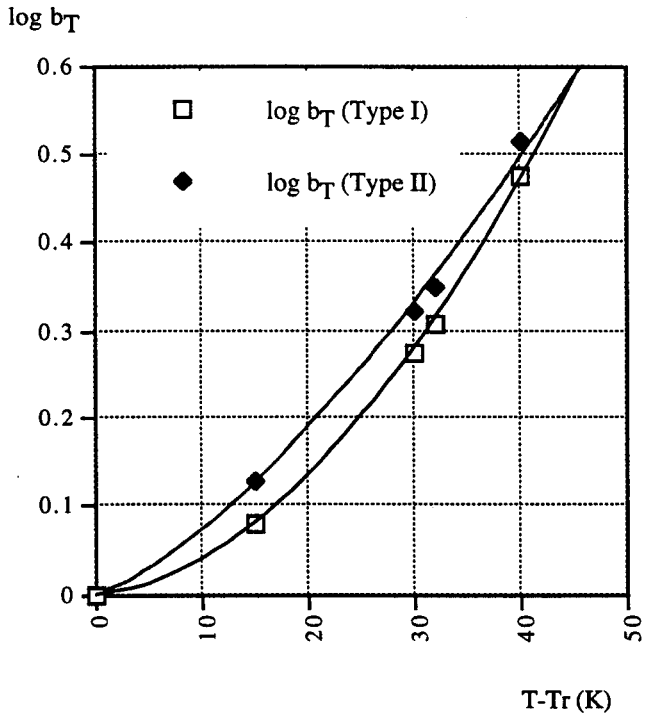

Fig. 6.4 Vertical shift factors, based on the WLF equation

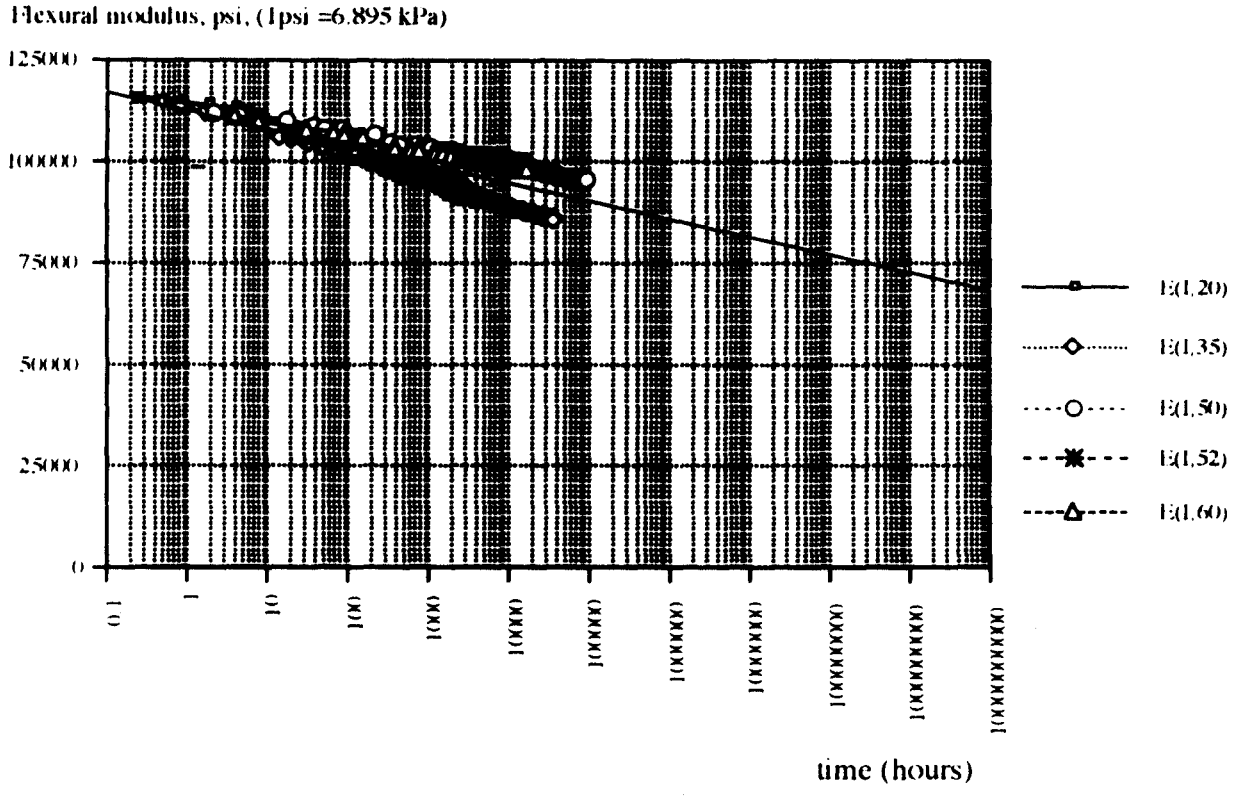

Fig. 6.5 Master curve , based on WLF equation for Type I specimen

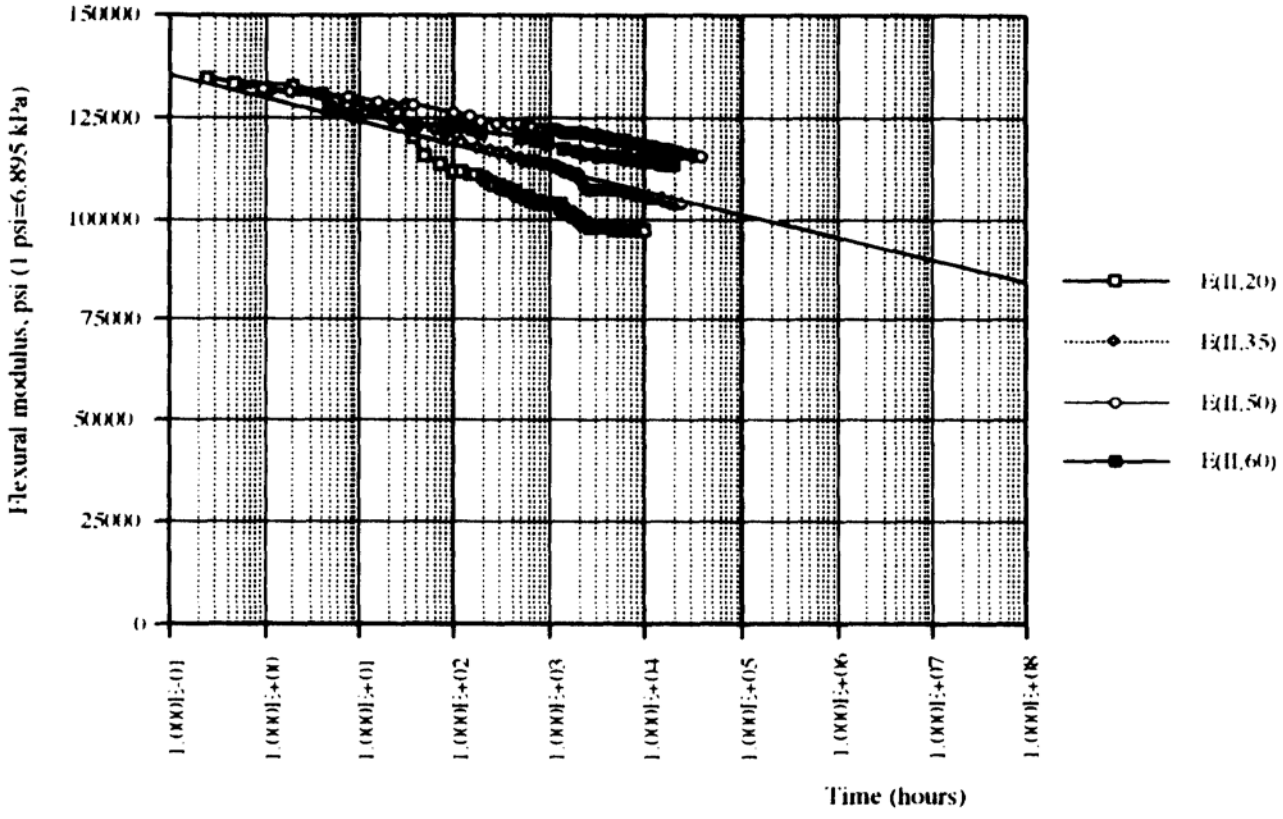

Fig. 6.6 Master curve , based on WLF equation for Type II specimen

Table 6.1 Long-Term Flexural Modulus, Based on WLF

Specimen types	25 ears	50 ears	100 ears
Type I	90.0 ksi (621 MPa)	88.8 ksi (612 MPa)	87.6 ksi (604 MPa)
Type II	99.1 ksi (683 MPa)	96.2 ksi (663 MPa)	95.0 ksi (655 MPa)

The decay of the flexural modulus after 100 years of service was about 24% of the initial modulus for Type I specimen and 29% for Type II. Therefore, the decay rate of the Type II specimen is a little larger than that of Type I, even though the 100 year modulus of Type II specimen is higher than that of Type I.

6.1.3 EVALUATION OF THE LONG-TERM MODULUS USING BIDIRECTIONAL SHIFTING METHOD (BSM)

The Bidirectional Shifting Method (BSM), which was introduced by Popelar et al, [1990], for consolidating elevated temperature data for polyethylene gas pipe materials, as an alternative method to predict the life, was used to construct master curves for non-pressurized HDPE sewer pipe material using creep test data. In this procedure, no curve fitting is needed which enables even a single data point, representing any viscoelastic phenomenon determined at a given test temperature to be shifted to another temperature Based on the time-temperature superposition principle, the horizontal and vertical shif functions, a_T and b_T, respectively, are given by:

$$a_T = \exp\left[-0.109\left(T - T_r\right)\right] \quad \text{----------(6.9)}$$

$$b_T = \exp\left[0.0116\left(T - T_r\right)\right] \quad \text{----------(6.10)}$$

The individual creep curves at different temperature levels (Figs 5.9 and 5.10) were assembled to establish the longer-time scale master curve by the bidirectional shift, referenced above. Fig. 6.7 and 6.8 show the change of horizontal and vertical shift factors at different temperature levels. Figs. 6.9 and 6.10 show the longer-time scale master curve based on bidirectional shifting for Type I and II specimens.

From the Figs. 6.9 and 6.10, the long-term (25, 50, and 100 years) moduli were estimated, in Table 6.2. The decay of the flexural modulus after 100 years of service was about 40% of the initial modulus for the Type I specimen and 47% for Type II. The rates of modulus decay were quite similar for both Type I and II specimens. Type I specimen showed better coherence of the master curves with good overlap of data at different temperatures, compared to Type II.

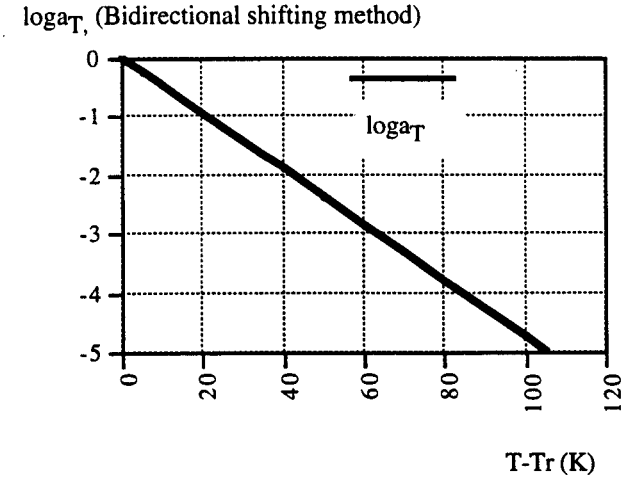

Fig. 6.7 Horizontal shift factors, based on the bidirectional shift method

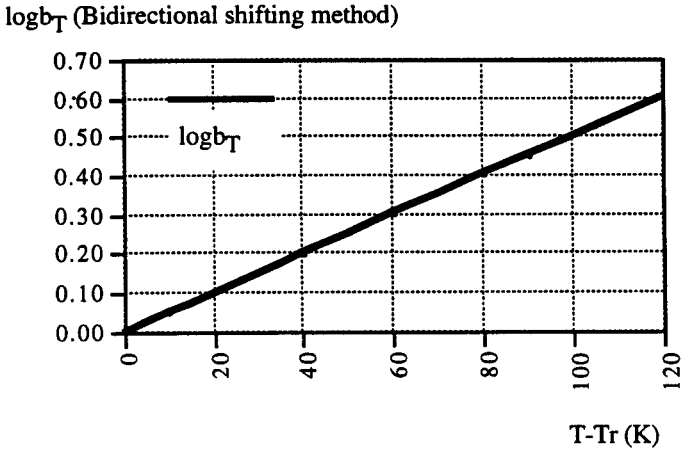

Fig. 6.8 Vertical shift factors, based on the bidirectional shift method

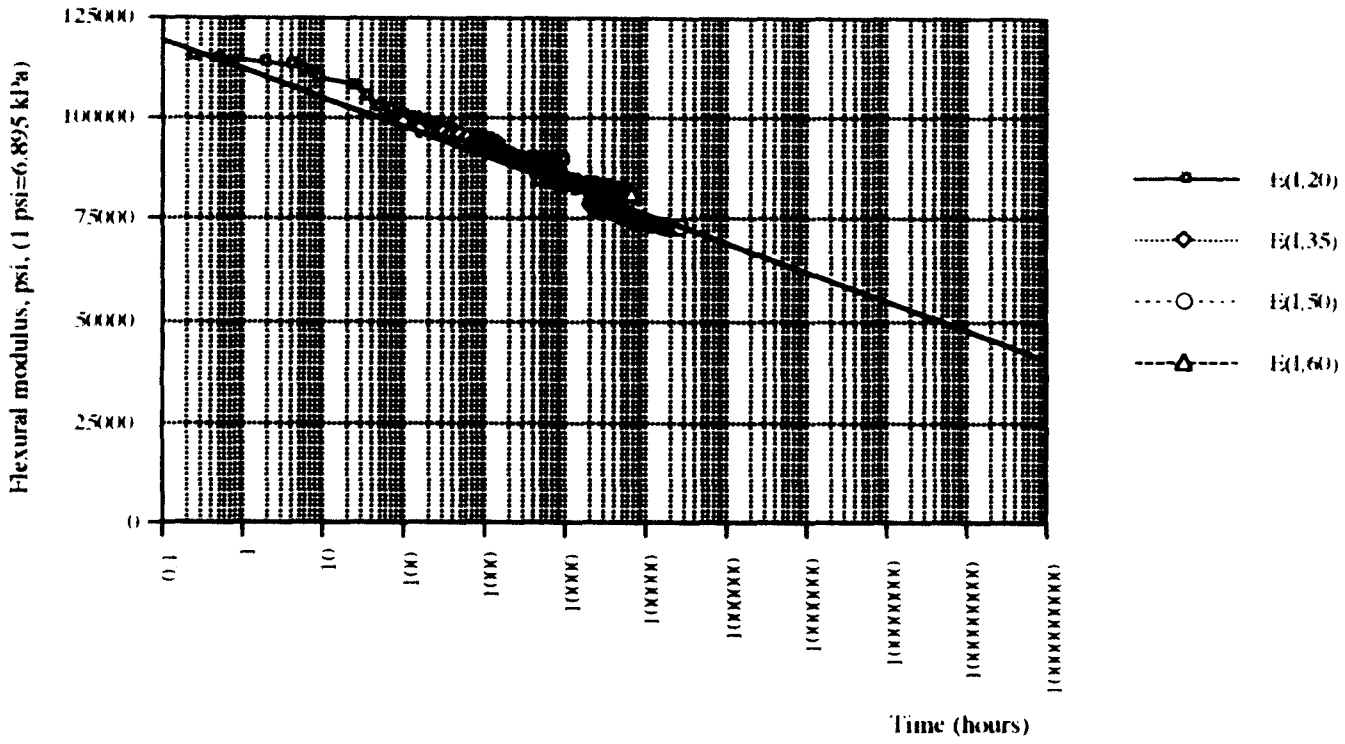

Fig. 6.9 Master curve, based on bidirectional method for Type I specimen

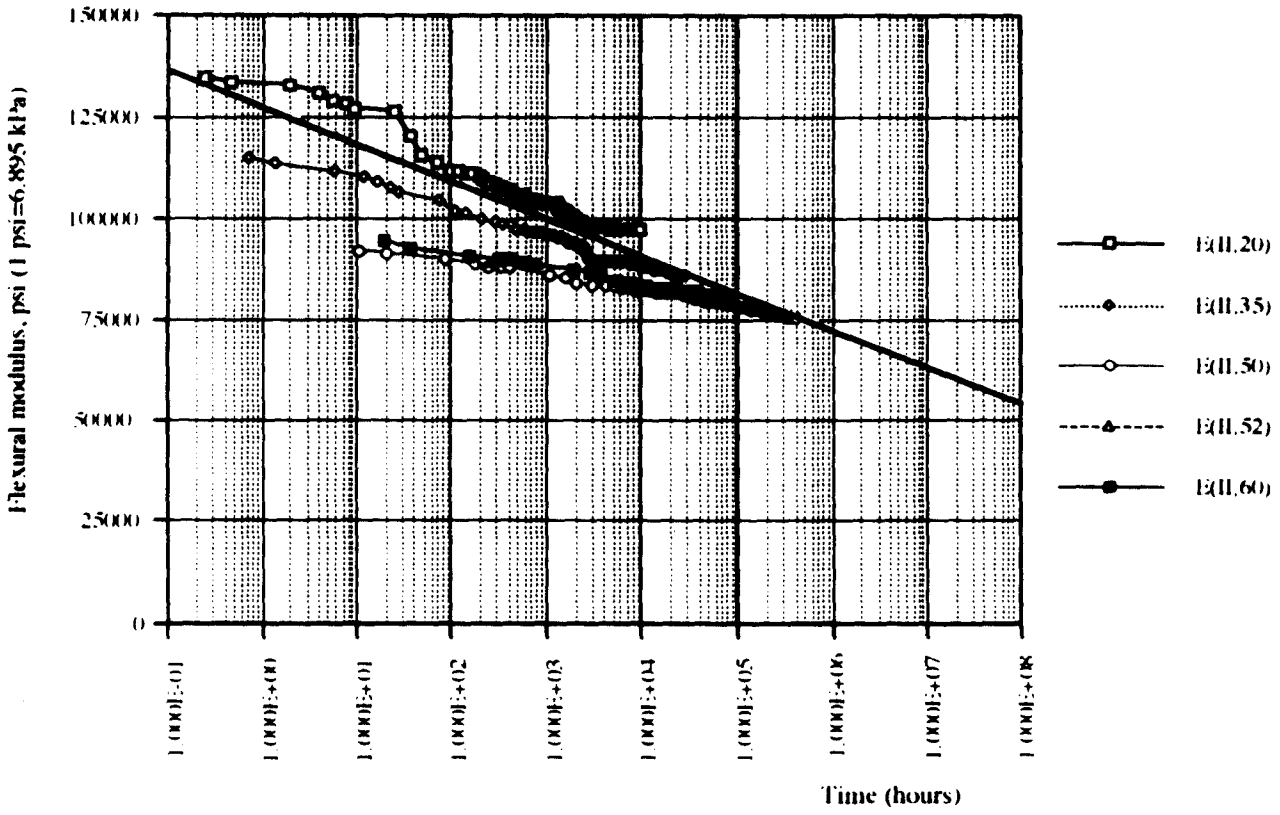

Fig. 6.10 Master curve, based on bidirectional method for Type II specimen

Table 6.2 Long-Term Flexural Modulus, Based on the the Bidirectional Shifting Method

Specimen types	25 years	50 years	100 years
Type I	75 ksi (517 MPa)	71.9 ksi (496 MPa)	69 ksi (476 MPa)
Type II	78.5 ksi (541 MPa)	74.5 ksi (514 MPa)	71.8 ksi (495 MPa)

6.2 COMPARISON OF ARRHENIUS EQUATION (AE)-BASED ANALYSIS, WLF TIME TEMPERATURE SUPERPOSITION, AND BIDIRECTIONAL SHIFTING METHOD (BSM)

The horizontal shift factors for each different method were compared in Fig. 6.11 after conversion of Fig. 6.1 to 6.2. Unlike amorphous polymers, for a HDPE pipe specimen, the semicrystalline polymer shows that horizontal shift factors of WLF equation do not match with those of Arrhenius equation, Fig. 6.11.

The master curves, based on the Arrhenius equation, are plotted for comparison with the WLF equation and the bidirectional shifting method, Figs. 6.12 and 6.13. Figs. 6.12 and 6.13 show the prediction of the long-term modulus, and the values (25, 50, and 100 years) are shown in Table 6.3. The decay of the flexural modulus after 100 years of service was about 32 % of initial modulus for Type I specimen and 36 % for Type II. The rates of the modulus decay were quite similar for both Type I and II specimens.

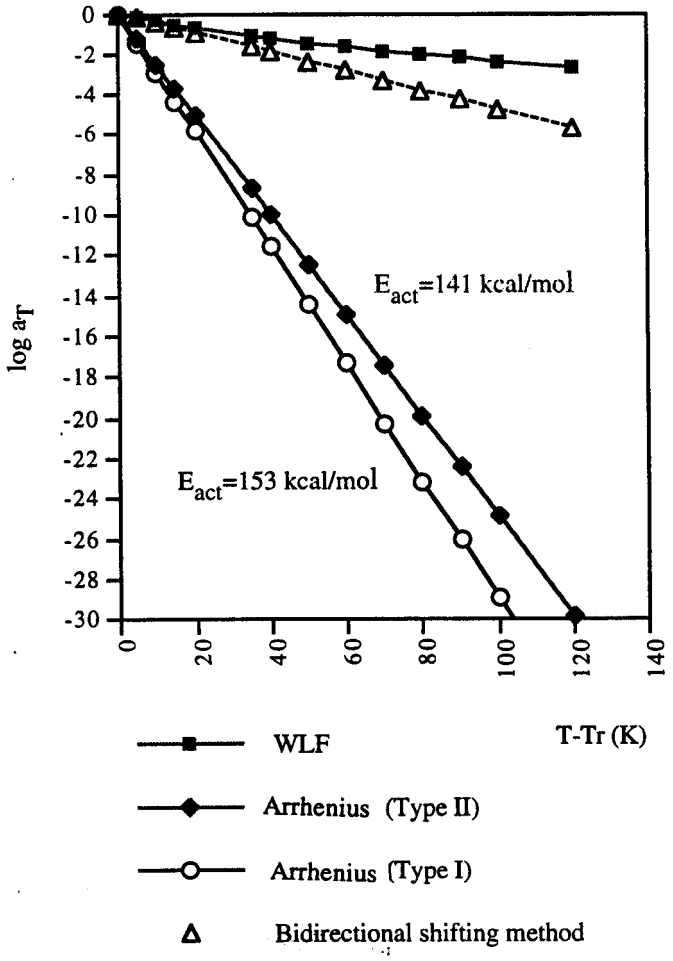

Fig. 6.11 Comparison of horizontal shift factors

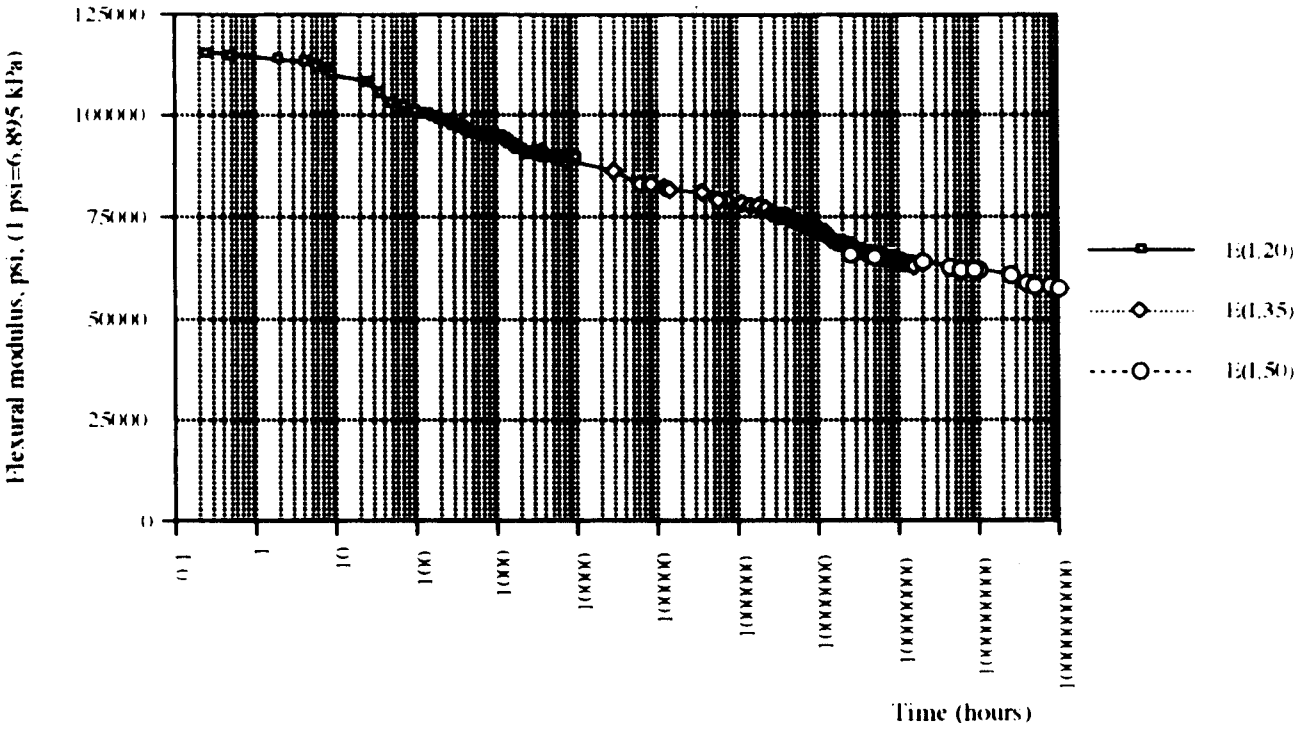

Fig. 6.12 Master curve for Type I specimen, based on Arrhenius equation

Fig. 6.13 Master curve for Type II specimen, based on Arrhenius equation

Table 6.3 Long-Term Flexural Modulus, Based on the Arrhenius Equation

Specimen types	25 ears	= 50 ears -T	100 ears
Type 1	82.5 ksi (569 MPa)	79.7 ksi (550 MPa)	78.1 ksi (539 MPa)
Type II	86.5 ksi (596 MPa)	84.3 ksi (581 MPa)	81.3 ksi (561 MPa)

The different prediction procedures for the long-term modulus of HDPE pipe specimens were compared by logarithmic regression curve fitting of individual master curves, and histograms, plotted in Figs. 6.14, 6.15, 6.16, and 6.17.

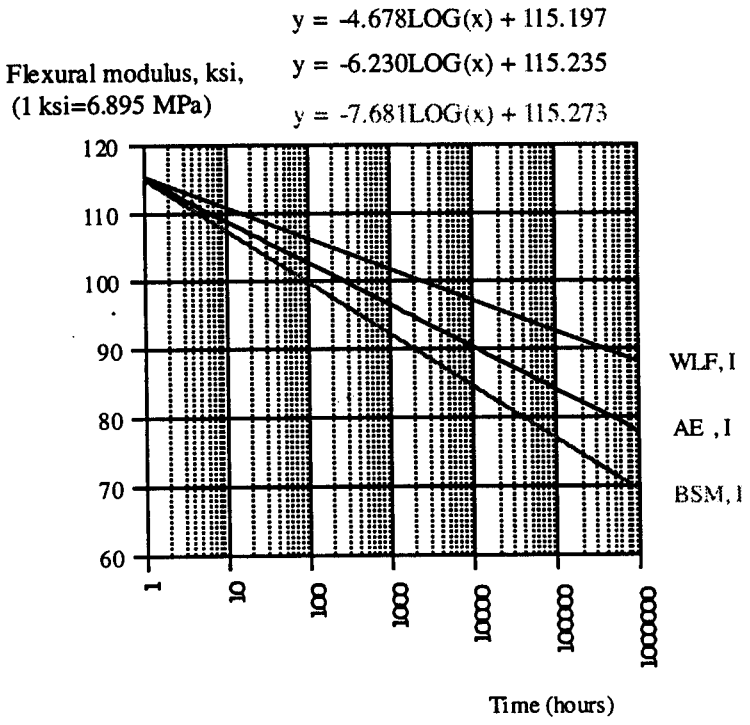

Fig. 6.14 Comparison of the prediction methods for the long-term property of Type I specimen

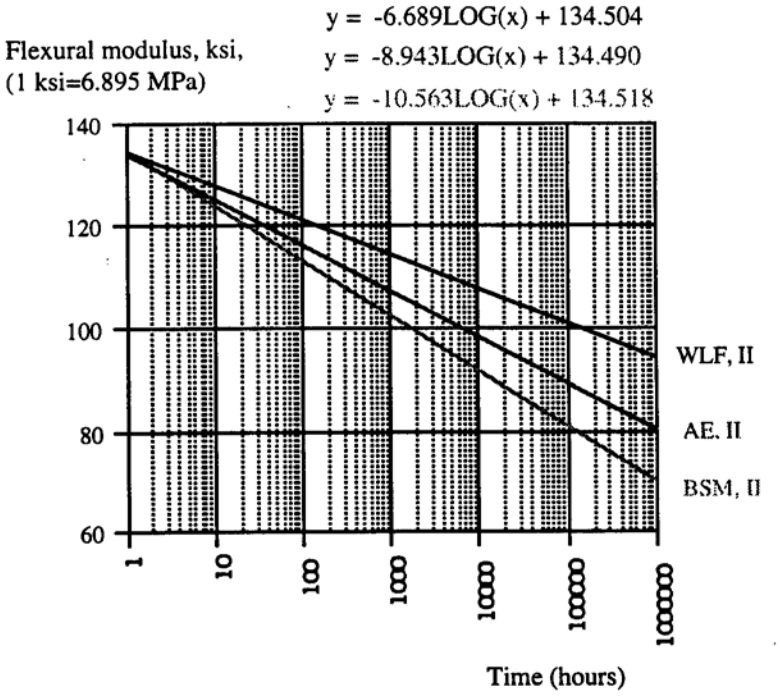

Fig. 6.15 Comparison of the prediction methods for the long-term property of Type II specimen

Based on the three different prediction methods of long-term properties, the overall three dimensional viscoelastic behavior of Type I and II specimens was plotted in Figs. 6.18 to 6.23. For the design of the HDPE pipe, the use of long-term modulus value, based on bidirectional shifting method (BSM) is the most conservative for the necessary calculations, e.g. deflection, buckling stresses, and bending strains.

The rate of modulus decay, based on WLF equations, was observed to be quite smaller than the values from other two methods with large vertical shifting corrections. This large vertical shift compared to the horizontal shift causes scattering of data, and makes prediction of the long-term modulus quite difficult, due to the change of degree of

crystallinity with temperature. Some research investigations were carried out to predict the service life of HDPE and MDPE geosynthetic material using the WLF equation. Aklonis and MacKnight, [1983], indicated that the WLF equation is not applicable to semicrystalline polymers, although it was proved to be valid and generally applicable to amorphous polymers. Therefore, use of the long-term modulus based on the WLF equation, simply choosing the universal constants C19=17.4 and C29=51.6 for the horizontal shift factor, aT, (Equation 5.5) may overestimate the service life of the HDPE pipe. The AE and BSM methods give master curves with good overlap of data from different temperature levels. These master curves show a maximum of 9.5 ksi (65 MPa) difference between the 100-year flexural moduli, based on the two methods.

BSM is the most conservative method to predict the long-term modulus, for the design procedure of pipe installation. The flexural modulus reductions after 100 years of service, are 40% and 46% of the initial modulus for Types I and II specimens, respectively. Due to the slight geometrical difference between the two different types of specimens, the 100-year moduli were 69 ksi (476 MPa) and 71.8 ksi (495 MPa) for Type l and II specimens, even though the Type II specimen had the higher rate of decay. Therefore, the HDPE pipe made with the new cell classification has a stiffness level good enough to meet the current specifications, 335420C, after 100 years of service. The IOC year flexural modulus of the new cell classification is close to the initial modulus for the commonly used cell classification, 324420C, in the U.S.

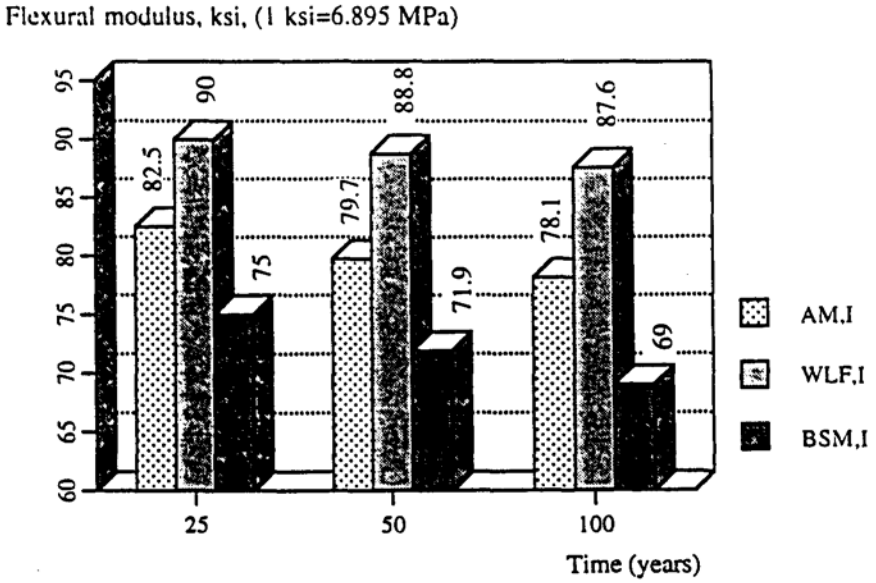

Fig. 6.16 Comparison of the prediction methods for 25, 50, 100 year modulus of Type I specimen

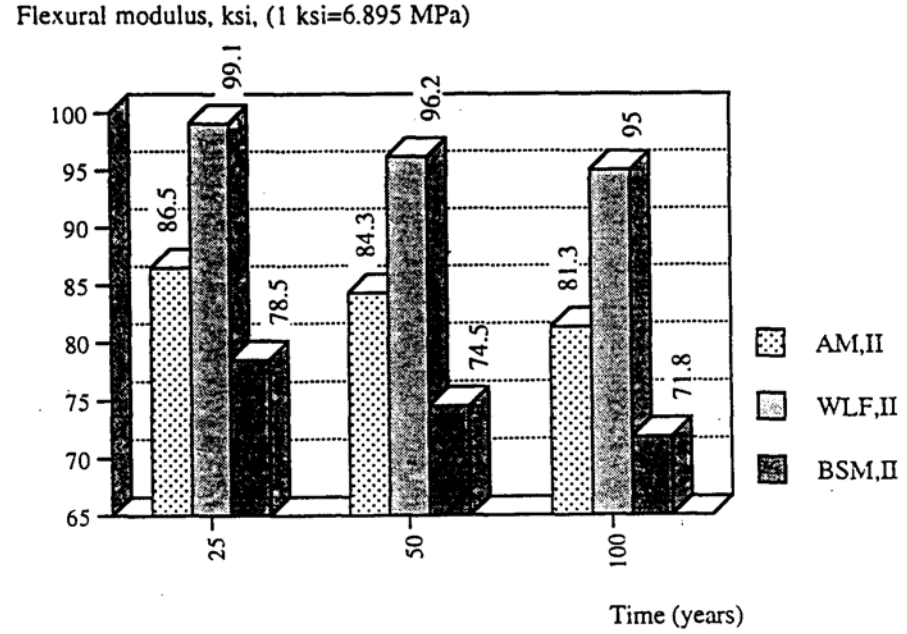

Fig. 6.17 Comparison of the prediction methods for 25, 50, 100 year modulus of Type II specimen

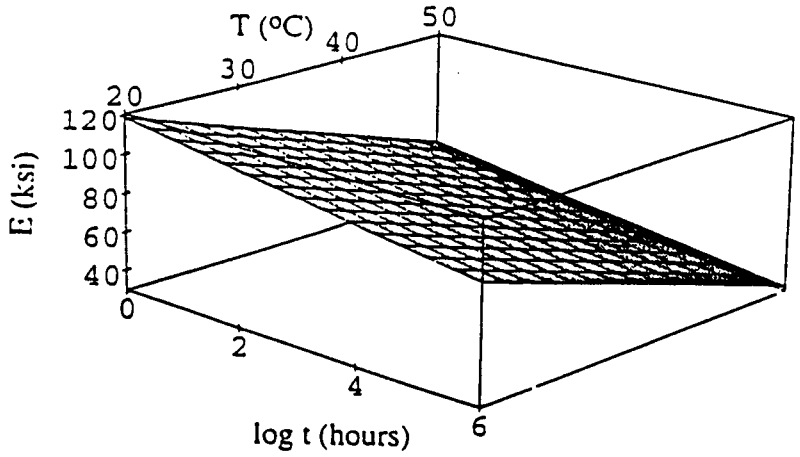

Fig. 6.18 Viscoelastic behavior of Type I specimen, based on WLF equation

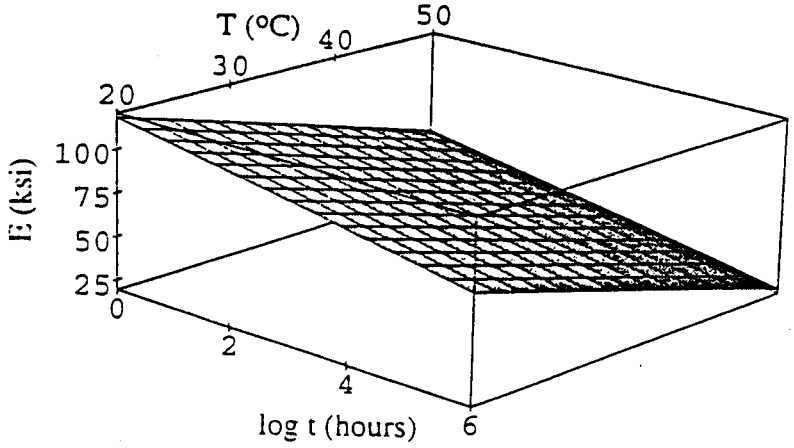

Fig. 6.19 Viscoelastic behavior of Type I specimen, based on Arrhenius equation

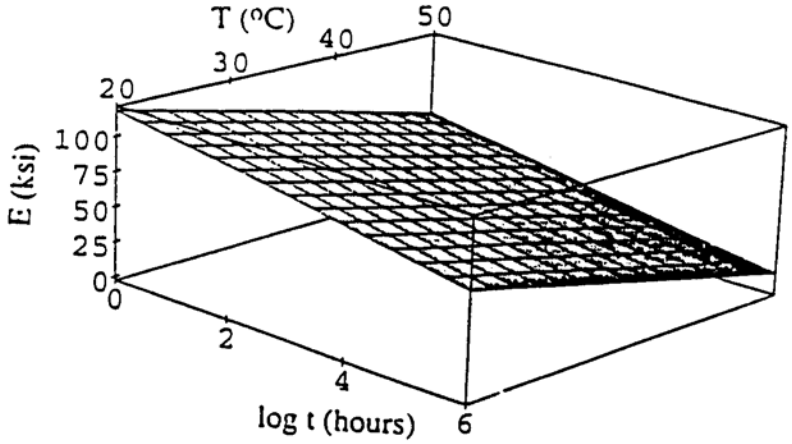

Fig. 6.20 Viscoelastic behavior of Type I specimen,
based on bidirectional shifting method

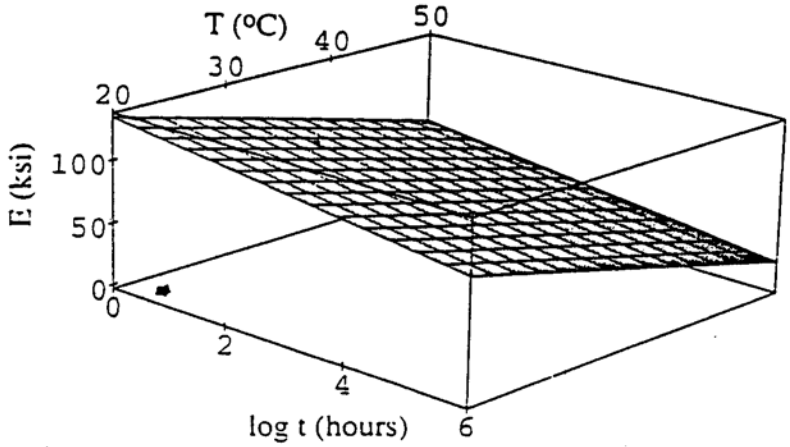

Fig. 6.21 Viscoelastic behavior of Type II specimen, based on WLF equation

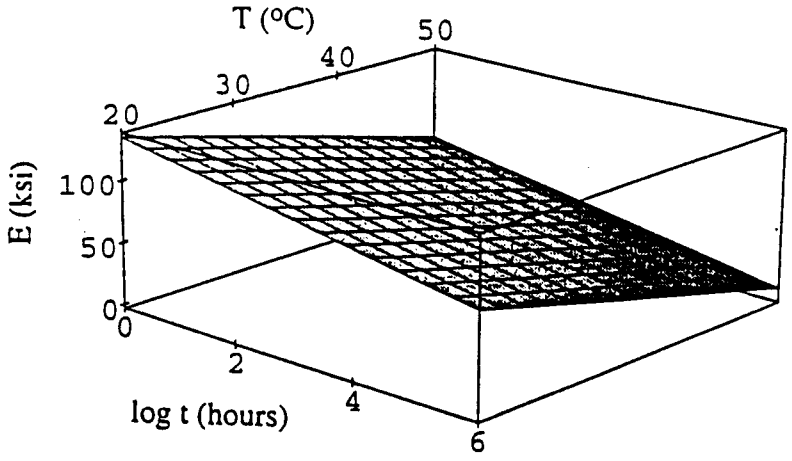

Fig. 6.22 Viscoelastic behavior of Type II specimen, based on Arrhenius equation

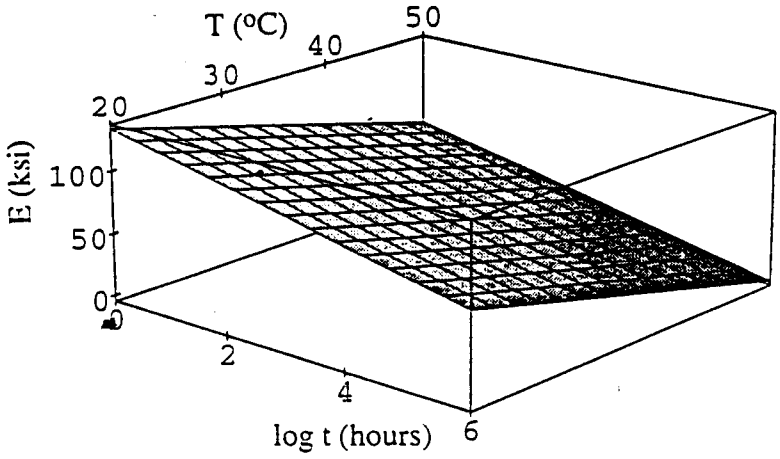

Fig. 6.23 Viscoelastic behavior of Type II specimen,
based on bidirectional shifting method

6.3 VISCOELASTIC MODELING

Based on creep test results, expanded to longer time scale (one million hours =100 years) by the BSM (bidirectional shifting method), Figs. 6.12 and 6.13, three different viscoelastic models were developed by backward substitution. Using multi-degree VoigtKelvin model, the viscoelastic behavior of the Type I and II HDPE pipe specimens (based on BSM) can be successfully expressed as mechanical analogs, which are combinations of springs and dashpots. Maxwell and Voigt models for the HDPE specimens were developed and compared with the Voigt-Kelvin model.

For the Maxwell model, a series combination of spring and dashpot (Maxwell elements) was used, Fig 6.24, [Aklonis and MacKnight, 1983]. The response of the model to creep is as follows:

$$D(t)=D+t/\eta \quad \text{---------- (6.11)}$$

where

$D=1/E_o=\epsilon_o/\sigma_o$=instantaneous response of Hookean spring, $(ksi)^{-1}$, $(MPa)^{-1}$

ϵ_o=instantaneous strain

σ_o=instantaneous stress, ksi (MPa) E=instantaneous modulus, ksi (MPa)

$\eta=\tau E$=viscosity of the liquid in the dashpot, ksi (MPa)

τ=proportionality constant

The average value of il was calculated from backward substitution in equation 6.11 at different time intervals using the creep test data, expanded by BSM. The creep compliance of the Maxwell model can be represented as follows:

For the Type I specimen

$$D(t) = 8.68 \times 10^{-3} + \frac{t}{1.38 \times 10^{6}}, \text{ (ksi)}^{-1} \quad \text{----------} (6.12)$$

For the Type II specimen

$$D(t) = 7.44 \times 10^{-3} + \frac{t}{1.29 \times 10^{6}}, \text{ (ksi)}^{-1} \quad \text{----------} (6.13)$$

The Voigt model, which consists of single spring and dashpot in parallel, Fig. 6.25, was used to evaluate the creep response of the HDPE pipe specimens. The average value of η was calculated in a manner similar to that for the Maxwell model. The creep compliance of the Voigt model, equation 6.14 can be represented by equations 6.15 and 6.16 for Type I and II specimens [Aklonis and MacKnight, 1983].

$$D(t) = D(1 - e^{-t/\tau}) \quad \text{----------} (6.14)$$

For the Type I specimen

$$D(t) = 8.68 \times 10^{-3}(1 - e^{-t/9660}) \text{ (ksi)}^{-1} \quad \text{----------} (6.15)$$

For the Type II specimen

$$D(t) = 7.44 \times 10^{-3}(1 - e^{-t/6918}) \text{ (ksi)}^{-1} \quad \text{----------} (6.16)$$

The multi-degree Voigt-Kelvin model is a generalization of the Voigt element that results from connecting Voigt elements in series, Fig. 6.26, [Aklonis and MacKnight, 1983], and the compliance function is as follows:

$$D(t) = \sum_{i=1}^{n} D_i(1 - e^{-t/\tau_i}) \quad \text{----------} (6.17)$$

The multi-degree Voigt-Kelvin model (with n=7) enables the representation of the viscoelastic response of HDPE pipe specimen realistically by calculation of creep compliance. The variations of ii for Type I and II specimens are shown in Table 6.4. Figs. 6.27 and 6.28 show the comparison of the three different viscoelastic models. The Maxwell model shows similar viscoelastic response only up to 10,000 hours, with other two models for both Type I and II specimens. However, the response of the single-degree Voigt model is similar to that of the multi-degree Voigt-Kelvin model for both specimen types. Therefore, the long-term (up to 100-year) creep compliance of HDPE pipe specimen can be predicted by a simple single-degree Voigt model but not the Maxwell model. Furthermore, the long term viscoelastic response of HDPE pipe can be fine-tuned by expanding the Voigt model, which yields the multi-degree Voigt-Kelvin model.

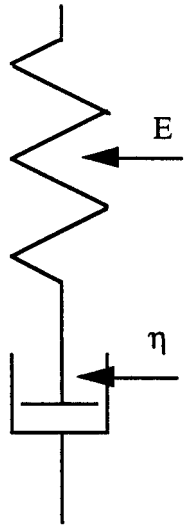

Fig. 6.24 Maxwell model

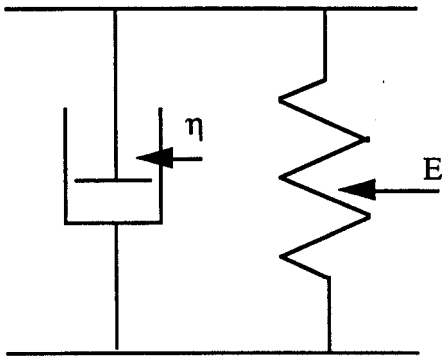

Fig. 6.25 Voigt model

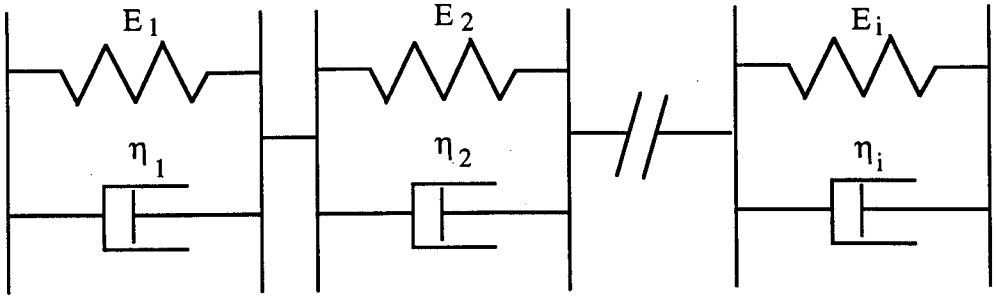

Fig. 6.26 Voigt-Kelvin model

Table 6.4 Proportionality Constants for the Voigt-Kelvin model

i	τ_i for Type I specimens	τ_i for Type II specimens
1	N/A	N/A
2	138	138
3	1,282	1,025
4	10,605	9,294
5	116,009	84,890
6	929,368	769,231
7	8,185,474	5,882,353

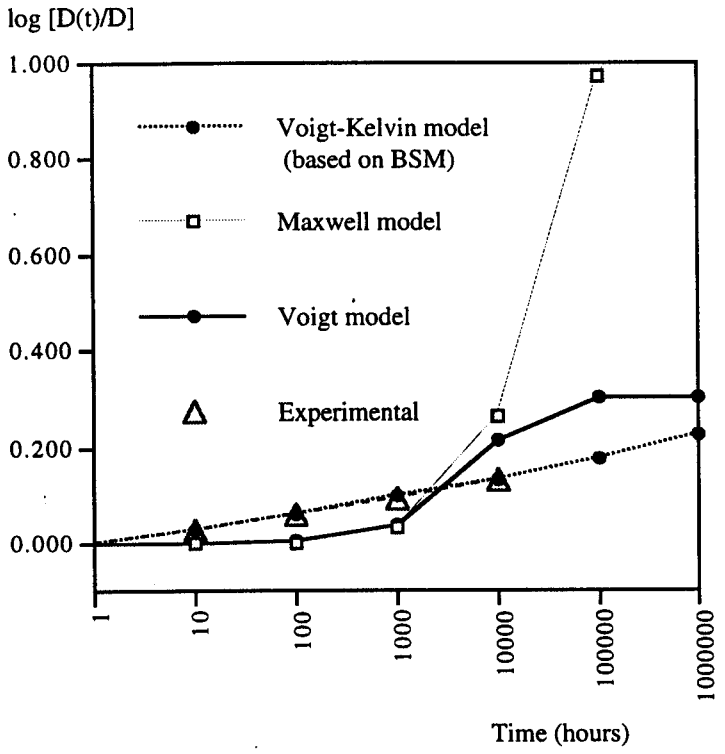

Fig. 6.27 Comparison of viscoelastic models for Type I specimen

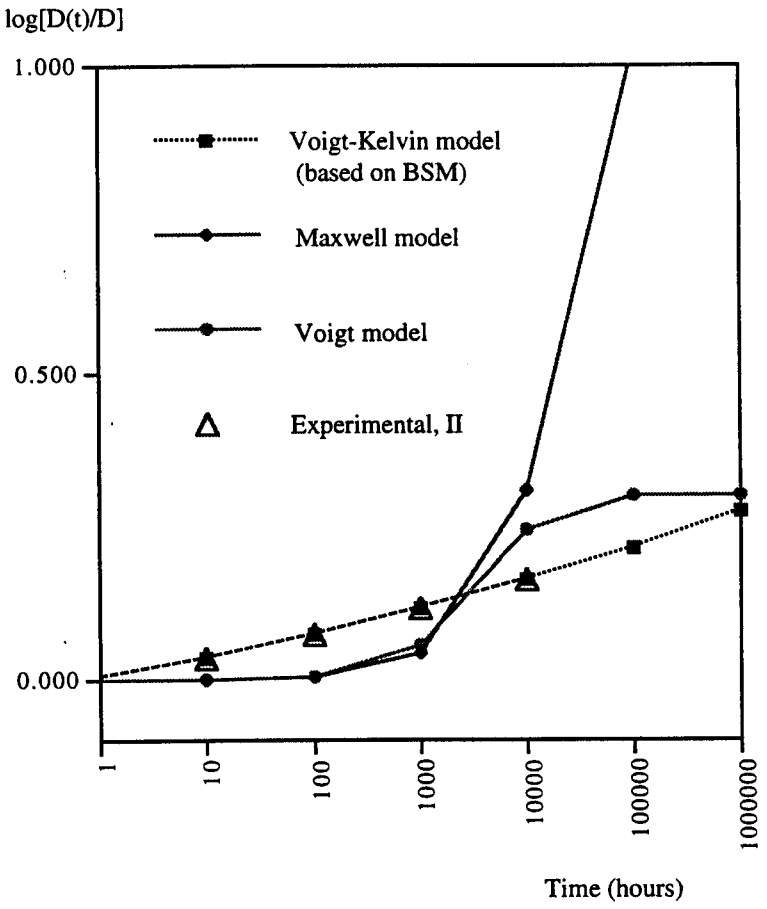

Fig. 6.28 Comparison of viscoelastic models for Type II specimen

6.4 FINITE ELEMENT ANALYSIS OF BURIED HDPE PIPE, SUBJECTED TO LIVE LOAD

Three-dimensional viscoelastic finite element analysis was used for the shallow depth buried HDPE pipe responding to vehicle live loads. Vehicles passing over the long span corrugated HDPE pipe induce a three-dimensional response that needs to be considered for design of the pipe installation to ensure long-term performance. The analysis includes the use of i) a two-dimensional finite element mesh across the pipe and harmonic modeling (a Fourier Integral) along the pipe axis, and ii) creep conformation data, D(t), based on the Voigt-Kelvin model (developed in Section 6.3) instead of using a constant value.

This was done using the Finite Element Methodology (FEM) application software, WANFE, developed by Moore, [1996]. The outputs of this three-dimensional FEM analysis were compared with those of the two-dimensional plane strain FEM analysis using CANDE 89 (Culvert Analysis and Design), developed by Katona, [1976, 1988], and Musser, [1989].

6.4.1 FINITE ELEMENT MODELING

Two different models were developed for i) 15 ft. (4.57 m) long span 42 in. (1.07 m) inside diameter HDPE pipe, subjected to concentrated tire pressure due to vehicle passing over the unpaved backfill surface, and ii) the long span 24 in. (610 mm) inside diameter, subjected to uniformly distributed loading on the pavement. The second model

was used for the comparative study with the experimental results from testing the buried HDPE pipe , subjected to live load.

Figs. 6.29 and 6.30 show the shallow-depth buried HDPE pipe responding to live load, applied on the surface of the backfill. Fig. 6.29 shows the possible maximum distribution of the axle loads when a heavy truck passes over the transverse centerline of the pipe, based on AASHTO H-20 Highway Load [CPPA, 1996]. Fig. 6.30 shows the uniform distribution of live load due to pavement on the backfill surface. The incremental soil response to live load was assumed to be linear elastic for South Florida clean sand and sand with little fines (Class II, SP elastic soil with almost no fines and Class III, SM, elastic soil with little fines) [ASTM D2487] [Moore and Brachman,1994].

Fig. 6.31 shows the schematic of finite-element pipe-soil mesh system, consisting of six-noded triangular soil elements and eight noded quadrilateral pipe elements. The preprocessed finite element meshes are shown in Figs 6.32, 6.33 and 6.34. Sixty four 8noded continuum elements and one thousand six hundred twenty six 6-noded triangles were used to model the pipe and soil for both pipe-soil systems, Figs 6.32, 6.33 and 6.34. The equivalent outside diameter and element thickness, which is long enough to cover at least one corrugation and valley, was used to simulate the correct circumferential and longitudinal stiffness of the corrugated HDPE pipe [Moore and Brachman,1994].

The defined prismatic pipe-soil system permits three-dimensional harmonic solutions. The coordinate directions, considered for this prismatic problem are X, Y, and Z, [Moore, 1996]. The finite element mesh, Figs. 6.33 and 6.34, was formed in the XY plane and harmonic analysis used in the Z direction (axial). Figs. 6.35 to 6.38 show four steps of the analysis of the buried HDPE pipe subjected to live load. Fig. 6.35 shows the

pipe subjected to surface live load in the XY plane (perpendicular to the pipe axis), and features some variation in the Z (axial) direction.

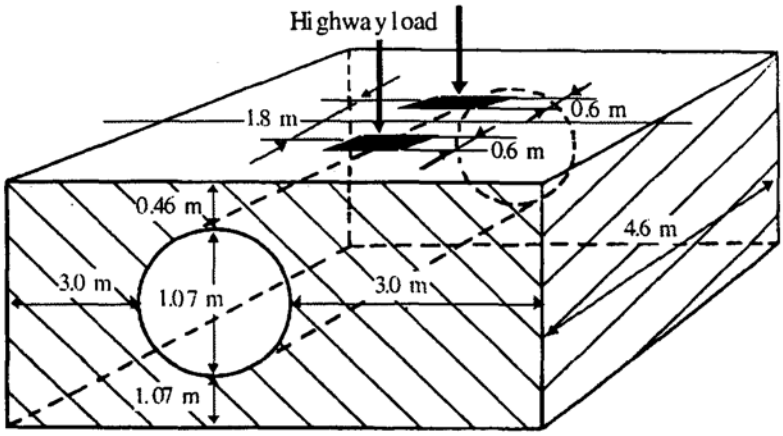

1 m=3.28 ft.

Fig. 6.29 Schematic of HDPE pipe-soil system, subjected to concentrated highway load

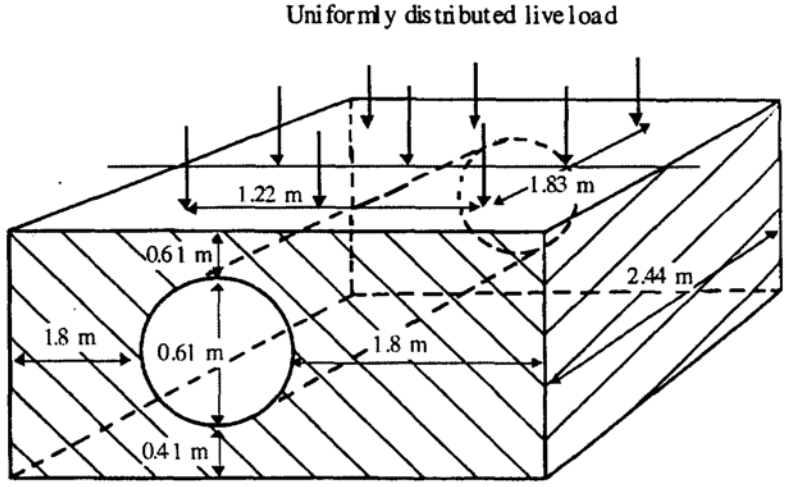

1 m=3.28 ft.

Fig.6.30 Schematic of HDPE pipe-soil system, subjected to uniformly distributed load - Simulation of test in the soil chamber

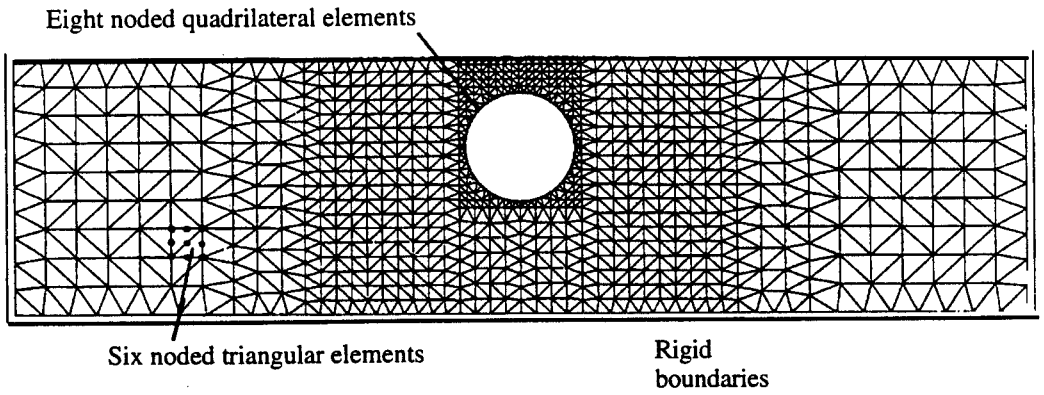

Fig. 6.31 Finite element mesh for the HDPE pipe-soil system [Moore, 1996]

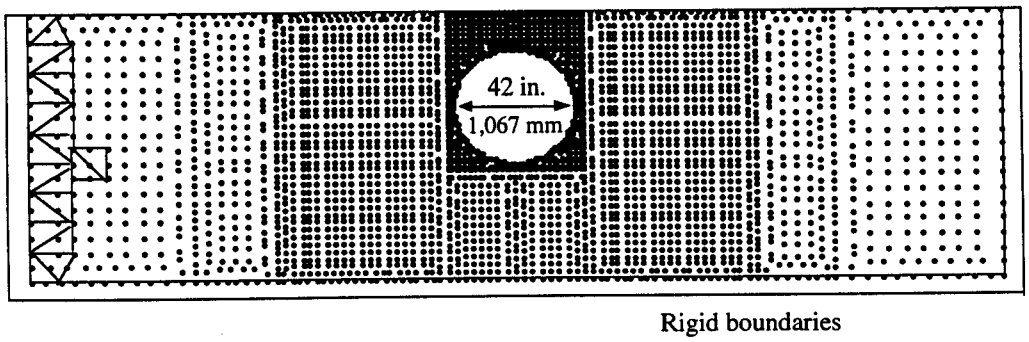

Fig. 6.32 Finite element mesh for the shallow depth buried HDPE pipe-soil system, [42 in. (1,067 mm) inside diameter] subjected to AASHTO footprint loading

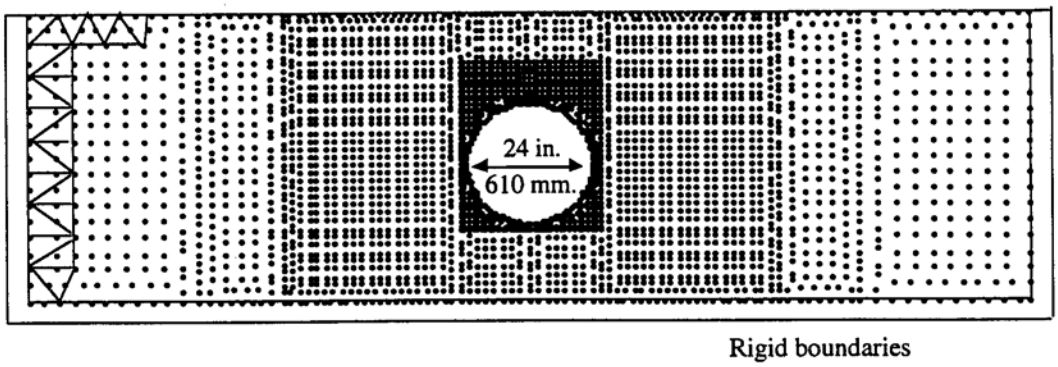

Fig. 6.33 Finite element mesh for buried HDPE pipe-soil system, [24 in. (610 mm) inside diameter] subjected to uniformly distributed loading

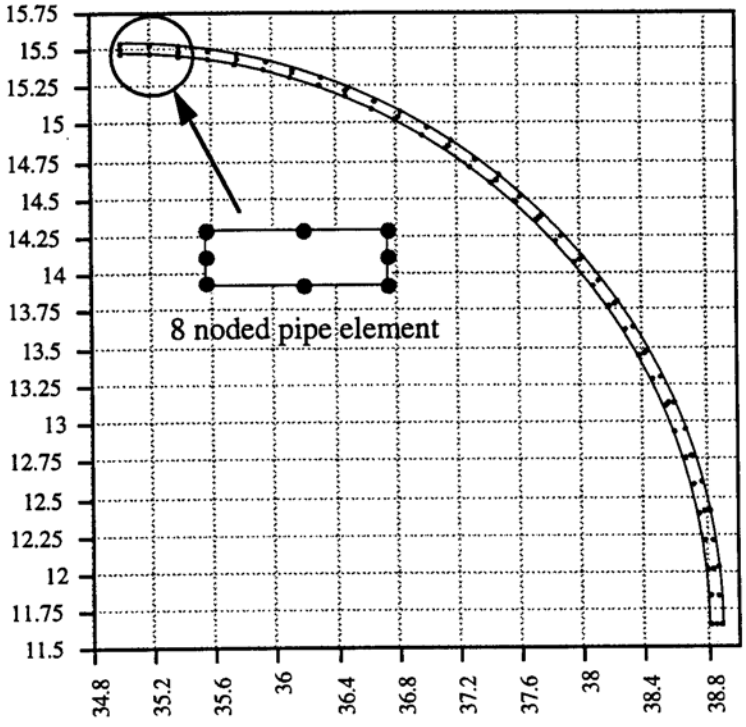

Fig. 6.34 Finite element mesh with eight-noded continuum elements for HDPE pipe

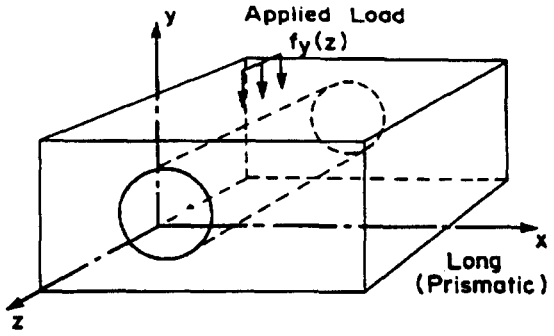

Fig. 6.35 HDPE pipe, subjected to surface live load [Moore and Brachman, 1994]

Fourier
Transform

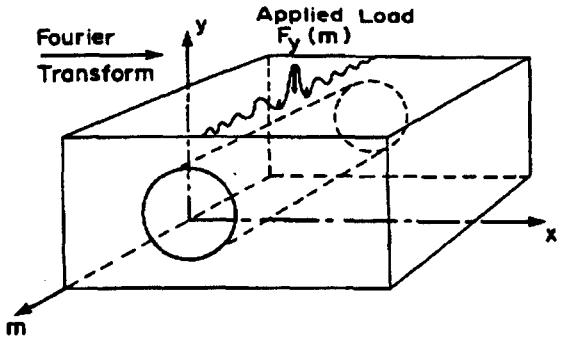

Fig. 6.36 Converted load variation with respect to the harmonic term, m
[Moore and Brachman, 1994]

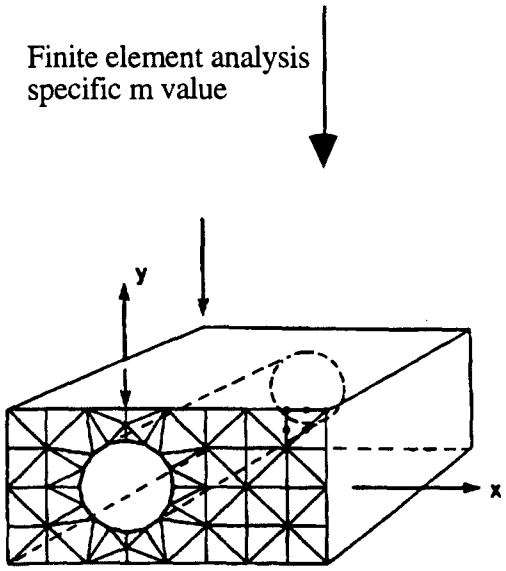

Fig. 6.37 Determination of harmonic displacements and stresses, $U_x(m)$, $U_y(m)$, $U_z(m)$, $S_{xx}(m)$, $S_{yy}(m)$, and $S_{zz}(m)$ [Moore and Brachman, 1994]

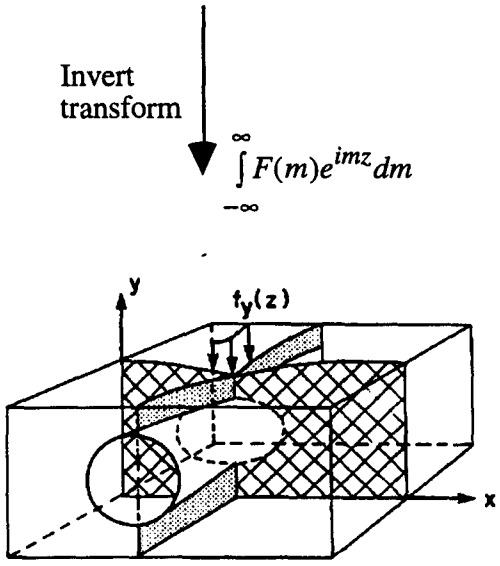

Fig. 6.38 Determination of displacements and stresses in real xyz space, $u_x(z)$, $u_y(z)$,$uz(z)$, $\sigma_{xx}(z)$, $\sigma_{yy}(z)$, and $\sigma_{zz}(z)$ [Moore and Brachman, 1994]

Assuming a long prismatic pipe-soil system, Fourier transformations were used to convert the load variation in the Z direction into variation with respect to the transform variable, m, which is equivalent to harmonic number, n, in the Fourier series, shown in Fig. 6.36 [Cheung, 1976]. A two-dimensional finite-element mesh was then used to model the pipe soil system in XY plane, and harmonic three-dimensional FEM was carried out by inverting the Fourier transform to harmonic displacements and stresses, Fig. 6.37. Fig. 6.38 shows that based on the principle of superposition, the harmonic response can be evaluated for a range of m values and displacements and stresses in the real XYZ coordinate system and can then be determined by summation [Moore and Brachman, 1994].

Using a two dimensional finite element mesh, three-dimensional results can be achieved, [Small and Wong, 1988]. The rectangular loading function (magnitude between -w and w) was defined in the direction of the pipe axis, Z, Fig. 6.39. The functions for the load f z , displacement u(z), and stresses. σ(z) can be transformed as follows:

$$F_c(m) = \int_0^{\infty} f(z)\cos mz\,dz \quad \text{----------} \quad (6.18)$$

$$U_c(m) = \int_0^{\infty} u(z)\cos mz\,dz \quad \text{----------} \quad (6.19)$$

$$S_c(m) = \int_0^{\infty} \sigma(z)\cos mz\,dz \quad \text{----------} \quad (6.20)$$

Fig. 6.40 shows the inverted form of the load function in Fig. 6.39. Harmonic finite element analysis can be performed to determine the nodal displacements, U_C (m), and

stresses. $S_C(m)$ for the particular transformed loading function. $F_C(m)$, [Zienkiewicz, 1979]. The real displacements and stresses can be recalculated by inversion of the Fourier transformation as follows:

$$u(z) = \frac{2}{\pi}\int_0^{\infty} U_c(m)\cos mz\,dm \quad \text{----------} \quad (6.21)$$

$$\sigma(z) = \frac{2}{\pi}\int_0^{\infty} S_c(m)\cos mz\,dm \quad \text{----------} \quad (6.22)$$

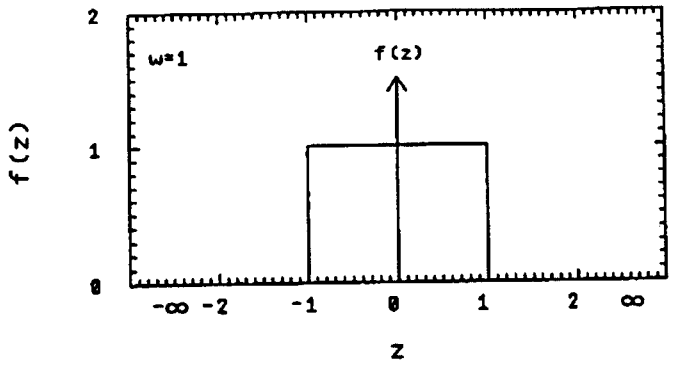

Fig. 6.39 Rectangular loading function, f(z) [Moore and Brachman, 1994]

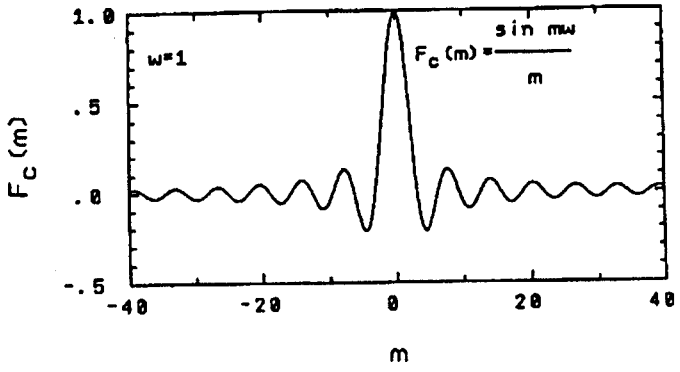

Fig. 6.40 Fourier transformation of loading function [Moore and Brachman, 1994]

6.4.2 THREE-DIMENSIONAL FEM ANALYSIS, SUBJECTED TO CONCENTRATED HIGHWAY LOADING

6.4.2.1 **Details of the Pipe-Soil System**

The 15 ft. (4.57 m) long, 42 in. (1.07 m) inside diameter HDPE pipe, is subjected to tire pressure due to a vehicle passing over the unpaved backfill surface. Based on the assumptions made for linear elastic soil and infinite length, the length was determined by the calculation of the characteristic length, X, which is equal to the distance between the two inflection points for a concentrated live load for a pipe on continuous elastic Winkler foundation [Cook and Young, 1985]. The characteristic length for an infinite pipe can be estimated by the principle of the beam on elastic foundation, equations 6.4 and 6.5 [Das, 1995] [Cook and Young, 1985]. Fig.6.41 shows the schematic of the infinite pipe on an elastic soil foundation.

$$\lambda = (3\pi/2\beta) \quad \text{----------} \quad (6.23)$$

where

$$\beta = \sqrt[4]{\frac{k}{EI}} \quad \text{----------} \quad (6.24)$$

in which

k=Spring coefficient for foundation (MPa, lb/in2) E

E=Modulus of elasticity of the pipe (MPa, psi)

I=Moment of inertia (mm^4, in^4.)

The calculated characteristic length, X, is equal to 13 ft. (4 m) so the length of pipe-soil system in this analysis was 15 ft. (4.57 m).

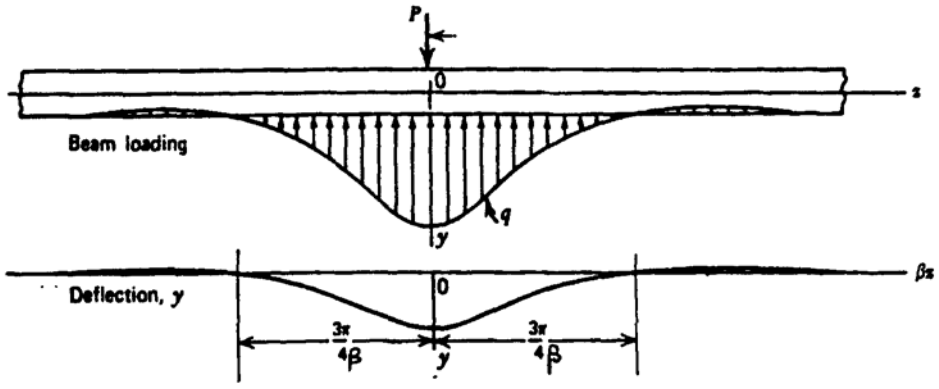

Fig. 6.41 Infinite pipe on an elastic soil foundation

Therefore, the pipe-soil system has a length to inside diameter ratio of 4.3:1. Details of the pipe specimen were as follows:

Specimen Details,

Type: Type 1

Cell Classification: 335420C

Corrugation Design: Annular

Size: 42 in. (1,067 mm) inside diameter 15 ft. (4.57 m) length.

The estimation of soil properties is quite difficult. The difficulty results from uniformity of relative compaction, size, and distribution. To resolve this difficulty for the selected two different backfill materials; the properties were determined based on the test results of sieve analysis in Section 5.4 with the current standards [ASTM D2321 and F894, 1995] [CPPA, 1996]. One type of backfill was used for the long-term performance and failure analysis and the other for soil effect analysis. The details of the selected types of soil were as follows:

1) South Florida Clean Sand,

Class: II, clean coarse grained soil, SP, poorly graded sands, little or no fines

Relative compaction: 85-95%, > 95%

Modulus, E': 2000 psi (13,800 kPa), 3000 psi (20,700 kPa) Poisson ratio, v: 0.3.

2) Sand with Little Fines

Class: III, Coarse-grained soils with fines, SM, silty sands, sands/silt mixtures

Relative compaction: , < 85%, 85-95%, > 95%

Modulus, E': 500 psi (3,500 kPa), 1,000 psi (7,000 kPa), 2000 psi (13,800 kPa)

Poisson ratio, v: 0.3

6.4.2.2 Highway Live Loading

Since most states use HDPE culverts across roads, the loads, from the heavy truck tires passing over the center line of the pipe were applied on the backfill surface of the pipesoil system. The distribution of the axle load of AASHTO H-20 Highway Load can be simplified conservatively, Fig. 6.29. All truck load was transferred to two rear wheels

passing over the centerline of pipe axis. Based on the AASHTO H-20 Highway Load configuration, Fig. 6.42, the axle loads were assumed to take the form of two footprints of vertical tire pressure of width 9.8 in. (250 mm) in the X direction and 23.6 in. (600 mm) in the Z direction, with central locations of each of these footprints 3 ft. (915 mm) apart in the z direction, Figs. 6.29 and 6.43.

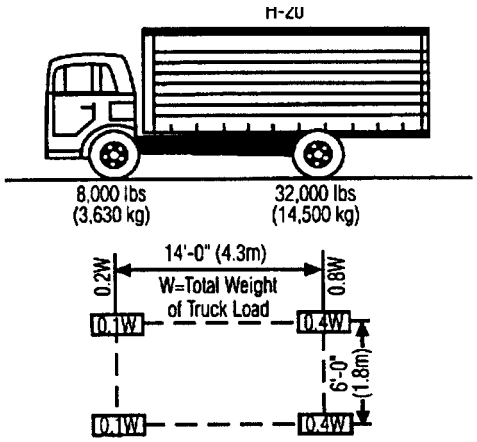

Fig. 6.42 AASHTO H-20 Highway Loading configuration [AASHTO, 1992]

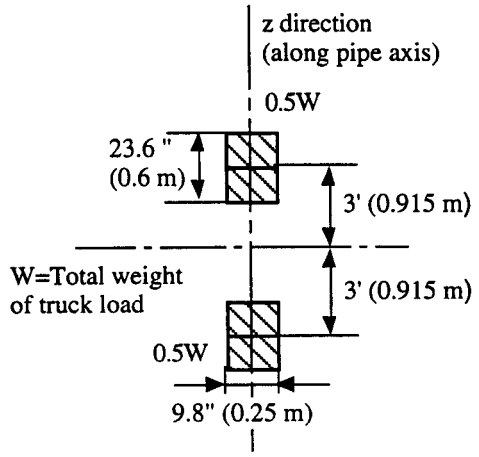

Fig. 6.43 Plan of simplified AASHTO H-20 Highway Loading on the centerline of the pipe-soil system

The two regions of live loading were modified by substituting this load function into equation 6.18. The transformed loading function is as follows:

$$F_c(m) = \frac{1}{m}\left[\sin(mz_s + mw) - \sin(mz_s)\right] \quad \text{----------} (6.25)$$

where

w=width of patches

z_s = distance from the centerline (z=0) to the patch

6.4.3 RESULTS OF THE THREE-DIMENSIONAL FEM ANALYSIS, SUBJECTED TO CONCENTRATED HIGHWAY LOADING

6.4.3.1 Long-Term Performance Analysis

A viscoelastic three-dimensional FEM analysis was carried out for the shallow depth buried HDPE pipe 15 ft. (4.57 m) long and 42 in. (1,067 mm) inside diameter, subjected to AASHTO H2O Highway Loading, 40 kips, (180 kN), shown in Figs. 6.29, 6.31, and 6.43. The backfill modulus was 2,000 psi (13.8 MPa) for South Florida clean sand with a relative compaction, 85-95%. Based on the Voigt-Kelvin model, developed for the Type I HDPE pipe, (equation 6.17 and Table 6.5), four separate analyses were performed for the input of initial, 25, 50, and 100-year moduli and the combined outputs are plotted in Fig. 6.44. Fig. 6.44 shows the vertical and horizontal changes of diameter for AASHTO H-20 Highway Load at 25, 50, and 100 years. The increase of 3.4 mm of vertical deflection, i.e. 0.4% of the long-term deflection of 35.5 mm, is for perfect material and installation conditions.

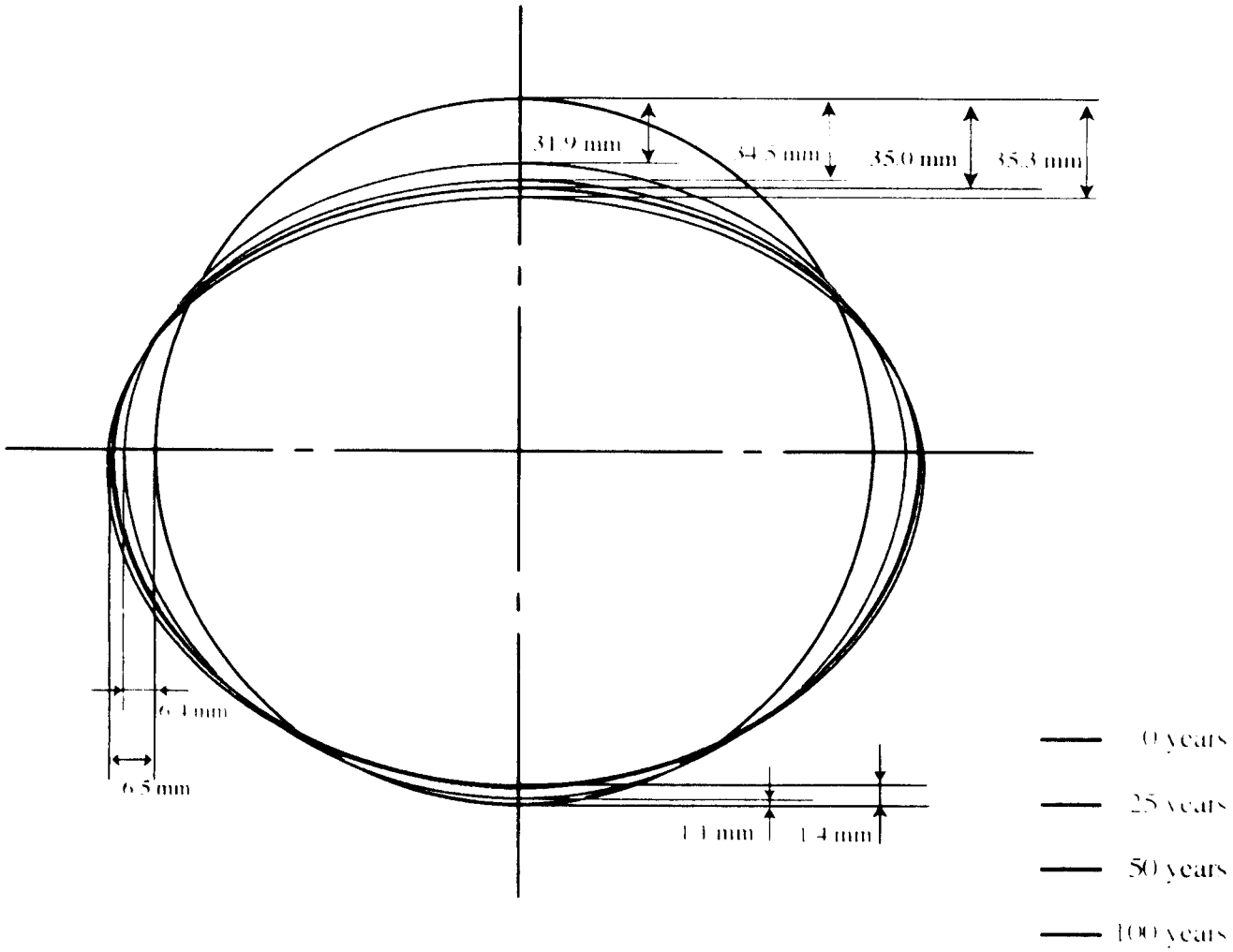

Fig. 6.44 Deformation of midsection at different ages

The pattern of deformation is not an symmetric oval shape. There is much more deflection at the top of the pipe than the bottom, whereas horizontal deformations are symmetric. Therefore, the deformation patterns of this analysis are similar to those determined from laboratory test results on the 24 in. (610 mm) pipe specimen, (Figs. 5.35 and 5.36), except for the bottom of the pipe. The maximum deformation occurred at the top of the pipe, and initial 3% vertical changes of inside diameter increased to 3.4% at 100 years (less than the failure limit 7.5%), [ASTM F894, 1995]. The vertical changes of inside diameter of the HDPE pipe, subjected to constant AASHTO H-20 Highway Load, increased only 0.4% after 100 year of service. Therefore, the design and installation criteria for initial 3% of change of inside diameter limit (out-of-roundness tolerance, ASTM F894-95) [Moore and Brachman, 1994] are conservative for long-term (maximum 100 years) performance of the pipe, buried in properly compacted uniform backfill. Figs. 6.45 to 6.48 show the initial stress distributions at the critical midsection of the pipe; it is easily noticed that the maximum stress was induced in the shoulder regions of the pipe. The magnitude of the maximum axial stress was about two-fifths of the maximum horizontal stress applied.

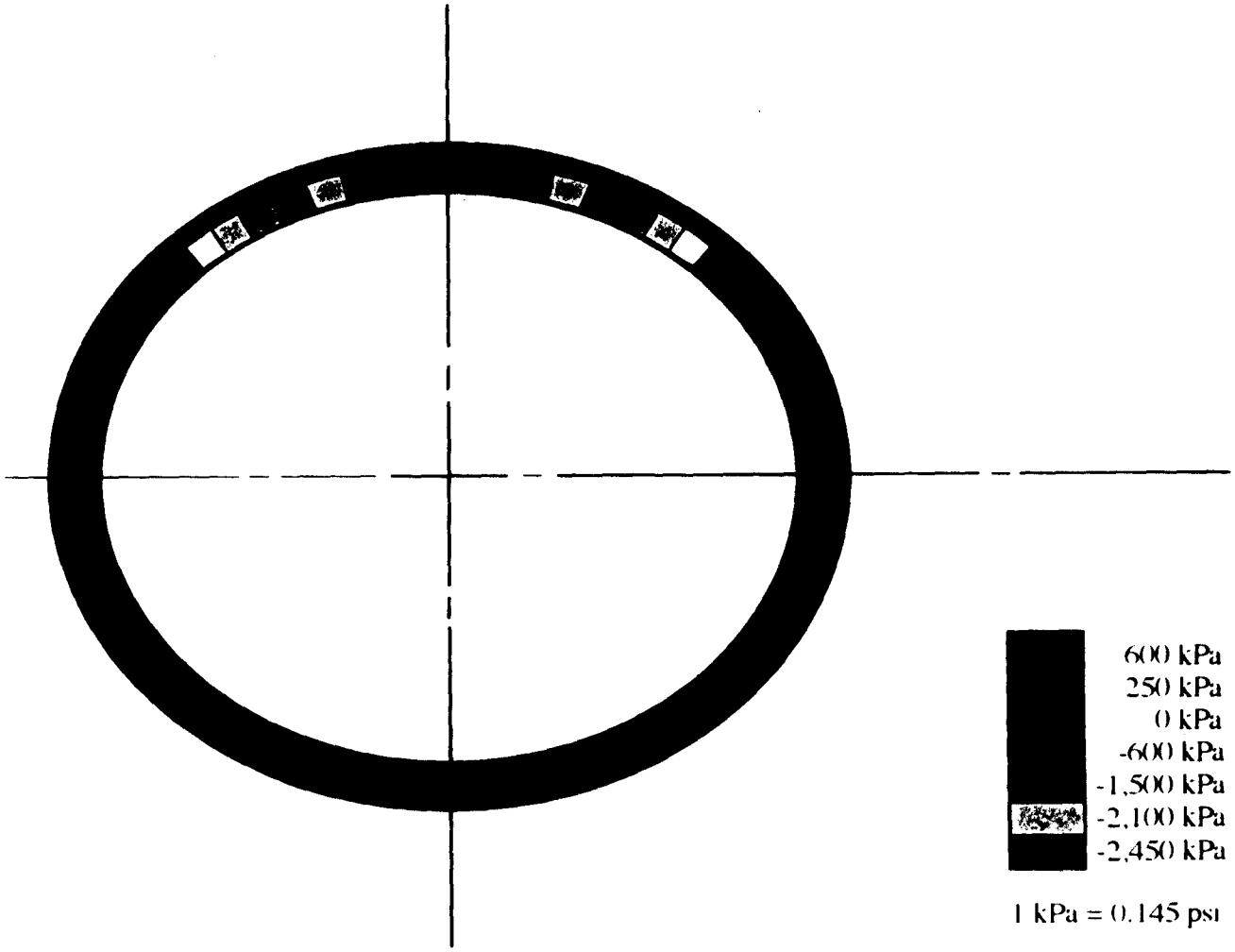

Fig. 6.45 Horizontal stress distribution on inner liner at mid-section

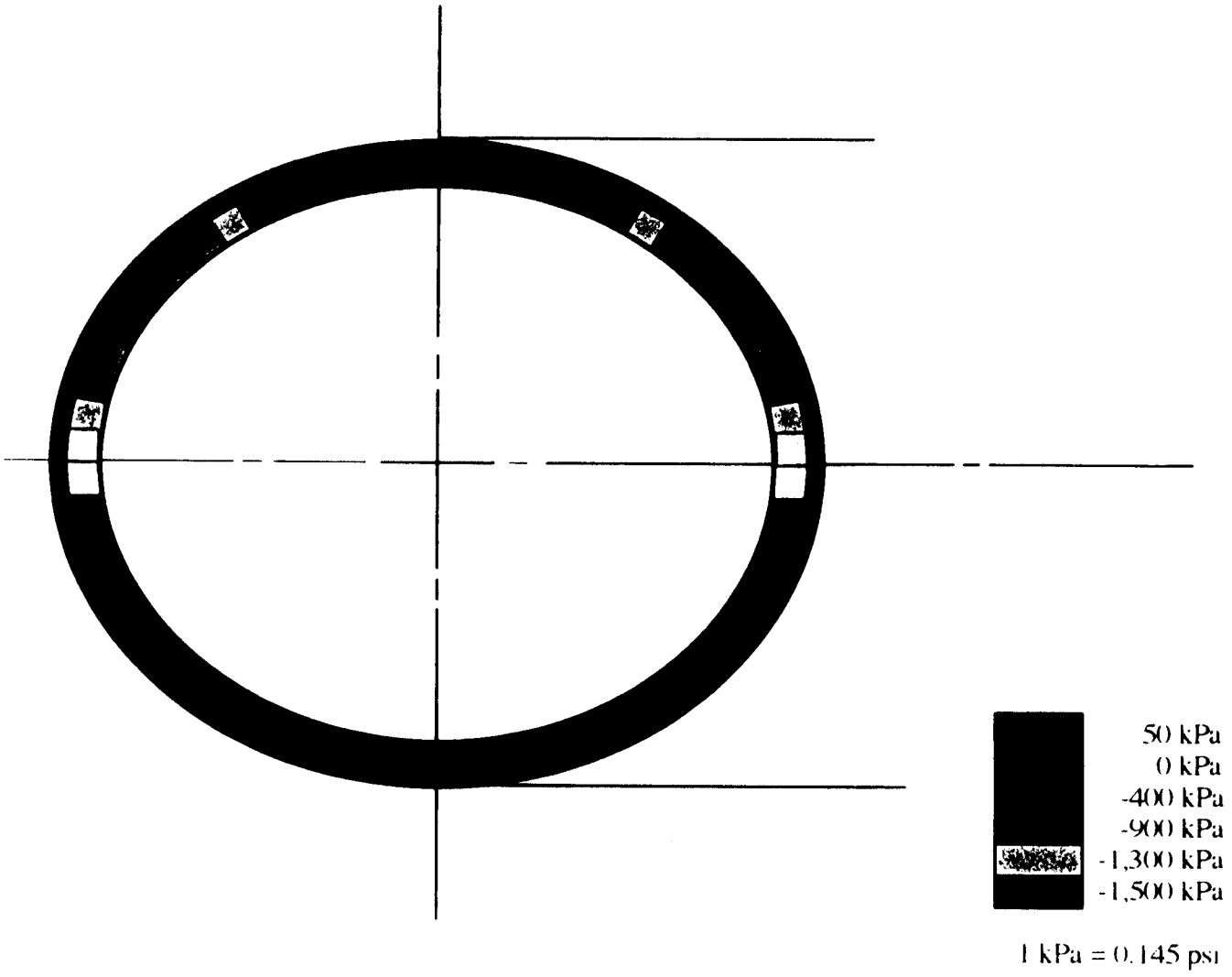

Fig. 6.46 Vertical stress distribution on inner liner at mid-section

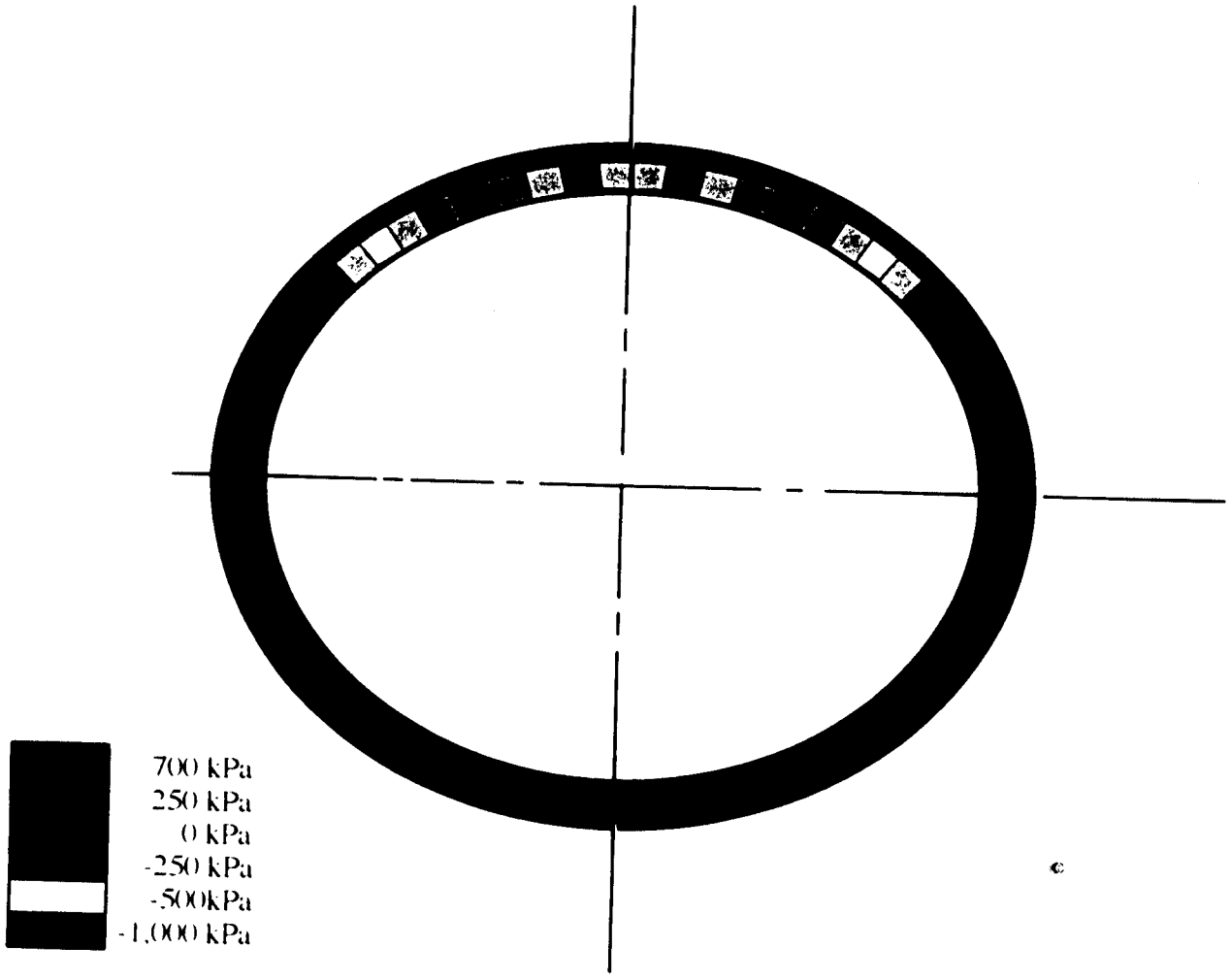

1 kPa = 0.145 psi

Fig. 6.47 Axial stress distribution on inner liner at mid-section

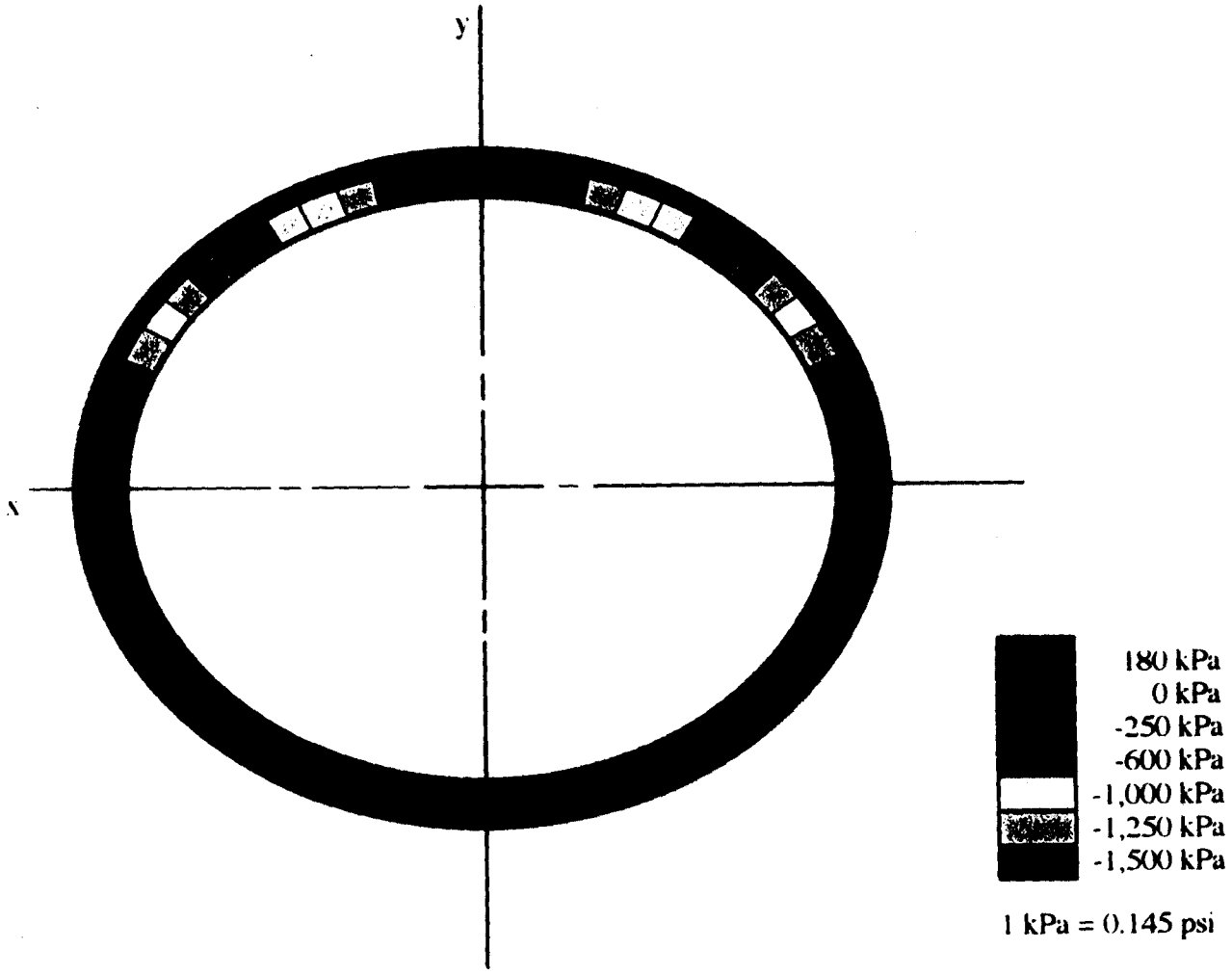

Fig. 6.48 Shear stress (x-y) distribution on inner liner at mid-section

6.4.3.2 Failure Analysis

Iterative three-dimensional FEM analyses were carried out for the 50-year old HDPE pipe, buried in shallow depth, applying incremental loading to the pipe-soil system, to determine the live load level for the failure of the pipe, (Figs. 6.29, 6.31, and 6.43). South Florida clean sand was used for the backfill material with modulus, 2,000 psi (13.8 MPa), for relative compaction, 85-95%, Class II, SP. The maximum vertical change of diameter reached to 7.5% at the load level, equals to 2.2 times the AASHTO H-20 Highway Load, 88 kips (392 kN). Figs. 6.49 to 6.52 show the stress distributions at midsection of the failed pipe after 50 years of service. Similar to mid-section stress distribution of the new pipe at service load, the shoulder region of the pipe section is subjected to maximum stresses in all the X, Y, and Z directions.

Compressive stresses were dominant in the X and Y directions, whereas the tensile stress, in the Z direction, at the bottom of the section has almost the same magnitude as the compressive stress at the top. The maximum axial stress was about one-third of the maximum horizontal stress. The maximum compressive axial stress in the shoulder region, 189 psi (1.3 MPa), was much less than the CPPA limit for the allowable axial stress level, 3,000 psi, based on yield strength of HDPE. It is necessary to evaluate the resultant stress level for each element. Then the failure mode and shape can be justified by evaluating the displacements and magnitudes of the effective stress level for each element.

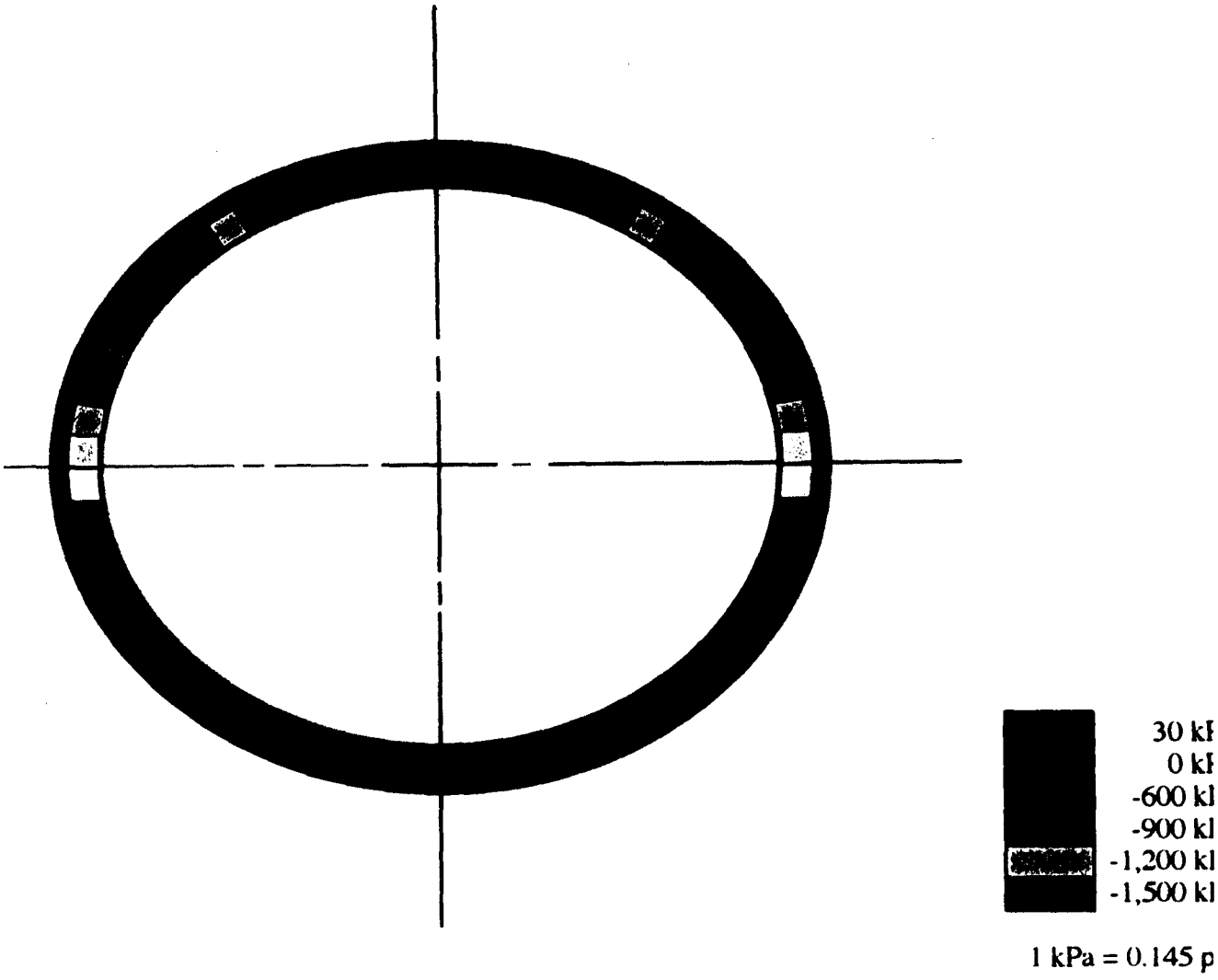

Fig. 6.50 Vertical stress distribution on inner liner at mid-section

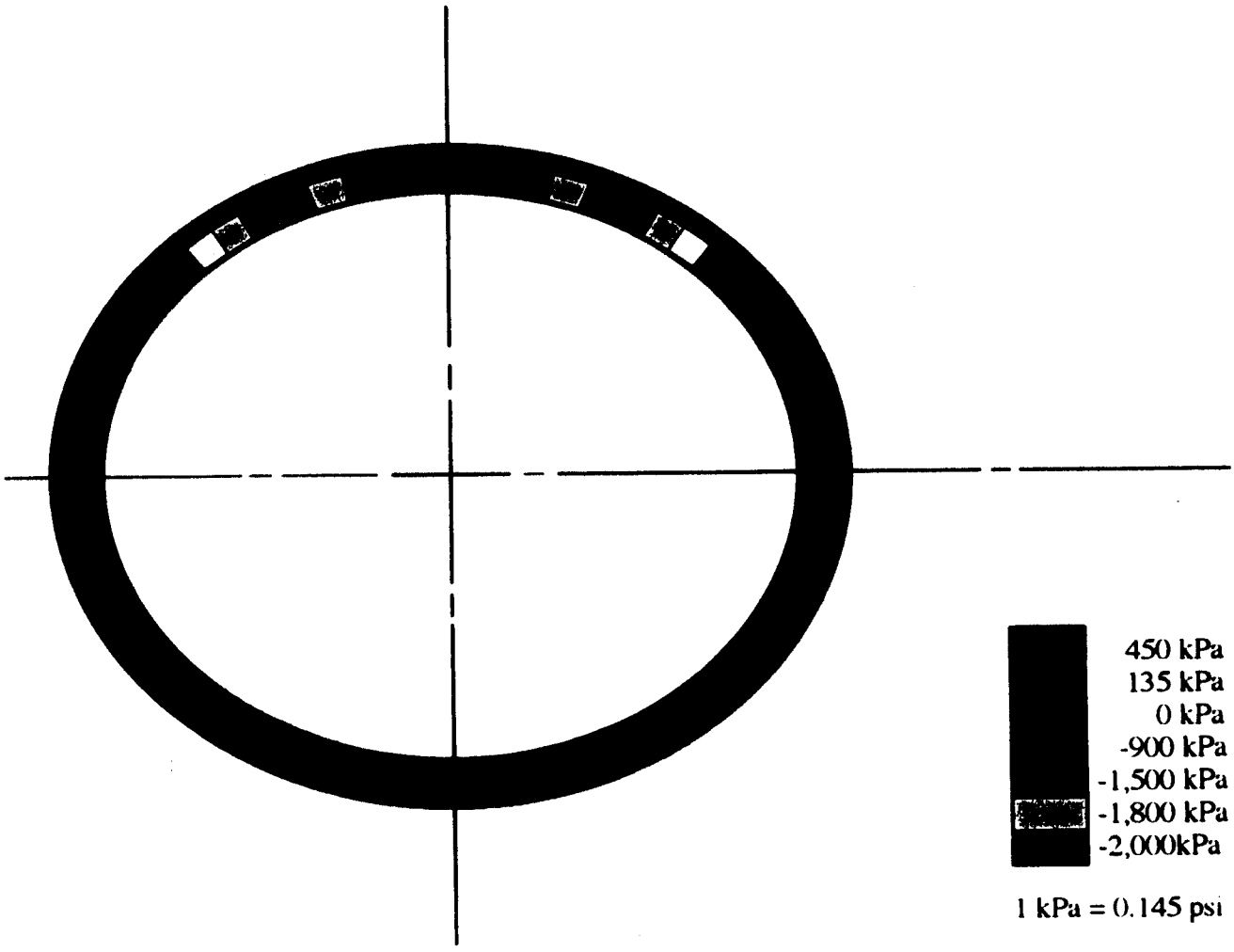

Fig. 6.49 Horizontal stress distribution on inner-liner at mid-section

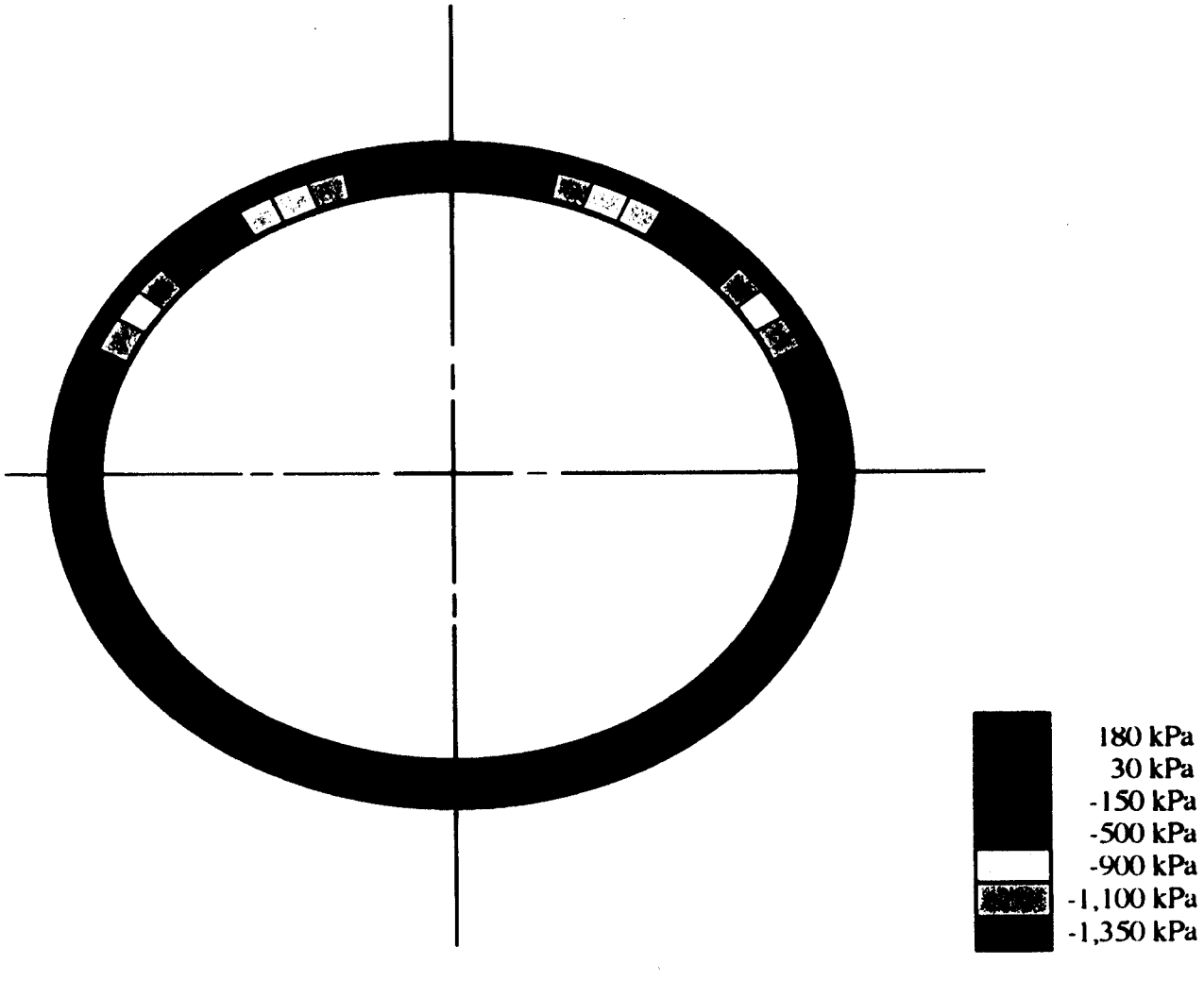

Fig. 6.51 Shear stress (x-y) distribution on inner liner at mid-section

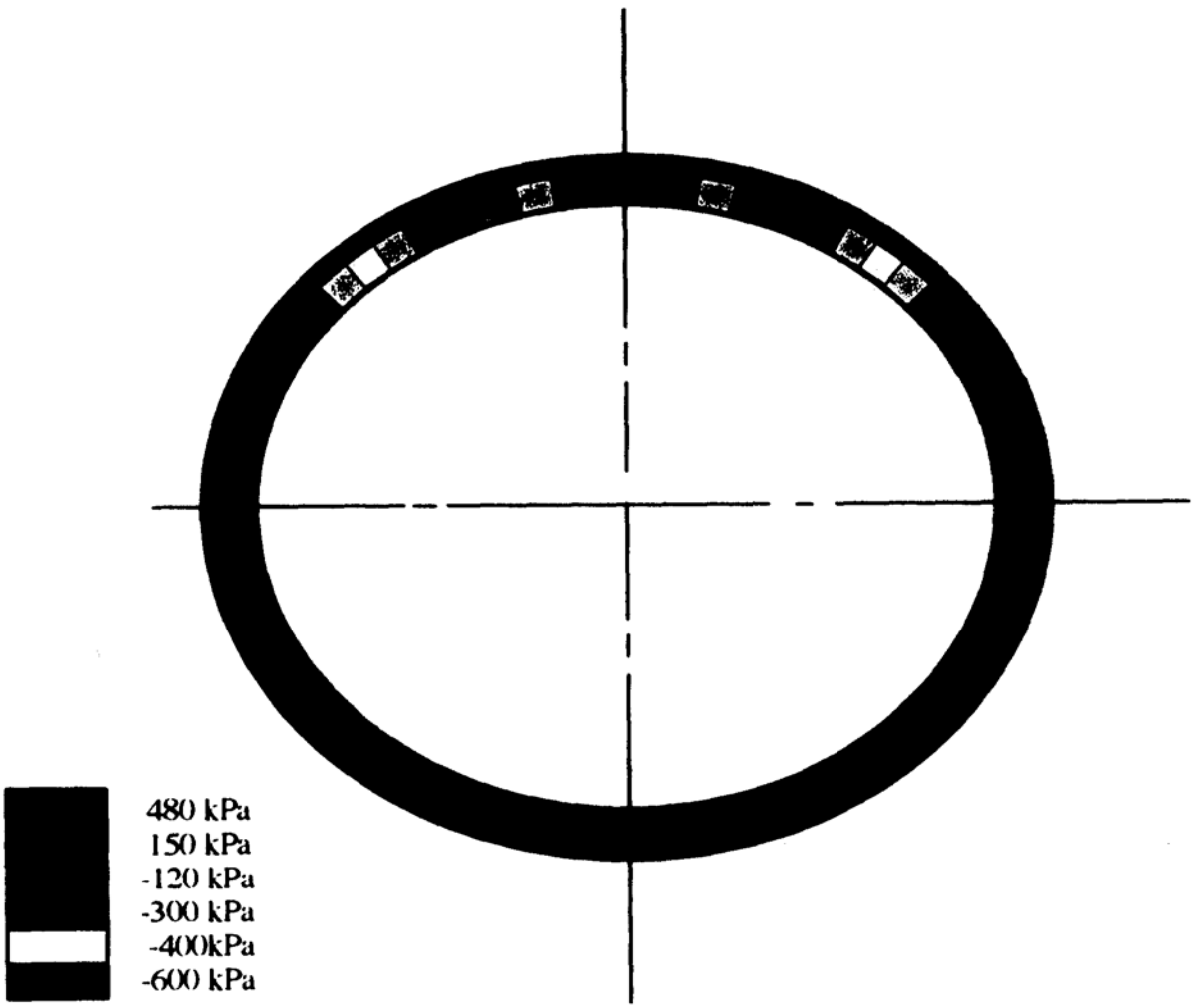

1 kPa = 0.145 psi

Fig. 6.52 Axial stress distribution on inner liner at mid-section

The effective stresses at the midsection were evaluated, based on the von Mises theory of failure, equation 6.26 [Cook and Young, 1983]:

$$\sigma_e = \frac{1}{\sqrt{2}}[(\sigma_x - \sigma_y)^2 + (\sigma_y - \sigma_z)^2 + (\sigma_z - \sigma_x)^2 + 6(\tau_{xy}^2 + \tau_{yz}^2 + \tau_{zx}^2)]^{1/2} \quad \text{--------} (6.26)$$

Fig. 6.53 shows the distribution of the midsection effective stress. The maximum effective stress, 841 psi (5.8 MPa) occurred red at the shoulder region of the midsection. This maximum effective stress level at pipe failure (with 7.5% change of I.D.) was much less than the tensile strength [at yield, 3.0 - < 3.5 ksi (21 - < 24 MPa)] of the HDPE pipe for the given cell classification [ASTM D3350, 1995]. Therefore, the magnitude of the maximum effective stress was only 28% of the tensile strength at yield. Based on this analysis, it was found that the critical shoulder region of 50-year old HDPE pipe is not expected to yield, even though it was subjected to live loading high enough to cause the maximum allowable deflection (7.5% change of I.D.). Failure occurs due to the maximum effective stress, which is not necessarily circumferential or axial due to non-uniform external pressure distribution along the pipe. The maximum axial stress was about 1/4 of the maximum effective stress in the shoulder region, Figs 6.52 and 6.53. Therefore, failure cannot be based on the CPPA performance limit for axial stress.

The fine post-processing was carried out to evaluate the failure mode and shape using five different software applications: WANFE, MS EXEL 5.0, FTP PRO, Cricket Graph III, and MacDraw Pro. Fig. 6.54 shows the post processed shape of the midsection at failure. The failure mode is characterized by the top flattening due to over-deflection. The deflection at the top of section is maximum based on the comparison of the horizontal and bottom deflections. Top

(especially 11 and 1 o'clock directions) caused by the live load, applied on the shallow depth pipe-soil system, Fig. 6.54.

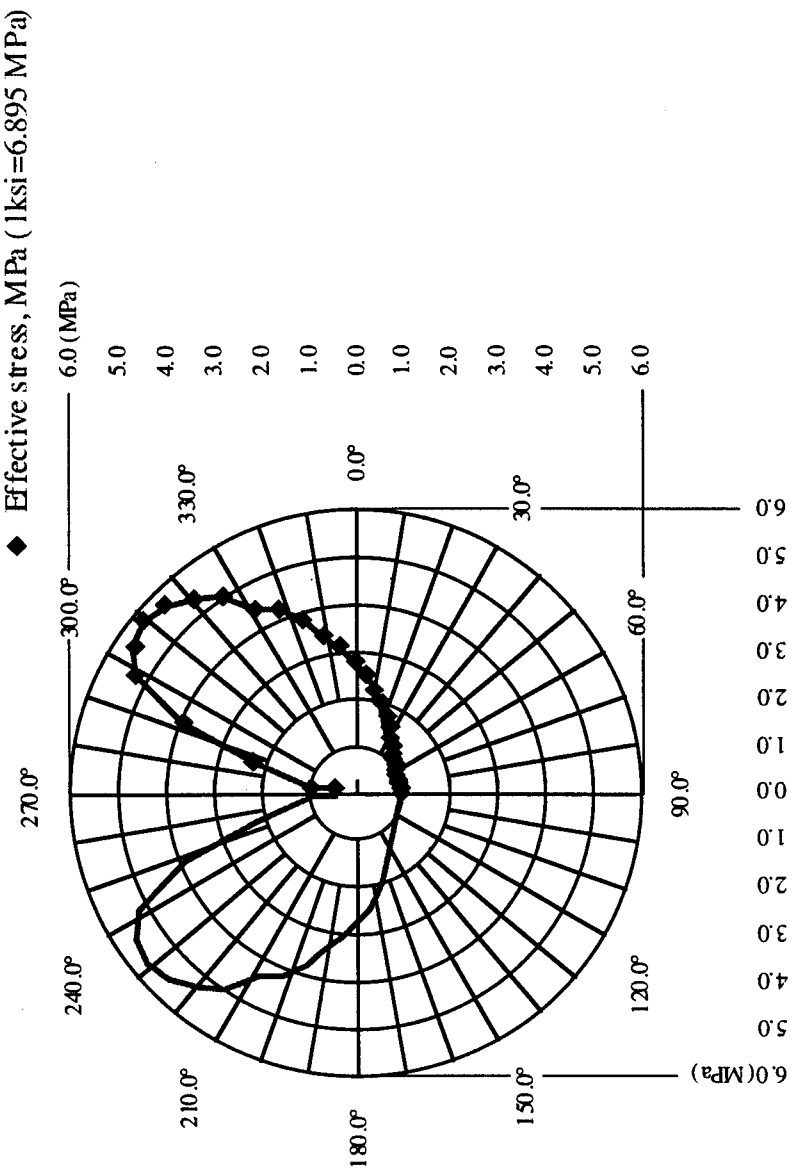

Fig. 6.53 Distribution of effective stresses at failure around mid section

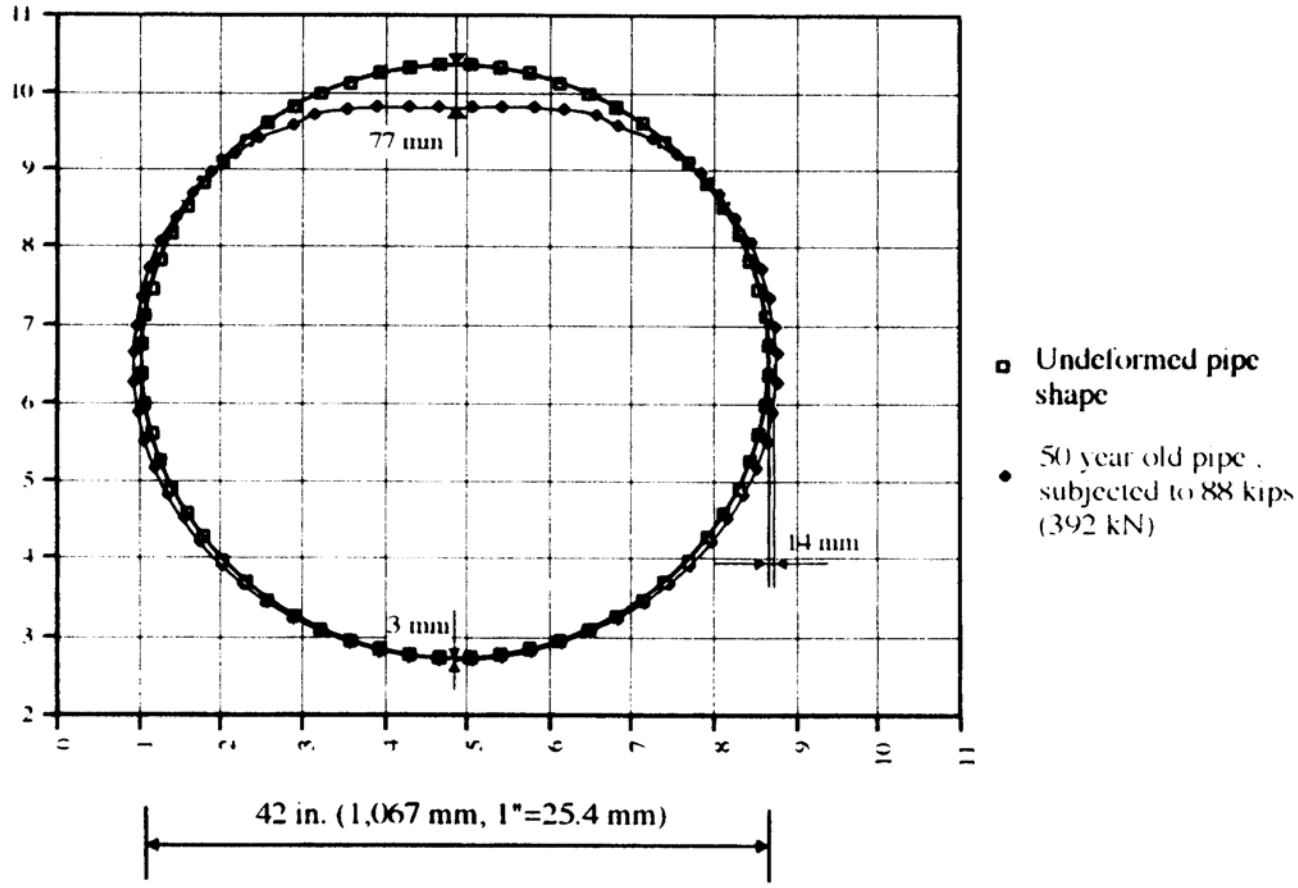

Fig. 6.54 Deformation at failure (7.5 %, change of inside diameter)

6.4.3.3 Soil Effect

Deflection of the shallow depth-buried HDPE pipe depends on the relative stiffness of the pipe and soil. Arching action can be reduced by a number of causes; for example: 1) change of physico-chemical stability, 2) change of relative compaction, 3) long term decomposition of the soil, or 4) swelling of the underlying clay. Therefore, it is important to evaluate the possible decrease of the arching effect for long-term performance. Threedimensional FEM analysis with different backfill material inputs enable the evaluation of the importance of soil effects on both the circumferential and longitudinal moments.

The three-dimensional FEM analysis of soil effect was carried out for the 50-year old shallow burial HDPE pipe [15 ft. (4.57 m) long, 42 in. (1,067 mm) inside diameter], subjected to AASHTO H-20 Highway Loading, 40 kips, (180 kN), shown in Figs. 6.29, 6.32, and 6.43. South Florida clean sand, Class II, SP, and sand with little fines, Class III, SM, for different relative compaction, was used for backfill material to simulate the long- term reduction of arching action and inadequate bedding condition due to changes of relative compaction with silt penetration.

Fig. 6.55 shows the post-processed midsection deformations for different backfill conditions, and Fig. 6.56 shows the relationship between backfill modulus and maximum change of diameter. After 50 years of service for AASHTO H-20 Highway Loading, the pipe buried in Class III, SM backfill soil with relative compaction, R=90%, performed adequately.

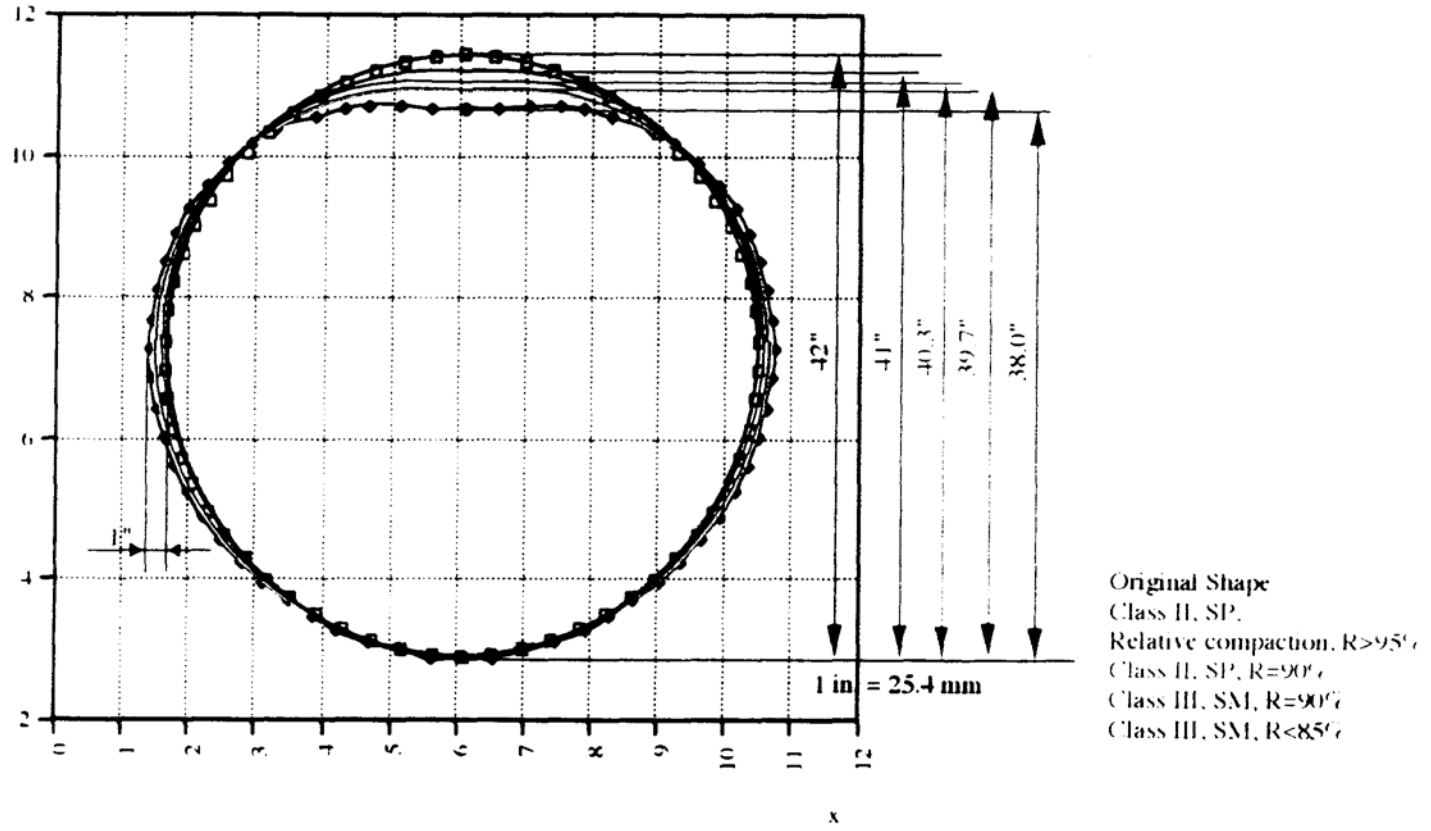

Fig. 6.55 Midsection deformations for different backfill conditions

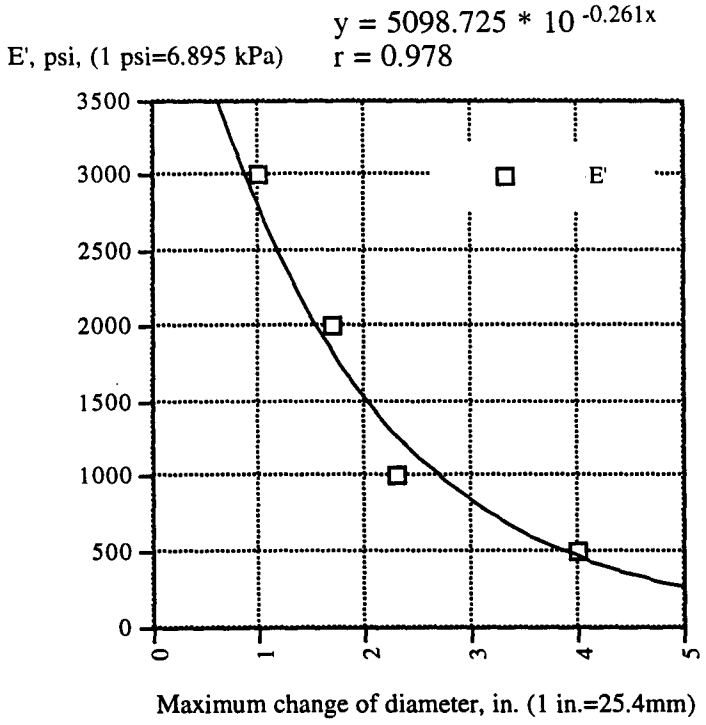

Fig. 6.56 Nonlinear relation between backfill modulus and maximum change of diameter

However, a small-degree reduction of the relative compaction for the backfill soil Class III, SM, can be detrimental to the long-term performance of the pipe due to the nonlinear relation between the backfill modulus and maximum change of diameter. Therefore, it is not recommended to use Class III backfill materials for the shallow-depth buried HDPE pipe, subjected to live load for the 100-year performance requirement.

Stress distributions of the pipe buried in different backfill conditions are shown in Figs. 6.57 to 6.60 There was sudden increase of axial compressive stresses in the

shoulder region between the relative compaction zones, R=90% and <85% for the Class III, SM, backfill. The stress distributions in the X and Y directions show similar patterns in the predominance of the compressive stress (with peak values in the shoulder region) for all different backfills, Figs 6.57, 6.58, and 6.59. Unlike the stress distributions in the X and Y directions, the magnitudes of axial stress in most regions show the maximum peak values for the Class III, SM, backfill with R<85%, Fig. 6.60. There are sudden jumps of axial compressive stresses at locations 57.5° and 111.5°, and tensile stress distributions in the bottom half (180° to 360^0) for the Class III, SM, backfill between R=90% and <85%.

Fig. 6.61 shows the resultant effective stress levels at mid-section for different backfill conditions. Fig. 6.62 shows the maximum axial stress contribution to the effective stress, at locations 57.5° and 111.5° for different backfill moduli. The contribution of the axial stress to the resultant effective stress is larger than that of the other stresses for the less stiff backfill soil, Figs. 6.60, 6.61, and 6.62. Therefore, it is quite important to carry out three-dimensional analysis to evaluate the axial stress distribution at the critical midsection of the pipe, especially for less stiff backfill material. Three-dimensional analysis is even more important for the less stiff backfill conditions.

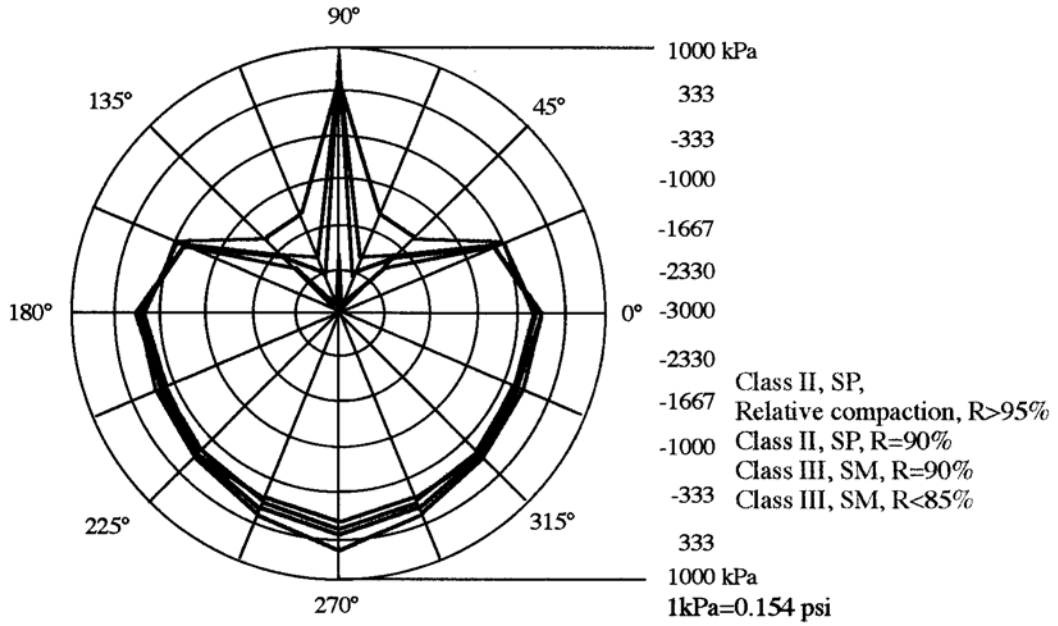

Fig. 6.57 Horizontal stress distributions at midsection for different backfill conditions

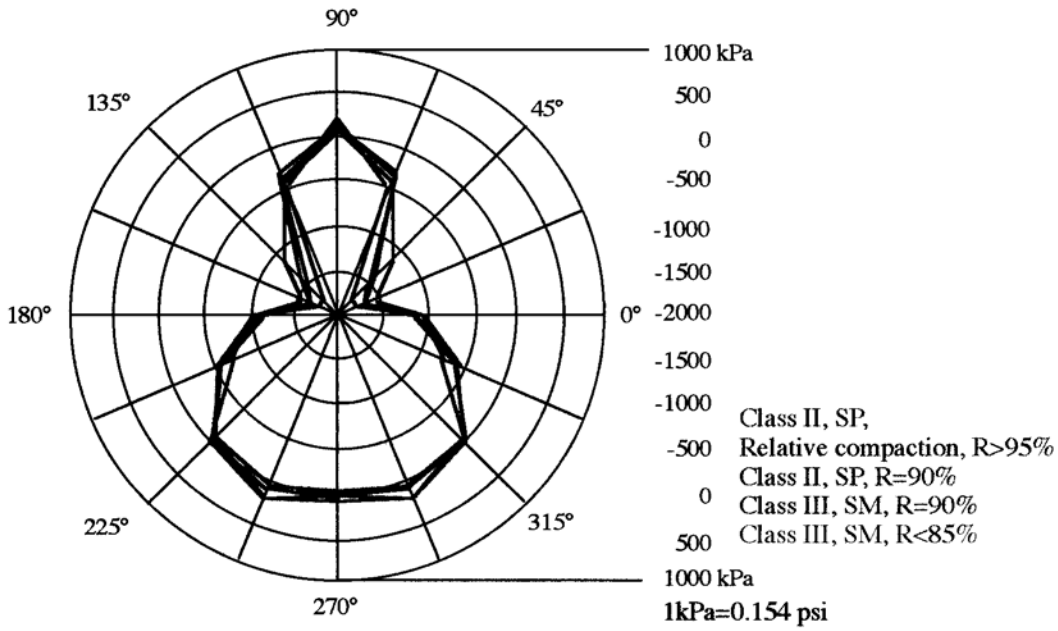

Fig. 6.58 Vertical stress distributions at midsection for different backfill conditions

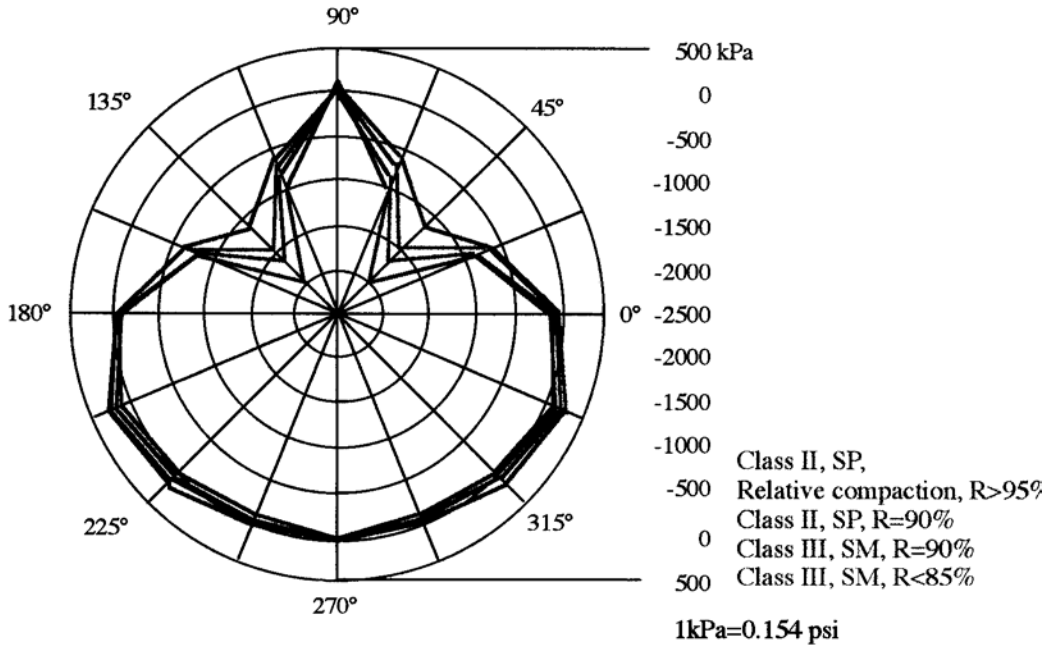

Fig. 6.59 Shear stress distributions at midsection for different backfill conditions

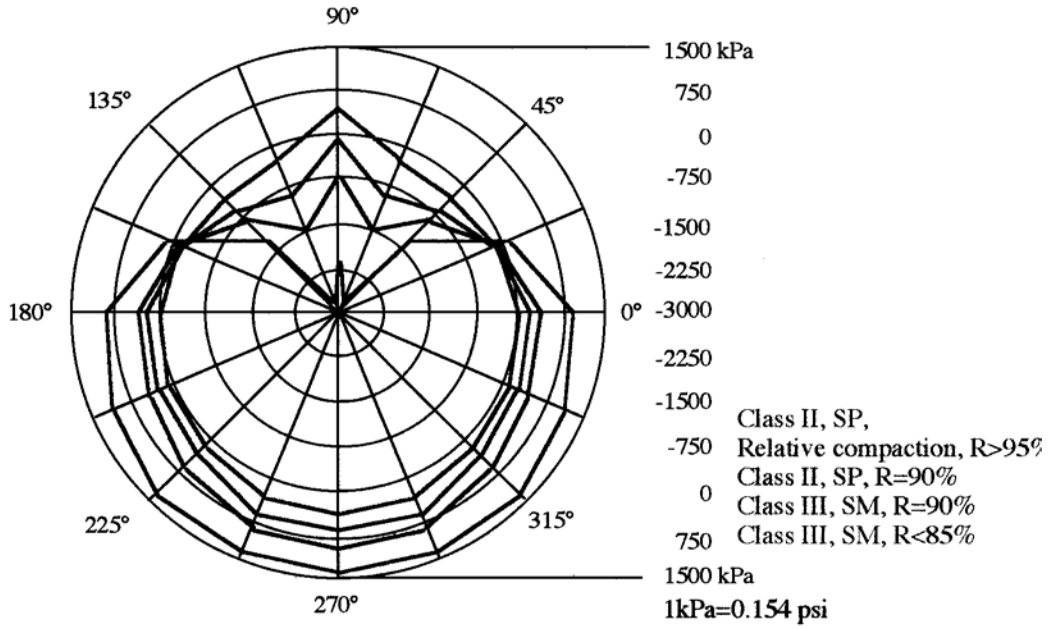

Fig. 6.60 Axial stress distribution at midsection for different backfill conditions

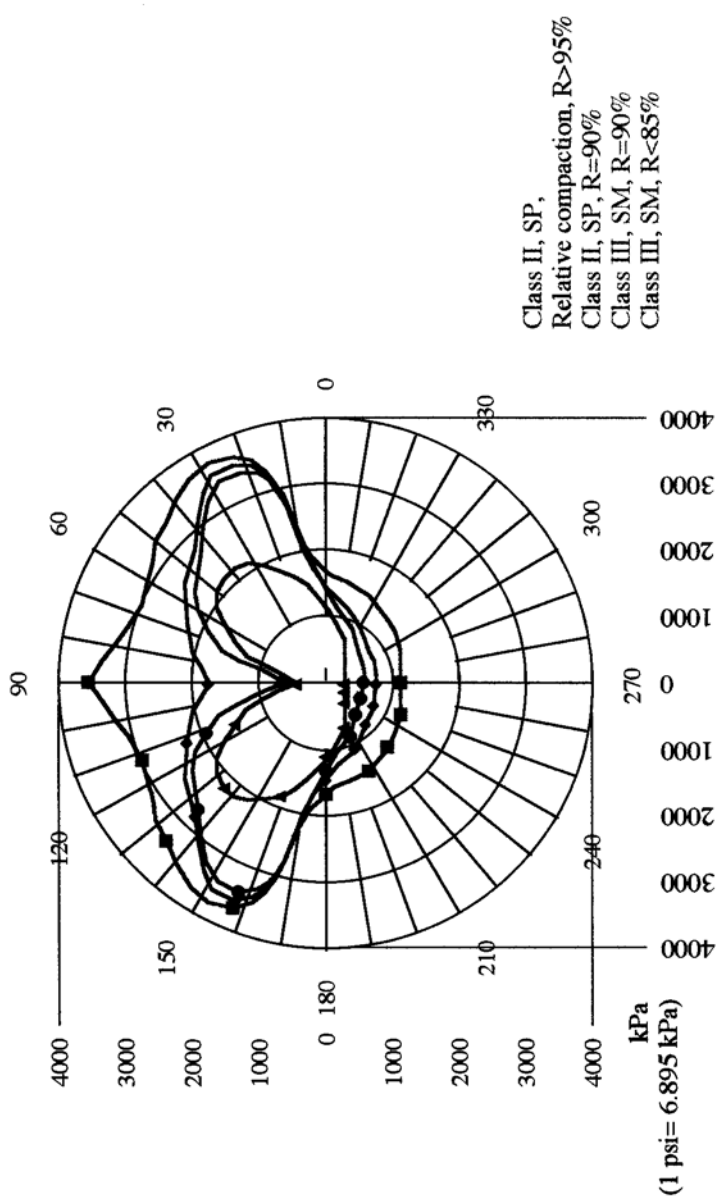

Fig. 6.61 Effective stress distribution at midsection for different backfill material

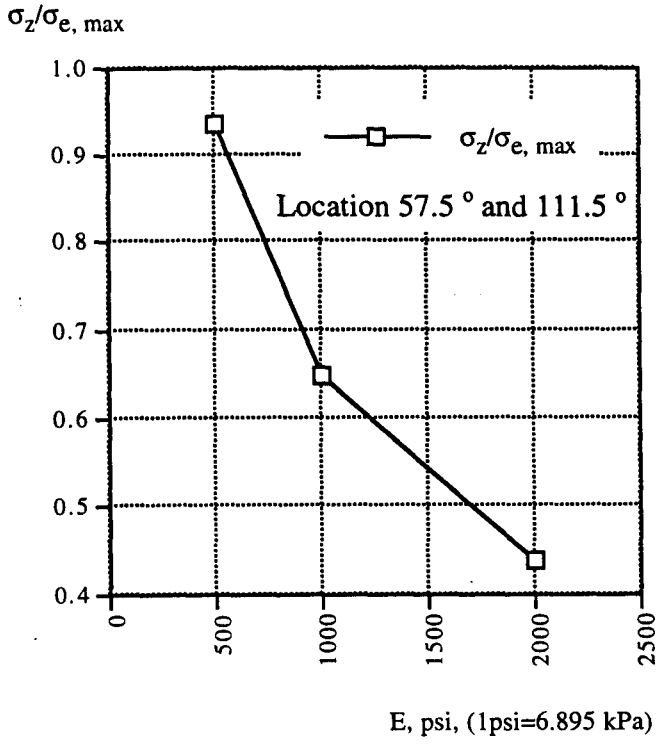

Fig. 6.62 Axial stress contribution to effective stress at locations 57.5° and 111.5°

6.4.4 THREE-DIMENSIONAL FEM ANALYSIS OF BURIED PIPE, SUBJECTED TO UNIFORMLY DISTRIBUTED LIVE LOADING

6.4.4.1 **Details of the Pipe-Soil System and Live Load**

A 8 ft. (2.44 m) long (to accommodate the characteristic length requirement), 24 in. (610 mm) inside diameter HDPE pipe, was subjected to uniformly distributed loading due to a vehicle passing over the paved backfill surface. The backfill material, selected in this analysis, was the same as the one used for the experimental investigation of the performance of the buried pipe, subjected to live loading. Details of the pipe specimen and the backfill material were as follows:

Specimen details

Type: Type I

Cell Classification: 335420C

Corrugation Design: Annular

Size: 24 in. (610 mm) inside diameter 8 ft. (2.03 m) length.

Details of backfill soil

South Florida Clean Sand,

Class II, clean coarse grained soil, SP, poorly graded sands, little or no fines

Relative compaction: 85-95%,

Modulus, E': 2000 psi (13,800 kPa), Poisson ratio, v = 0.3

The uniform distribution of AASHTO H-20 Highway Loading was applied on the surface of the backfill. Based on the dimensions of the experimental test setup, the live loads were uniformly distributed on the middle surface area of width 4 ft. (1.22 m) in the X (transverse) direction and length 6 ft. (1.83 m) in the Z (axial) direction, shown in Figs. 6.30. The live loading was modified by substituting this load function into equation 6.18. The transformed loading function was as follows:

$$F_c(m) = \frac{\sin(mw)}{m} \quad \text{----------} \quad (6.27)$$

Where

w=width

m=harmonic transform variable

6.4.4.2 Results of Three-Dimensional FEM Analysis, Subjected to Uniformly Distributed Live Load

Iterative three-dimensional elastic FEM analysis was carried out for the shallow depth buried HDPE pipe 8 ft (2.44 m) long, 24 in. (610 mm) inside diameter, subjected to heavy live load levels, one to eight times the AASHTO H2O Highway Loading, i.e. 40 kips (180 kN) to 320 kips (2.2 MN), on the paved backfill surface. Fig. 6.63 shows the vertical and horizontal changes of diameter for different load levels.

The maximum vertical change of diameter reached, 7.5%, is at the load level, which is 8.4 times AASHTO H-20 Highway Loading, 336 kips (1.5 MN). The deformation pattern is not symmetric oval shape. The results of this analysis agree with those of the

laboratory tests on the 24 in. (610 mm) pipe specimen, except for the bottom deflections, shown in Fig. 6.63. There is much more deflection at the top of the pipe than the bottom, whereas the horizontal deformations are symmetric. The maximum vertical change of diameter is larger than the maximum horizontal change of diameter, and the difference between the two increases with load.

Figs. 6.64 and 6.65 show the stress distributions (X, Y, and Z directions) at the critical mid-section of the pipe at failure, and the effective stress distributions at different load levels. The maximum compressive stresses occurred at the shoulder region for all X, Y, and Z directions. The compressive stresses were dominant in the X and Y directions, whereas the tensile stress in the Z direction was maximum at the bottom, 143 psi (986 kPa). The magnitude of the axial stress at the critical shoulder region, -63 psi (-431 kPa), was approximately 26% of the maximum horizontal stress, -237 psi (-1,636 kPa) and 16% of the maximum effective stress, 403 psi (2,776 kPa) at the shoulder. Therefore, it is necessary to carry out three-dimensional analysis to evaluate the magnitude of the axial stress, which contributes significantly to the resultant effective stress that causes failure.

Compared with the mid-section stress distribution at pipe failure due to concentrated loading in Section 6.4.3.2, the differences between the maximum and minimum stress levels in all X, Y and Z directions were less than that for the pipe subjected to concentrated loading at shallower cover depth. The interesting findings include i) similarity of maximum effective stress distributions with maximum peak values at the shoulder for both concentrated and uniform loading conditions, ii) maximum axial stress at the bottom in tension for uniform loading, and iii) in compression at the shoulder for the concentrated loading condition.

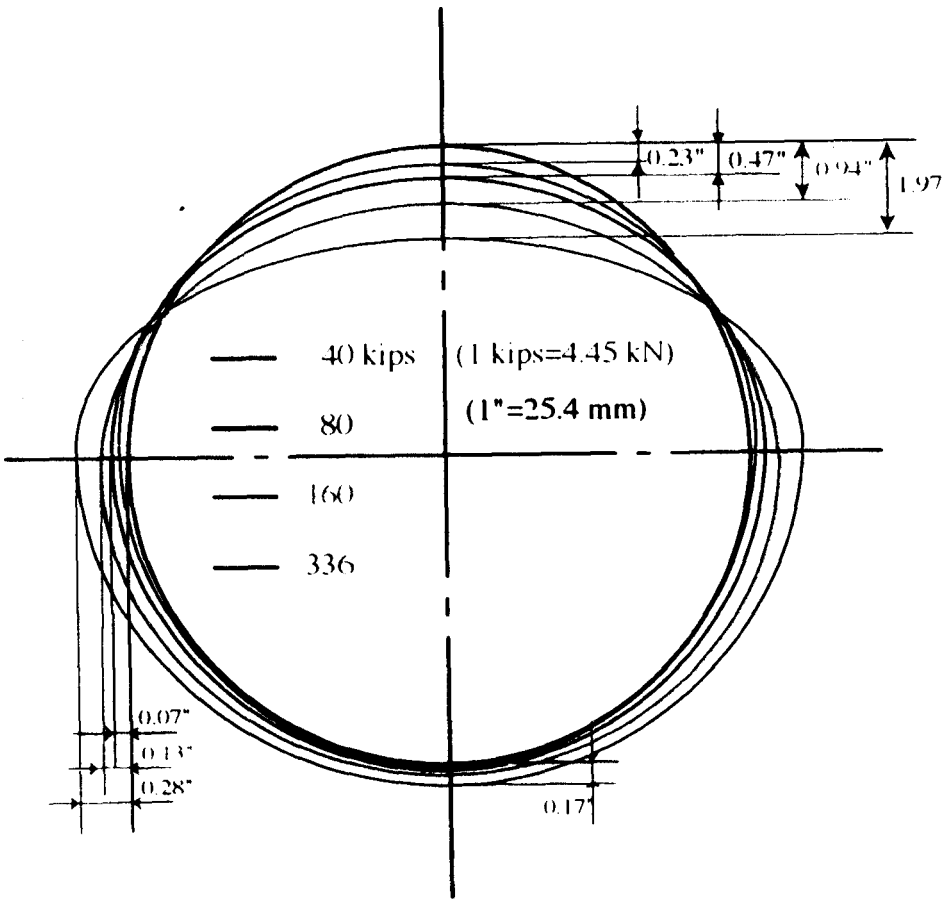

Fig. 6. 63 Midsection deformation at different live load levels, based cm three dimensional FEM analysis

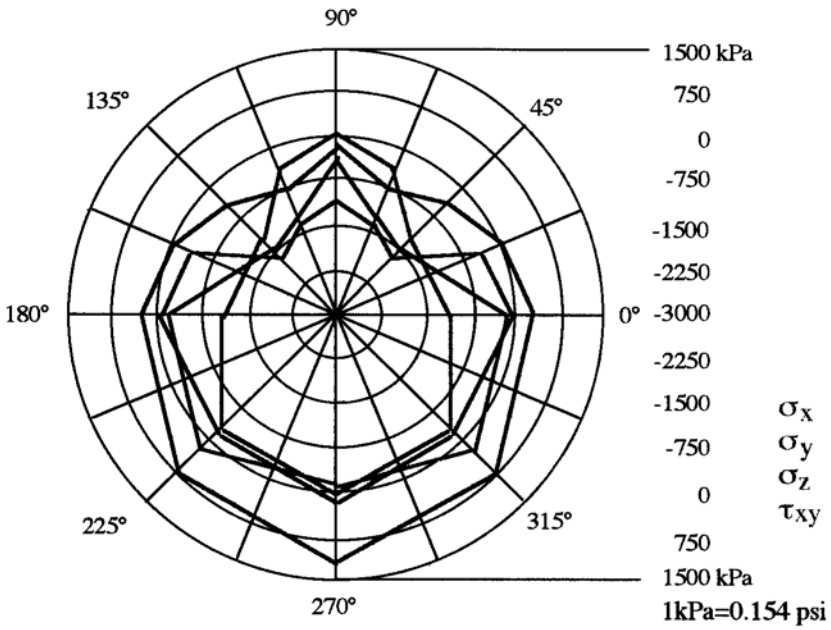

Fig. 6.64 Midsection stress distribution at failure

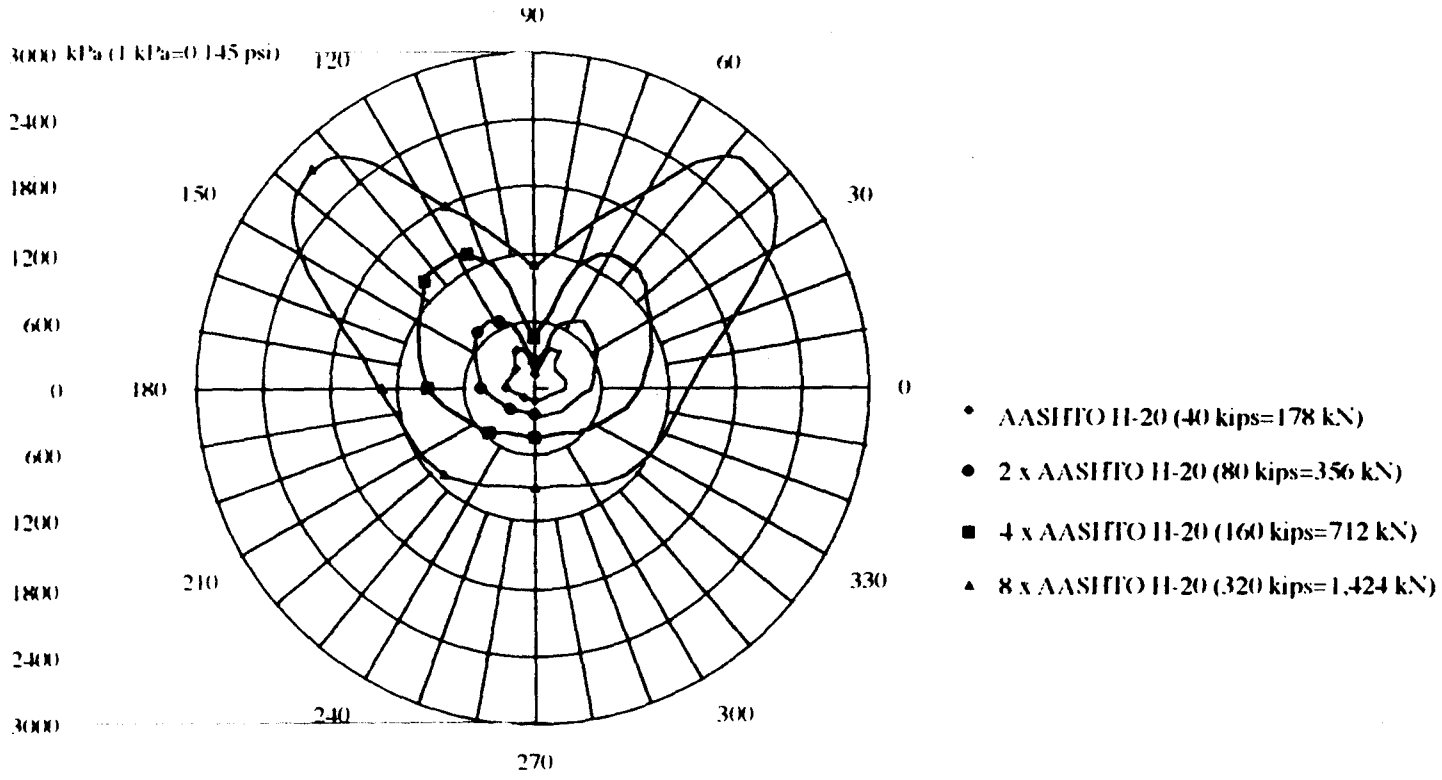

Fig. 6.65 Midsection effective stress distribution

Therefore, it is inferred that the uniformity of hoop and axial stress distributions, and the axial stress contribution to failure will depend on the type of loading and cover depth to pipe diameter ratio. However, the failure modes are the same for both loading conditions.

6.4.5. COMPARISON ANALYSES

Comparison analyses on the performance of buried HDPE pipe, subjected to live load were carried out to evaluate the differences of results from i) the experimental investigation, ii) the Iowa method (modified Spangler equation), iii) Two-dimensional FEM analysis using the software application, CANDE-89, developed by Katona et al. [1976] and Musser [1989], and iv) Three-dimensional FEM analysis, using the software WANFE, Moore [1996].

6.4.5.1 **Details of the Two-Dimensional FEM Analysis**

CANDE-89 [Katona et al., 1976] [Musser, 1989] was used for the twodimensional FEM analysis of the HDPE pipe, subjected to uniform load, based on incremental virtual work using a displacement formulation. A stress-strain law for HDPE pipe was assumed up to yield stress level, 3,000 psi (21 MPa). The isotropic linear elastic soil model was defined by a constant value of Poisson's ratio, 0.3 and backfill modulus, 2,000 psi, (13.8 MPa) for Class II, SP, R=90%, backfill soil, used in the experimental investigation [Musser, 1989]. The live load had to be converted to equivalent truncated soil overburden pressure for this analysis.

The solution utilizes automated mesh routines that internally construct the finite element mesh. Details of the elements and nodes are shown in Figs 6.66 and 6.67.

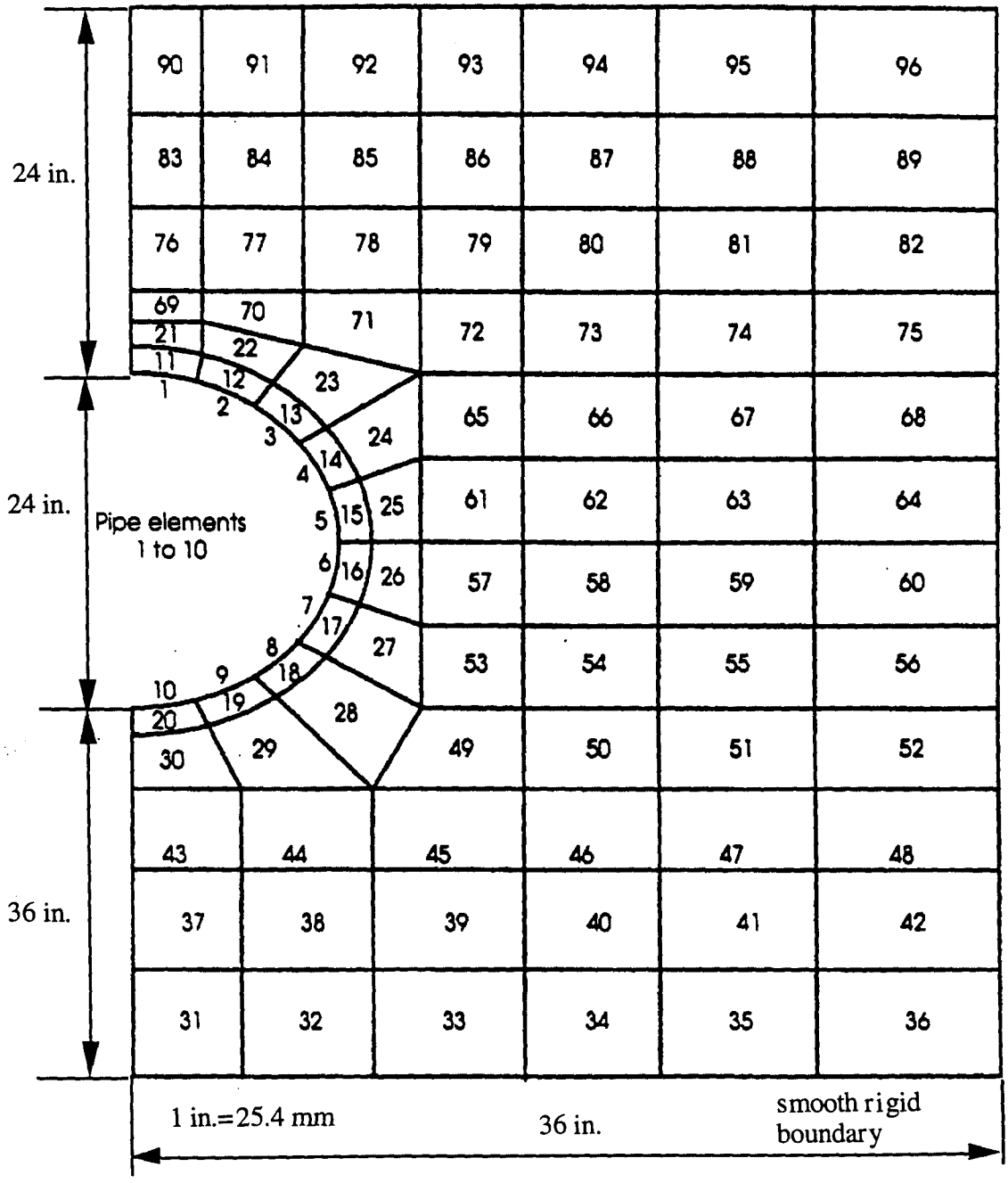

Fig. 6.66 Element numbering of the finite element mesh

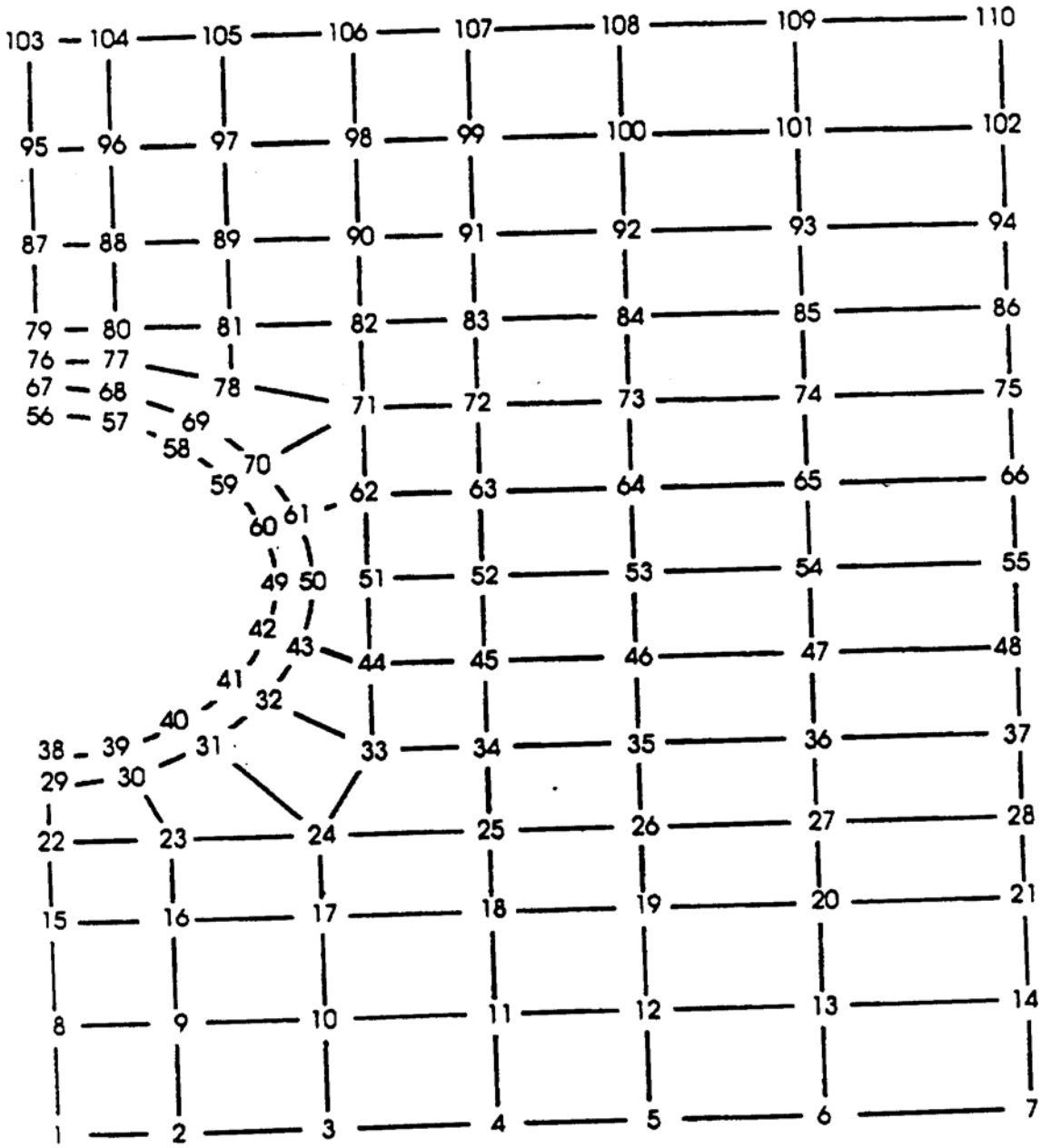

Fig. 6.67 Details of node numbering [Musser, 1989]

Eighty-six quadrilateral elements with four center nodes for each element, and ten beam-column elements with a node at each end, were used for the soil and pipe respectively.

The details of the specimen were as follows:

Specimen Details

Type: Type I

Cell Classification: 335420C

Corrugation Design: Annular

Size: 24 in. (610 mm) inside diameter 8 ft. (2.03 m) length.

6.4.5.2 Comparison

The results of the experimental investigation, and the three-dimensional FEM analysis were compared with the two-dimensional FEM analysis, following conversion of uniformly distributed three dimensional live load on paved backfill into an equivalent truncated soil overburden pressure. Fig. 6.68 shows the vertical and horizontal changes of diameter at different live load levels, based on the two-dimensional FEM analysis. Fig.6.68 shows more downward vertical deflection at the bottom of the pipe due to settlement of embedded zone, and more horizontal deflection at the spring line, than those from the three-dimensional FEM analysis and the experimental investigation, Figs. 5.35 and 6.63. Figs. 6.69 and 6.70 show further details of the performance differences in the two and three dimensional FEM analyses, experimental investigation, and Iowa formula. Increments of change of diameter with load, based on three and two-dimensional FEM analyses were quite similar to experimental test results.

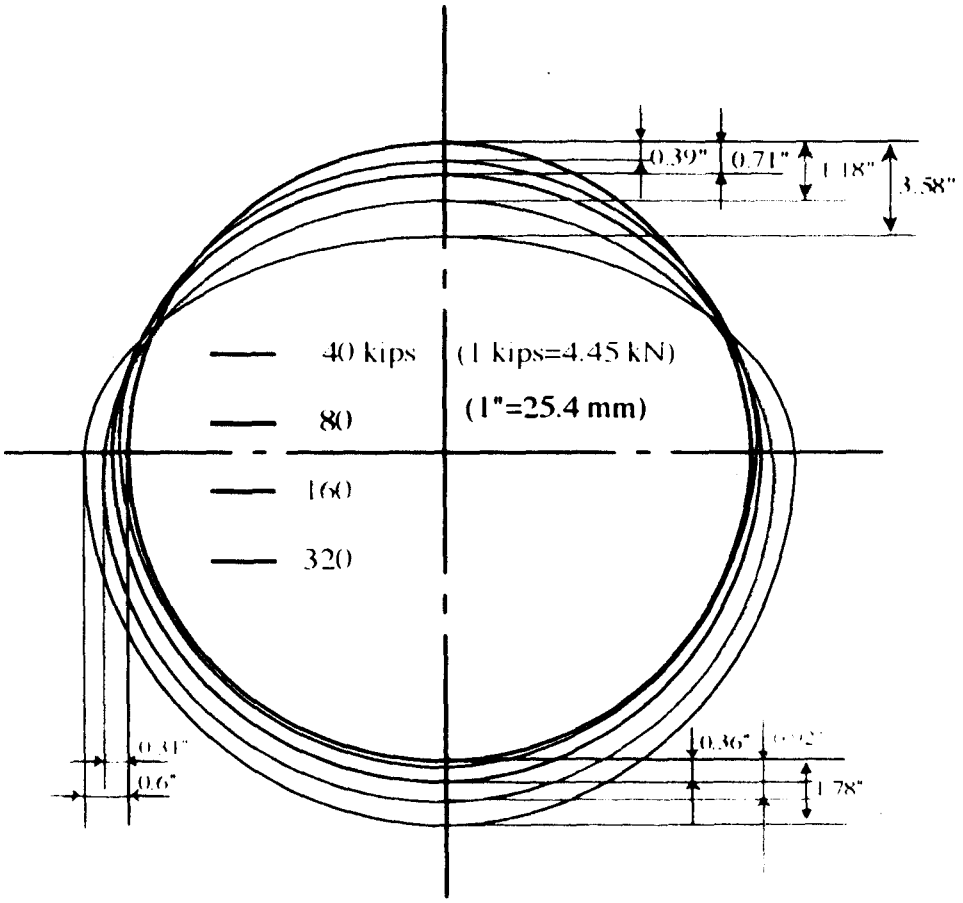

Fig. 6. 68 Deformation at different live load levels, based can two dimensional FEM

However, the increments, based on the Iowa formula have higher values than those, based on the experiment. Therefore, prediction of the maximum changes of diameter, based on the Iowa formula, is quite conservative for the design of the HDPE pipe.

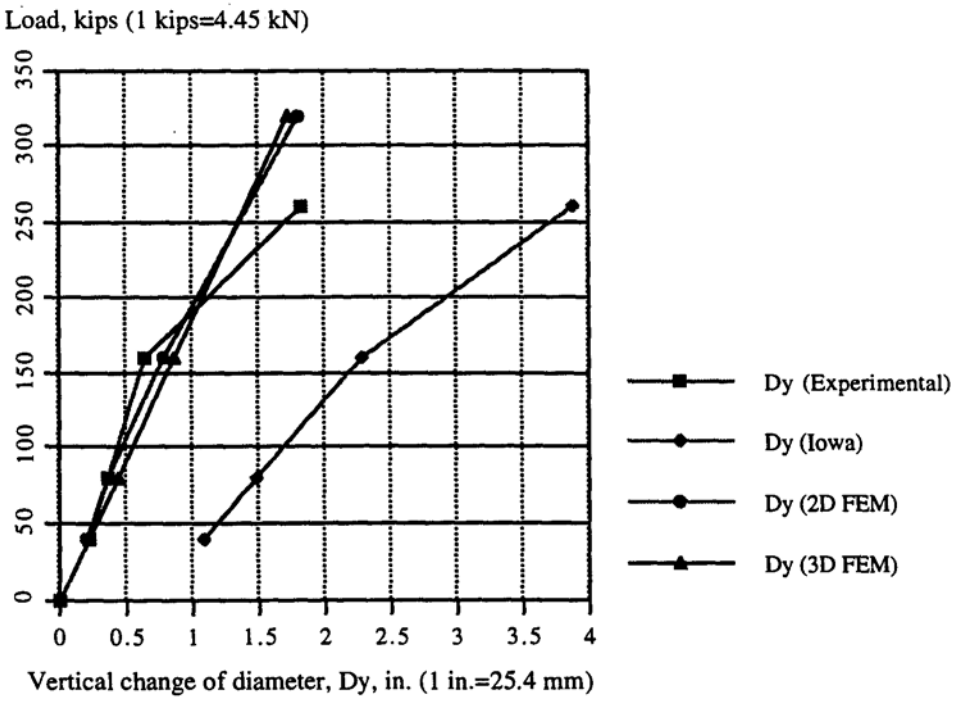

Fig. 6.69 Comparison of vertical changes of diameter

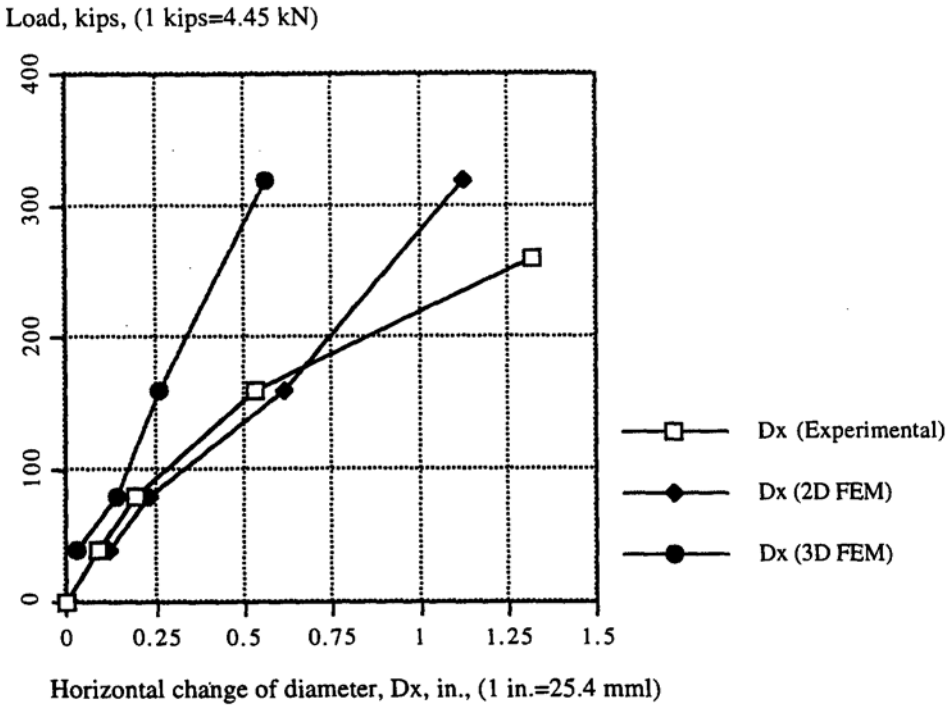

Fig. 6.70 Comparison of horizontal changes of diameter

Vertical changes of diameter, from two and three-dimensional FEM analyses were larger than the test values. Three-dimensional FEM analysis showed more vertical deformation and less horizontal deformations than the 2-D anlaysis. Even though, there was good agreement between the test results and the three-dimensional FEM analysis, the settlement at the bedding (below the bottom of pipe section), based on the two-dimensional FEM analysis was much larger. In the experimental test results and the two and three-dimensional FEM analyses, there were reasonably good agreements for the cross-sectional deformations at any live load level below 160 kips (712 kN), where the buried HDPE pipe showed elastic behavior. Therefore, both two and three-dimensional FEM analytical investigations are quite efficient for the shallow-depth buried HDPE pipe, subjected to live

load level up to four times the AASHTO H-20 Highway Loading, 160 kips (712 kN), on the paved backfill.

The hoop stress distributions at different load levels, based on two-dimensional FEM analysis are shown in Fig. 6.71 with the maximum hoop stress plotted at each load level, based on three-dimensional FEM analysis for comparison. Three-dimensional analysis indicated the maximum hoop stress, occurred at the shoulder (45^0 and 135º, whereas the two-dimensional analysis showed that it occurred at the spring line (180^0 and 0º) for all the live load levels. Two-dimensional analysis gave higher values of the maximum hoop stress than three-dimensional analysis, but the values at the shoulder were very close for all the live load levels, Fig. 6.71.

In Figs. 5.28 to 5.31, the maximum hoop stress, that corresponds to the experimental value for the maximum circumferential strain at the shoulder for each live load level, was less than that evaluated by either two or three-dimensional FEM analysis.

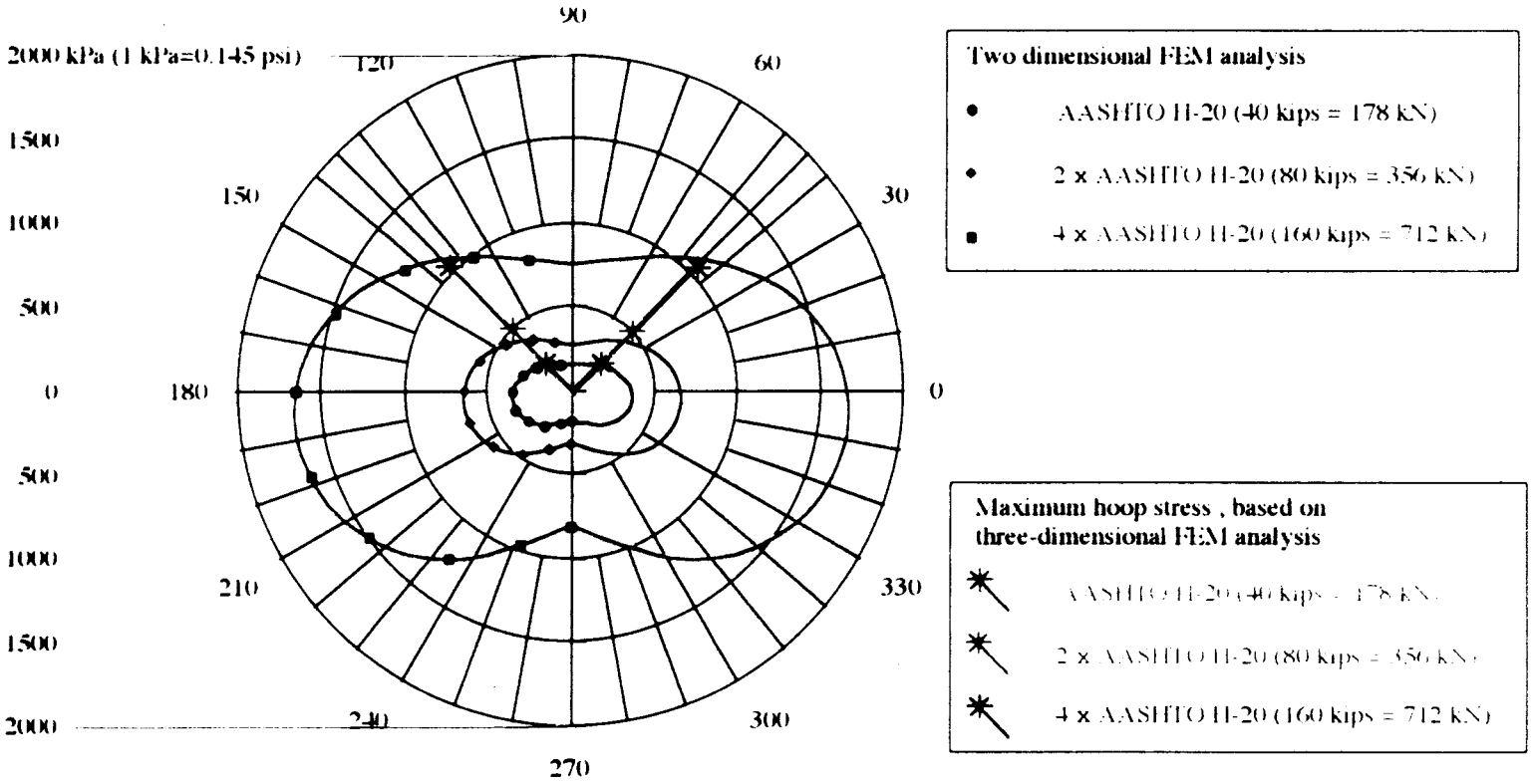

Fig. 6.71 Hoop stress distribution (absolute value) at different load levels

For example, the experimentally evaluated maximum hoop stress value at the shoulder, 910 kPa (132 psi) was less than 1,483 kPa (215 psi) and 1,055 kPa (153 psi), based on two and three-dimensional analyses for the live load level, four times the AASHTO H-20 highway load, 712 kN (160 kips). The bottom axial strain at the bottom vs. live load curves, show the agreement between experimental and analytical results in Fig. 6.72. The experimental results matched better with the three-dimensional FEM analysis than two dimensional analysis and showed the maximum hoop stress at the shoulders (45° and 135°). The two-dimensional plane-strain FEM CANDE analysis overestimates the thrust, and the design of the pipe installation based on this, becomes quite conservative.

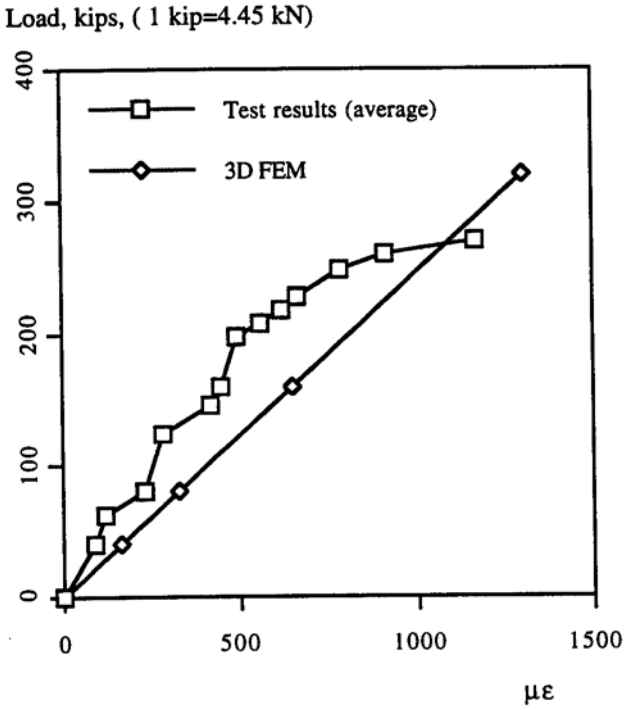

Fig. 6.72 Comparison of the bottom axial strain vs. live load-experimental and analytical investigations

The hoop stress distribution at failure (7.5% change of inside diameter), based on two dimensional FEM analysis, is plotted in Fig. 6.73, with the effective stress distribution and the maximum hoop stress, based on three-dimensional FEM analysis for comparison. The maximum compressive hoop stress, -4.0 MPa (-577 psi) occurred at the spring line (180^0 and 0^0), for two-dimensional FEM analysis, whereas the maximum resultant effective stress, -2.0 MPa (-289 psi) occurred at the shoulder (45° and 135^0) for three-dimensional analysis. The maximum hoop stress value, based on two-dimensional analysis is about twice the value of the resultant effective stress at the shoulder from three dimensional analysis. These maximum stress levels, -4.0 MPa (-577 psi) and -2.0 MPa (289 psi) are quite smaller than the yield strength of HDPE, [21-24 MPa (3,000-3,500 psi)], for the given cell class 4. Therefore, based on both experimental and analytical evaluations for shallow burial pipe, live load can cause over deflection-induced failure before any part of the pipe is subjected to yield stress.

6.4.6 **CIRCUMFERENTIAL BUCKLING**

A change in the geometry of the pipe under compression, it will result in the loss of its stability to resist loading. Because the instability can lead to a failure of the pipe, it is essential to take it into account for design of the pipe-soil system installation. The elastic buckling theory, based on the energy concept [Chelapati and Allgood, 1972], AASHTO specification [AASHTO, 1992], and Moser's formula for buckling [Moser, 1990] were used to verify instability at 7.5% change of inside diameter.

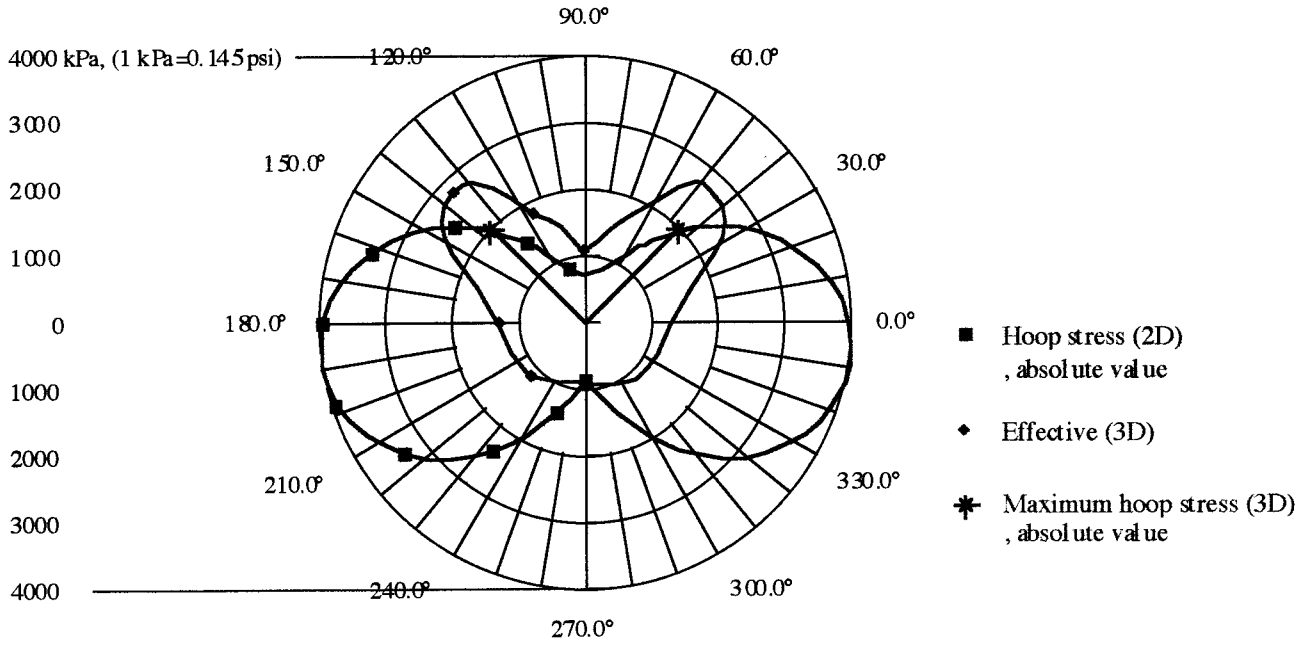

Fig. 6.73 Distribuions of hoop and effective stresses at failure

6.4.6.1 Buckling Analysis for the Shallow-Depth Buried HDPE Pipe, Subjected to Foot-Print Live Loading

Buckling analysis was carried out for the HDPE pipe, that was analyzed for failure in the previous Section 6.4.3.2, Failure Analysis, to evaluate whether buckling caused top flattening. The shoulder region (especially the 11 and 1 o'clock directions) can experience buckling, because for a flexible pipe, it can often cause flattening or reversal of curvature, shown in Fig. 6.54. The AASHTO buckling formula is based on a 50-year service life. Input data for failure analysis was substituted in the buckling equations (3.2) and (3.3) and P_{cr}, critical buckling pressure [Moser, 1990], and f_{cr}, the critical buckling stress [AASHTO, 1992] were calculated as follows:

$$P_{cr} = 2\sqrt{\frac{E'}{1-\nu}\left(\frac{EI}{R^3}\right)} = 270 \text{ psi (1.9 MPa)} \quad \text{----------} (6.28)$$

where

P_{cr}=critical buckling pressure, (Mpa, psi)

E'=soil modulus, (MPa, psi)

v=poisson's ratio, (dimensionless)

E--modulus of elasticity, (MPa, psi)

I=moment of inertia, ($mm^4/mm.$, $in.^4/in.$)

R=pipe radius, (mm, in.)

and

$$f_{cr} = 0.77(R / A\phi)\sqrt{\frac{BE'EI}{0.149R^3}} = 870 \text{ Psi (6 MPa)} \quad \text{---------} (6.29)$$

where

f_{cr}=critical buckling stress, (MPa, psi)

B=water buoyancy factor (dimensionless)=1- $0.33h_w/h$

h_w =height of water above top of pipe, (m, ft.)

h=height of ground surface above top of pipe, (m, ft.)

E--long term modulus of elasticity (50 year), (MPa, psi)

I=moment of inertia, (mm^4/mm, $in.^4$ /in.)

E'= soil modulus, (MPa, psi)

R=effective radius, (mm, in.)=c+III/2

c=distance from inside surface to the neutral axis, (mm, in.)

Aϕ=pipe wall area (0.083 mm^2/mm, in^2/ft.)

Moser's buckling formula is much more conservative than the AASHTO formula by a factor of three. The maximum hoop stress, applied in the shoulder region, 609 psi (4.2 MPa) was smaller than f_{cr}. Therefore, the pipe, buried in backfill soil (Class II, SP, R=90%), is not subjected to buckling before it fails due to over deflection.

6.4.6.2 Buckling Analysis for the Shallow-Depth Buried HDPE Pipe, Subjected to Uniformly Distributed Load.

The experimental test results showed no buckling at deflection-based failure, (Section 5.7). P_{cr}, critical buckling pressure [Moser, 1990], and f_{cr}, critical buckling stress [AASHTO, 1992], in equations (3.2 and 3.3) for the Type I pipe specimen were as follows: P_{cr} = 327 psi (2.25 MPa) and f_{cr} = 696 psi (4.8 MPa). The maximum hoop stress level corresponding to the strain values at the shoulder for 7.5% of the vertical change of diameter, 264 psi (1.8 MPa), was smaller than P_{cr} and f_{cr}. Therefore, the over deflection occurred and caused failure before the HDPE pipe experienced buckling for the given backfill and load conditions.

In a similar manner, the maximum hoop stresses, based on two and three-dimensional FEM analyses were compared with P_{cr} = 327 psi (2.25 MPa) and f_{cr} = 696 psi (4.8 MPa). The maximum hoop stress level at the shoulder, 284 psi (2.0 MPa), based on three-dimensional analysis, is smaller than the calculated value, P_{cr} = 327 psi (2.25 MPa) and f_{cr} = 696 psi (4.8 MPa). The maximum hoop stress level at the springline, 580 (4.0 MPa), based on two-dimensional analysis, is larger than Pcr and smaller than f_{cr}. Even though the maximum hoop stress at the spring line was overestimated by two dimensional analysis, the stress level is smaller than fcr . Therefore, the shallow-depth buried HDPE pipe, subjected to live load on paved backfill, does not experience buckling before it fails, and the failure mode is overdeflection, which may further develop to reverse the curvature.

The closed form solution of elastic buckling, based on energy concepts [Chelapati and Allgood, 1972], was carried out using CANDE-89 analysis to evaluate the buckling resistance of the shallow-depth buried pipe, subjected to a uniformly distributed live

loading [Katona et al., 1976] [Musser, 1989]. The uniformly distributed three-dimensional live load on paved backfill was simulated by equivalent truncated soil overburden pressure. The assumptions were as follows: 1) both soil and pipe are linear elastic, and 2) uniform compression loading. The assumption of uniform compression was implied with the suggested safety factor, 3, by Katona et al. [1976]. The critical hydrostatic buckling external pressure is given as follows:

$$P_{cr} = 6\sqrt{M_s(1-K_s)EI / D^3} \quad \text{----------} (6.30)$$

where

M_S = confined modulus of soil

K_S = lateral coefficient of soil

EI = in-plane bending stiffness of pipe

D = pipe diameter

The safety factor for buckling at pipe failure (7.5% change of inside diameter) was calculated as follows:

$$SF_{buckling} = P_{cr} / P_{av} = 1.73 \quad \text{----------} (6.31)$$

where

P_{av} = average pressure on pipe

The suggested safety factor, 3, compensating for the assumptions made above for smooth wall plastic pipe, seems to be the most conservative for the corrugated HDPE pipe. The reason is that the smooth wall pipe, is much more susceptible to buckling than the corrugated one. Thus, the approximate method for determining critical buckling pressure, $SF_{buckling}$, gives a value 1 for the corrugated HDPE pipe.

6.4.7 EVALUATION OF AXIAL STRESS VARIATION ALONG THE PIPE

For the in-situ HDPE pipe in a long-term period of service (up to 100 years), it is difficult to expect that the surrounding backfill environment stays uniform along the pipe as at the installation stage. The backfill modulus can vary along pipe because the degree of saturation increases. The backfill modulus can vary along the pipe because the degree of saturation and the density of backfill soil change with time [Drumm et al., 1997]. Also, improper installation of pipe and backfill soil can cause the non-uniformity. Therefore, it was necessary to evaluate the long-term performance of the pipe, buried in non-uniform backfill conditions. The FEM software used, CANDE89 [Musser, 1989] [Katona et al., 1976] for two-dimensional analysis and WANFE [Moore, 1996] for three-dimensional analysis, cannot take into account non-uniform longitudinal soil properties; for example, sandy soil changing from dry to saturated/dense to loose conditions.

Two-dimensional finite element modeling, coupled with harmonic analysis and finite difference approximation in the longitudinal direction, enables the evaluation of the three-dimensional response of shallow-depth buried HDPE piping in non-uniform backfill by assembling finite segments from infinite lengths in the different soil media and introducing deflection compatibility at the soil interfaces by regression analysis. The input moduli are the initial modulus for instantaneous response and the moduli, obtained from the seven-degree Voigt-Kelvin model, defined in Section 6.3 for long-term behavior. The associated stresses are computed by finite differencing the deflected profile. The axial stresses, based on the finite element analyses were compared with those from the simplified calculation method, based on an infinite beam on an elastic foundation analysis. Each backfill condition was assumed as a continuous linear elastic foundation (Winkler model)

[Cook and Young, 1985]. Type I pipe buried in differerent backfill conditions with nonuniform saturation was analyzed. The details of the specimen, subjected to AASHTO H-20 Highway Loading, were shown as follows:

Specimen Details

Type: I

Cell Classification: 335420C

Corrugation Design: Annular

Size: 24 in.(610 nun) inside diameter 25 ft. (7.62 m) length.

Figs. 6.74 and 6.75 show the schematic of the pipe-soil systems, subjected to AASHTO H-20 Highway live loading [CPPA, 1996]. Similar to the previous analyses in the Sections 6.4.4 and 6.4.5, the length of the specimen pipe was determined considering the characteristic length for the pipe in saturated loose sand, λ=21 ft. (6.4 m), which is equal to the distance between the two inflection points for a concentrated live load for a pipe on a continuous elastic Winkler foundation, equations 6.23 and 6.24. The pavement is assumed to be laid on the backfill, and the sinusoidal live load applied at the top of the backfill cover, shown in Figs. 6.74 (a) and 6.74 (b) [Martin, 1958] [Tia et al, 1997]. The live loading was uniformly distributed at each transverse section of the pipe-soil system. The simulated non-uniform backfill conditions as follows: i) saturated soil of one-sixth of the pipe length, 50 in. (1.27 m) from both ends to simulate poor drainage conditions, and ii) improper installation similar to that observed at a field inspection of HDPE pipe, buried in the median of I-75 near the Wildwood exit, was simulated by embedding one sixth of the pipe length from the left end in saturated loose sand, Fig. 6.75.

The moduli of elasticity for the different backfill conditions were estimated by the modified Vesic equation as follows [Vesic 1961, Das 1995].

$$k' = 0.65\sqrt[12]{\frac{E' D^4}{EI}}\left(\frac{E'}{D(1-\mu^2)}\right) \text{----------} (6.32)$$

where

k'= coefficient of subgrade modulus , lb/in^3, (kN/m^3)

E' = modulus of elasticity of soil, lb/in^2, (N/mm^2)

D = mean diameter of pipe, in., (mm)

μ = Poisson's ratio of soil

E = flexural modulus of pipe, lb/in^2, (N/mm^2)

I = moment of inertia of pipe cross section, in^4, (mm^4)

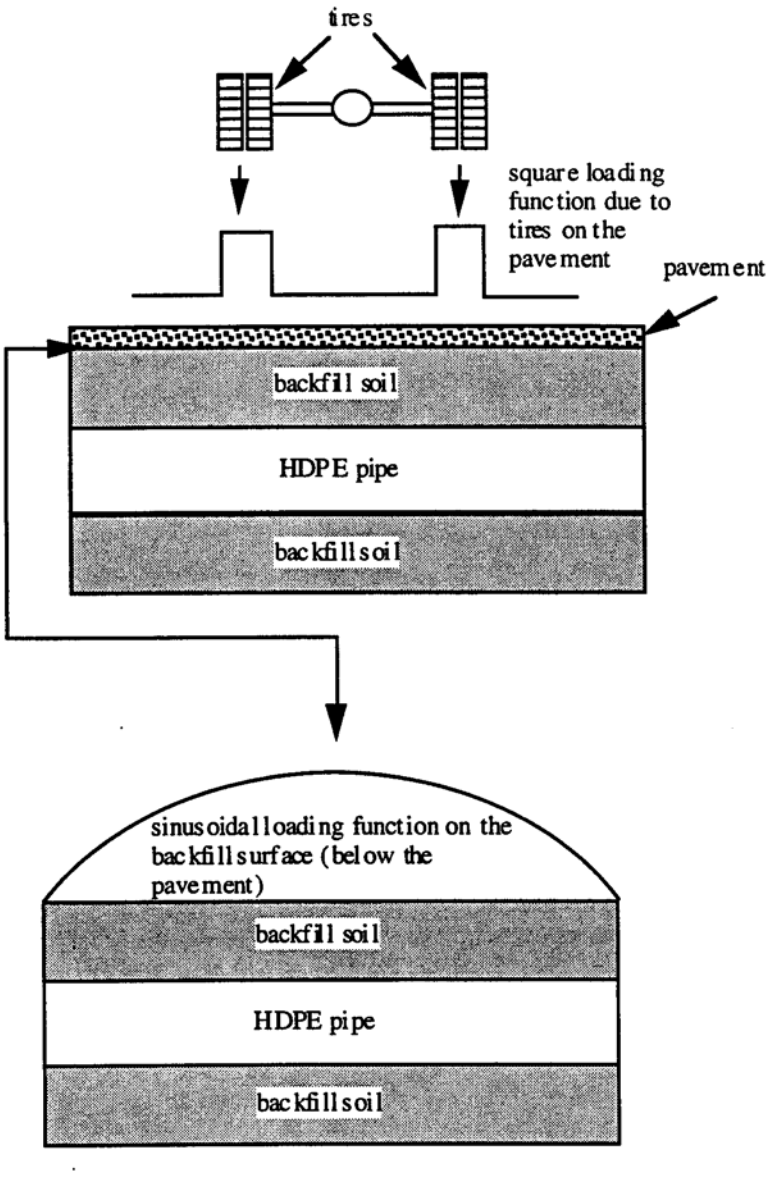

Fig. 6.74 a) Sinusoidal loading function on the backfill due to a square loading function on the pavement

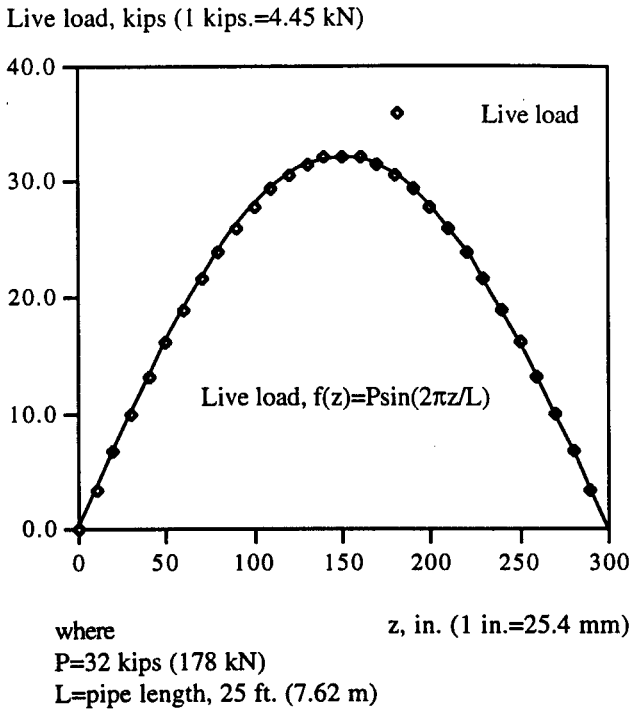

Fig. 6.74 b) Loading function on the backfill, due to AASHTO H-20 Highway Load

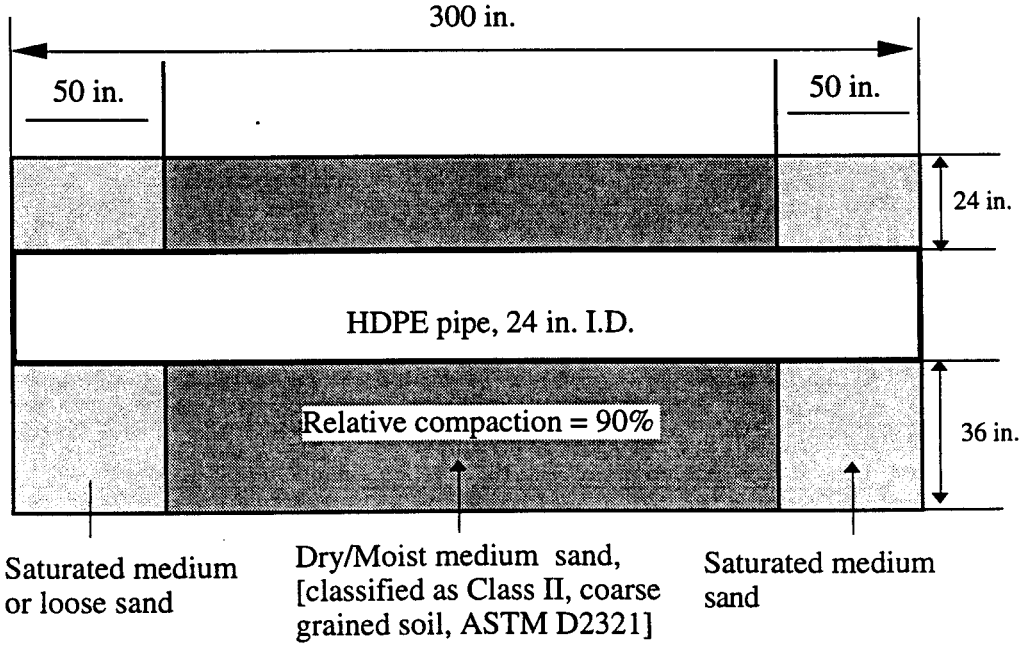

Fig. 6.75 Schematic of the pipe in non-uniform backfill

Tables 6.5 and 6.6 shows the unit weights and elastic moduli for the sand in different conditions [Dunn et al, 1980], [Das, 1995].

Table 6.5 Modulus of Elasticity, psi (kPa), of the Different Sandy Soils [Das, 1995]

Conditions	Loose	Medium	Dense
Drained	1,500 (10.3)	2,500 (17.5)	5,000 (34.5)
Saturated	244 (1.7)	805 (5.6)	2,886 (20.2)

Table 6.5 Unit weight, lb/ft^3 (kN/m^3), of the Different Sandy Soils [Dunn et al, 1980]

Conditions	Loose	Medium	Dense
Drained	90 (14.1)	104 (16.3)	109 (17.1)
Saturated	118 (18.5)	122 (19.2)	130 (20.4)

Finite element analyses (using the software CANDE89 and WANFE) with the same models, used in Sections 6.4.4 and 6.4.5 and the simplified calculation method (using the theory of beam on Winkler foundation), were carried out to estimate the deflections of the pipe at each cross-section and central difference approximations of the second derivatives were used to evaluate the changes of axial stress along the pipe as follows:

$$y_i'' = \frac{y_{i+1} - 2y_i + y_{i-1}}{(\Delta x^2)} \quad \text{----------} \quad (6.33)$$

$$\sigma_b = -Er_m y_i'' \quad \text{----------} \quad (6.34)$$

where

y=deflection

i=section number, 1 to 30,

Δx=interval between each segement, 10 in. (254 mm)

σb=axial stress due to bending, psi (N/mm2)

E=flexural modulus of the pipe, psi (N/mm2)

r_m=mean radius, in. (mm)

In view of the complexity, associated with three-dimensional prismatic elements and the time constraints, an approximate analysis was developed by assembling finite segments from infinite lengths in the different soil media, and introducing deflection compatibility at the soil interfaces by regression analysis. WANFE uses two-dimensional finite elements: i) in the cross section, coupled with longitudinal harmonics for the shallow burial pipe, and ii) in the longitudinal section, coupled with circumferential harmonics for deep burial pipe in the uniform backfill condition. The schematics of the assembly procedure are presented in Fig. 6.76. Similarly, deflections at each individual cross sections based on CANDE89 solution were assembled by regression analysis in the same manner as for WANFE. The associated stresses were computed by finite differencing the deflected profile.

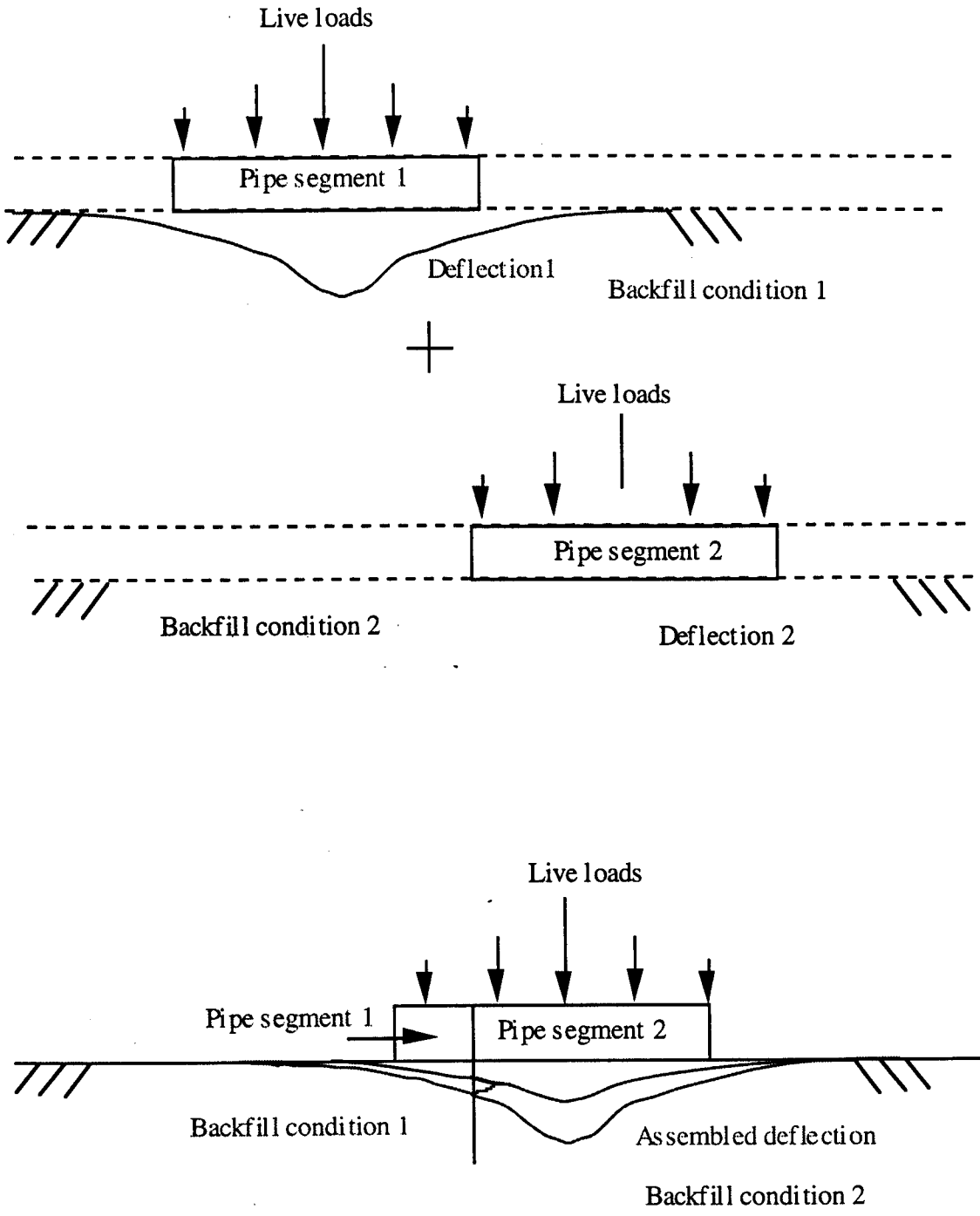

Fig. 6.76 Principle of segment assembly

6.4.7.1 **Results, Based on FEM Analysis**

Viscoelastic finite element analyses with finite difference approximation were used to evaluate changes of axial stress along the pipe, buried in medium dense sand backfill (Calss II, coarse grained soil with relative compaction=90%) . The soil of one fifth of the pipe length, 50 in. (1.27 m) from both ends was saturated, Fig 6.75. Assembly of deflections for. saturated and dry conditions were needed for three dimensional FEM analysis using WANFE, whereas the two dimensional analysis CANDE89 required the assembly of all individual cross-sectional profiles due to the load applied at each section. Schematics of the assembly procedure have been presented in Fig 6.76. Because of the fact that WANFE requires the uniform backfill property along the pipe, approximation for the satruated and dry segments were made where each pipe segment is considered an infinite beam on elastic foundation, Fig. 6.76. Regression analysis with 6th degree of polynomial smoothly represented the deflection compatibility at the soil interfaces.

Figs.6.77 and 6.78 show the results based on two and three dimensional FEM analyses. Deflection and axial stress variations (top and bottom of the pipe) along the pipe axis show the adverse effect of saturation indicating sudden increment of bending moment at interface between saturated and dry/moist regions. The deflection and stress variations, based on the two different analyses are quite similar and the two dimensional FEM analysis (CANDE89) showed slightly higher maximum deflection and stress values than the three dimensional analysis (WANFE). The maximum compressive axial stress, 804 psi (5.54 MPa), occurred at the top of the pipe and maximum tensile axial stress, 623 psi (4.3 MPa), at the bottom of the pipe, near the interface between the saturated and dry or moist region.

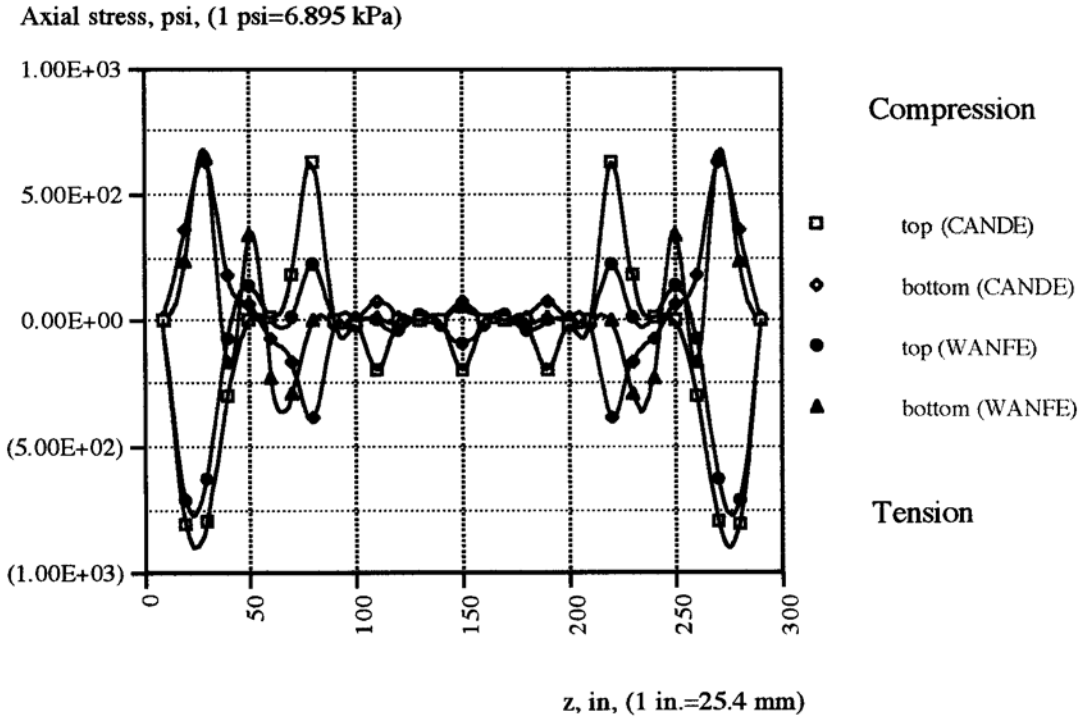

Fig. 6.78 Axial stress variation along the pipe in medium dense sand, saturated one-sixth of the pipe length from each end

Long-term variations of deflection and axial stress along the pipe were also evaluated by two dimensional FEM analysis. 50-year and 100-year flexural moduli, 71.9 and 69 ksi (496 and 476 MPa), were obtained from the seven-degree Voigt-Kelvin model, (developed from creep test results) in Section 6.3. The 50 and 100 year-deflection and stress variations are shown in Figs. from 6.79 to 6.82. It is noticed that the deformations and maximum tensile, and compressive stresses at the top and bottom of pipe increase with time adjacent to the saturated/dry soil interface. Fig. 6.83 shows the increment of axial stresses (tensile/compressive) near the interface with time.

Additionally, the extreme condition of improper installation, observed at a field inspection (HDPE pipe, buried in the median of I-75 near the Wildwood exit) was simulated by embedding one-sixth of the pipe length from the left end in saturated loose sand , Fig. 6.75. Two-dimensional FEM analysis with FDM approximation in the axial, Z, direction was carried out to evaluate the HDPE pipe performance. The soft backfill condition at one end caused a sudden jump of both deflection and axial stress near the saturated loose/dry medium sand interface, Figs. 6.84 and 6.85. The maximum tensile stress at the bottom of the pipe and the compressive stress at the top were 1,594 psi (11 MPa) and 2,647 psi (18.3 MPa), respectively.

$$y = -1.79E\text{-}13x^6 + 1.61E\text{-}10x^5 - 5.57E\text{-}08x^4 + 9.31E\text{-}06x^3 - 7.61E\text{-}04x^2 + 2.64E\text{-}02x + 1.68E\text{-}01$$

$$y = -1.13E\text{-}13x^6 + 1.02E\text{-}10x^5 - 3.51E\text{-}08x^4 + 5.80E\text{-}06x^3 - 4.61E\text{-}04x^2 + 1.46E\text{-}02x + 1.23E\text{-}01$$

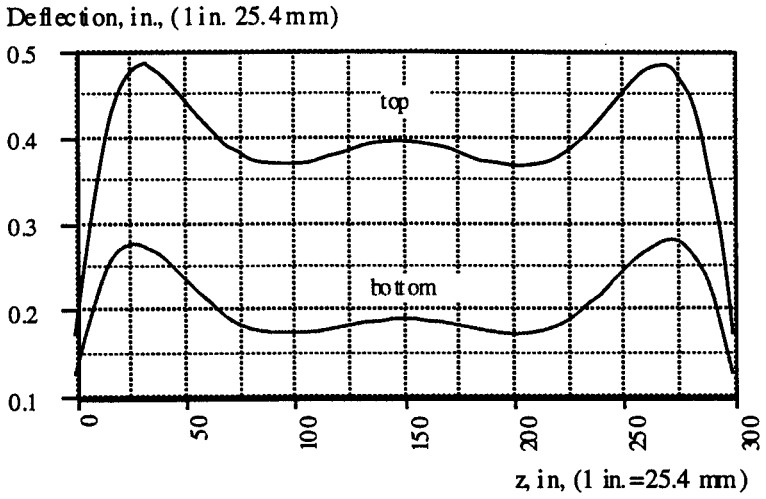

Fig. 6.79 Deflection variation along the 50-year old pipe

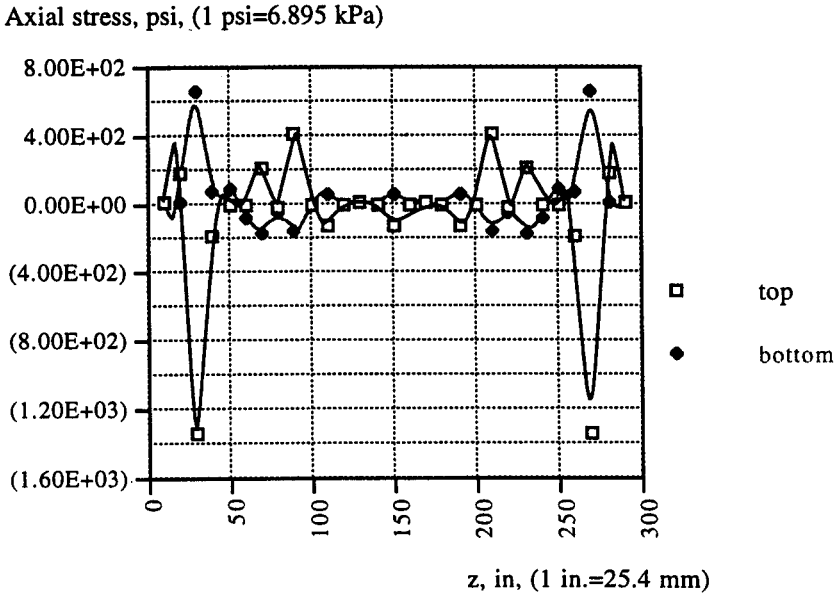

Fig. 6.80 Axial stress variation along 50-year old the pipe

$$y = -2.48E\text{-}13x^6 + 2.23E\text{-}10x^5 - 7.69E\text{-}08x^4 + 1.27E\text{-}05x^3 - 1.02E\text{-}03x2 + 3.36E\text{-}02x + 1.43E\text{-}01$$

$$y = -1.52E\text{-}13x^6 + 1.37E\text{-}10x^5 - 4.72E\text{-}08x^4 + 7.80E\text{-}06x^3 - 6.20E\text{-}04x^2 + 1.96E\text{-}02x + 1.04E\text{-}01$$

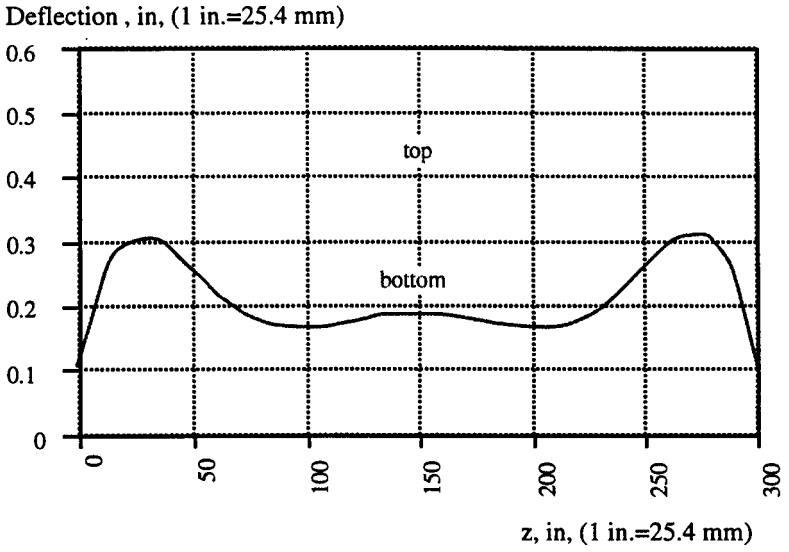

Fig. 6.81 Deflection variation along the 100-year old pipe

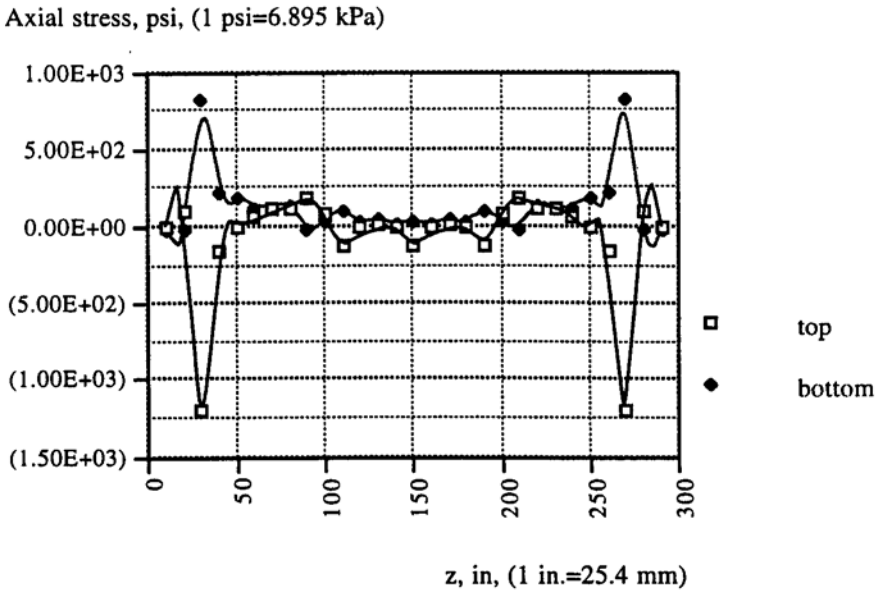

Fig. 6.82 Axial stress variation along the 100-year old pipe

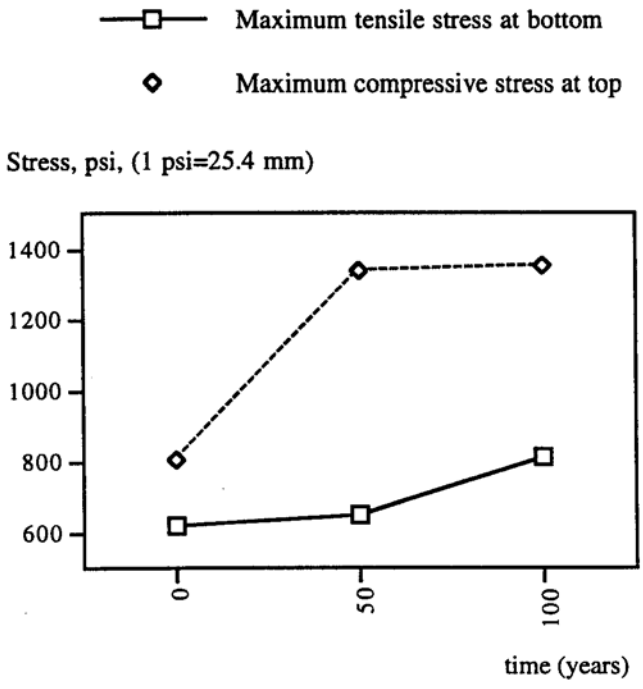

Fig. 6.83 Axial stresses near the saturated/dry interface

$$y = 2.06E\text{-}17x^8 - 2.59E\text{-}14x^7 + 1.31E\text{-}11x^6 - 3.31E\text{-}09x^5 + 4.28E\text{-}07x^4 - 2.28E\text{-}05x^3 - 2.13E\text{-}04x^2 + 4.30E\text{-}02x + 7.03E\text{-}01$$

$$y = 1.41E\text{-}17x^8 - 1.79E\text{-}14x^7 + 9.07E\text{-}12x^6 - 2.33E\text{-}09x^5 + 3.11E\text{-}07x^4 - 1.84E\text{-}05x^3 + 1.00E\text{-}04x^2 + 1.83E\text{-}02x + 6.17E\text{-}01$$

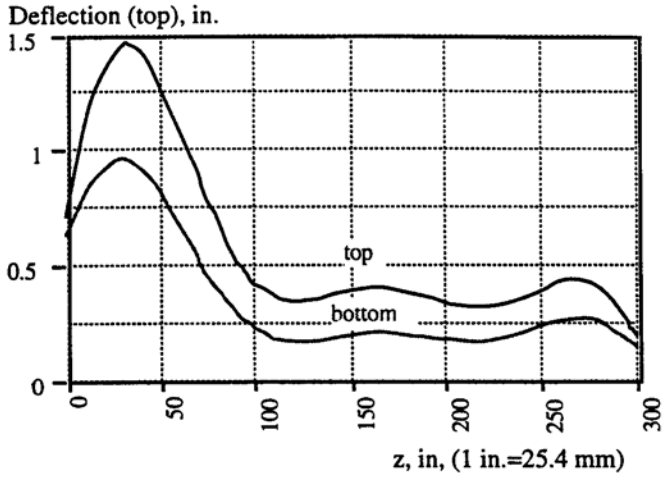

Fig. 6.84 Deflection variation along the pipe in dry medium sand, with saturated loose sand one sixth of the pipe length from the left end

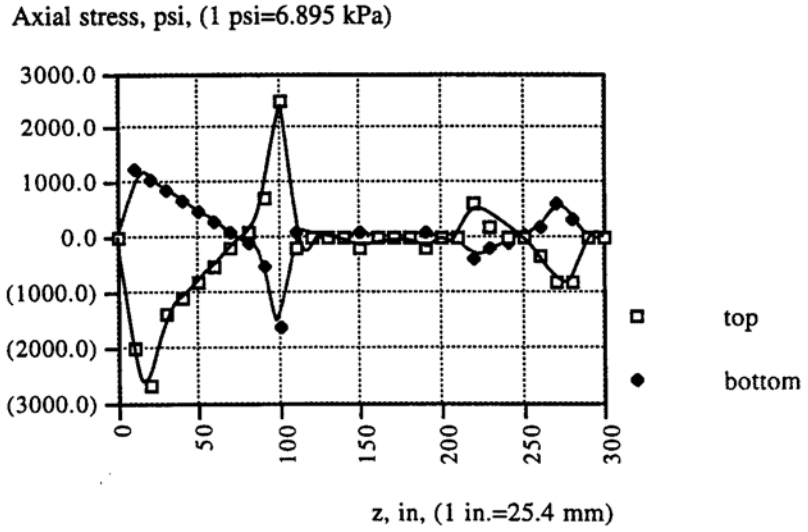

Fig. 6.85 Axial stress variation along the pipe in dry medium sand, with saturated loose sand one sixth of the pipe length from the left end

Even though the stress levels are lower than the yield strength of 3,000 psi (21 MPa), the local stress at an initially defective zone can be raised high enough to initiate SCG (Slow Crack Growth). This SCG can propagate further and possibly change to RCP (Rapid Crack Propagation).

6.4.7.2 **Simplified Calculation Method**

Based on the theory of the beam on continuous elastic foundation (Winkler model), a simplified calculation, was carried out [Cook and Young, 1985]. The deflections were estimated by segment assembly as follows: i) superposition of all individual segment deflected profiles due to live loads, AASHTO H-20 and backfill dead load, and ii) assembly of saturated and dry segment deflected profiles by enforcing deflection compatibility at the soil interfaces by regression analysis. The

$$y_i = \frac{\beta P_i}{2k} e^{-\beta z_i} [\cos(\beta z_i) + \sin\cos(\beta z_i)] \quad \text{----------} (6.35)$$

$$y = q / k \quad \text{----------} (6.36)$$

where

$$\beta = \sqrt[4]{\frac{k}{EI}}$$

k=spring coefficient for foundation (MPa, psi), 34.6 psi (0.24 MPa) for dry and 107.3 psi (0.74 MPa) for saturated medium sand [Das, 1995]

E=modulus of elasticity of the pipe (MPa,

I=moment of inertia (mm^4, in^4.)

q--uniformly distributed backfill dead load on the pipe (lb/in, N/mm)

The assembled deflection profiles are shown in Figs. 6.86 and 6.87. Similar to FEM analyses in the previous Section, 6.4.7.2, the variation of axial stress at the bottom of the pipe can be evaluated by using FDM and compared with the results of two-dimensional FEM analysis, Fig. 6.88. The values of maximum deflection and tensile stress, from the direct simplified calculation method, are less than those based on two-dimensional FEM analysis. However, the both methodologies agree quite well, showing similar patterns of stress variation with good overlapping of data, Fig. 6.88. Therefore, comparing Figs. 6.78 and 6.88, it is indicated that all of the three different approaches show very close patterns of stress variation. The two-dimensional FEM analysis, compared with FDM approximation longitudinal stresses is the most conservative methodology to evaluate the longitudinal performance of the pipe buried in non-uniform backfill conditions. Tables 6.7 and 6.8 show the evaluation of maximum tensile and compressive stresses, based on the three different analyses.

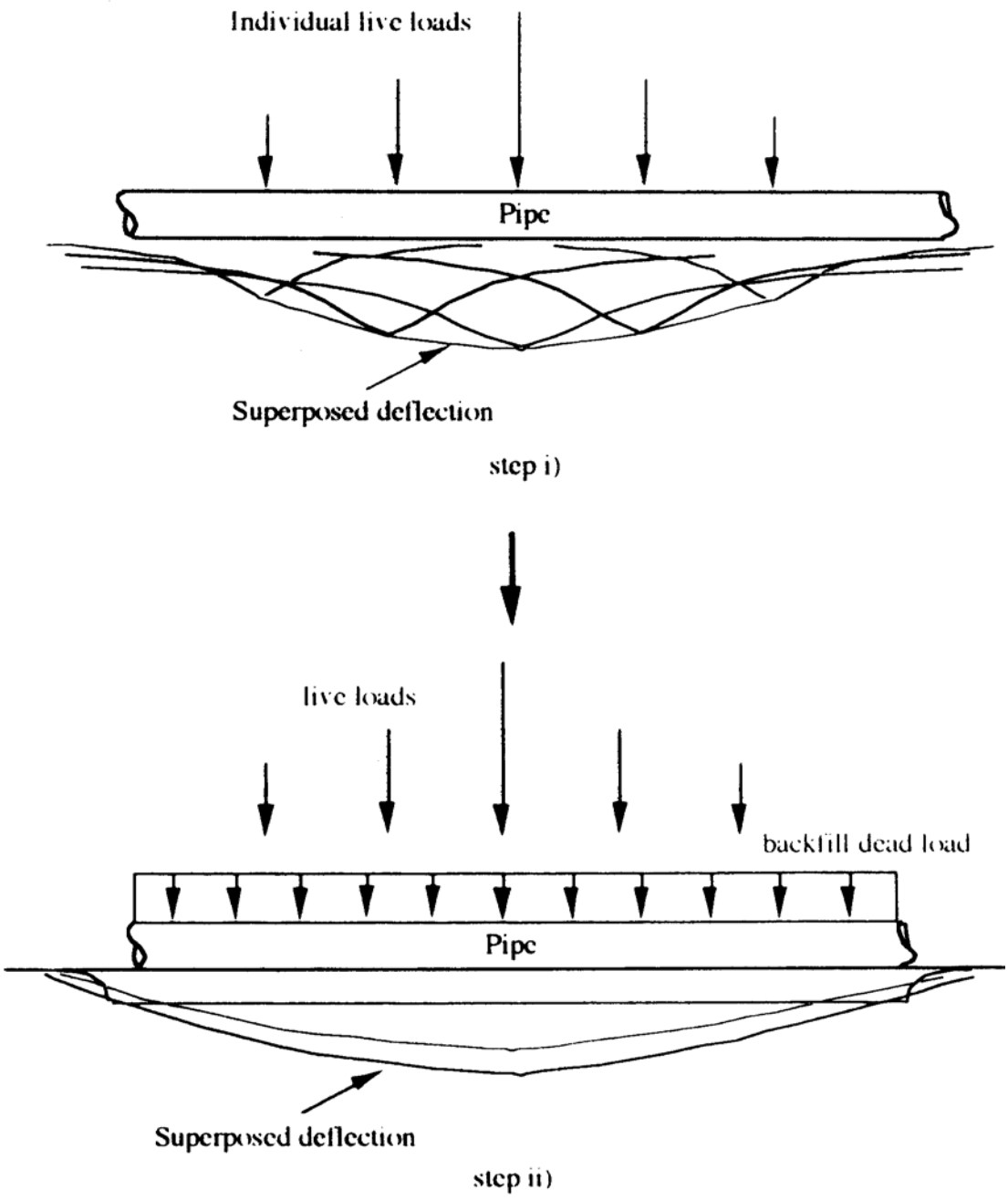

Fig. 6.86 Details of step i) and ii) deflection superposition for the simplified calculation method

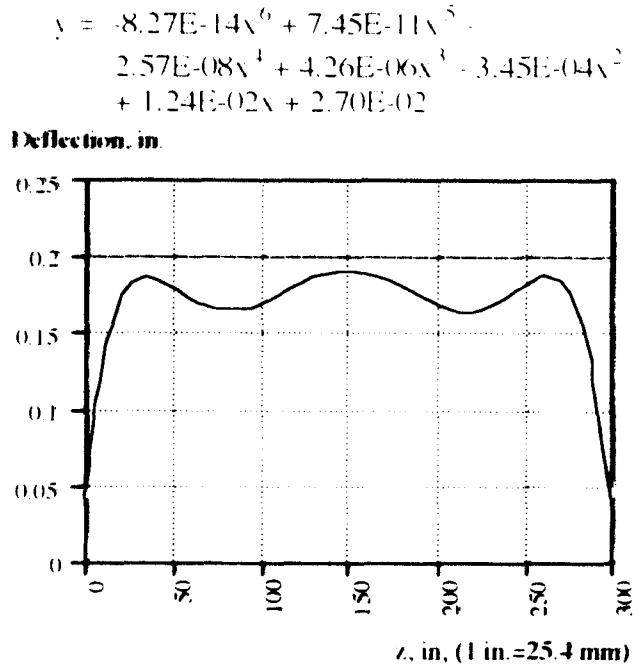

Fig. 6.87 Deflection variation (based on the simplified calculation method) along the pipe

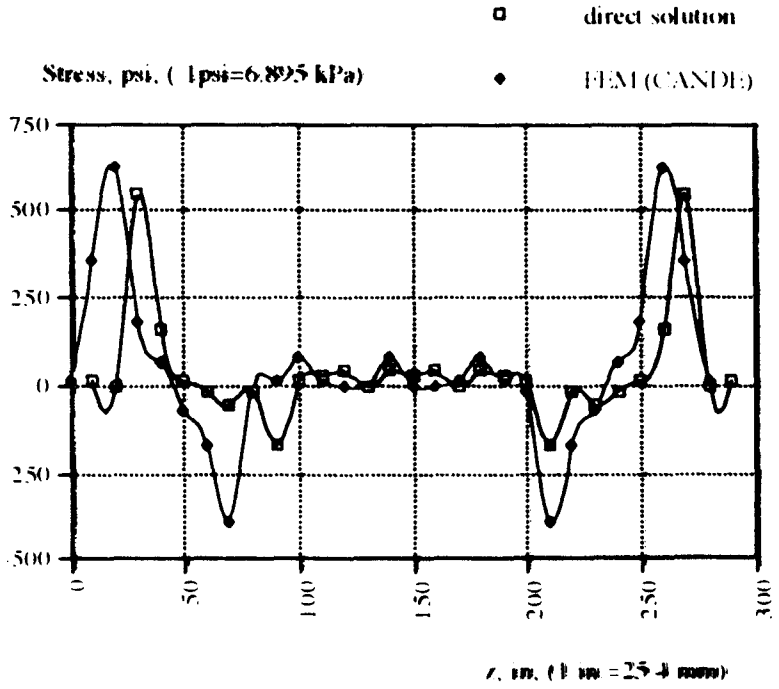

Fig. 6.88 Comparison of stress variation, based on the simplified calculation method and 2D FEM analysis along the pipe

Table 6.7 Maximum Axial Stress, Evaluated by 2D FEM analysis for the Pipe Buried in Non-Uniform Backfill Condition, Saturated Loose/Dry Medium/Saturated Medium Sand

Methodology	Tensile stress (bottom), psi, (MPa)	Compressive stress (top), psi, (MPa)
2D FEM	1,594 (11)	2,647 (18.3)

Table 6.8 Maximum Axial Stress, Evaluated by Different Methodologies for the Pipe Buried in a Non-Uniform Backfill Conditions, Saturated-Dry Medium Sand

Methodology	Tensile stress (bottom), psi, (MPa)	Compressive stress (top), psi, (MPa)
2D FEM	Instantaneous, 623 (4.3) 50 years, 653 (4.5) 100 years, 816 (5.6)	Instantaneous,804 (5.5) 50 years, 1,340 (9.2) 100 years,1354 (9.3)
3D FEM	Instantaneous, 651 (4.5)	Instantaneous, 706 (4.9)
Simplified Calculation Method	Instantaneous, 544 (3.8)	

6.4.7.2 **Joint Integrity**

The performance of the two different types of joints was evaluated by comparing maximum tensile stress near the saturated-dry interface and the required minimum strength of each type of joint. The two different types of joints are as follows: 1) coupler with polyisoprene O ring gasket (Type I), and 2) spin-welded joint (e.g. connection of the bell end with the corrugated length for Type II pipe). The minimum strength of each type of joint and the equivalent axial stress level at the bottom of the pipe are shown in Table 6.9.

Table 6.9 Current Data for Minimum Strength of Joint and Axial Stress on the Pipe

Type of joint	Internal pressure for initiation of leakage	Corresponding axial stress	Axial stress due to differential settlement
Coupler with O ring	10.8 psi (74.5 kPa) (ASTM D3212)	707 psi	816 psi at 100 years
Spin-Welded	320 psi (2.2 MPa) (ASTM D3261) - Heat fusion	743 psi	816 psi at 100 years

The axial stresses for initiation of leakage were obtained from the ASTM testing standard specifications, shown in Table 6.10, and compared with the maximum axial tensile stress due to differential settlement at the saturated-dry medium sand interface, shown in Table 6.9. The coupler with the polyisoprene O ring gasket and spin-welded joint (connection of the bell end with the corrugated length for Type II pipe) connecting the pipe at the interface, saturated-dry medium sand backfill was determined as adequate for 50 years; but after that, increasing differential settlement of the segments leads to higher tensile stresses at the interface and opening or cracking of the joints, Tables 6.9 and 6.10.

6.4.7.4 Flexural Buckling Resistance

The effect of the distribution of the bending moment along the pipe buried in non-uniform backfill conditions on its flexural buckling strength was investigated. When the pipe is subjected to a non-constant bending moment throughout the length due to non-uniform condition of the backfill material, flexural buckling of the pipe can occur and cause possible cracking or joint opening [Chen and Lui, 1987].

The critical elastic buckling moment is as follows:

$$M_{cr} = C_b \times M_{ocr} \quad \text{----------} \quad (6.38)$$

where

$$M_{ocr} = \frac{\pi}{L}\sqrt{EIGJ} \quad \text{----------} \quad (6.39)$$

in which

Mcr-elastic buckling moment, lb-in, (N-mm)

Mocr=elastic buckling moment under uniform moment, lb-in, (N-mm)

C_b=equivalent moment factor

EI=bending stiffness, lb-in^2, (N-mm^2)

GJ=torsional stiffness, lb-in^2, (N$^-$mm^2)

Based on the Kirby and Nethercot's (1979) empirical relation for various loading conditions, C_b for the HDPE pipe, buried in non-uniform backfill can be calculated as follows:

$$C_b = \frac{12}{3(M_1 / M_{max}) + 4(M_2 / M_{max}) + 3(M_3 / M_{max}) + 2} \quad \text{------ (6.40)}$$

where M_1,M_2, and M_3 are the moments at the quarter-point, mid-point, and three-quarter point of the beam, respectively, and Mmax is the maximum moment of the pipe. The critical equivalent moment factor, C_b=1.87, was estimated for the HDPE pipe in the saturated-dry medium sand backfill condition, subjected to the sinusoidal live loading. The critical moment, M_{gr}=951 kips-ft (1.27 MN-m), and the critical buckling stress σ_{cr}=1,307 psi (9.0 kPa). Therefore, considering Table 6.9, it was found that the pipe buried in the non-uniform saturated backfill condition (saturated-dry medium sand) under highway live loading can be subjected to flexural buckling at 50 years of service. The critical buckling stress, 6cr=1,307 was less than 1,340, the applied compressive stress at the top of the specimen near the interface.

Due to the viscoelastic behavior of the HDPE, the pipe can be subjected to flexural buckling or joint opening, even though it may perform well for the first few years. It is quite clear that there are two important parameters which cannot be overlooked of underestimated. One is the viscoelastic behavior of the HDPE pipe, and the other is the non-uniform backfill condition.

CHAPTER 7

DISCUSSION

The discussion of the findings is focused on certain recent concerns, associated with the HDPE piping related to cell classification, environmental stress cracking resistance, deflection, buckling, top flattening, non-uniform backfill condition, joint integrity, leakage, tearing and delamination of liner, longitudinal bending, circumferential cracking, creep, creep rupture, slow crack growth, rapid crack propagation, long term performance, and service life prediction.

In HDPE, stress cracking is most commonly thought to occur when the tie molecules which link crystalline and amorphous regions slowly slip out from the region of crystallinity involving entangled loose ends of tie molecules [Lustiger, 1983]. Fracture occurs between crystalline regions involving the amorphous polymer, without apparent deformation with relatively smooth fracture face morphology [Peggs and Kanninen, 1995]. Test results of environmental stress cracking resistance (ESCR) testing indicated excellent performance of both Type I and II HDPE specimens in the extremely harsh environment [100 % IGEPAL, CO-630, concentration at 50 °C, (112 OF)], endorsing the new cell classification, 335420C. Initial pin-point surface depressions did not play any role of

stress raisers to initiate cracking, shown in Fig. 5.1. Therefore, the depressions that occur in the manufacturing process do not have to be considered as initial flaws. The AASHTO type ESCR testing is a good accelerated testing method to evaluate relative ESCR among different cell classified HDPE pipe specimens, but not an accelerated simulation of in-situ conditions, since IGEPAL dissolves in the amorphous phase and not in the crystalline one, and the degree of crystallinity depends on temperature [Koerner et al., 1992].

The potential for stress cracking of plastic pipe is not a function of material properties alone, as geometry plays an important role [Gabriel, Bennett, and Schneir [1996]. The NCTL (Notch Constant Tensile Load), ASTM D5397, does not address the relationship between stiffness and stress crack initiation with the focus on geometry. Studies of this nature require more specimens, with different size notches at different temperature levels, and IGEPAL_ concentrations to address the notch sensitivity, crack propagation rate, temperature effects, concentration of the non-ionic detergent, and time. Therefore, the acceleration factor for the in-situ simulation can be estimated by evaluating the critical notch sizes and crack propagation rates at different exposure conditions.

Test results of parallel plate loading and creep enable the prediction of long term performance of HDPE pipe with several different techniques. This modified ASTM D2412 test for creep at super-ambient temperature levels can overcome the limitation of the HDB (Hydrostatic Design Basis, commonly used for smooth wall pressurized pipe) testing, which has only marginal value in its ability to predict the long-term service performance of gravity flow non-pressure pipes, with cost/benefit aspects that are not persuasive [Gabriel et al., 1996].

As Aklonis and MacKnight, (1983) pointed out, WLF time-temperature superposition is not an effective methodology for the prediction of the long-term behavior of semicrystalline HDPE pipe. The long-term master curve, based on the WLF method showed more scattering of data than those based on the Arrhenius and bidirectional shifting methods, due to temperature dependency of the crystallinity in HDPE. Based on the most conservative bidirectional shifting method, the flexural modulus reductions after 100 years of service, are 40% and 46% of the initial modulus for Type I and II specimens respectively. Due to the slight geometrical difference between the two different types of specimens, the 100-year moduli were 69 ksi (476 MPa) and 71.8 ksi (495 MPa) for Type I and II specimens, even though the Type II specimen had the higher rate of decay. Therefore, the HDPE pipe made with the new cell classification has a stiffness level good enough to meet the current specifications for flexural modulus, 335420C, after 100 years of service.

The 100-year flexural modulus of the new cell classification is close to the initial modulus for the commonly used cell classification, 324420C. However, it must be pointed out that the period of 100 years refers to only the cell classification, and not the long-term life, which has to be based also on other parameters, i.e. material imperfections, quality of installation etc. The single-degree Voigt model, which consists of a spring and dash pot in parallel can be used for the approximate estimation of the creep response of the HDPE; however, the response can be more accurately represented by the seven-degree VoigtKelvin model which consists of a series of Voigt elements. Considering the geometrical differences between the two types of specimens, the parallel plate loading test (ASTM D2412 type) for each different pipe size enables the evaluation of the flexural modulus in a more precise manner. Type I pipe has a slightly larger diameter and moment of inertia than

Type II pipe for the nominal size 12 in. (305 mm) I. D. pipe. The opposite is the case for the 24 in. (610 mm) I.D. pipe.

Prediction of long-term properties can be enhanced by comparing the long-term stress relaxation and creep with more specimens and exposure conditions (temperature and time). Based on the creep test results, fine-tuning of the prediction can be achieved by increasing the test temperature levels from the ambient temperature to 50 OC, (112 OF). It is necessary to carry out parallel plate testing for all testing temperature levels to evaluate the initial modulus at different temperatures. The exposure time need not be strictly 10,000 hours for all testing temperature levels to construct the 100-year scale master curve for the HDPE pipe of cell classification 335420C. For example, extrapolation and calculation of activation energy for Ahrrenius modeling, based on curve fitting with a larger number of temperature levels, is more precise than the common three-point curve fitting.

It is not recommended to use any detergent (e.g. IGEPAL, CO 630) for creep or stress relaxation tests to reduce the test period, because of the instability at high temperatures and the lack of correlation between the detergent concentration and rate of degradation. Oxidation reactions can occur quite fast at super-ambient temperatures and lead to erroneous predictions of the long-term properties of HDPE pipe specimens, exposed to the detergents, and to an unacceptably large scatter in the data [Sholten et al, 1989]. Because of the strong time and temperature dependence of polyethylene, application of super-ambient temperatures alone can accelerate the failure mechanism in a more precise viscoelastic manner for the service life prediction of the HDPE pipe.

Moser [1993, 1994] observed that "the normal and real modulus is the instantaneous stress divided into the instantaneous short term strain parameter for design and most materials must be designed on a life basis". This was based on Hydrostatic

Design Basis (HDB) strength testing of the PVC pipe that had been in service for 15 years, in which the modulus after unloading was the same as that when the pipe was manufactured. The properties of HDPE pipe (viscoelastic material) are dependent on time, temperature, stress, and rate of loading. Instantaneous testing cannot be expected to simulate material behavior when subjected to stress or deformation for an extended period of time. For life prediction, consideration should be given to the estimation of long-term property values of the modulus and strength under exposure conditions (pipe-soil interaction) that simulate the end-use applications. More importantly, the integral of the time-dependent modulus over the life cycle period must be considered for viscoelastic behavior.

The use of a pseudoviscoelastic modulus for the elastic modulus implies the tacit use of a principle of viscoelasticity known as the "correspondence principle". This principle states that the stresses in a viscoelastic body subjected only to constant applied forces, will be exactly the same as they are in an elastic body subjected to the same set of tractions [Christensen, 1971]. In contradistinction to constant internally pressurized pipe in the gas industry, non-pressure pipe is subjected to mixed force and displacement boundary conditions, which make creep and relaxation characterization testing essential for an analysis of the potential for service failure.

Creep, expressed in terms of the decreasing modulus contributing to increasing deformation, (i.e. loss of stiffness), and creep-rupture, expressed in terms of decreasing life with increasing stress and temperature, are important parameters for life prediction. The transition from ductile to brittle behavior enables the realistic estimation of life from the creep-rupture plot. Geometry, associated with the pipe curvature and the connectivity of the corrugations with lining, can affect creep and creep-rupture behavior. It can also reduce

the buckling strength at the wall. It is necessary to identify unexpected failure-initiating defects and to understand at what rate induced cracks will propagate, and how much they affect the reduction of service life, Figs. 3.2 , 3.3, and 3.4.

Experimental and analytical investigations for the performance of shallow depth buried HDPE pipe, subjected to live load, confirmed that pressure distribution around the HDPE pipe at shallow-depth is not uniform; the vertical changes of inside diameter were greater than the horizontal changes and the maximum circumferential strain occurred at the shoulder region (45° and 135^0) of the pipe cross section. The failure mode was characterized by over-deflection with the top flattening and reversing in curvature, and over-deflection preceding yielding and buckling. The pipe can deflect or distort without kinking or buckling, and remain structurally stable until it deflects 7.5% vertical change of diameter; However, the excessive deflection with flattening can limit the flow or cause leakage [Goddard, 1994] [Hashash, 1991].

The testing required a high load level to cause a 7.5% change diameter at the given backfill condition, Class II, SP, R>90% , requiring two hydraulic jacks, instead of the air bag loading, used by Selig et al. (1993) and water jacket loading by Rogers et al. (1995), for similar HDPE pipe-soil interaction tests. The test setup simulated the shallow burial pipe condition similar to the test setup used by Rogers et al. (1995) unlike the test setup used by Selig et al. (1993) for the deep burial study of pipe-soil interaction. The test setup had a much higher applicable load capacity; up to 400 kips (1.8 MN) more than that of Roger et al. (1995).

For HDPE piping, longitudinal stress should not exceed 3,000 psi (20.7 MPa) and the bending strain should not exceed 0.05 [CPPA, 1996]. However, the test results

indicated that the maximum axial strain at failure is approximately 0.002 (at 7.5% vertical change of diameter), which is much less than the CPPA limit referred to above. It seems that the limit, which is based on yielding due to longitudinal bending, is not reasonable for the general failure criteria of the buried HDPE pipe subjected to live load. The maximum circumferential strain occurred at the shoulder region (45^0 or 135^0) of the specimen, whereas the minimum circumferential strain occurred at the haunch (225^0 or 315^0) for each live load level, Figs 5.28 to 5.31.

Tensile circumferential strains occurred at all the regions except at the haunches (225^0 or 315^0) for all the live load levels. This is quite similar to the findings of Rogers et al. (1995). The strain values measured at the single and double wall locations were close to each other. Similar to the test results for longitudinal strains, there was no significant difference between the single and double-wall locations for the circumferential strain measurement. Axial strain, which is much less than the CPPA (Corrugated Polyethylene Pipe Association) limit, plays an important role to cause non-uniform over-deflection in a three-dimensional manner.

From flexural testing of the specimens in air, it was found that the failure mode is in plastic yielding without cracking, buckling, or debonding between inner and outer liners. The range of midspan axial strain at initiation of yielding (increase of deflection without load increment) is about 2,500-6,000 g (0.0025-0.006%), which was much less than the CPPA limit of 50,000 p. (5%). This indicates that the CPPA strain limit based on the uniaxial yielding of coupons, is not realistic for the limit state of the in-situ pipe. The soil tight joint has a large deflection capacity that will allow differential settlement due to possible non-uniform backfill conditions. Additionally, the joint can relieve the large longitudinal stress along the pipe due to the differential settlement. Because of the variety

of joints, it would be necessary to compare the flexural strengths of the pipes with different joint types.

Similar to the viscoelastic behavior of the polymer itself, an isochronous effect in the pipe soil system was also observed. These findings are based on the unnotched pipe, subjected to uniformly distributed live load with proper uniform backfill. The findings can be extended by long-term foot print loading on an initially defective pipe, to evaluate the effectiveness of the variables (axial stress due to bending, creep/creep rupture, nonuniformity of backfill, and size of the possible initial damage, e.g. notch that can occur during the manufacturing, transportation, or installation on the long-term performance of the HDPE pipe.

The results of the two and three-dimensional finite element analyses and experimental investigation agree quite well, until the load level exceeds four times the AASHTO H-20 Highway Load. The estimation of the maximum change of inside diameter, based on the Iowa equation is quite conservative, compared to the values from the analytical and experimental investigations, Figs. 6.69 and 6.70. The three-dimensional finite element analysis for pipe-soil interaction overcomes the limitations of the Iowa deflection analysis, which uses empirical constants, and the two-dimensional FEM analysis, which does not include the longitudinal effect.

The FEM software used, CANDE 89 [Musser, 1989, Katona et al., 1976] for two-dimensional analysis, and WANFE [Moore, 1996] have limitations for modeling of the corrugation and valley without prismatic finite elements, and cannot take into account non-uniform longitudinal soil properties; for example, sandy soil changing from dry to saturated/dense to loose conditions. The uniform outside diameter and element length,

which is long enough to cover at least one corrugation and one valley, were used to simulate the correct circumferential and longitudinal stiffness of the corrugated HDPE pipe. South Florida clean sand (Class II, SP) with relative compaction 85-95% is a excellent backfill material, which can support HDPE pipe very well for highway culvert applications. However, the predicted period cannot exceed 50 years, in view of the material and constructional uncertainties.

Special cautions are required in less stiff Class III, SM, backfill soil, compared to Class I and II. A higher degree of relative compaction and thicker cover depth are required to support the pipe as well as stiffer backfill soils for long-term performance of the pipe. For shallow-depth application, it is recommended to use backfill materials with a flexural modulus of at least 2,000 psi to ensure long term (50-year) performance of the HDPE pipe, subjected to live load. Based on the FEM analysis, failure occurs due to the effective stress, which is not necessarily circumferential or axial due to non-uniform external pressure distribution along the pipe. The magnitude of the maximum tensile axial stress is about 1/8 of the maximum effective stress in the shoulder region (clockwise from horizontal), Figs 6.52 and 6.53. Therefore, the axial stress contribution to failure cannot be simply underestimated, based on the CPPA performance limit (maximum stress 3000 psi, 20.7 MPa, and minimum strain 0.05) [CPPA, 1996]. The larger contribution of the axial stress to the resultant effective stress is for the less stiff backfill soil. Therefore, three-dimensional analysis is even more important for less stiff backfill conditions.

For long-term service (up to 50 years), it is difficult to ensure that the surrounding backfill environment will remain uniform along the pipe as in the installation stage. The backfill modulus can decrease if the degree of saturation increases. The backfill modulus can also vary along the pipe because of the degree of saturation and density of backfill soil

changing with time [Drumm et al., 1997]. Also, improper installation of the pipe and backfill soil can cause non-uniformity. Therefore, it was necessary to evaluate the longterm performance of the pipe, buried in non-uniform backfill conditions as follows: i) saturated soil for one-sixth of the pipe length, 50 in. (1.27 m), from both ends to simulate poor drainage conditions and ii) improper installation similar to that observed at a field inspection of HDPE pipe, buried in the median of I-75 near the Wildwood exit, was simulated by embedding one-sixth of the pipe length from the left end in saturated loose sand, Fig. 6.75.

The deflection profile of the long in-situ pipe was determined for the characteristic length, X=21 ft. (6.4 m), which is equal to the distance between the two inflection points for a concentrated live load for a pipe on Winkler foundation, equations 6.23 and 6.24. WANFE uses two-dimensional finite elements: i) in the cross section, coupled with longitudinal harmonics for the shallow burial pipe, and ii) in the longitudinal section, coupled with circumferential harmonics for deep burial pipe in the uniform backfill condition.

In view of the complexity, associated with three-dimensional prismatic elements and the time constraints, an approximate analysis was developed by assembling finite segments from infinite lengths in the different soil media, and introducing deflection compatibility at the soil interfaces by regression analysis. The method is approximate because rotation compatibilty is not enforced. Similarly deflections at each individual cross section, based on the CANDE 89 solution, were assembled with regression analysis in the same manner as for WANFE. Each backfill condition was assumed as a continuous elastic Winkler foundation [Cook and Young, 1985]. The associated stresses were computed by finite differencing the deflected profile. The schematics of the assembly procedure have

been presented in Fig. 6.76. Based on the theory of the beam on a Winkler foundation, a simplified analysis was carried out to compare and verify the results from two and three-dimensional FEM analysis. Similar to the FEM analysis coupled with the finite difference method, the segment deflection profiles due to live and backfill dead loads were assembled, with regression, Fig. 6.85. There was good agreement of the axial stress values, adjacent to non-uniform backfill interfaces, with those obtained from the two and three-dimensional FEM analyses and the simplified analysis.

The coupler with the polyisoprene O ring gasket and heat fusion joints (connections of the bell end with the corrugated lengths) connecting the pipe at the saturated-dry interface of the medium sand backfill was determined as adequate for 50 years, but after that, increasing differential settlement of the segments leads to higher tensile stresses at the interface and opening or cracking of the joints, Tables 6.9 and 6.10, ASTM D3212 and D3261.

Flexural buckling of the pipe can occur and cause possible cracking or joint opening when the pipe is subjected to non-constant bending moment throughout the length due to non-uniform condition of the backfill material. It was found that the pipe, buried in the non-uniform (saturated-dry medium sand) subjected to highway live loading, can be subjected to flexural buckling at 50 years of service. The critical buckling stress, 6cr=1,307 psi was less than 1,340 psi, the applied compressive stress at the top of the specimen near the interface.

FEM analysis and the simplified calculation with finite difference approximation showed possible joint opening and flexural buckling adjacent to the saturated-dry interface due to longitudinal bending, within the normal life period of the pipe. Therefore, the QC

(Quality Control)/QA (Quality Assurance) condition must be clearly specified for the installation, maintenance, and repair of the HDPE piping to reduce the problems associated with non-uniform backfill condition. These are addressed in ASTM D2321 Sections 5, and 6 (1997) and AASHTO LRFD Bridge Design Specification Sections 12.4.1 and 12.6.2.(1994) for backfill materials, embedment density, moisture content of embedment, settlement, and water control.

Failure can occur as a result of some unknown material performance characteristic, or some unexpected local service condition that initiates a crack at a "flaw" in the material. For long-term applications, both pipe deflection levels and the specific grade of the plastic used must be controlled. The striking feature of failure can be its local nature. The individual pipe wall profile must be evaluated in regard to its specific geometry, and the stresses and strains quantified to properly determine the long-term performance of the HDPE pipe. Local buckling can occur due to one or more combinations of deflection and ring compression for each specific profile. Cracking occurs due to stress concentrationamplified tension stresses (strains) and residual stresses in the profile. Local stresses that cause local failure (cracking) trigger the global failure. In the same manner, test results of the field inspection proved that the improper installation of the pipe can cause excessive local stresses, crack initiation, slow crack growth (SCG), and finally lead to rapid crack propagation (RCP). It is essential to evaluate the role and sensitivity of the critical element, which can undergo the local-global transition (SCG-RCP).

The critical element, in-turn, is defined, as the initial failure source of global fracture [Reifsnider et al., 1996]. Studies of this nature require long-term experimental and analytical investigations for pipe-soil interaction with specimens, including varying notch sizes with different exposure conditions (temperature, time, and live load level). The usefulness of the findings, in this analytical and experimental study, will be enhanced by

life prediction of the shallow burial HDPE pipe subjected to foot-print live loading, based on the critical element concept for evaluating temperature dependent creep/creep rupture mechanisms, localized buckling, liner tearing, and debonding.

CHAPTER 8

CONCLUSIONS

1. The short term environmental stress cracking resistance (ESCR) of the HDPE pipe with the new cell-classification is satisfactory notwithstanding pin-point surface depressions. Therefore, the depressions, that occur in the manufacturing process do not have to be considered as initial flaws; but these need to be evaluated for long-term sustained load conditions. AASHTO type ESCR testing is a good accelerated testing method to evaluate t e relative ESCR values for different cell classified HDPE pipe specimens, but not for accelerated simulation of in-situ conditions.

2. Arrhenius Equation-based analysis (AE) and the Bidirectional Shift Method (BSM) for the H PE pipe with the new cell classification, 335420C, are the appropriate methods to predict the long-term flexural modulus of the HDPE pipe, with the BSM being more conservative. The long-term master curve, based on the WLF method, showed more scattering of data than those on the Arrhenius and bidirectional shifting methods, due to temperature dependency of the crystallinity in HDPE. The WLF time-temperature superposition method is not recommended for the HDPE pipe with the new cell classification, in spite of some reports to the contrary for HDPE and MDPE geomembrane

liners. After 100 years of service, the flexural modulus of the HDPE pipe decreases to 47% of the initial value, indicating reduction of buckling strength which should be based on long-term modulus not on initial modulus.

3. Due to the imperfect installation or non-uniform backfill condition, the unfavorable SCG (Slow Crack Growth) can initiate, propagate, and develop to RCP (Rapid Crack Growth). Therefore, the failure mode is not restricted to SCG; transitioning to RCP implies catastrophic failure.

4. Proper installation conditions associated with uniformly distributed live load, adequate cover, and proper uniform compaction (relative compaction, R=85-95%) significantly reduce, but do not eliminate axial stresses. The failure mode of the pipe is characterized by the top flattening due to over-deflection, which precedes buckling or cracking, when it is subjected to the ultimate live load level. Vehicular traffic live load can be simulated better by tire foot-print loading than uniformly distributed load. Both loading patterns are in conformance with the DOTs in most states using HDPE culverts across roads. For the live load and the backfill combinations of i) foot-print/uniform and ii) uniformly distributed/non-uniform, large axial stresses can be induced leading to failure, associated with tearing, joint opening, and buckling. The coupler, with the polyisoprene O ring gasket and spin-welded joint (e.g. by connection of the bell end with the corrugated length for Type 11 pipe), connecting the pipe at the interface of the saturated-dry medium sand backfill was determined as adequate for 50 years, but after that, increasing differential settlement of the segments leads to higher tensile stresses at the interface and opening or cracking of the joints.

5. For shallow-depth applications, backfill materials with flexural moduli of at least 2,000 psi are required for long-term performance of 50 years for the HDPE pipe, subjected to live load. For the footprint live loading/uniform backfill with Class 11, SP, backfill combination, failure occurs due to the maximum effective stress, which is not necessarily circumferential or axial due to non-uniform external pressure distribution along the pipe. The magnitude of the maximum axial stress (87 psi, 0.6 MPa) is about 1/10 of the maximum resultant effective stress (835 psi, 5.8 MPa) in the shoulder region at failure (7.5% change of diameter). Therefore, the axial stress contribution to failure cannot be simply underestimated, based on the CPPA performance limit for yielding (maximum stress 3000 psi, 20.7 MPa, and minimum strain 0.05), [CPPA, 1996]. The greater contribution of the axial stress to the resultant effective stress is for the less stiff backfill soil.

6. The flexural failure mode of the pipe is by plastic yielding without cracking, buckling, or debonding between inner and outer liners.

7. The non-uniformity of backfill can be caused by partial saturation of the backfill or imperfect installation. This can induce large bending moments at the interface of the different soil media leading to critical long-term joint performance and buckling. Furthermore, the effect of the non-uniform backfill condition on long-term performance needs to be evaluated in different geological environments.

8. QA (Quality Assurance)/QC (Quality Control) conditions must be clearly specified for the installation, maintenance, and repair of the HDPE piping to reduce the problems associated with non-uniform backfill condition, for example, ASTM D2321 Sections 5, and 6, (1997) and AASHTO LRFD Bridge Design Specification Sections 12.4.1 and

12.6.2.(1994) for backfill materials, embedment density, moisture content of embedment, settlement, and water control.

9. The principal modes of failure can be characterized by their local nature. Local buckling can occur when sufficient compressive strain, due to any combination of deflection and ring compression, occurs for each specific profile. Cracking occurs due to stress concentration-amplified localized tension stresses (strains) and residual stresses in the profile. Local stresses that initiate local failure (cracking) trigger global failure. Geometry, associated with the pipe curvature and the connectivity of the corrugations with lining, can affect the creep and creep-rupture behavior. It can also reduce the buckling strength at the wall. Studies of this nature require long-term experimental and analytical investigations for pipe-soil interaction of specimens, with varying sizes of notches and different exposure conditions (temperature, time, and live load level). The use of threedimensional FEM analysis with brick elements, to model the individual pipe wall in regard to its specific geometry, will enable more accurate analysis of the long-term performance of the pipe, compared to the two-dimensional mesh model with harmonic analysis in the third direction.

10. It is difficult to draw definitive conclusions regarding life prediction, in view of the uncertainties associated with material imperfections, i.e. notches, material property changes (transition from creep to creep-rupture), changed backfill properties (saturation, improper installation).

11. An on-going experimental and analytical investigation at Florida Atlantic University, funded by FDOT, is addressing the life prediction of shallow burial HDPE pipe subjected to footprint Hive loading based on temperature-dependent creep / creep-rupture

mechanisms, localized buckling, liner kaving, and debonding. This study will enable more reliable estimates of life.

12. Until the findings of the FAU and other projects, for example, a recently initiated NCHRP study 4-26 entitled "Thermoplastic Drainage Pipe, Design and Testing" are available, it is not recommended that the 50-year life estimate be changed.

REFERENCES

1. AASHTO, "Interim Specifications-Bridges-1994", Section 18, AASHTO (American Association of State Highway Transfortation Officials), pp.323- 327, 1994.

2. AASHTO, "Standard Specifications for Highway Bridges-1994", AASHTO, 1992.

3. AASHTO M294-93, : Standard Specification for Corrugated Polyethylene Pipe, 12 to 36 in. Diameter, AASHTO, pp.745-749, 1993.

4. Adams, D.N., Tennyson, M., and Selig, E.T., "Polyethylene Pipe Under High Fill", Analysis, Design, and Behavior of Underground Culverts, TRB Report #1231, pp. 88-95, 1989.

5. Aklonis, J. J. and Macknight, W. J, "Introduction to Polymer Viscoelasticity", pp. 47-50, John Wiley and Sons, New York, 1983.

6. Ahn, W., An Experimental and Analytical Investigation of Viscoelastic Pipe Soil Interaction, Ph. D. Dissertation, 1998-Supervisor: D.V. Reddy.

7. Amarasiri, A., Jayawickrama,N., and Senadheera, S.P., "Use of Large Diameter HDPE Pipes in Highway Construction: Current State of Practice", Proc. TRB 78th Annual Meeting Washinton DC, 1999.

8. ASTM D 2412-92: Standard Test Methods for Determination of External Loading Characteristics of Plastic Pipe by Parallel-Plate Loading; Vol. 08.04, Plastic pipe and Building Products, Annual Book of ASTM Standards, pp. 142-146, 1995.

9. ASTM D 3350-84: Standard Specification for Polyethylene Plastics Pipe and Fitting Materials; Vol. 08.04, Plastic pipe and Building Products, Annual Book of ASTM Standards, pp. 479-483, 1995.

10. ASTM D 2990-93a: Standard Test Methods for Tensile, Compressive, and Flexural Creep, and Creep-Rupture of Plastics; Vol. 08.04, Plastic pipe and Building Products, Annual Book of ASTM Standards, pp. 189-206, 1995.

11. ASTM F894-92: Standard Specification for Polyethylene (PE) Large Diameter Profile Wall Sewer and Drain Pipe, Vol. 08.04, Plastic pipe and Building Products, Annual Book of ASTM Standards, pp. 998-1005, 1995.

12. ASTM D 2321-89: Standard Practice for Underground Installation of Thermoplastic Pipe for Sewers and Other Gravity-Flow Applications, Vol. 08.04, Plastic pipe and Building Products, Annual Book of ASTM Standards, pp. 133-141, 1993.

13. ASTM D 3839-89: Standard Practice for Under Ground Installation of Fiberglass Pipe, Vol. 08.04, Plastic pipe and Building Products, Annual Book of ASTM Standards, pp. 534-543, 1993.

14. Chen, W. F. and Lui, E. M., "Structural Stability Theory and Implementation', Elsevier Science Publishing Co. Inc., New York, 1987.

15. Cheung, Y. K., "Finite Strip Method in Structural Analysis", Pergamon Press, Elmsford, N.Y., 1976.

16. Clark, C.M., "Expansive-Soil Effect on Buried Pipe", Journal of the American Water Works Association, 63: pp. 424-427, 1971.

17. Cook, R. D. and Young, W. C., "Advanced Mechanics of Materials", Macmillan Publishing Company, New York, 1985

18. CPPA, "Structural Design Method for Corrugated Polyethylene Pipe", Corrugated Polyethylene Pipe Association, 1996

19. Culley, R.W., "Structural Tests on Large Diameter Polyethylene Culvert Pipe", Saskatchawan Department of Highway and Transportation, Technical Report 31, Regina, Saskatchawan, pp. 27-28, Feb. 1982.

20. Das, B. M., "Principles of Foundation Engineering", PWS Publshing Co., Third Edition, 1995.

21. Dunn, I. S., Anderson, L. R., and Kiefer, F. W., "Fundamentals of Geotechnical Analysis", John Wiley & Sons, Inc., New York, 1980.

22. Drumm, E. C., Reeves, J. S., Madgett, M. R., and Trolinger, W. D., "Subgrade Resilient Modulus Correction for Saturation Effects", Journal of Geotechnical and Geoenvironmental Engineering,Vol. 123, No. 7, ASCE, pp.663-670. July, 1997.

23. Ferry, J. D., Viscoelastic Properties of Polymers, 3rd Edition, John Wiley and Sons, 1955.

24. Florida Department of Transportation (FDOT), "Roadway and Traffic Design Standards", January 1995.

25. Gabriel, L.H., Bennett, O.N., Schneier, B., "Polyethylene Pipe Specifications", NCHRP Project 20-7, Task 68, Final Report, Jan. 1996.

26. Goddard, J.B, "Research Problem Statement for TRB Committee A2C06 on Culverts and Hydraulic Structures", 1995.

27. Goddard, J.B, "Plastic Pipe Design", Technical Report 4. 103, ADS Specifier Manual, Advanced Drainge systems, Inc. Columbus, OH, November, 1994.

28. Gere, J. M. and Timoshenko, S. P., "Mechnics of Materials", PWS-Kent Publshing Company, Boston, 1990.

29. Hancor, "Drainage Handbook", Manual # 26781, Hancor Inc., Findlay, OH, 1996

30. Hall and Foreman, Inc., "Corrugated Polyethylene Pipe, Victorville, California", Investigative Report, Oct. 1993.

31. Hashash, N. M. A., "Design and Analysis of Deeply buried Polyethylene Drainge Pipes", Ph. D Dissertation, submitted to the University of Massachusetts, September, 1991.

32. Joint Cooperative Committee of the Southern California Chapter American Public Works Association and Southern California Districts Associated General Contractors of California, "Greenbook Standard Specification for Public works Construction", BNI Building News, pp. 257-265, Los Angeles, CA, 1994.

33. Johnson, L., "HDPE Pipe, San Diego, California, Test Site #1, HDPE Pipe Task Group Report for Standard Specifications for Public Works Construction, Sep. 1993.

34. Kajartanson, B.H., Lohnes, R.A., and Klaiber, F.W., "A Full-Scale Field Test of the Uplift Resistance of a Corrugated Metal Pipe Culvert", TRB Preprint Paper #950471, pp. 27-38, Jan. 1995.

35. Kanninen, M. F., Peggs, I. D., and Popelar, C. H., "A Methodology for Forecasting the Lifetimes of Geomembranes that Fail by Slow Crack Growth", Proc. of Geosynthetics 93, Vancouver, Canada, pp.831-844, 1993.

36. Katona, M.G., Smith, J.M., Odello, R.S., and Allgood, J.R., "CANDE-A Modern Approach for the Structural Design and Analysis of Buried Culverts", Civil Engineering Laboratory, Port Hueneme, CA, NTIS Report #PB 275807, 466 pp. October 1976.

37. Katona, M.G., "Allowable Fill Height for Corrugated Polyethylene Pipe", Transportation Research Record, 1191, pp.30-38, 1988.

38. Kirby, P.A. and Nethercot, D. A., "Design for Structural Stability", Constrado Monographs, Granada Publishing, suffolk, UK, 1979.

39. Klaiber, F.W., Lohnes, R.A., Wipf, T.J., and Phares, B.M. "Investigation of High Density Polyethylene Pipe Applications", Final Report: Phase I submitted to Iowa Department of Transportation, January 1996, (IDOT Project HR-373)

40. Koerner, R. M., Lord Jr., A. E., and Hsuan, Y. H., "Arrhenius Modeling to Predict Geosynthetic Degradation", Geotextiles and Geomembranes, Vol. 11, pp. 151-183, 1992.

41. Lohnes, R.A., Klaiber, F.W., and Austin, T.A., "Uplift Failures of Corrugated Metal Pipe", TRB Preprint Paper No. 950502, pp. 22-32, Jan. 1995.

42. Lustiger, A., "The Molecular Mechanism of Slow Crack Growth in Ployethylene", Proceedings of Eighth Plastic Fuel Gas Pps Sympodium, American Gas Association, Arlington, VA, USA, pp. 55-56.

43. Martin, R. G. and Wallace, "Design and Construction of Asphalt Pavement", McGraw-Hill, Book Co, Inc., New York, 1958.

44. McGrath, T. J.and Chambers, R. E." Recent Trend in Installation Standards For Plastic Pipe", Buried Plastic Technology, ASTM STP 1093, edited by Buczala, G. S. and Cassady, M. J., ASTM, 1990, pp.281-293.

45. Miyano, Yasushi "Long Term Prediction Method for Static, Creep, and Fatigue Strengths of CFRP Composites", Progress in Durability Analysis of Composite Systems, Fukuda and Reifsnider (eds), 1996

46. Moore, I.D., and Laidlaw, T.C., "Corrugation Buckling in HDPE Pipes - Measurements and Analysis", TRB 76th Annual Meeting, Paper No. 970565, Jan. 1997.

47. Moore, I. D., "WANFE User's Guide", Geotechnical Research Centre, University of Western Ontario, Canada, 1996.

48. Moore, I. D. and Hu, F., "Response of profiled HDPE Pipe in Hoop Compression", TRB Preprint Paper No. 950823, January 1995.

49. Moore, I. D. and Brachman, R. W. "Three-Dimensional Analysis of Flexible Circular Culverts", Journal of Geotechnical Engineering, Vol. 120, No.10, American Society of Civil Engineers, pp.1829-1845, Oct. 1994.

50. Morris, R.E., "Principal Causes and Remedies of Water Main Breaks", Journal of the American Water Works Association, 54: pp. 782-798, 1967.

51. Moser, A. P., "The Structural Performance of Buried 48 in. Diameter N-12 HC Polyethylene Pipes", Technical Report 4-104, Advanced Drainage Systems Inc., Sep. 1994.

52. Moser, A. P, "Buried Pipe Design", McGraw Hill, 1990

53. Musser, S.E. "CANDE-89 Culvert ANalysis and DEsign User Manual", U.S. Department of Transportation, Federal Highway Administration, Publication No. FHWA-RD-89-169, June 1989.

54. Peggs, I. D., and Kanninen, "HDPE Geosynthetics: Premature Failures and Their Prediction", Journal of Geosysnthetics International, 1995. Vol, 2, No. 1, pp. 327-339.

55. Plastic Pipe Line,"The Slow Crack Growth Test for Comparing and Selecting Polyethylene Piping Material", Quarterly newsletter about plastic pipe research, Gas Research Institute, Vol.5, No.1. 1994.

56. Popelar, C. H., "A Comparison of the Rate Process Method and the Bidirectional Shifting Method", Thirteenth Plastic Fuel Gas Pipe Symposium, San Antonio, TX, pp. 140-151, 1993.

57. Rajani, B., Zhan, C., and Kuraoka, S., "Pipe-Soil Interaction Analysis of Jointed Water Mains", Ca. Geotech. J. 33: pp. 393-404, 1996.

58. Reddy, D. V., Evaluation of Plastic Piping for Pipe Culverts and Storm Sewers, State Project No. 99700-3312-010, WPI # 0510757 Florida Department of Transportation, 1995-98.

59. Reddy, D.V., Long Term Performance of Buried High Density Polyethylene Plastic Piping, State Project No. 99700-3312-010, WPI # 0510757 Project, Florida Department of Transportation, 1997-99.

60. Reifsnider, K.L., Case, S., and Xu, Y. L., "A Micro-Kinetic Approach to Durability Analysis: The Critical Element Method", Progress in Durability Analysis of Composite Systems, edited by Cardon, A. H., Fukuda, H., and Reifsnider, K.L., Balkema Publishers, pp.3-11.

61. Rogers, C. D. F., Fleming, P. R., Loeppy, M. W. J., and Faragher, E., "Buried Plastic Pipe-Performance Versus Prediction", Proc. on Second ASCE Conference on in Underground Pipeline Engineering, pp. 1-12, Seattle, June 1995.

62. Sclairpipe, "Engineered Large Diameter Polyethylene Piping Systems", DuPont Canada Inc., Canada, 1976.

63. Selig, E.T., "Long Term performance of Polyethylene Pipe Under High Fill", Geotechnical Report, Part II, Submitted to Pennsylvania Department of Transportation, Feb. 1995.

64. Selig, E.T., DiFrancesco, L.C., and McGrath, T.J., "Laboratory Test buried Pipe in Hoop Compression," Buried pipe Technology, 2nd Vol. ASTM STP1222, Dave Eckstein, Ed. ASTM, pp.1-11, 1993.

65. Sholten, F.L., Pister, T., and Venema, B., "A More Reliable Detergent for Constant Load Experiment on Polyethylene", Polymer Testing, Elesevier Science Publishers Ltd, London, 1989, pp.385-405.

66. Small, J. C.and Wong, K. W., "The Use of Integral Transforms in Solving Three Dimensional Problems in Geomechanics", Comp. and Geomechanics, 6(3), pp.199-216, 1988.

67. Spangler, M.G.,Soil Engineerin, Harper and Row Publishing Co., NY. 1982.

68. Strand, D, "Miramar Landfill, City of San Diego, California, Test Sites #1 and #2", HDPE Task Force for Green Book Standard Specifications for Public Works Construction, Oct. 1993.

69. Tia, M., Ruth, B. E., Lee, M., and Liu, D., "Developement of Relationships between SHRP Asphalt Test Parameters and Structural Mixtures For Mechanistic Aanlysis and Rehabilitation Design of Flexible Pavement", Draft Final Report to Florida Department of Transportation, Department of Civil Engineering, Univ. of Florida, 1997.

70. Tobolsky, A. V., Properties and Structure of Polymers, J. Wiley and Sons, New York, 1960.

71. Vesic, A. S., "Bending of Beams Resting on Isotropic Solid,"Journal of the Engineering Mechanics Division, American Society of Civil Enginerrs, Vol. 87, pp.35-53, 1961.

72. Webb, N.and Selig, E.T., "Long Term Performance of polyethylene pipe Under High Fill", Geotechnical Report #PDT92-397F, Tech Report-Part 1, Research Project #88-14 Penn. DOT, Harrisburg, PA, Dec. 1994.

73. Woods, D.W., Krause-Singh, J., and Hindman, J., "Estimation of Long-Term Stress Capacity of HDPE Materials by Tensile Stress-Rupture Testing," Technical Report, Hauser Laboratories, Boulder, CO, 1996.

74. Zienkiewicz, O. C., "The Finite Element Method in Engineering Science", McGrow Hill, New York, N.Y., 1979.